

Identification of molecular glues of 14-3-3 Protein-Protein Interactions

Citation for published version (APA):

Soini, L. (2021). *Identification of molecular glues of 14-3-3 Protein-Protein Interactions*. [Phd Thesis 1 (Research TU/e / Graduation TU/e), Biomedical Engineering]. Eindhoven University of Technology.

Document status and date:

Published: 06/07/2021

Document Version:

Publisher's PDF, also known as Version of Record (includes final page, issue and volume numbers)

Please check the document version of this publication:

- A submitted manuscript is the version of the article upon submission and before peer-review. There can be important differences between the submitted version and the official published version of record. People interested in the research are advised to contact the author for the final version of the publication, or visit the DOI to the publisher's website.
- The final author version and the galley proof are versions of the publication after peer review.
- The final published version features the final layout of the paper including the volume, issue and page numbers.

[Link to publication](#)

General rights

Copyright and moral rights for the publications made accessible in the public portal are retained by the authors and/or other copyright owners and it is a condition of accessing publications that users recognise and abide by the legal requirements associated with these rights.

- Users may download and print one copy of any publication from the public portal for the purpose of private study or research.
- You may not further distribute the material or use it for any profit-making activity or commercial gain
- You may freely distribute the URL identifying the publication in the public portal.

If the publication is distributed under the terms of Article 25fa of the Dutch Copyright Act, indicated by the "Taverne" license above, please follow below link for the End User Agreement:

www.tue.nl/taverne

Take down policy

If you believe that this document breaches copyright please contact us at:

openaccess@tue.nl

providing details and we will investigate your claim.

Identification of molecular glues of 14-3-3 Protein-Protein Interactions

PROEFSCHRIFT

ter verkrijging van de graad van doctor aan de Technische Universiteit Eindhoven,
op gezag van de rector magnificus prof.dr.ir. F.P.T. Baaijens, voor een commissie
aangewezen door het College voor Promoties, in het openbaar te verdedigen op
dinsdag 6 juli 2021 om 11:00 uur

door

Lorenzo Soini

geboren te Rovereto, Italië

Dit proefschrift is goedgekeurd door de promotoren en de samenstelling van de promotiecommissie is als volgt:

voorzitter:	Prof. Dr. M. Merkx
I ^e promotor:	Dr. C. Ottmann
copromotor:	Dr. J. Davis (UCB Pharma, Slough, UK)
leden:	Prof. Dr. L. Brunsveld Dr. L. Albertazzi Prof. Dr. T. Grossmann (Vrije Universiteit Amsterdam, NL) Prof. Dr. T. Obsil (Charles University, Prague, CZ) Prof. Dr. A. Tolomelli (University of Bologna, IT)
adviseur:	Dr. S. Leysen (UCB Pharma, Slough, UK)

Het onderzoek of ontwerp dat in dit proefschrift wordt beschreven is uitgevoerd in overeenstemming met de TU/e Gedragscode Wetenschapsbeoefening.

L. Soini ©

A catalogue record is available from the Eindhoven University of Technology Library

ISBN: 978-90-386-5319-8

This research (TASPPI – Targeted Small Molecule Stabilisation of Protein-Protein Interactions) has been financially supported by the Innovative Training Network, funded by the H2020 Marie Curie Actions of the European Commission under Grant Agreement 675179.

Table of Contents

List of Abbreviations	i
Chapter 1	1
Introduction	1
1.1 Protein-Protein Interactions	2
1.2 Molecular Glues and Protein Degradors: rising stars in PPI modulation	4
1.3 The 14-3-3 protein family	10
1.4 Aim and Outline of the Thesis	15
1.5 References	17
Chapter 2	25
A Biophysical and Structural Analysis of the Interaction of BLNK with 14-3-3 Proteins	25
2.1 Introduction	26
2.2 Results and Discussion	27
2.3 Conclusions and Perspectives	37
2.4 Material and Methods	38
2.5 Supporting Information	39
2.6 References	45
Chapter 3	49
A Structural and Biophysical Characterization of the 14-3-3/SLP76 Protein-Protein Interaction	49
3.1 Introduction	50
3.2 Results and Discussion	51
3.3 Conclusions	61
3.4 Material and Methods	62
3.5 Supporting Information	64
3.6 References	68
Chapter 4	71
TR-FRET and FP Assay Development for the discovery of 14-3-3/SLP76 PPI stabilisers	71
4.1 Introduction	72
4.2 Results and Discussion	74
4.3 Conclusions	82
4.4 Material and Methods	83
4.5 References	85
Chapter 5	87
Identification of Molecular Glues of the SLP76/14-3-3 Protein-Protein Interaction	87
5.1 Introduction	88
5.2 Results and Discussion	89
5.3 Conclusions	116
5.4 Material and Methods	119
5.5 Supporting Information	122
5.6 References	130

Chapter 6	135
Structural and Biophysical characterization of the GADS/14-3-3 PPI	135
6.1 Introduction	136
6.2 Results and Discussion	137
6.3 Conclusions	144
6.4 Material and Methods	145
6.5 Supporting Information	147
6.6 References	148
Chapter 7	151
The characterization of potential 14-3-3 interaction sites on the bone regulator protein Schnurri-3	151
7.1 Introduction	152
7.2 Results and Discussion	153
7.3 Conclusions	158
7.4 Material and Methods	159
7.5 Supporting Information	160
7.6 References	161
Chapter 8	163
Epilogue	163
8.1 Introduction	164
8.2 The challenges associated with studying multivalent 14-3-3 interactions and full-length 14-3-3 binding partners	164
8.3 SLP76 as potential therapeutic target	167
8.4 References	170
Summary	171
Curriculum Vitae	173
List of Publications	175
Acknowledgments	177

List of Abbreviations

AD	Assay Development
AF647	Alexa Fluor 647
AKT	Protein Kinase B
AMP	Adenosine Monophosphate
ASU	Asymmetric Unit
BAD	Bcl-2 Associated Agonist of Cell Death
BAK	Bcl-2 Homologous Antagonist
Bcl-2	B-cell Lymphoma 2
Bcl-xL	B-cell Lymphoma-Extra Large
BCR	B-cell Receptor
BET	Bromodomain and Extraterminal Motif
BLNK	B-cell Linker Protein
BRD	Bromodomain
CN-A	Cotylenin-A
CRBN	Protein Cereblon
CsA	Cyclosporin A
DLBCL	Diffuse Large B-cell Lymphoma
DUBs	Deubiquitinating Enzymes
ER	Oestrogen Receptor
FC-A	Fusicoccin-A
FDA	Food and Drug Administration
FITC	Fluorescein Isothiocyanate
FL	Full-Length
FP	Fluorescence Polarization
GADS	GRB-2 related adaptor protein 2
HDM2	Double Minute 2 Protein
HPK1	Hematopoietic Progenitor Kinase 1
HTRF	Homogeneous Time Resolved Fluorescence
HTS	High Throughput Screening
IAP	Inhibitor of Apoptosis Protein
IDR	Intrinsically Disordered Region
IMiDs	Immunomodulatory Imide Drugs
ITC	Isothermal Titration Calorimetry
K _d	Dissociation Constant
LAT	Linker for Activation of T-cell
LC-MS	Liquid Chromatography-Mass Spectrometry
MS	Mass Spectrometry
mTOR	mammalian Target Of Rapamycin
NMR	Nuclear Magnetic Resonance
PDB	Protein Data Bank
PhoRCs	Phosphatase Recruiting Chimeras
PKA	Protein Kinase A
PMA	Plasma Membrane H ⁺ -ATPase
PPI	Protein-Protein Interaction
PROTACs	Proteolysis Targeting Chimeras
PTKs	Protein Tyrosine Kinases
PTMs	Post-Translational Modifications
SAM	Sterile Alpha Motif
SAR	Structure-Activity Relationship
SARDs	Selective Androgen Receptor Degraders
SEC	Size Exclusion Chromatography
SERDs	Selective Oestrogen Receptor Degraders
SH2	Src Homology 2 Domain
SHN3	Schnurri-3
SLP76	SH2 domain-containing protein of 76 kDa
SOC	Super Optimal broth with Catabolite repression
SPLAMs	Splicing Inhibitor Sulfonamides

- List of Abbreviations -

SPR	Surface Plasmon Resonance
Sumo	Small Ubiquitin-like Modifier
TCR	T-cell Receptor
TEV	Tobacco Etch Virus
TPD	Targeted Protein Degradation
TR-FRET	Time-Resolved Fluorescence Energy Transfer
Ub	Ubiquitin
UPS	Ubiquitin-Proteasome System
WT	Wild Type

Chapter 1

Introduction

Abstract

There are approximately 650,000 protein-protein interactions (PPIs) governing diverse signalling pathways in the human organism. Targeting PPIs has become a common approach to tackle various diseases since their misregulation in important pathways has been related to several human conditions, providing insight into their therapeutic potential. First, different approaches can be used to modulate PPIs. Initially, therapeutic effects were mostly sought by inhibiting PPIs. However, by gaining insight into the mode of action of certain therapeutic compounds, it became clear that stabilising (i.e. enhancing) PPIs can also provide a useful approach. The latter strategy is recently gaining a lot of attention, as stabilising naturally occurring interactions, or even inducing novel interactions of a target protein with E3 ubiquitin ligases forms the basis of the targeted protein degradation (TPD) approach. 14-3-3 proteins are a family with an interactome of over 500 binding partners which facilitate many of the processes within the cell. 14-3-3 involvement has also been associated with ubiquitination and degradation pathways of certain proteins, suggesting it could be possible to enhance or lower their degradation by modulating the 14-3-3 interactions which ultimately lead to an increased or decreased level of their ubiquitination.

1.1 Protein-Protein Interactions

Proteins are the gearwheels that makes the complex cellular engine work. They are responsible for most cellular biological processes in the cell such as signal transduction, expression and degradation of other macromolecules, transport, motility and catalysis ¹. The overwhelming variety of functions performed by these macromolecules is achieved by the high degree of structural complexity that the twenty amino acids can provide. A simple strand of amino sequence can fold and generate secondary structure motifs and three-dimensional domains that ultimately define their function.

In the last decades, a huge effort has been put into the sequencing of the protein-coding genes that compose the human genome, settling on the order of magnitude of 20,000-25,000 genes ². The proteome, however, is far more complex considering that one gene can encode more than one protein. Although the number is still the object of debate, the human proteome is estimated to be in the range of tens of thousands to the hundreds of thousands of proteins ³⁻⁵. UniProt reports a count of 75,776 reviewed non-redundant proteins ⁶. Modifications among highly related proteins encoded by the same gene, like post-translational modifications (PTMs), increase complexity and provide chemical diversity making the association of a definitive number to the proteome extremely challenging ^{3,7}. Although in the early days of protein analysis the focus was mainly on single proteins, they rarely live out their life span without interacting with other proteins to execute their function ^{1,8}. This bring us to the concept of protein-protein interactions (PPIs) and the protein interactome, which has been estimated to be around 650,000 protein interactions ⁹. Attempts to define the types of PPIs have been described in the literature ¹⁰. Although it is possible to distinguish PPIs in obligate/non-obligate complexes; transient and permanent complexes; weak and strong interactions one must bear in mind that exceptions are more frequent than rules ^{10,11}. Reversible transient interactions are, however, extremely important for cellular processes and combined with the reversible nature of PTMs provide an extremely sophisticated and fine-tuned machine ¹¹.

Understanding of protein-protein interactions (PPIs) and protein complexes requires careful analysis to fully comprehend their mechanism and have a chance of modulating their function.

1.1.1 The PPIs Modulation Challenge

From a drug discovery perspective, the sheer number of PPIs make them attractive therapeutic targets. In fact, dysfunctions in PPIs have been correlated to many human diseases ¹². A study mapping the pharmacological space revealed that only a few hundred human proteins are targeted by orally available small molecule drugs ¹³. The first three protein classes for which the majority of drugs have been developed are enzymes, receptors and ion channels ¹⁴. On one hand this leaves a big gap that is waiting to be filled with drugs targeting PPIs. On the other hand PPIs have always been considered challenging, compared to the more conventional targets mentioned above ^{15,16}. Clearly defined features such as pockets and grooves that regulate and modulate the function of enzymes and receptors are often lacking on the more flat and broad surfaces formed by PPIs. Most often, there is also no starting point provided by a natural ligand, as is commonly the case for an enzyme or receptor ¹⁶⁻¹⁸.

The elucidation of crystal structures of proteins and protein complexes combined with the alanine-scanning mutagenesis approach helped to uncover the mechanisms and atomic structures of molecular recognition sites, the so called “hot spots”¹⁹⁻²¹. Hot spots are specific residues, often conserved, that contribute to the majority of the binding free energies of protein complexes^{22,23}. The most recurrent residues found in hot spots are tryptophan, tyrosine and arginine^{19,22}. The knowledge of the preferred ways with which proteins interact has allowed the potential for rational drug design¹⁵.

Despite the challenges of targeting PPIs, the last two decades have witnessed successful stories unfold, bringing small molecules from their early discovery stage to the most advanced clinical trials^{18,24}. Examples of such stories can be found within the Bcl-2 family of proteins where the inhibitor Navitoclax/ABT-263 (AbbVie) reached Phase II in cancer treatment by inhibiting the Bcl-xL/Bcl-2 interaction with BH3 domains of proapoptotic proteins like BAK and BAD (Figure 1.1a)^{25,26}. The more Bcl-2 selective compound Venetoclax/ABT-199 has been recently approved by the Food and Drug Administration (FDA) for the treatment of chronic lymphocytic leukemia (CLL)²⁷. Another example in the cancer area is the HDM2/p53 PPI disruptor Idasanutlin/RG7388 (Roche), a Nutlin analogue²⁸, which progressed into Phase III (Figure 1.1b, the Nutlin analogue Nutlin-2 is displayed in the figure). Moving from the cancer therapeutic area, Apabetalone/RVX-208 (Resverlogix) specifically inhibits the BET bromodomains from interacting with the lipid ApoA1 protein^{29,30}. This causes up-regulation of lipid ApoA1, a long time therapeutic goal that helped the compound to reach Phase III (Figure 1.1c).

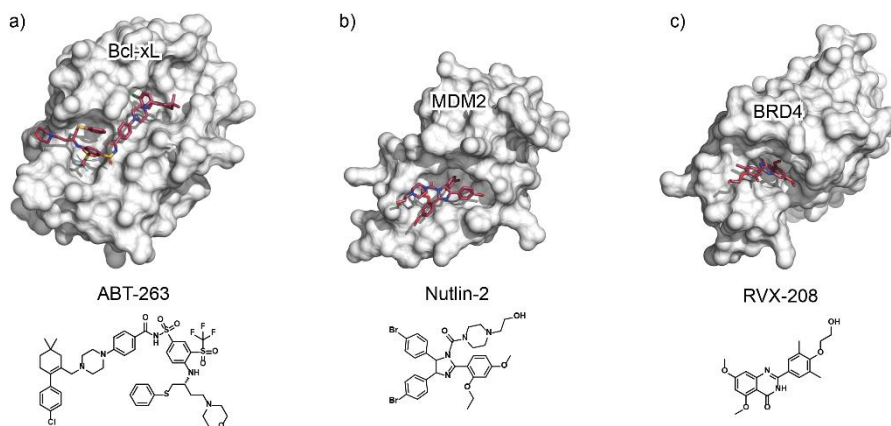


Figure 1.1 | Crystal and chemical structure of PPI inhibitors bound to their target. a) Sticks and surface representation of the inhibitor ABT-263 bound to Bcl-xL (PDB ID: 4QNQ). ABT-263 chemical structure is reported below. b) Sticks and surface representation of the inhibitor Nutlin-2 bound to MDM2 (PDB ID: 1RV1). Nutlin-2 chemical structure is reported below. c) Sticks and surface representation of the inhibitor RVX-208 bound to a BRD4 domain (PDB ID: 4MR4). RVX-208 chemical structure is reported below.

The examples mentioned above are all PPI inhibitors. Inhibition is the first approach to PPI modulation that has been addressed systematically and, to some extent, is the most intuitive. Inhibiting a PPI in order to achieve a desired therapeutic effect is, however, not the only available path. More recently, PPI stabilisation, has gained more and more attention from the scientific community. PPI stabilisation has two key advantages over the more classical inhibitory approach. First, stabilisers can in theory afford to be less potent compared to inhibitors as they do not have to displace any natural binder to achieve a function, but rather enhance an already present interaction. Secondly, stabilisers often bind to a transient, unique interface formed by two (or more) interacting proteins that contribute to an extremely selective pocket that would minimise off-target effects ³¹⁻³³. A study performed on protein crystal structures available in the Protein Data Bank (PDB) revealed some similarity between the cavities formed by PPIs and the ones present on more conventional targets supporting the feasibility of the PPI stabilisation approach ³⁴. Moreover, compound libraries that historically have been designed with more conventional targets in mind may still find utility in the search for stabilisers.

Interestingly, some small molecule stabilisers or molecular glues (an interchangeable concept) have been present in disguise on the market for decades. The retrospective uncovering of their mechanism of action has made molecular glues an area of investigation which is now gaining more and more attention by both academia and the pharmaceutical industry ^{35,36}. An equally fascinating concept that overlaps with molecular glues is targeted protein degradation (TPD) ³⁷.

1.2 Molecular Glues and Protein Degraders: rising stars in PPI modulation

Targeting PPIs by means of molecular glues can unlock the so far considered undruggable pool of scaffolding, adaptor proteins and transcriptional factors that regulate many cellular processes ^{37,38}.

1.2.1 Natural macrocycles as molecular glues

Among the first compounds identified as molecular glues were Cyclosporin A (CsA), Rapamycin and FK506 (Figure 1.3) ³⁵. These compounds all possess immunosuppressive activity acting as molecular glues to inhibit T-Cell Activation. CsA binds to Cyclophilin and Calcineurin proteins leading to IL-2 inactivation ^{39,40}. FK506 forms a ternary complex with the proteins FKBP12 and Calcineurin inhibiting the enzymatic phosphatase activity of Calcineurin ^{39,40}. Finally, Rapamycin glues the two proteins FKBP12 and mTOR, inhibiting mTOR kinase activity (Figure 1.3) ^{41,42}. All three of these natural products have become clinically important immunosuppressives to prevent transplant rejection and treat other auto-immune disorders. These examples demonstrate the fundamental importance of exploiting molecular glues to modulate cellular pathways and stimulate therapeutic outcomes.

1.2.2 Protein degraders

Before discussing the most relevant protein degraders currently under study and the strategies implemented by them, an introduction on the ubiquitin-proteasome system is due.

The UPS, ubiquitin-proteasome system, is an extremely sophisticated biological mechanism specific to eukaryotic cells that can silence targeted proteins by degrading them (Figure 1.2) ⁴³. Contrary to phosphorylation, protein degradation is irreversible but alongside phosphorylation controls most of the signalling pathways ⁴⁴. The proteolysis of targeted proteins is triggered by a cascade of enzymatic reactions carried out by three types of enzymes: an activating enzyme E1, a conjugating enzyme E2 and a ubiquitin protein ligase E3 ^{43,45}. Proteins are selected for degradation by small, 76-amino acid long, polypeptides called ubiquitins that bind covalently on lysine of the targeted protein. The transfer of ubiquitin to the target protein is facilitated by the enzymes E1 and E2. The E3 protein ligase facilitates the proximity induced transfer of ubiquitin from E2 to the target protein (Figure 1.2) ^{45,46}. The cycle is repeated until at least three ubiquitin proteins are linked to the targeted protein. This marks the protein for degradation by the proteasome ⁴⁵. Being such an essential controlling mechanism in substantially every biological pathway of the cellular system, aberrations in the UPS can be related to many different human disease areas like cancer, neurodegenerative diseases and immune system disorders ^{44,47,48}. The UPS is not only being targeted directly to therapeutically address human conditions. It is also being exploited by sophisticated, engineered synthetic molecules to reprogram protein degradation of selected target proteins involved in therapeutically relevant pathways (Figure 1.2) ⁴⁹.

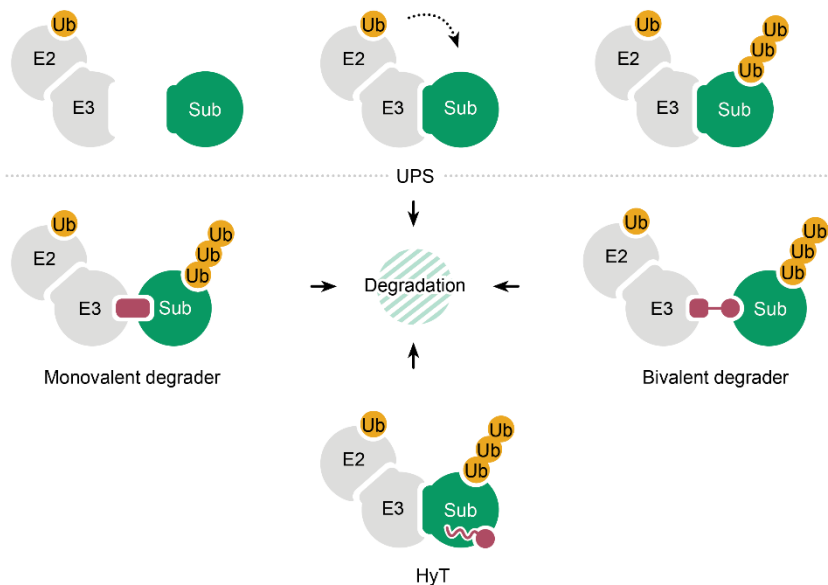


Figure 1.2 | Cartoon representation of the ubiquitin-proteasome system (UPS) and strategies to therapeutically exploit it. In the ubiquitin-proteasome system a natural E3 ligase

substrate (Sub) is recruited and polyubiquitinated. The ubiquitination targets the substrate for degradation. Artificial strategies have been shown to exploit the UPS for the degradation of desired therapeutic targets. A couple examples are illustrated, such as the implementation of monovalent agents, bivalent agents or hydrophobic tagging (HyT).

Targeted protein degradation by means of either monovalent or bivalent molecules is a rising strategy in drug discovery. If compared to the more traditional inhibitors of protein function, protein degraders require only a transient event for function in order to target the protein for degradation⁵⁰. They are also free from the stoichiometric occupancy rule since they can be recycled immediately after the target has been degraded. Functioning more like tags, they do not have to bind to specific “active” sites of the protein. This allows to engage proteins so far considered undruggable⁵¹. Moreover, a kinetic advantage is provided by the fact that the target proteins have to be re-synthesised extending its duration of action and avoiding potential feedback mechanisms that would trigger overexpression of an inhibited protein⁵⁰. The regulation of intracellular protein concentration can be achieved by other methods such as RNA interference or antisense oligonucleotides^{52,53}. A TPD approach however can provide the pharmacological advantages of a small molecule drug consistent with the Lipinski Rule of Five^{49,54}.

Monovalent protein degraders

Direct protein degradation has been achieved by selective oestrogen degraders, SERDs, and selective androgen receptor degraders, SARDs. The progenitor of these small molecules is the FDA approved drug Fulvestrant used in breast cancer treatment (Figure 1.3)⁵⁵. The mechanism by which Fulvestrant acts as an oestrogen receptor (ER) antagonist has only been discovered retrospectively. Fulvestrant is in fact responsible of inducing conformational changes that increase hydrophobicity on the ER surface, targeting it for degradation^{56,57}. A considerable amount of effort has been put into the development of both SARDs and SERDs of either steroidal and non-steroidal origin and have been extensively reviewed^{58,59}. Another example of a monovalent degrader is ASTX660, a BIR3-binding domain IAP (inhibitor of apoptosis protein) antagonist, which destabilises and induces cIAP degradation. This increases dimerization and autoubiquitylation of the latter, restoring the apoptosis pathway (Figure 1.3)⁶⁰. Bcl6 is a transcription factor of which dysregulation leads to conditions such as diffuse large B cell lymphoma (DLBCL). Small molecules like BI-3802 have been shown to induce Bcl6 degradation, resulting in an inhibition of its action in the disease progression (Figure 1.3)⁶¹.

Monovalent small molecules acting as a molecular glue as well as a protein degrader are also known and they are represented by the Immunomodulatory Imide drugs (IMiDs) and by the Splicing Inhibitor Sulfonamides (SPLAMs) class of molecules⁵⁹. Thalidomide, Lenalidomide (Figure 1.3) and Pomalidomide (IMiDs) have all been identified as Cereblon (CRBN) binders. CRBN is the substrate receptor of an E3 ligase complex known as CRL4^{CRBN}^{62,63}. IMiDs can recruit non-native substrates for the CRL4^{CRBN} complex by acting as molecular glues, bridging interactions between CRBN and neo-substrates. Investigations on the mechanisms of action of these molecules combined with the elucidation of crystal structures in which these molecules have been co-crystallised, suggest that IMiDs induce conformational changes on CRBN

making it capable of recruiting different substrates⁶⁴. Interestingly, these conformational changes appear to be IMiDs-structure dependent, revealing a huge potential for this class of molecules. IMiDs have been related to CRBN neo-substrates such as the lymphoid transcription factors Ikaros and Aiolos (IKZF1 and IKZF3) resulting in IL-2 upregulation in T-cells^{65,66}. IMiDs are also related to the Casein Kinase 1 α of which a crystal structure has been solved lately⁶⁴. Among the latest generation of IMiDs that have been developed Avadomide (C-122) (Figure 1.3) is currently being tested in clinical trials for DLBCL treatment⁶⁷.

The last class of protein degraders with a small molecule molecular glue mode of action are the splicing inhibitor sulphonamides (SPLAMs). Indisulam (Figure 1.3) has been reported to mediate the recruitment of the RBM39 splicing factor to the CUL4-DCAF15 E3 ligase protein complex causing its degradation. Indisulam has been proven effective as an anticancer agent⁶⁸.

Bivalent protein degraders

Bivalent protein degraders normally consist of two distinct chemical moieties required for the molecule to function. The bifunctional aspect of these tools generally provides a modular action that can be redirected on multiple targets, conferring a general transferability³⁷.

The first example of bivalent protein degraders exploits the natural recognition of hydrophobicity on proteins of interest to target them for degradation. Partially folded proteins would display hydrophobic portions on their surfaces as a result of an incomplete folding and are therefore naturally degraded. The artificial inclusion of hydrophobic tags on proteins by means of small molecules can interfere with their correct folding process, hence targeting them for degradation⁶⁹. Hydrophobic tagging can be achieved by tagging small molecules with adamantane or Boc₃Arg chemical moieties (Figure 1.3). For instance, an adamantyl moiety has been linked to a ligand of kinase HER3, a therapeutic cancer target. The resulting bivalent molecule TX2-121-1 has been shown to induce HER3 degradation *via* the proteasome pathway⁷⁰. Boc₃Arg tagged ligands are also reported to induce degradation of targeted proteins such as GST-1 and DHFR⁷¹.

The second, and certainly one of the most ground-breaking technologies of the last decade is represented by the Proteolysis Targeting Chimeras class of molecules or, more simply, PROTACs. PROTACs are a class of bifunctional molecules designed and engineered for binding to an E3 ligase neo-substrate and to an E3 ligase protein complex. They are normally an assembly of three components: first a chemical moiety that binds to the desired protein to be degraded, second a chemical moiety that binds to an E3 protein complex and third an artificial linker connecting these two binding motifs. The proximity induced by the PROTACs agent, although it is not always a sufficient condition, causes the neo-substrate to be polyubiquitinated and therefore targeted for degradation⁷². The PROTACs strategy does not only consist of bringing an E3 ligase and a target protein in proximity. Indeed, there are a variety of different parameters such as the affinity of the “warheads” to their respective target; the length, the attachment location and the chemical nature of the linker, and the choice of E3 ligase, that provide PROTACs with an extremely high potential for target selectivity⁷³. The first synthetic PROTACs proof of concept was first

described 20 years ago by Sakamoto et al. ⁷⁴ in which an IκBα inspired phosphopeptide was linked to the MetAP-2 protein antagonist OVA, generating the Protac-1 bivalent degrader. Protac-1 was in fact reported to degrade MetAP-2 *via* ubiquitination by recruiting it on the SCF^{β-TRCP} E3 ligase protein complex. The fact that MetAP-2 was not a substrate for SCF^{β-TRCP} revealed the hidden potential of the PROTACs approach ⁷⁴. A second generation of PROTACs exploited non-peptidic, more drug-like small molecules to recruit substrates to E3 ligases. Those could boast better stability and cellular permeability ⁷³. So far, the E3 ligases that have been involved in the PROTACs approach for targeted degradation are MDM2, IAP1, VHL and CRBN ⁷⁵. The major success came from the recruitment of the E3 ligases VHL and CRBN that gave birth to the PROTACs molecules MZ1 ⁷⁶ (first ternary crystal structure: Brd4^{BD2}/MZ1/VHL) (Figure 1.3), ARV-771 ⁷⁷ and ARV-825 ⁷⁸. The PROTACs molecules were engineered to degrade ERRα, RIPK2, Brd4/3/2 ⁷⁵ and other targets not listed here.

As a concluding remark, a recent work has demonstrated how bivalent molecules can be exploited to modulate post-translational modifications other than ubiquitination ⁷⁹. Yamazoe et al. developed tool compounds, Phosphatase Recruiting Chimeras (PhoRCs), able to hijack the protein phosphatase-1 (PP1) to dephosphorylate the oncogenic kinases EGFR and AKT ⁷⁹. Although far from being a mature approach, the ability to modulate phosphorylation intracellularly represents an attractive strategy for the future ⁸⁰.

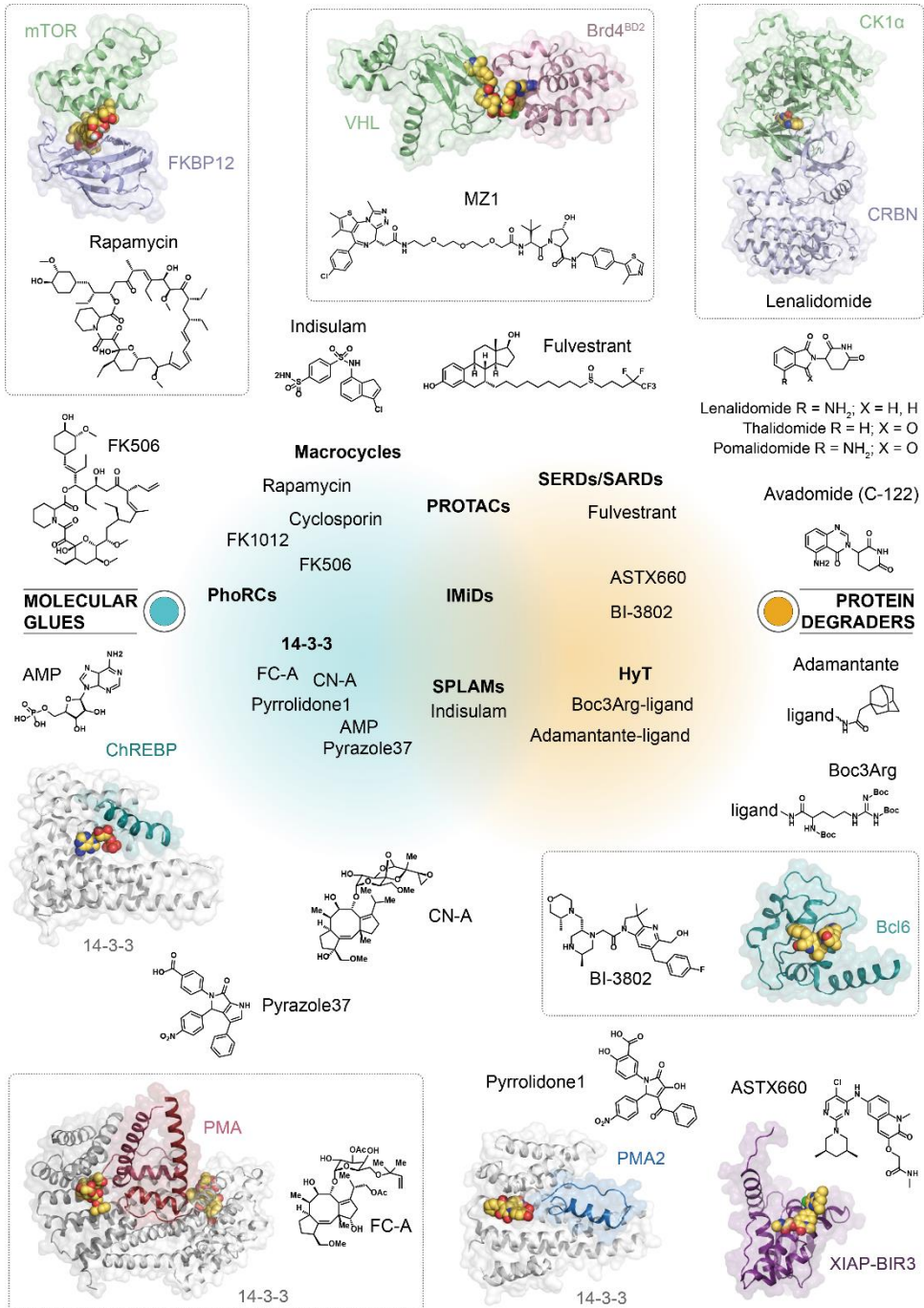


Figure 1.3 | Examples of protein degraders and molecular glues mentioned in this chapter.

The circle graph in the middle highlight how the molecular glues and protein degrader mechanism of action sometimes overlap like in the case of PROTACs, IMiDs and SPLAMs. Ternary Rapamycin/FKBP12/mTOR complex (1FAP)⁸¹. Ternary MZ1/ Brd4^{BD2}/VHL complex (5T35)⁷⁶. Ternary Lenalidomide/CK1 α /CRBN complex (5FQD)⁶⁴. Ternary AMP/14-3-3/ChREBP complex (5F74)⁸². Ternary FC-A/14-3-3/PMA complex (2O98)⁸³. Ternary Pyrrolidone1/14-3-3/PMA2 complex (3M51)⁸⁴. Binary ASTX660/XIAP-BIR3 complex (5OQW)⁸⁵. Binary BI-3802/Bcl6 complex (5MW2)⁶¹.

1.3 The 14-3-3 protein family

A class of proteins on which extensive small molecule modulation work has been performed in the last decades, are the regulatory family of proteins collectively referred to as 14-3-3. In the next section we will briefly cover general aspects of the 14-3-3 protein family, stabilisers of 14-3-3 protein interactions and the involvement of 14-3-3 proteins in ubiquitination pathways.

1.3.1 14-3-3 proteins structure and biology

14-3-3 proteins are one of the most abundant families of adaptor proteins in eukaryotic cells. By definition, they do not possess any enzymatic activity but rather act as hub proteins contributing to signal transduction by facilitating the formation of transient signalling protein complexes^{86,87}. 14-3-3 proteins were first identified as part of calf brain proteins and owe their name to a specific migration pattern on DEAE cellulose chromatography and starch gel electrophoresis⁸⁸. Depending on the organism, a lower or higher number of 14-3-3 isoforms can be detected. To date, seven different isoforms have been identified in humans (β , ϵ , η , γ , τ , ζ and σ). An initial number of nine was claimed but two isoforms turned out to be phosphorylated versions of already existing isoforms⁸⁹. Extensive research on 14-3-3 proteins led to the discovery of their presence among a considerable number of different cellular pathways such as modulation of catalytic enzymes^{90,91}, regulation of protein subcellular localization⁹², regulation of the cytoskeleton⁹³, apoptosis and cell cycle regulation⁹⁴⁻⁹⁶. Moreover, the 14-3-3 interactome is currently estimated to be around 500 binding partners⁹⁷. Being such a ubiquitously present class of molecules, 14-3-3 proteins are found in most of human tissues and therefore they are involved in many human diseases⁹⁸. 14-3-3 is extremely highly expressed in brain tissue; hence it has been detected in neurofibrillary tangles bound to Tau in Alzheimer's disease affected patients⁹⁹. Moreover, 14-3-3 has been associated with Lewy body formation in Parkinson's disease¹⁰⁰. 14-3-3 presence has also been well document in many types of cancer¹⁰¹.

The first crystal structure of 14-3-3, 14-3-3 ζ , was released in 1995 by Liu et al.¹⁰² and helped in the elucidation of the 14-3-3 mechanism of action. From a structural perspective, 14-3-3 proteins are dimeric highly α -helical proteins. 9 α -helices spaced out by short loops constitute one monomer which is bound to the second monomer in an antiparallel fashion¹⁰³. The dimerization process, either by heterodimerization or homodimerization, is controlled by salt bridges (Arg18/Glu89, Asp21/Lys85, and Glu5/Lys74) and hydrophobic contacts between monomers¹⁰⁴. The binding of target proteins to 14-3-3

occurs *via* recognition of one of 3 specific phosphorylated motifs on the binding partner: mode I) RSXpS/pTXP, mode II) RXY/FXpS/pTXP and mode III) pS/pTX1-2-COOH (X: any residue; p: phosphorylation) (Figure 1.4a) ^{105,106}. 14-3-3 proteins engage their binding partners using two amphipathic grooves which are extremely conserved among the isoforms. More solvent exposed residues possess a higher degree of variability and the C-terminal tail is extremely variable and disordered (Figure 1.4a) ¹⁰³. Over the last two decades the number of crystal structures of 14-3-3 proteins bound to their targets increased exponentially, providing valuable insights in both the understanding of the 14-3-3 binding mechanism and the possibility of modulating 14-3-3 PPI with small molecules ¹⁰⁷. However, the representation of 14-3-3 binding partners is mostly limited to short synthetic phosphorylated peptides (Figure 1.4a) and to date, only 6 crystal structures with full-length or partially truncated proteins are deposited in the PDB. 5 of these structures were solved by protein crystallography and 1 by cryo-electron microscopy (Figure 1.4b-g) ¹⁰⁸. The high intrinsic disorder present in most of the 14-3-3 binding partners represents an obstacle in routinely solving these structures ^{109,110}.

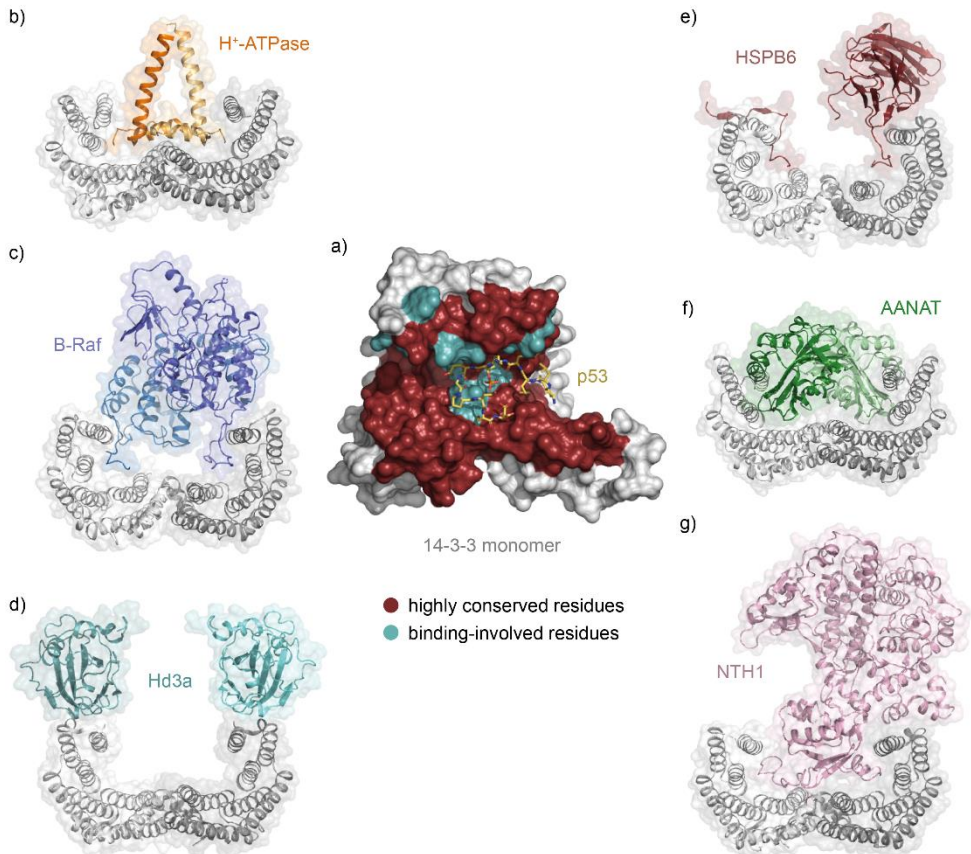


Figure 1.4 | 14-3-3 monomer structure and structures of 14-3-3 in complex with full-length or partially truncated proteins. a) An example of 14-3-3 in complex with a synthetic phosphorylated

peptide, in this case derived from p53 shown in yellow sticks, engaging the 14-3-3 binding groove. Poorly conserved residues among the 14-3-3 isoforms are shown as white surface, while highly conserved residues are shown as ruby red surface. The residues shown as cyan surface are essential for interacting with binding partners. b) 14-3-3/H⁺ATPase binary complex (PDB ID: 2O98)⁸³. c) 14-3-3/B-Raf binary complex (PDB ID: 6UAN)¹¹¹. d) 14-3-3/Hd3a binary complex (PDB ID: 3AXY)¹¹². e) 14-3-3/HSBP6 binary complex (PDB ID: 5LTW)¹¹³. f) 14-3-3/AANAT binary complex (PDB ID: 1IB1)⁹⁰. g) 14-3-3/NTH1 binary complex (PDB ID: 5N6N)¹¹⁴.

1.3.2 14-3-3 molecular glues

The stabilisation of 14-3-3 PPIs has been the focus of many academic early stage drug discovery projects in the last decades. The inspiration came, as in most cases, from nature. The wilt-inducing toxin Fusicoccin-A (FC-A), a diterpene glycoside produced by the *Phomopsis amygdali* fungus, was first isolated in 1964¹¹⁵. Like the Rapamycin case discussed before, the elucidation of the FC-A binding mechanism and finding it was acting as a molecular glue happened retrospectively. FC-A was in fact identified as a binder of the protein complex composed of 14-3-3 and the regulatory domain of the plasma membrane H⁺-ATPase (PMA) (Figure 1.3)¹¹⁶. FC-A activates plant plasma membranes by stimulating H⁺ pumping which leads to wilting. This mechanism was characterized structurally in 2007^{83,117}. The disclosure of the FC-A mechanism allowed it to be used as a valuable tool to stabilise other 14-3-3 PPIs, including in human cells. One example is the stabilisation of the 14-3-3/ER α complex, which results in the inhibition of ER α transcriptional activity¹¹⁸. Another example is the 14-3-3/CFTR interaction for which stabilisation results in increased CFTR trafficking to the cell membrane¹¹⁹. A structurally related compound to FC-A is Cotylenin-A (CN-A). It has been reported to possess anti-tumour activity in a few human cancers (Figure 1.3)^{120,121}. 14-3-3 has been reported to be a cofactor for Raf kinase activity and a published structure of CN-A bound to the 14-3-3/Raf complex provided useful insight as to how CN-A can provide antitumor activity^{122,123}.

Non-natural stabilisers of 14-3-3 PPIs were also discovered. The main example is Pyrrolidone1, which was identified by an HTS conducted on the 14-3-3/PMA2 complex using a surface-based format⁸⁴. A more potent molecule derived from the optimisation of Pyrrolidone 1, Pyrazole37 (Figure 1.3), was identified later by converting the Pyrrolidone1 moiety to a more rigid one¹²⁴. Another example is the adenosine monophosphate molecule AMP which has been reported to directly stabilise the 14-3-3/ChREBP PPI. An interesting feature of this PPI is that it also occurs *via* non-phosphorylated ChREBP. A crystal structure reveals that AMP engages the 14-3-3 binding groove with a phosphate that also bridges the interaction with ChREBP (Figure 1.3)⁸². 14-3-3 proteins regulate ChREBP subcellular localization upon changing glucose levels¹²⁵. Routes to develop more potent and specific versions of these molecules have been pursued and the field is rapidly moving forward¹²⁶⁻¹²⁸.

In particular, fragment-based approaches for the identification of 14-3-3 PPI stabilisers have seen a considerable amount of progress in the last few years^{129,130}. 14-3-3 proteins in complex with short phosphorylated peptides have demonstrated to be a binary system highly amenable to crystallisation. It is therefore very suitable for structural fragment-based approaches. Recently, methods have been developed that allow the discovery of fragments binding covalently (tethering) to complexes of 14-3-3 and

phosphopeptides derived from binding partners *via* disulphide or aldimine bonds. As some of these fragments demonstrate stabilisation of the targeted 14-3-3 interaction, they provide promising starting points for the development of non-covalent stabilisers ^{131,132}.

1.3.3 14-3-3 in the context of protein degradation

The role of 14-3-3 proteins in protein degradation and ubiquitination pathways has not been studied systematically but a few examples are reported in which 14-3-3 is, to different degrees, involved in protein degradation and ubiquitination pathways.

14-3-3 γ has been reported to play a crucial scaffolding role in the cell cycle DNA damage checkpoint pathway. 14-3-3 γ in fact mediates the interaction between the Chk1 kinase, upon its autophosphorylation on Ser296, and the Cdc25A phosphatase. This induces Cdc25A phosphorylation on Ser76, a site that appears to regulate its ubiquitination and degradation ¹³³. The degradation of Cdc25A inhibits mitotic entry upon DNA damage ¹³⁴. This example describes the scaffolding action of 14-3-3 proteins. Although the scaffolding mechanism has been described, this specific 14-3-3 mode of action has not been widely reported and a structural confirmation is yet to come ^{103,108}. 14-3-3 proteins also play a role in ubiquitin-independent protein degradation as in the case of the kinase inhibitor p21 by directly promoting its interaction with the 20S proteasome. The downregulation of p21 associated with 14-3-3 overexpression is correlated with shorter breast cancer patient survival ¹³⁵. The interaction between 14-3-3 proteins and deubiquitinating enzymes (DUBs) has also been reported. Specifically, 14-3-3 was shown to inhibit the catalytic activity of UBPY ¹³⁶. The 14-3-3 and UBPY interaction has been described in the context of the Cushing's Disease (CD) where mutations of the UBPY gene lead to an impaired 14-3-3/UBPY interaction and upregulation of EGFR signalling, ultimately culminating in CD symptoms ^{137,138}. In the context of the Hippo pathway, LATS1/2 kinases phosphorylate the transcriptional regulator factors YAP and TAZ allowing the docking of 14-3-3 proteins to their phosphorylation sites. The binding of 14-3-3 proteins induces cytoplasmic retention of YAP and TAZ where a subsequent phosphorylation by Casein kinase 1 δ / ϵ triggers the recruitment of the SCF E3 ubiquitin ligase which leads to the degradation of YAP and TAZ ^{139,140}. In this case 14-3-3 acts more coordinatively to inhibit YAP and TAZ oncogenic activity by spatially controlling their localization ¹⁴¹. Interestingly, 14-3-3 proteins have also been reported to shield proteins from degradation by occluding their ubiquitination sites, an opposite scenario of what was discussed above. An example is the interaction with the Cdt2 protein, an important regulator of cell proliferation which is upregulated in a few human cancers. 14-3-3 γ interacts with Cdt2 shielding it from ubiquitin-mediated degradation. This results in cell cycle progression ¹⁴². Another protein target that has been suggested to benefit from 14-3-3 ubiquitination shielding activity are the FOXO family of transcriptional factors. They are involved in apoptosis regulation, cell-cycle progression, and oxidative stress resistance ¹⁴³. One type of FOXO regulation occurs *via* AKT phosphorylation which results in FOXO translocation from the nucleus to the cytoplasm. In the cytoplasm higher expression FOXO3 levels has been correlated to increased expression of 14-3-3 explained by 14-3-3 having a role protecting FOXO3 from either dephosphorylation and degradation ^{144,145}. Examples where 14-3-3 is itself object of degradation are also reported but these lie outside of the aim of the discussion.

In T-cell receptor (TCR) and B-cell receptor (BCR) signalling, 14-3-3 proteins have been recently correlated to phosphorylation driven negative feedback mechanisms that, in some cases, are related to ubiquitination pathways. The adaptor proteins SLP76, BLNK and BTK are in fact reported to undergo ubiquitination and consequently degradation upon 14-3-3 binding, leading to attenuation of the immune response ¹⁴⁶⁻¹⁴⁹. Interestingly, the loss of the phosphorylation responsible for the engagement of 14-3-3 with these proteins reduces their degradation. The elucidation of these three mechanisms has not been fully elucidated, however the remarkable similarities between these targets highlights the strong role of 14-3-3 in these pathways. In the case of GADS, once again 14-3-3 has been suggested to scaffold the formation of a ternary complex with SLP76 which modulates the immune response. Although this specific target has not been linked to the ubiquitination pathways yet, its degradation as a consequence of 14-3-3 binding has not been excluded ¹⁵⁰. An extensive description of the mechanism between 14-3-3 proteins and the targets mentioned in this paragraph is reported in Chapter 2 for BLNK, Chapter 3 for SLP76 and Chapter 6 for GADS in which an insight into the structural basis of these interactions will also be provided.

Although the mechanisms by which 14-3-3 proteins interfere with the UPS and protein degradation is not completely understood yet, modulating 14-3-3 PPIs represents an intriguing new opportunity for the indirect modulation of protein degradation.

1.4 Aim and Outline of the Thesis

The modulation of PPIs represents a challenge for the drug discovery field and offers the potential for therapeutic intervention in many human conditions. In **Chapter 1** of this thesis, the importance of PPIs and the challenges that come with modulating their function are extensively covered. The approaches to address modulation of PPIs are many, but recently more and more attention has been given to stabilising PPIs with molecular glues to achieve therapeutic effects. Targeting proteins for degradation (TPD) is another emerging approach currently attracting intense interest to modulate signalling pathways. 14-3-3 proteins and certain proteins in their interactome could provide an interesting area of research to bridge the PPI stabilisation and TPD approaches.

The major objective of this thesis was to identify novel stabilisers of therapeutically interesting 14-3-3 PPIs which could form the basis of future research in this area with the intriguing possibility of an alternative approach to promote protein degradation. To achieve this, the thesis workflow and aims are organised on different levels. On the first level, 14-3-3 interactions were studied with synthetic peptides in structural and biophysical experiments of several candidate proteins with the principle focus on SLP76 and BLNK. These are two adaptor proteins with key roles in TCR and BCR cell signalling respectively and both interact with 14-3-3 in a highly similar fashion. On a second level, larger protein constructs of these proteins were generated in preparation for the third level, which consisted of the development of an HTS screening methodology for the identification of small molecule modulators of a specific 14-3-3 PPI. The HTS screening methodology focused on these protein constructs rather than small phospho-peptides more typically used in the 14-3-3 field to date. The intent was to screen using more physiologically relevant constructs and provide an opportunity to discover 14-3-3 modulators beyond the canonical 14-3-3 phospho-peptide binding site. If successful, this could provide an approach of general utility to the 14-3-3 field.

Chapter 2 is dedicated to the structural and biophysical characterization of the 14-3-3/BLNK PPI. BLNK is an adaptor protein involved in the signalling pathway downstream of BCRs which modulates the immune response. A negative feedback mechanism reveals that BLNK is targeted for degradation after interaction with 14-3-3 proteins. The work reported in this chapter studies the interaction between 14-3-3 and BLNK, focusing on two BLNK phosphorylation sites which suggest the existence of a gate-keeper model of interaction.

Chapter 3 reports on the study of SLP76, a remarkably similar target to BLNK. In contrast to BLNK, SLP76 orchestrates the signalling downstream of TCRs but similarly interacts with 14-3-3 and modulates the immune response. The insight into the interaction is provided by X-ray crystallography, FP and ITC confirming the importance of the SLP76 Ser376 residue. A full-length protein and a truncated version of SLP76, containing an SH2 domain, are generated and the binding with 14-3-3 was characterised. Particular attention is given to the SLP76-SH2 construct which will prove essential for the next chapter. A precise determination of K_D and stoichiometry is in fact being carried out against 14-3-3γ.

In **Chapter 4**, the BLNK-SH2 and SLP76-SH2 construct generated in the previous chapters were used to develop a TR-FRET based assay against 14-3-3 γ with the intent of implementing a High Throughput Screening campaign (HTS). In **Chapter 5**, the results of an HTS of a chemically diverse 20,000 small molecule library on the 14-3-3 γ /SLP76-SH2 system is reported. Multiple novel stabilisers were identified and will be disclosed as promising modulators of the 14-3-3 γ /SLP76-SH2 PPI. A library of derivative molecules is also screened against the same system. The orthogonal testing of the identified compounds on the 14-3-3 γ /SLP76pS376 peptide system suggests that several of the compounds do not engage the known 14-3-3 pocket.

Chapter 6 and **Chapter 7** carries on with an extensive characterisation of other 14-3-3 binding partners: GADS, Chapter 6, and Schnurri3 (SHN3), Chapter 7. While for GADS, an adaptor protein involved in the immune response signalling, the interaction with 14-3-3 was already known, that was not the case for the bone regulator protein SHN3. The characterization techniques involved were X-ray crystallography, FP and ITC. Three novel crystal structures of 14-3-3 σ with synthetic peptides are described. Moreover, the SHN3pS452 case forms a disulphide bond with 14-3-3 σ which is a finding to take into consideration when planning further studies on this target. A preliminary expression and solubility test of a few constructs was performed on GADS and SLP76. Finally, biophysical data of the constructs generated as part of the entire work are reported.

The **epilogue** analyses the challenges and limitations of the work presented in this thesis. Additionally, it focuses on the work that has been performed on the 14-3-3/SLP76 PPI on a cellular level exploiting Flow Cytometry Technology. A few of the compounds identified as part of the HTS process were tested in Jurkat Cells to assess if they had functional activity. This part of work is in its early days and will certainly need a follow-up to confirm whether the compounds identified in this work can promote proteasomal degradation of SLP76 *in vivo*.

1.5 References

- 1 Keskin, O., Gursoy, A., Ma, B. & Nussinov, R. Principles of protein-protein interactions: what are the preferred ways for proteins to interact? *Chem Rev* **108**, 1225-1244, doi:10.1021/cro40409x (2008).
- 2 International Human Genome Sequencing, C. Finishing the euchromatic sequence of the human genome. *Nature* **431**, 931-945, doi:10.1038/nature03001 (2004).
- 3 Ponomarenko, E. A. *et al.* The Size of the Human Proteome: The Width and Depth. *Int J Anal Chem* **2016**, 7436849, doi:10.1155/2016/7436849 (2016).
- 4 Wilhelm, M. *et al.* Mass-spectrometry-based draft of the human proteome. *Nature* **509**, 582-587, doi:10.1038/nature13319 (2014).
- 5 Kim, M. S. *et al.* A draft map of the human proteome. *Nature* **509**, 575-581, doi:10.1038/nature13302 (2014).
- 6 UniProt, C. UniProt: the universal protein knowledgebase in 2021. *Nucleic Acids Res* **49**, D480-D489, doi:10.1093/nar/gkaa1100 (2021).
- 7 Smith, L. M., Kelleher, N. L. & Consortium for Top Down, P. Proteoform: a single term describing protein complexity. *Nat Methods* **10**, 186-187, doi:10.1038/nmeth.2369 (2013).
- 8 Jones, S. & Thornton, J. M. Principles of protein-protein interactions. *Proc Natl Acad Sci U S A* **93**, 13-20 (1996).
- 9 Stumpf, M. P. *et al.* Estimating the size of the human interactome. *Proc Natl Acad Sci U S A* **105**, 6959-6964, doi:10.1073/pnas.0708078105 (2008).
- 10 Irene, I. M. A. & Thornton, J. M. Diversity of protein-protein interactions. *The EMBO Journal* **22**, 3486-3492, doi:10.1093/emboj/cdg359 (2003).
- 11 Perkins, J. R., Diboun, I., Dessailly, B. H., Lees, J. G. & Orengo, C. Transient protein-protein interactions: structural, functional, and network properties. *Structure* **18**, 1233-1243, doi:10.1016/j.str.2010.08.007 (2010).
- 12 Ryan, D. P. & Matthews, J. M. Protein-protein interactions in human disease. *Curr Opin Struct Biol* **15**, 441-446, doi:10.1016/j.sbi.2005.06.001 (2005).
- 13 Paolini, G. V., Shapland, R. H., van Hoorn, W. P., Mason, J. S. & Hopkins, A. L. Global mapping of pharmacological space. *Nat Biotechnol* **24**, 805-815, doi:10.1038/nbt1228 (2006).
- 14 Overington, J. P., Al-Lazikani, B. & Hopkins, A. L. How many drug targets are there? *Nat Rev Drug Discov* **5**, 993-996, doi:10.1038/nrd2199 (2006).
- 15 Scott, D. E., Bayly, A. R., Abell, C. & Skidmore, J. Small molecules, big targets: drug discovery faces the protein-protein interaction challenge. *Nat Rev Drug Discov* **15**, 533-550, doi:10.1038/nrd.2016.29 (2016).
- 16 Wells, J. A. & McClendon, C. L. Reaching for high-hanging fruit in drug discovery at protein-protein interfaces. *Nature* **450**, 1001-1009, doi:10.1038/nature06526 (2007).
- 17 Ottmann, C. Protein-Protein Interactions. *Drug Discov Today Technol* **24**, 1-2, doi:10.1016/j.ddtec.2017.11.008 (2017).
- 18 Petta, I., Lievens, S., Libert, C., Tavernier, J. & De Bosscher, K. Modulation of Protein-Protein Interactions for the Development of Novel Therapeutics. *Mol Ther* **24**, 707-718, doi:10.1038/mt.2015.214 (2016).
- 19 Moreira, I. S., Fernandes, P. A. & Ramos, M. J. Hot spots--a review of the protein-protein interface determinant amino-acid residues. *Proteins* **68**, 803-812, doi:10.1002/prot.21396 (2007).
- 20 DeLano, W. L. Unraveling hot spots in binding interfaces: progress and challenges. *Curr Opin Struct Biol* **12**, 14-20, doi:10.1016/s0959-440x(02)00283-x (2002).
- 21 Lo Conte, L., Chothia, C. & Janin, J. The atomic structure of protein-protein recognition sites. *J Mol Biol* **285**, 2177-2198, doi:10.1006/jmbi.1998.2439 (1999).
- 22 Thorn, K. S. & Bogan, A. A. ASEdb: a database of alanine mutations and their effects on the free energy of binding in protein interactions. *Bioinformatics* **17**, 284-285, doi:10.1093/bioinformatics/17.3.284 (2001).
- 23 Bogan, A. A. & Thorn, K. S. Anatomy of hot spots in protein interfaces. *J Mol Biol* **280**, 1-9, doi:10.1006/jmbi.1998.1843 (1998).
- 24 Arkin, M. R., Tang, Y. & Wells, J. A. Small-molecule inhibitors of protein-protein interactions: progressing toward the reality. *Chem Biol* **21**, 1102-1114, doi:10.1016/j.chembiol.2014.09.001 (2014).
- 25 Tse, C. *et al.* ABT-263: a potent and orally bioavailable Bcl-2 family inhibitor. *Cancer Res* **68**, 3421-3428, doi:10.1158/0008-5472.CAN-07-5836 (2008).

- 26 Ashkenazi, A., Fairbrother, W. J., Levenson, J. D. & Souers, A. J. From basic apoptosis
discoveries to advanced selective BCL-2 family inhibitors. *Nat Rev Drug Discov* **16**, 273-284,
doi:10.1038/nrd.2016.253 (2017).
- 27 Stilgenbauer, S. *et al.* Venetoclax in relapsed or refractory chronic lymphocytic leukaemia with
17p deletion: a multicentre, open-label, phase 2 study.
- 28 Vassilev, L. T. *et al.* In vivo activation of the p53 pathway by small-molecule antagonists of
MDM2. *Science* **303**, 844-848, doi:10.1126/science.1092472 (2004).
- 29 Bailey, D. *et al.* RVX-208: a small molecule that increases apolipoprotein A-I and high-density
lipoprotein cholesterol in vitro and in vivo. *J Am Coll Cardiol* **55**, 2580-2589,
doi:10.1016/j.jacc.2010.02.035 (2010).
- 30 Picaud, S. *et al.* RVX-208, an inhibitor of BET transcriptional regulators with selectivity for the
second bromodomain. *Proc Natl Acad Sci U S A* **110**, 19754-19759,
doi:10.1073/pnas.1310658110 (2013).
- 31 Thiel, P., Kaiser, M. & Ottmann, C. Small-molecule stabilization of protein-protein interactions:
an underestimated concept in drug discovery? *Angew Chem Int Ed Engl* **51**, 2012-2018,
doi:10.1002/anie.201107616 (2012).
- 32 Bier, D., Thiel, P., Briels, J. & Ottmann, C. Stabilization of Protein-Protein Interactions in
chemical biology and drug discovery. *Prog Biophys Mol Biol* **119**, 10-19,
doi:10.1016/j.pbiomolbio.2015.05.002 (2015).
- 33 Zarzycka, B. *et al.* Stabilization of protein-protein interaction complexes through small
molecules. *Drug Discov Today* **21**, 48-57, doi:10.1016/j.drudis.2015.09.011 (2016).
- 34 Block, P., Weskamp, N., Wolf, A. & Klebe, G. Strategies to search and design stabilizers of
protein-protein interactions: a feasibility study. *Proteins* **68**, 170-186, doi:10.1002/prot.21296
(2007).
- 35 Schreiber, S. L. The Rise of Molecular Glues. *Cell* **184**, 3-9, doi:10.1016/j.cell.2020.12.020
(2021).
- 36 Deshaies, R. J. Protein degradation: Prime time for PROTACs. *Nat Chem Biol* **11**, 634-635,
doi:10.1038/nchembio.1887 (2015).
- 37 Lai, A. C. & Crews, C. M. Induced protein degradation: an emerging drug discovery paradigm.
Nature Reviews Drug Discovery **16**, 101-114, doi:10.1038/nrd.2016.211 (2016).
- 38 Che, Y., Gilbert, A. M., Shanmugasundaram, V. & Noe, M. C. Inducing protein-protein
interactions with molecular glues. *Bioorg Med Chem Lett* **28**, 2585-2592,
doi:10.1016/j.bmcl.2018.04.046 (2018).
- 39 Schreiber, S. L. & Crabtree, G. R. The mechanism of action of cyclosporin A and FK506.
Immunology Today **13**, 136-142, doi:10.1016/0167-5699(92)90111-j (1992).
- 40 Liu, J. *et al.* Calcineurin is a common target of cyclophilin-cyclosporin A and FKBP-FK506
complexes. *Cell* **66**, 807-815, doi:10.1016/0092-8674(91)90124-h (1991).
- 41 Brown, E. J. *et al.* A mammalian protein targeted by G1-arresting rapamycin-receptor complex.
Nature **369**, 756-758, doi:10.1038/369756a0 (1994).
- 42 Dumont, F. J. & Su, Q. Mechanism of action of the immunosuppressant rapamycin. *Life
Sciences* **58**, 373-395, doi:10.1016/0024-3205(95)02233-3 (1995).
- 43 Hershko, A. & Ciechanover, A. The ubiquitin system. *Annu Rev Biochem* **67**, 425-479,
doi:10.1146/annurev.biochem.67.1.425 (1998).
- 44 Nalepa, G., Rolfe, M. & Harper, J. W. Drug discovery in the ubiquitin-proteasome system. *Nat
Rev Drug Discov* **5**, 596-613, doi:10.1038/nrd2056 (2006).
- 45 Wolf, D. H. & Hilt, W. The proteasome: a proteolytic nanomachine of cell regulation and waste
disposal. *Biochim Biophys Acta* **1695**, 19-31, doi:10.1016/j.bbamcr.2004.10.007 (2004).
- 46 Pickart, C. M. & Eddins, M. J. Ubiquitin: structures, functions, mechanisms. *Biochim Biophys
Acta* **1695**, 55-72, doi:10.1016/j.bbamcr.2004.09.019 (2004).
- 47 Ciechanover, A. & Schwartz, A. L. The ubiquitin system: pathogenesis of human diseases and
drug targeting. *Biochim Biophys Acta* **1695**, 3-17, doi:10.1016/j.bbamcr.2004.09.018 (2004).
- 48 Popovic, D., Vucic, D. & Dikic, I. Ubiquitination in disease pathogenesis and treatment. *Nat
Med* **20**, 1242-1253, doi:10.1038/nm.3739 (2014).
- 49 Valeur, E., Narjes, F., Ottmann, C. & Plowright, A. T. Emerging modes-of-action in drug
discovery. *Medchemcomm* **10**, 1550-1568, doi:10.1039/c9md00263d (2019).
- 50 Crews, C. M., Georg, G. & Wang, S. Inducing Protein Degradation as a Therapeutic Strategy. *J
Med Chem* **59**, 5129-5130, doi:10.1021/acs.jmedchem.6b00735 (2016).
- 51 Neklesa, T. K., Winkler, J. D. & Crews, C. M. Targeted protein degradation by PROTACs.
Pharmacol Ther **174**, 138-144, doi:10.1016/j.pharmthera.2017.02.027 (2017).

- 52 Rinaldi, C. & Wood, M. J. A. Antisense oligonucleotides: the next frontier for treatment of
neurological disorders. *Nature Reviews Neurology* **14**, 9-21, doi:10.1038/nrneurol.2017.148
(2017).
- 53 Setten, R. L., Rossi, J. J. & Han, S. P. The current state and future directions of RNAi-based
therapeutics. *Nat Rev Drug Discov* **18**, 421-446, doi:10.1038/s41573-019-0017-4 (2019).
- 54 Lipinski, C. A., Lombardo, F., Dominy, B. W. & Feeney, P. J. Experimental and computational
approaches to estimate solubility and permeability in drug discovery and development settings.
Adv Drug Deliv Rev **46**, 3-26, doi:10.1016/s0169-409x(00)00129-0 (2001).
- 55 Nathan, M. R. & Schmid, P. A Review of Fulvestrant in Breast Cancer. *Oncol Ther* **5**, 17-29,
doi:10.1007/s40487-017-0046-2 (2017).
- 56 Moverare-Skrtic, S. *et al.* The estrogen receptor antagonist ICI 182,780 can act both as an
agonist and an inverse agonist when estrogen receptor alpha AF-2 is modified. *Proc Natl Acad
Sci U S A* **111**, 1180-1185, doi:10.1073/pnas.1322910111 (2014).
- 57 Wu, Y. L. *et al.* Structural basis for an unexpected mode of SERM-mediated ER antagonism.
Mol Cell **18**, 413-424, doi:10.1016/j.molcel.2005.04.014 (2005).
- 58 Patel, H. K. & Bihani, T. Selective estrogen receptor modulators (SERMs) and selective estrogen
receptor degraders (SERDs) in cancer treatment. *Pharmacol Ther* **186**, 1-24,
doi:10.1016/j.pharmthera.2017.12.012 (2018).
- 59 Hanan, E. J. *et al.* Monomeric Targeted Protein Degraders. *J Med Chem* **63**, 11330-11361,
doi:10.1021/acs.jmedchem.0c00093 (2020).
- 60 Johnson, C. N. *et al.* A Fragment-Derived Clinical Candidate for Antagonism of X-Linked and
Cellular Inhibitor of Apoptosis Proteins: 1-(6-[(4-Fluorophenyl)methyl]-5-(hydroxymethyl)-
3,3-dimethyl-1H,2H,3H-pyrrolo[3,2-b]pyridin-1-yl)-2-[(2R,5R)-5-methyl-2-[(3R)-3-
methylmorpholin-4-yl)methyl]piperazin-1-yl]ethan-1-one (ASTX660). *Journal of Medicinal
Chemistry* **61**, 7314-7329, doi:10.1021/acs.jmedchem.8b00900 (2018).
- 61 Kerres, N. *et al.* Chemically Induced Degradation of the Oncogenic Transcription Factor BCL6.
Cell Rep **20**, 2860-2875, doi:10.1016/j.celrep.2017.08.081 (2017).
- 62 Lopez-Girona, A. *et al.* Cereblon is a direct protein target for immunomodulatory and
antiproliferative activities of lenalidomide and pomalidomide. *Leukemia* **26**, 2326-2335,
doi:10.1038/leu.2012.119 (2012).
- 63 Ito, T. *et al.* Identification of a primary target of thalidomide teratogenicity. *Science* **327**, 1345-
1350, doi:10.1126/science.1177319 (2010).
- 64 Petzold, G., Fischer, E. S. & Thoma, N. H. Structural basis of lenalidomide-induced CK1alpha
degradation by the CRL4(CRBN) ubiquitin ligase. *Nature* **532**, 127-130,
doi:10.1038/nature16979 (2016).
- 65 Lu, G. *et al.* The myeloma drug lenalidomide promotes the cereblon-dependent destruction of
Ikaros proteins. *Science* **343**, 305-309, doi:10.1126/science.1244917 (2014).
- 66 Kronke, J. *et al.* Lenalidomide causes selective degradation of IKZF1 and IKZF3 in multiple
myeloma cells. *Science* **343**, 301-305, doi:10.1126/science.1244851 (2014).
- 67 Hagner, P. R. *et al.* CC-122, a pleiotropic pathway modifier, mimics an interferon response and
has antitumor activity in DLBCL. *Blood* **126**, 779-789, doi:10.1182/blood-2015-02-628669
(2015).
- 68 Han, T. *et al.* Anticancer sulfonamides target splicing by inducing RBM39 degradation via
recruitment to DCAF15. *Science* **356**, doi:10.1126/science.aal3755 (2017).
- 69 Neklesa, T. K. & Crews, C. M. Chemical biology: Greasy tags for protein removal. *Nature* **487**,
308-309, doi:10.1038/487308a (2012).
- 70 Xie, T. *et al.* Pharmacological targeting of the pseudokinase Her3. *Nat Chem Biol* **10**, 1006-
1012, doi:10.1038/nchembio.1658 (2014).
- 71 Long, M. J., Gollapalli, D. R. & Hedstrom, L. Inhibitor mediated protein degradation. *Chem
Biol* **19**, 629-637, doi:10.1016/j.chembiol.2012.04.008 (2012).
- 72 Zhang, Y., Loh, C., Chen, J. & Mainolfi, N. Targeted protein degradation mechanisms. *Drug
Discov Today Technol* **31**, 53-60, doi:10.1016/j.ddtec.2019.01.001 (2019).
- 73 Hughes, S. J. & Ciulli, A. Molecular recognition of ternary complexes: a new dimension in the
structure-guided design of chemical degraders. *Essays Biochem* **61**, 505-516,
doi:10.1042/EBC20170041 (2017).
- 74 Sakamoto, K. M. *et al.* Protacs: chimeric molecules that target proteins to the Skp1-Cullin-F box
complex for ubiquitination and degradation. *Proc Natl Acad Sci U S A* **98**, 8554-8559,
doi:10.1073/pnas.141230798 (2001).
- 75 Cromm, P. M. & Crews, C. M. Targeted Protein Degradation: from Chemical Biology to Drug
Discovery. *Cell Chem Biol* **24**, 1181-1190, doi:10.1016/j.chembiol.2017.05.024 (2017).

- 76 Gadd, M. S. *et al.* Structural basis of PROTAC cooperative recognition for selective protein
degradation. *Nat Chem Biol* **13**, 514-521, doi:10.1038/nchembio.2329 (2017).
- 77 Raina, K. *et al.* PROTAC-induced BET protein degradation as a therapy for castration-resistant
prostate cancer. *Proceedings of the National Academy of Sciences* **113**, 7124-7129,
doi:10.1073/pnas.1521738113 (2016).
- 78 Lu, J. *et al.* Hijacking the E3 Ubiquitin Ligase Cereblon to Efficiently Target BRD4. *Chem Biol*
22, 755-763, doi:10.1016/j.chembiol.2015.05.009 (2015).
- 79 Yamazoe, S. *et al.* Heterobifunctional Molecules Induce Dephosphorylation of Kinases-A Proof
of Concept Study. *J Med Chem* **63**, 2807-2813, doi:10.1021/acs.jmedchem.9b01167 (2020).
- 80 Conway, S. J. Bifunctional Molecules beyond PROTACs. *J Med Chem* **63**, 2802-2806,
doi:10.1021/acs.jmedchem.0c00293 (2020).
- 81 Choi, J., Chen, J., Schreiber, S. L. & Clardy, J. Structure of the FKBP12-Rapamycin Complex
Interacting with Binding Domain of Human FRAP. *Science* **273**, 239-242,
doi:10.1126/science.273.5272.239 (1996).
- 82 Sato, S. *et al.* Metabolite Regulation of Nuclear Localization of Carbohydrate-response
Element-binding Protein (ChREBP): ROLE OF AMP AS AN ALLOSTERIC INHIBITOR. *J Biol
Chem* **291**, 10515-10527, doi:10.1074/jbc.M115.708982 (2016).
- 83 Ottmann, C. *et al.* Structure of a 14-3-3 coordinated hexamer of the plant plasma membrane
H⁺ -ATPase by combining X-ray crystallography and electron cryomicroscopy. *Mol Cell* **25**,
427-440, doi:10.1016/j.molcel.2006.12.017 (2007).
- 84 Rose, R. *et al.* Identification and structure of small-molecule stabilizers of 14-3-3 protein-
protein interactions. *Angew Chem Int Ed Engl* **49**, 4129-4132, doi:10.1002/anie.200907203
(2010).
- 85 Ward, G. A. *et al.* ASTX660, a Novel Non-peptidomimetic Antagonist of cIAP1/2 and XIAP,
Potently Induces TNFalpha-Dependent Apoptosis in Cancer Cell Lines and Inhibits Tumor
Growth. *Mol Cancer Ther* **17**, 1381-1391, doi:10.1158/1535-7163.MCT-17-0848 (2018).
- 86 Flynn, D. C. Adaptor proteins. *Oncogene* **20**, 6270-6272 (2001).
- 87 Tzivion, G. & Avruch, J. 14-3-3 proteins: active cofactors in cellular regulation by
serine/threonine phosphorylation. *J Biol Chem* **277**, 3061-3064, doi:10.1074/jbc.R100059200
(2002).
- 88 Moore, B. W. Specific acidic proteins of the nervous system. *Physiological and Biochemical
Aspects of Nervous Integration.*, 343-359 (1967).
- 89 Aitken, A. 14-3-3 proteins: a historic overview. *Semin Cancer Biol* **16**, 162-172,
doi:10.1016/j.semcancer.2006.03.005 (2006).
- 90 Obsil, T., Ghirlando, R., Klein, D. C., Ganguly, S. & Dyda, F. Crystal Structure of the 14-3-
3 ζ :Serotonin N-Acetyltransferase Complex. *Cell* **105**, 257-267, doi:10.1016/S0092-
8674(01)00316-6 (2001).
- 91 Fantl, W. J. *et al.* Activation of Raf-1 by 14-3-3 proteins. *Nature* **371**, 612-614,
doi:10.1038/371612a0 (1994).
- 92 Obsilova, V. *et al.* 14-3-3 Protein interacts with nuclear localization sequence of forkhead
transcription factor FoxO4. *Biochemistry* **44**, 11608-11617, doi:10.1021/bi050618r (2005).
- 93 Sluchanko, N. N. & Gusev, N. B. 14-3-3 Proteins and regulation of cytoskeleton. *Biochemistry
(Moscow)* **75**, 1528-1546, doi:10.1134/S0006297910130031 (2011).
- 94 Mackintosh, C. Dynamic interactions between 14-3-3 proteins and phosphoproteins regulate
diverse cellular processes. *Biochem J* **381**, 329-342, doi:10.1042/BJ20031332 (2004).
- 95 Gardino, A. K. & Yaffe, M. B. 14-3-3 proteins as signaling integration points for cell cycle control
and apoptosis. *Semin Cell Dev Biol* **22**, 688-695, doi:10.1016/j.semcdb.2011.09.008 (2011).
- 96 Hermeking, H. & Benzinger, A. 14-3-3 proteins in cell cycle regulation. *Seminars in Cancer
Biology* **16**, 183-192, doi:10.1016/j.semcancer.2006.03.002 (2006).
- 97 Johnson, C. *et al.* Visualization and biochemical analyses of the emerging mammalian 14-3-3-
phosphoproteome. *Mol Cell Proteomics* **10**, M110 005751, doi:10.1074/mcp.M110.005751
(2011).
- 98 Zhao, J., Meyerkord, C. L., Du, Y., Khuri, F. R. & Fu, H. 14-3-3 proteins as potential therapeutic
targets. *Semin Cell Dev Biol* **22**, 705-712, doi:10.1016/j.semcdb.2011.09.012 (2011).
- 99 Layfield, R. *et al.* Neurofibrillary tangles of Alzheimer's disease brains contain 14-3-3 proteins.
Neurosci Lett **209**, 57-60, doi:10.1016/0304-3940(96)12598-2 (1996).
- 100 Kawamoto, Y. *et al.* 14-3-3 proteins in Lewy bodies in Parkinson disease and diffuse Lewy body
disease brains. *J Neuropathol Exp Neurol* **61**, 245-253, doi:10.1093/jnen/61.3.245 (2002).
- 101 Hermeking, H. The 14-3-3 cancer connection. *Nature Reviews Cancer* **3**, 931-943,
doi:10.1038/nrc1230 (2003).

- 102 Liu, D. *et al.* Crystal structure of the zeta isoform of the 14-3-3 protein. *Nature* **376**, 191-194,
doi:10.1038/376191a0 (1995).
- 103 Obsil, T. & Obsilova, V. Structural basis of 14-3-3 protein functions. *Semin Cell Dev Biol* **22**,
663-672, doi:10.1016/j.semcdb.2011.09.001 (2011).
- 104 Gardino, A. K., Smerdon, S. J. & Yaffe, M. B. Structural determinants of 14-3-3 binding
specificities and regulation of subcellular localization of 14-3-3-ligand complexes: a comparison
of the X-ray crystal structures of all human 14-3-3 isoforms. *Semin Cancer Biol* **16**, 173-182,
doi:10.1016/j.semcancer.2006.03.007 (2006).
- 105 Muslin, A. J., Tanner, J. W., Allen, P. M. & Shaw, A. S. Interaction of 14-3-3 with Signaling
Proteins Is Mediated by the Recognition of Phosphoserine. *Cell* **84**, 889-897,
doi:10.1016/S0092-8674(00)81067-3 (1996).
- 106 Yaffe, M. B. *et al.* The structural basis for 14-3-3:phosphopeptide binding specificity. *Cell* **91**,
961-971, doi:http://doi.org/10.1016/S0092-8674(00)80487-0 (1997).
- 107 Stevers, L. M. *et al.* Modulators of 14-3-3 Protein-Protein Interactions. *J Med Chem* **61**, 3755-
3778, doi:10.1021/acs.jmedchem.7b00574 (2018).
- 108 Sluchanko, N. N. Association of Multiple Phosphorylated Proteins with the 14-3-3 Regulatory
Hubs: Problems and Perspectives. *J Mol Biol* **430**, 20-26, doi:10.1016/j.jmb.2017.11.010
(2018).
- 109 Sluchanko, N. N. & Bustos, D. M. Intrinsic disorder associated with 14-3-3 proteins and their
partners. *Prog Mol Biol Transl Sci* **166**, 19-61, doi:10.1016/bs.pmbts.2019.03.007 (2019).
- 110 Bustos, D. M. & Iglesias, A. A. Intrinsic disorder is a key characteristic in partners that bind 14-
3-3 proteins. *Proteins* **63**, 35-42, doi:10.1002/prot.20888 (2006).
- 111 Kondo, Y. *et al.* Cryo-EM structure of a dimeric B-Raf:14-3-3 complex reveals asymmetry in the
active sites of B-Raf kinases. *Science* **366**, 109-115, doi:10.1126/science.aay0543 (2019).
- 112 Taoka, K. *et al.* 14-3-3 proteins act as intracellular receptors for rice Hd3a florigen. *Nature* **476**,
332-335, doi:10.1038/nature10272 (2011).
- 113 Sluchanko, N. N. *et al.* Structural Basis for the Interaction of a Human Small Heat Shock Protein
with the 14-3-3 Universal Signaling Regulator. *Structure* **25**, 305-316,
doi:10.1016/j.str.2016.12.005 (2017).
- 114 Alblova, M. *et al.* Molecular basis of the 14-3-3 protein-dependent activation of yeast neutral
trehalase Nth1. *Proc Natl Acad Sci U S A*, doi:10.1073/pnas.1714491114 (2017).
- 115 Ballio, A. *et al.* Fusicocin: a New Wilting Toxin produced by *Fusicoccum amygdali* Del. *Nature*
203, 297-297, doi:10.1038/203297a0 (1964).
- 116 Oecking, C., Eckerskorn, C. & Weiler, E. W. The fusicocin receptor of plants is a member of the
14-3-3 superfamily of eukaryotic regulatory proteins. *FEBS Letters* **352**, 163-166,
doi:10.1016/0014-5793(94)00949-x (1994).
- 117 Wurtele, M., Jelich-Ottmann, C., Wittinghofer, A. & Oecking, C. Structural view of a fungal
toxin acting on a 14-3-3 regulatory complex. *EMBO J* **22**, 987-994, doi:10.1093/emboj/cdg104
(2003).
- 118 De Vries-van Leeuwen, I. J. *et al.* Interaction of 14-3-3 proteins with the estrogen receptor alpha
F domain provides a drug target interface. *Proc Natl Acad Sci U S A* **110**, 8894-8899,
doi:10.1073/pnas.1220809110 (2013).
- 119 Stevers, L. M. *et al.* Characterization and small-molecule stabilization of the multisite tandem
binding between 14-3-3 and the R domain of CFTR. *Proc Natl Acad Sci U S A* **113**, E1152-1161,
doi:10.1073/pnas.1516631113 (2016).
- 120 Sassa, T., Tojyo, T. & Munakata, K. Isolation of a new plant growth substance with cytokinin-
like activity. *Nature* **227**, 379, doi:10.1038/227379a0 (1970).
- 121 Ottmann, C. *et al.* A structural rationale for selective stabilization of anti-tumor interactions of
14-3-3 proteins by cotylenin A. *J Mol Biol* **386**, 913-919, doi:10.1016/j.jmb.2009.01.005
(2009).
- 122 Tzivion, G., Luo, Z. & Avruch, J. A dimeric 14-3-3 protein is an essential cofactor for Raf kinase
activity. *Nature* **394**, 88-92, doi:10.1038/27938 (1998).
- 123 Molzan, M. *et al.* Stabilization of physical RAF/14-3-3 interaction by cotylenin A as treatment
strategy for RAS mutant cancers. *ACS Chem Biol* **8**, 1869-1875, doi:10.1021/cb4003464 (2013).
- 124 Richter, A., Rose, R., Hedberg, C., Waldmann, H. & Ottmann, C. An optimised small-molecule
stabiliser of the 14-3-3-PMA2 protein-protein interaction. *Chemistry* **18**, 6520-6527,
doi:10.1002/chem.201103761 (2012).
- 125 Sakiyama, H. *et al.* Regulation of nuclear import/export of carbohydrate response element-
binding protein (ChREBP): interaction of an alpha-helix of ChREBP with the 14-3-3 proteins

- and regulation by phosphorylation. *J Biol Chem* **283**, 24899-24908, doi:10.1074/jbc.M804308200 (2008).
- 126 Andrei, S. A. *et al.* Rationally Designed Semisynthetic Natural Product Analogues for Stabilization of 14-3-3 Protein-Protein Interactions. *Angew Chem Int Ed Engl* **57**, 13470-13474, doi:10.1002/anie.201806584 (2018).
- 127 Bosica, F. *et al.* Design of Drug-Like Protein-Protein Interaction Stabilizers Guided By Chelation-Controlled Bioactive Conformation Stabilization. *Chemistry* **26**, 7131-7139, doi:10.1002/chem.202001608 (2020).
- 128 Milroy, L. G., Grossmann, T. N., Hennig, S., Brunsveld, L. & Ottmann, C. Modulators of protein-protein interactions. *Chem Rev* **114**, 4695-4748, doi:10.1021/cr400698c (2014).
- 129 Valenti, D. *et al.* Set-up and screening of a fragment library targeting the 14-3-3 protein interface. *Medchemcomm* **10**, 1796-1802, doi:10.1039/c9md00215d (2019).
- 130 Guillory, X. *et al.* Fragment-based Differential Targeting of PPI Stabilizer Interfaces. *J Med Chem* **63**, 6694-6707, doi:10.1021/acs.jmedchem.9b01942 (2020).
- 131 Sijbesma, E. *et al.* Site-Directed Fragment-Based Screening for the Discovery of Protein-Protein Interaction Stabilizers. *J Am Chem Soc* **141**, 3524-3531, doi:10.1021/jacs.8b11658 (2019).
- 132 Wolter, M. *et al.* Fragment-Based Stabilizers of Protein-Protein Interactions through Imine-Based Tethering. *Angew Chem Int Ed Engl*, doi:10.1002/anie.202008585 (2020).
- 133 Jin, J. *et al.* SCFbeta-TRCP links Chk1 signaling to degradation of the Cdc25A protein phosphatase. *Genes Dev* **17**, 3062-3074, doi:10.1101/gad.1157503 (2003).
- 134 Kasahara, K. *et al.* 14-3-3gamma mediates Cdc25A proteolysis to block premature mitotic entry after DNA damage. *EMBO J* **29**, 2802-2812, doi:10.1038/emboj.2010.157 (2010).
- 135 Wang, B. *et al.* 14-3-3Tau regulates ubiquitin-independent proteasomal degradation of p21, a novel mechanism of p21 downregulation in breast cancer. *Mol Cell Biol* **30**, 1508-1527, doi:10.1128/MCB.01335-09 (2010).
- 136 Mizuno, E., Kitamura, N. & Komada, M. 14-3-3-dependent inhibition of the deubiquitinating activity of UBPY and its cancellation in the M phase. *Exp Cell Res* **313**, 3624-3634, doi:10.1016/j.yexcr.2007.07.028 (2007).
- 137 Centorrino, F., Ballone, A., Wolter, M. & Ottmann, C. Biophysical and structural insight into the USP8/14-3-3 interaction. *FEBS Lett* **592**, 1211-1220, doi:10.1002/1873-3468.13017 (2018).
- 138 Reincke, M. *et al.* Mutations in the deubiquitinase gene USP8 cause Cushing's disease. *Nat Genet* **47**, 31-38, doi:10.1038/ng.3166 (2015).
- 139 Pocaterra, A., Romani, P. & Dupont, S. YAP/TAZ functions and their regulation at a glance. *J Cell Sci* **133**, doi:10.1242/jcs.230425 (2020).
- 140 Meng, Z., Moroishi, T. & Guan, K. L. Mechanisms of Hippo pathway regulation. *Genes Dev* **30**, 1-17, doi:10.1101/gad.274027.115 (2016).
- 141 Zhao, B., Li, L., Tumaneng, K., Wang, C. Y. & Guan, K. L. A coordinated phosphorylation by Lats and CK1 regulates YAP stability through SCF(beta-TRCP). *Genes Dev* **24**, 72-85, doi:10.1101/gad.1843810 (2010).
- 142 Dar, A., Wu, D., Lee, N., Shibata, E. & Dutta, A. 14-3-3 proteins play a role in the cell cycle by shielding cdt2 from ubiquitin-mediated degradation. *Mol Cell Biol* **34**, 4049-4061, doi:10.1128/MCB.00838-14 (2014).
- 143 Carter, M. E. & Brunet, A. FOXO transcription factors. *Curr Biol* **17**, R113-114, doi:10.1016/j.cub.2007.01.008 (2007).
- 144 Tzivion, G., Dobson, M. & Ramakrishnan, G. FoxO transcription factors; Regulation by AKT and 14-3-3 proteins. *Biochim Biophys Acta* **1813**, 1938-1945, doi:10.1016/j.bbamcr.2011.06.002 (2011).
- 145 Dobson, M. *et al.* Bimodal regulation of FoxO3 by AKT and 14-3-3. *Biochim Biophys Acta* **1813**, 1453-1464, doi:10.1016/j.bbamcr.2011.05.001 (2011).
- 146 Wang, X. *et al.* Down-regulation of B cell receptor signaling by hematopoietic progenitor kinase 1 (HPK1)-mediated phosphorylation and ubiquitination of activated B cell linker protein (BLNK). *J Biol Chem* **287**, 11037-11048, doi:10.1074/jbc.M111.310946 (2012).
- 147 Wang, X. *et al.* Attenuation of T cell receptor signaling by serine phosphorylation-mediated lysine 30 ubiquitination of SLP-76 protein. *J Biol Chem* **287**, 34091-34100, doi:10.1074/jbc.M112.371062 (2012).
- 148 Mohammad, D. K., Nore, B. F. & Smith, C. I. E. Terminating B cell receptor signaling. *Oncotarget* **8**, 109857-109858, doi:10.18632/oncotarget.22986 (2017).
- 149 Mohammad, D. K. *et al.* Dual phosphorylation of Btk by Akt/protein kinase b provides docking for 14-3-3zeta, regulates shuttling, and attenuates both tonic and induced signaling in B cells. *Mol Cell Biol* **33**, 3214-3226, doi:10.1128/MCB.00247-13 (2013).

- 150 Lasserre, R. *et al.* Release of serine/threonine-phosphorylated adaptors from signaling microclusters down-regulates T cell activation. *J Cell Biol* **195**, 839-853, doi:10.1083/jcb.201103105 (2011).

Chapter 2

A Biophysical and Structural Analysis of the Interaction of BLNK with 14-3-3 Proteins

Abstract

B-cell linker protein (BLNK) is an adaptor protein that orchestrates signalling downstream of B-cell receptors. It has been reported to undergo proteasomal degradation upon binding to 14-3-3 proteins. Here, we report the first biophysical and structural study of this protein-protein interaction (PPI). Specifically, we investigated the binding of mono- and di-phosphorylated BLNK peptides to 14-3-3 using fluorescent polarization (FP) and isothermal titration calorimetry assays (ITC). Our results suggest that BLNK interacts with 14-3-3 according to the gatekeeper model, where HPK1 mediated phosphorylation of Thr152 (pT152) allows BLNK anchoring to 14-3-3, and an additional phosphorylation of Ser285 (pS285) by AKT, then further improves the affinity. We have also solved a crystal structure of the BLNKpT152 peptide bound to 14-3-3 σ . Finally, we test the binding of four recombinant, phosphorylated BLNK protein constructs to 14-3-3 proteins. These constructs could serve as important tool for compound discovery programs aiming to modulate the interaction with 14-3-3, or other BLNK binding partners.

Part of this work has been published as: **Soini, L.**, Leysen, S., Davis, J. & Ottmann, C. A biophysical and structural analysis of the interaction of BLNK with 14-3-3 proteins. *J Struct Biol* **212**, 107662.

2.1 Introduction

B-cell linker protein, also known as BLNK, is a 50 kDa adaptor protein expressed in B-cells. It is composed of three different regions: a N-terminal acidic region, a central proline rich domain (mostly disordered) and a C-terminal SH2 domain ¹. Following antigen mediated B-cell receptor (BCR) stimulation, BLNK is phosphorylated by protein tyrosine kinases (PTKs), and then recruited to the cell membrane where it orchestrates and activates a subset of proteins e.g. GRB2, VAV, BTK, NCK, PLC γ 2 and HPK1 via formation of a multimolecular complex ^{2,3}. The formation of this protein complex stimulates downstream effectors such as the nuclear factors NF- κ B and NFAT ^{4,5}, and is crucial for Ca²⁺ flux regulation ⁶⁻⁸ and cytoskeleton reorganization ⁹.

Importantly, a negative feedback regulation mechanism attenuates BCR signalling through HPK1 induced phosphorylation of BLNK residue Thr152 ¹⁰. Hematopoietic progenitor kinase 1 (HPK1) is a Ste20-like serine/threonine kinase that is activated upon antigen stimulation of BCRs ¹¹⁻¹³. HPK1 downregulation leads to an increase in the immune response of antigen immunized mice, making them prone to develop autoimmune diseases ^{14,15}. Also, downregulation of HPK1 is linked to the human autoimmune disease lupus erythematosus ¹⁶. Wang et al. showed that the HPK1 induced phosphorylation of BLNK at Thr152 induced its association with 14-3-3, leading to BLNK ubiquitination by an as yet unidentified E3 ligase, and subsequent proteolytic degradation ¹⁰. Mohammad et al. suggested that phosphorylation at Ser285 by AKT could also contribute to the interaction of BLNK with 14-3-3 ¹⁷.

14-3-3 proteins are a family present in all eukaryotic cells. Humans have seven highly conserved isoforms named: β , γ , ϵ , ζ , η , σ , τ ^{18,19}. They are adaptor proteins that perform important biological roles within cells, one of which is either to mask or expose ubiquitination sites ^{10,20,21}. 14-3-3 are highly helical, dimeric proteins that contain two symmetrical amphipathic binding grooves, which accommodate mostly Ser/Thr-phosphorylated binding motifs of their partner proteins ^{18,22}. The presence of two or more cooperative Ser/Thr interaction sites on a 14-3-3 target protein, is a well-established concept, commonly described as the “gatekeeper model” ^{23,24}. When multiple sites situated on the same polypeptide chain, bind individually to 14-3-3 it is usually possible to distinguish a high affinity (“gatekeeper”) and a low affinity site, with the latter often too weak to establish contact with 14-3-3 by itself. However, when the two sites bind simultaneously, after the gatekeeper has provided the anchor point, the weak site is able to interact with the second 14-3-3 monomeric unit, thereby enhancing the binding affinity dramatically ²⁵. The presence on BLNK of two potential 14-3-3 interaction sites therefore makes a detailed study of its binding mechanisms important to understand BLNK signalling pathways downstream of the BCR.

In this work, we probe the presence of a gatekeeper model between 14-3-3 and synthetic mono- and di- phosphorylated BLNK peptides, using a combination of structural and biophysical characterization techniques. In addition, we studied the interaction of BLNK with two 14-3-3 isoforms using four recombinant BLNK protein constructs.

2.2 Results and Discussion

2.2.1 Thr152 is the gatekeeper controlling the interaction of BLNK with 14-3-3

Since production of recombinant proteins with site specific phosphorylation can be challenging, a successful approach to facilitate investigations of 14-3-3 PPI, is to use synthetic phosphorylated peptides that represent the partner protein's 14-3-3 binding motif ²⁶.

The BLNKpT152 peptide was designed starting from the native BLNK protein sequence. A total length of 12 amino acid residues was chosen to mimic the 14-3-3 anchor point: ARLTSpT152LPALTA (Figure 2.1a). The peptide was synthesized and purified in an acetylated N-terminal version and in a FITC-labelled N-terminal version for ITC and FP measurements respectively. To prove that the peptide is indeed a 14-3-3 binder, a FP ligand binding assay was performed against all 7 human 14-3-3 full-length isoforms (Figure 2.1b). All 14-3-3 isoforms interact with the BLNKpT152 peptide and showed affinities covering a range between 1 and 40 μ M, ranked in the following order (strongest to weakest): $\gamma > \eta > \beta > \zeta > \epsilon > \tau > \sigma$. This only partially corresponded with the trend previously reported in literature: $\gamma > \tau > \eta > \epsilon > \beta > \sigma > \zeta$ ¹⁰. The comparison of both trends, however, must be done cautiously considering they were obtained using very different techniques (i.e. BLNKpT152 peptide in FP/ITC vs cellular BLNK in GST pulldown assays). Still, both trends agreed with 14-3-3 γ as the isoform with the highest affinity. 14-3-3 γ was consequently used for all the following comparative studies, giving more practical assay conditions to work with. To further validate the assay, a dose-response inhibition was performed on the 14-3-3 γ /BLNKpT152 system exploiting the known 14-3-3 inhibitor R18 ²⁷ (Figure S 2.1a). A progressive drop in polarization values, proportional to the increase in R18 concentration, was observed. This confirms BLNKpT152 specificity for the 14-3-3 binding sites. In addition, a direct ITC binding assay was performed to orthogonally confirm binding of the BLNKpT152 peptide to the γ (Figure 2.2), ζ (Figure S 2.2) and σ (Figure S 2.2) 14-3-3 isoforms. The binding ranking between the 14-3-3 isoforms was also confirmed by ITC: $\gamma > \zeta > \sigma$ (Figure 2.2), (Figure S 2.2).

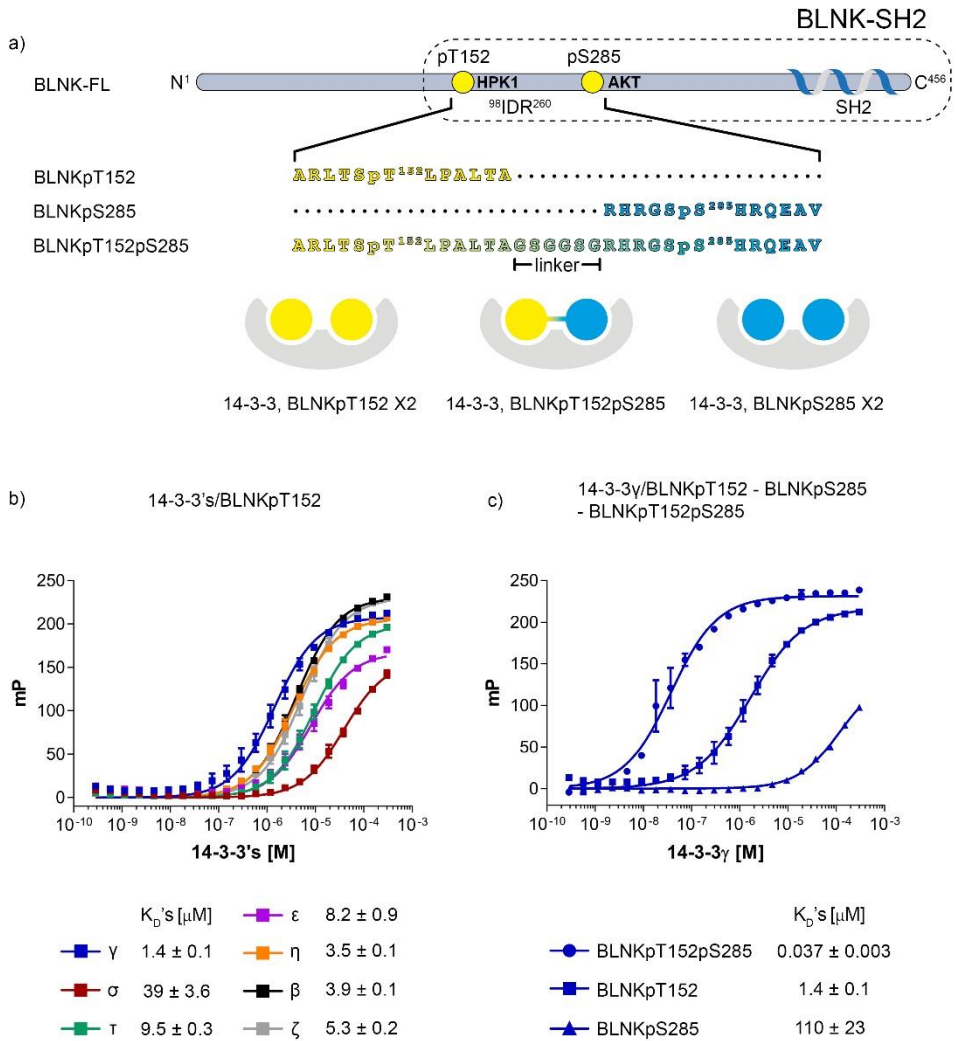


Figure 2.1| Fluorescence polarization binding of the BLNK peptides (BLNKpT152, BLNKpS285 and BLNKpT152pS185) to 14-3-3 proteins. a) Representation of BLNK protein. Sequences of the peptides used in this study, and cartoon representation of the gate-keeper model. b) FP assay of all 14-3-3 isoforms binding to BLNKpT152. K_D values are reported with their standard error. c) FP assay showing the binding curves of the peptides BLNKpT152, BLNKpS285 and BLNKpT152pS185 binding to 14-3-3γ. K_D values are reported with their standard error.

To investigate the hypothesis that BLNK and 14-3-3 interact via the gatekeeper model, two more peptides were designed and obtained in N-terminal FITC-labelled and acetylated versions: BLNKpS285 and BLNKpT152pS285. Like the BLNKpT152 peptide, BLNKpS285 is 12 residues long:

RHRGSpS285HRQEAV (Figure 2.1a). The BLNKpT152pS285 peptide contains the BLNKpT152 and BLNKpS285 peptides sequences linked by an artificial GSGGSG linker: ARLTSpT152LPALTAGSGGSGRHRGSpS285HRQEAV (Fig. 1a). The binding to 14-3-3 of the BLNKpS285 and the BLNKpT152pS285 peptides was tested in an FP ligand binding assay against the 14-3-3 γ isoform (Figure 2.1c). The binding to the other 14-3-3 isoforms was also tested (Figure S 2.3). The peptides are ranked according to their affinity to 14-3-3 γ (strongest to weakest): BLNKpT152pS285 > BLNKpT152 > BLNKpS285. The data suggest that the BLNKpS285 is the weak site (its K_D can only be approximated) and BLNKpT152 is the gatekeeper site. When the two sites are combined in a single, double-phosphorylated peptide, BLNKpT152pS285, the affinity increased 37-fold compared to BLNKpT152 alone, and 110-fold, compared to BLNKpS285. The data from the BLNKpT152pS285 peptide were analysed using a one-site and two-site model. As expected, a two-site binding model is a better fit for the doubly phosphorylated peptide, supporting two distinct binding events with estimated K_D high and low values of 28 nM (\pm 3.5 nM) and 1.9 μ M (\pm 2.1 μ M) respectively (Figure S 2.1b). However, for illustrative purposes we include results from all 3 peptides using a one-site model to enable an easy comparison of the data which shows a left-shift of binding curve for BLNKpT152pS285 with an apparent K_D of 37 nM (\pm 3.3 nM) (Figure 2.1c).

The binding was orthogonally confirmed performing a direct ITC binding assay of the peptides against 14-3-3 γ (Figure 2.2). The K_D 's derived by ITC were highly consistent with the FP data confirming the affinity ranking of the three peptides to 14-3-3 γ : BLNKpT152pS285 > BLNKpT152 > BLNKpS285. The estimated K_D values are 27 nM (\pm 6.7 nM), 1.5 μ M (\pm 19 nM) and 39.7 μ M (\pm 6.69 μ M) respectively (Figure 2.2).

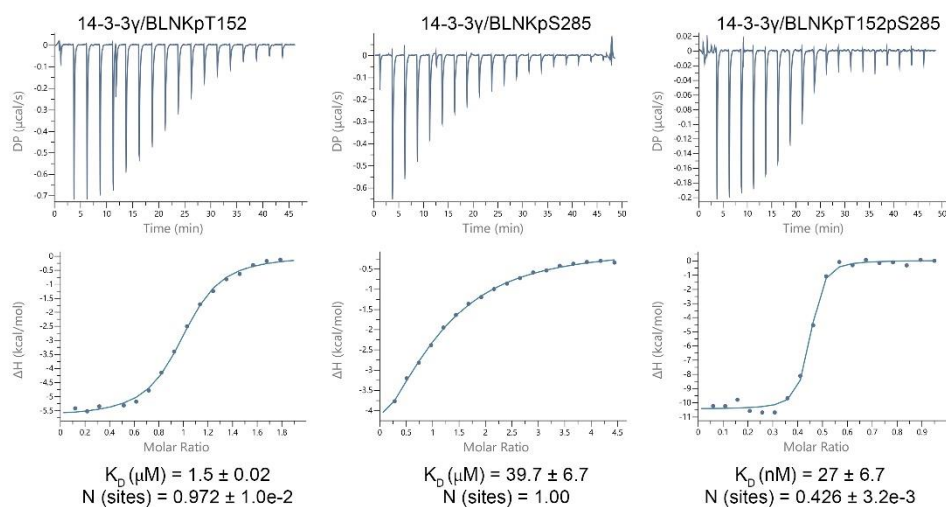


Figure 2.2| Isothermal titration calorimetry binding of the BLNK peptides (BLNKpT152, BLNKpS285 and BLNKpT152pS185) to 14-3-3 proteins. ITC measurements for binding of

peptides BLNKpT152, BLNKpS285 and BLNKpT152pS185 to 14-3-3 γ . K_D values are reported with their standard error.

Additionally, it can be noticed that in the mono-phosphorylated cases the stoichiometry is close to 1, where in the di-phosphorylated case the stoichiometry is close to 0.5. When the stoichiometry is 1, two identical copies of mono-phosphorylated peptides occupy two identical grooves on one 14-3-3 dimer. When the stoichiometry is 0.5, one copy of di-phosphorylated peptide occupies two grooves on one 14-3-3 dimer, one for each site. This observation strongly suggests that the weak site pS285 is responsible for the increase in affinity of the BLNKpT152pS285 and that the two phospho-residues engage the 14-3-3 dimer binding grooves simultaneously (Figure 2.1a).

2.2.2 Crystal structure of the 14-3-3 σ /BLNKpT152 complex

To structurally elucidate the binding between 14-3-3 and the BLNKpT152 peptide, X-ray protein crystallography was applied. 14-3-3 σ was used since this isoform is known to readily produce high-resolution diffracting crystals. Furthermore, 14-3-3 isoforms are highly conserved in the amphipathic binding groove responsible for the interaction with partner proteins.

The crystals diffracted to a resolution of 1.88 Å and the structure was solved by molecular replacement using the structure of 14-3-3 σ in complex with the YAppS127 peptide (PDB ID: 3MHR) ²⁸. All data collection and refinement statistics are reported in (Table S 2.1). 14-3-3 σ crystallised in the typical space group C2221, with one monomer present in the asymmetric unit (ASU) (Figure 2.3a). The BLNKpT152 peptide could be modelled within the 14-3-3 σ amphipathic binding groove with clear electron density for 8 of its 12 amino acids (Figure 2.3b). The binding of BLNKpT152 in the 14-3-3 binding groove is consistent with other 14-3-3 σ /phospho-peptide structures deposited in the PDB. Some examples are the complexes 14-3-3 σ /LRRK2pS910 (PDB ID: 5MYC) ²⁹, 14-3-3 σ /p53pT387 (PDB ID: 5MHC) ³⁰, 14-3-3 σ /YAppS127 (PDB ID: 3MHR) ²⁸ and 14-3-3 σ /PADI6pS446 (PDB ID: 4DAT) ³¹. The crucial anchor points of the peptide to 14-3-3 is provided by the residues buried in the 14-3-3 binding groove (Figure 2.3c): Lys49, Arg56, Tyr130 and Arg129 which interact via polar bonds with pThr152 on the peptide. Polar bonds are also provided by Lys122, Asn175 and Glu182 of 14-3-3 that bind the far ends of BLNKpT152 at Pro154, Ser151, Thr150 and Arg148 respectively. Additional hydrophobic contacts are generated on the upper part of the amphipathic binding groove by the residues Ile219, Leu222 and Leu229 of 14-3-3 with Leu153 and Leu159 of BLNKpT152 respectively (Figure 2.3c). The combination of biophysical assays and X-ray crystallography establish the BLNKpT152 peptide as a 14-3-3 binder.

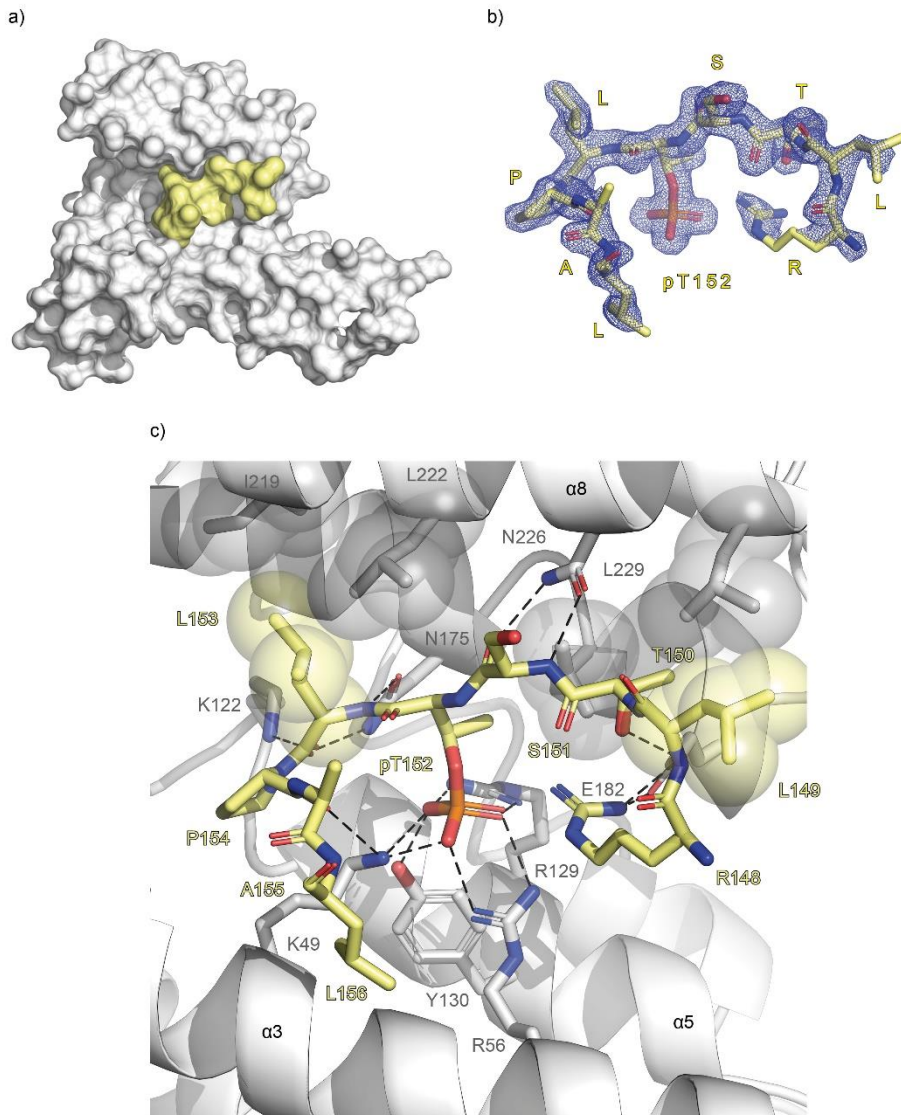


Figure 2.3 | Crystal structure of the 14-3-3 σ /BLNKpT152 binary complex at a 1.88 Å resolution. a) Surface representation of the ASU of the 14-3-3 σ /BLNKpT152 crystal structure. The 14-3-3 σ monomer and the BLNKpT152 peptide are displayed in grey and yellow surfaces, respectively. b) 2F_o-F_c refined map contoured at $\sigma=1$ of the BLNKpT152 peptide. Interpretable residues are highlighted in yellow cases. c) Representation of the BLNKpT152 peptide (yellow sticks) bound to the 14-3-3 σ amphipathic groove (grey cartoon). Polar contacts are represented as black dotted lines and hydrophobic contacts are represented with semi-transparent spheres contoured around the residue side chains.

Crystallisation of the binary complexes 14-3-3 σ /BLNKpS285 and 14-3-3 γ /BLNKpT152pS285 was attempted, but we were unable to obtain crystals that diffracted well.

2.2.3 Exploring the 14-3-3/BLNK PPI using four BLNK protein constructs

In order to study 14-3-3 PPIs, a practical and accepted approach is to mimic 14-3-3 binding partners using short synthetic phosphorylated peptides (more than 100 structures are deposited in the PDB). This approach greatly simplifies generation of reagents, allowing the use of highly sample consuming characterisation techniques like X-ray protein crystallography and ITC. On one hand this has provided a large structural information pool on 14-3-3 and its many binding partners, on the other hand the characterisation of more complex systems involving full-length or truncated protein constructs is far behind ³². More complete systems are needed for a better understanding of 14-3-3 biology and to more faithfully reproduce interactions within the cells. This is also crucial in drug discovery, where working with short synthetic peptides to represent the 14-3-3 binding partner instead of the full-length protein carries two risks. First, one could miss potential druggable sites when searching for inhibitors or stabilisers of the targeted PPI. Vice versa, while working with peptides one might risk targeting a site which could be absent in the context of the full-length protein.

We therefore produced larger protein constructs of BLNK, to study its interaction with 14-3-3 on a protein level as well. A full-length protein version of BLNK (BLNK-FL) has been expressed and purified, and subsequently phosphorylated *in vitro* using HPK1. This kinase has been reported to phosphorylate Thr152 on BLNK ¹⁰ (Figure S 2.4a). To confirm whether the phosphorylation is required for the binding to 14-3-3 at the protein level, BLNK-FL has been incubated with 14-3-3 ζ in its phosphorylated form (pBLNK-FL) and in its non-phosphorylated form (BLNK-FL) (Figure 2.4a). The two samples have then been loaded on an analytical size exclusion column. A superposition of the two elution profiles showed a left shift towards a higher molecular mass when mixing 14-3-3 ζ with pBLNK-FL, suggesting the formation of a complex when BLNK is phosphorylated. Fractions of the elution peaks were collected and analysed by SDS/PAGE, confirming the formation of a 14-3-3 ζ /pBLNK-FL complex and not of the 14-3-3 ζ /BLNK-FL one (Figure 2.4c). Native mass spectrometry confirmed the formation of a complex in the presence of the phosphorylation. The mass of the complex suggests it consists of one 14-3-3 dimer bound to one copy of pBLNK-FL (Figure 2.4b).

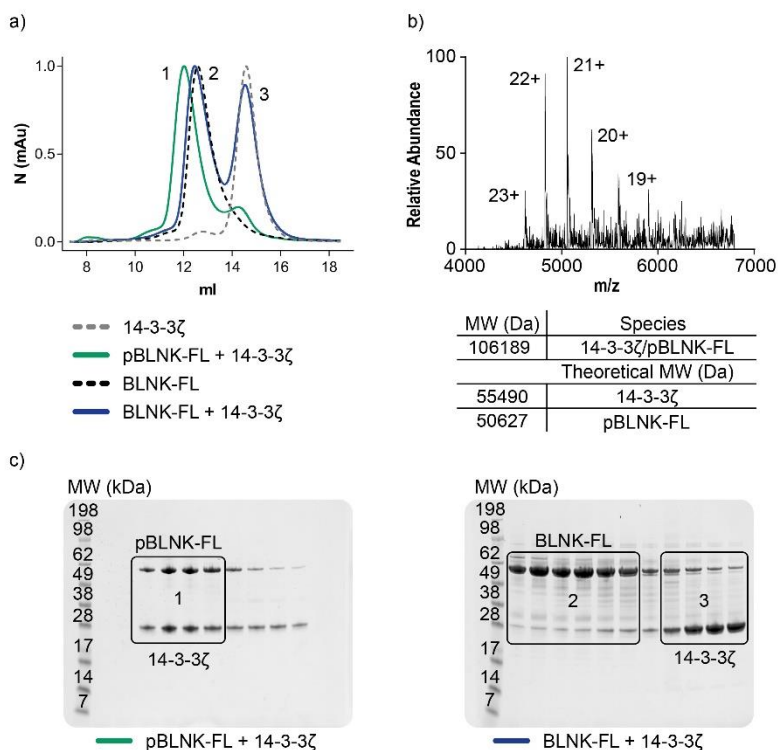


Figure 2.4 | Binding of the pBLNK-FL construct to 14-3-3 proteins. a) Size exclusion chromatograms superposition of the samples: 14-3-3ζ/BLNK-FL and 14-3-3ζ/pBLNK-FL. The mAU intensity has been normalized. The elution profile of the single proteins has also been reported for comparison. b) Native mass spectrometry spectrum of the 14-3-3ζ/pBLNK-FL complex. The experimental calculated molecular weight of the complex is reported on the graph and below the theoretical molecular weight of the single components as reference. c) SDS-PAGE analysis for the size-exclusion profiles of the BLNK-FL/14-3-3ζ and pBLNK-FL/14-3-3ζ mixtures. The content of peak 1 shows band attributable to 14-3-3ζ and pBLNK-FL of equal intensity confirming the presence of a complex. The content of peaks 2 and 3 show bands attributable to BLNK-FL and 14-3-3ζ respectively, eluted at two different elution volumes.

A second full-length construct was expressed and purified with a T152E mutation: BLNK-E (Figure 2.5a). The implementation of glutamic or aspartic acid is sometimes used to mimic the highly negatively charged phosphate group of a phosphorylated serine or threonine³³⁻³⁵. We have chosen the glutamic acid because it better mimics also the length of a phosphorylated threonine or serine. The binding to 14-3-3 of this construct has been tested with SEC (size exclusion chromatography) and ITC. For the SEC experiment the proteins were pre-incubated and mixed in a 1:1 stoichiometric ratio and consequently loaded onto a SEC column. The single components 14-3-3ζ and BLNK-E were loaded separately as controls. An additional control sample composed of a mixture of wild type BLNK-FL and 14-3-3ζ was also added (Figure 2.5b). From these SEC profiles it appears that no complex formation happened between the

phosphomimetic construct BLNK-E and 14-3-3. This was confirmed after having tested the system in an isothermal titration calorimetry assay (Figure 2.5c).

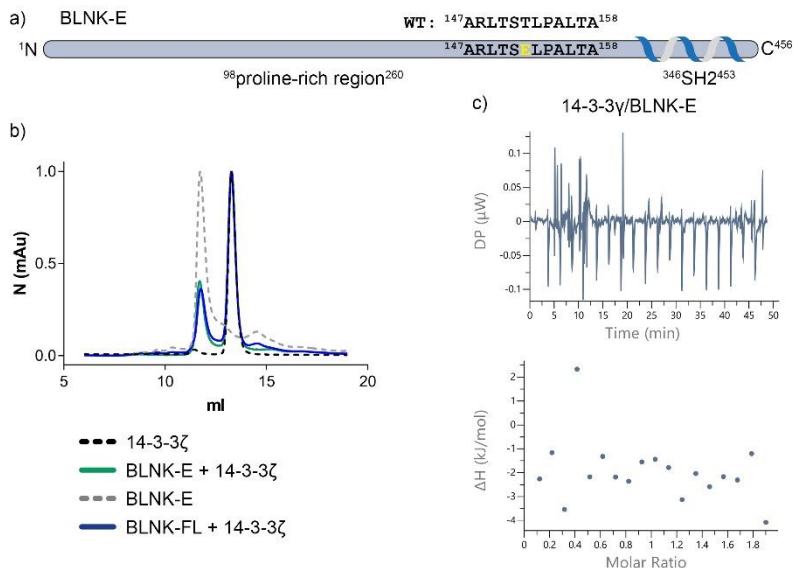


Figure 2.5 | Analysis of the BLNK-E construct. a) Cartoon representation of the mutated BLNK phosphomimetic construct: T152E. The mutation is highlighted with yellow letters. WT: wild type. b) Superposition of size exclusion profiles of 14-3-3ζ, BLNK-FL, BLNK-E and their mixtures. The elution volumes of the single proteins taken as a reference superpose exactly to the protein mixtures suggesting that no 14-3-3ζ/BLNK-E complex has formed. c) ITC experiment of 14-3-3γ titrated on BLNK-E. The assay shows very little heat formation attributable to the titration and no binding curve, confirming that no interaction occurs between 14-3-3 proteins and BLNK-E.

These observations strengthen the already widely accepted concept of how important phosphorylation is to engage 14-3-3 proteins. The binding cannot be rescued by the use of phosphomimetics even when dealing with full-length protein constructs³²⁻³⁶. In the BLNK case the phosphorylation of Thr152 has proven to be essential for the binding.

The third construct, BLNK-PKA, was expressed together with the kinase PKA. The BLNK-PKA construct was mutated in order to be recognized by the kinase PKA, which is supposed to promptly phosphorylate the substrate in the expression phase. The same workflow of experiments was applied to the BLNK construct designed for the PKA co-expression (Figure 2.6a). The phosphorylation of the BLNK-PKA construct was checked by mass spectrometry, of which the deconvolution spectra are shown in (Figure S 2.4b). The molecular mass of the wild type construct is also reported and has been used to calculate the number of phosphorylation events. Species with two and four phosphorylations were identified for BLNK-PKA. Phosphorylation site mapping experiments would be necessary for the identification of the precise location of these phosphorylations. However, such experiment was considered

to be beyond the scope of this work. From the SEC profiles it is clear that a left shift of the sample containing the mixture of 14-3-3 ζ and BLNK-PKA occurred (Figure 2.6b). The left shift can be compared with the superposition of the single proteins taken as a control: 14-3-3 ζ and BLNK-PKA. If the proteins had not interacted with each other, the two peaks of the green profile would have been perfectly superimposable (Figure 2.6b). This experiment suggested that indeed a complex has formed between 14-3-3 ζ and BLNK-PKA. The isothermal titration calorimetry experiment confirmed this observation, as binding curves were generated upon titration of 14-3-3 γ onto BLNK-PKA (Figure 2.6c).

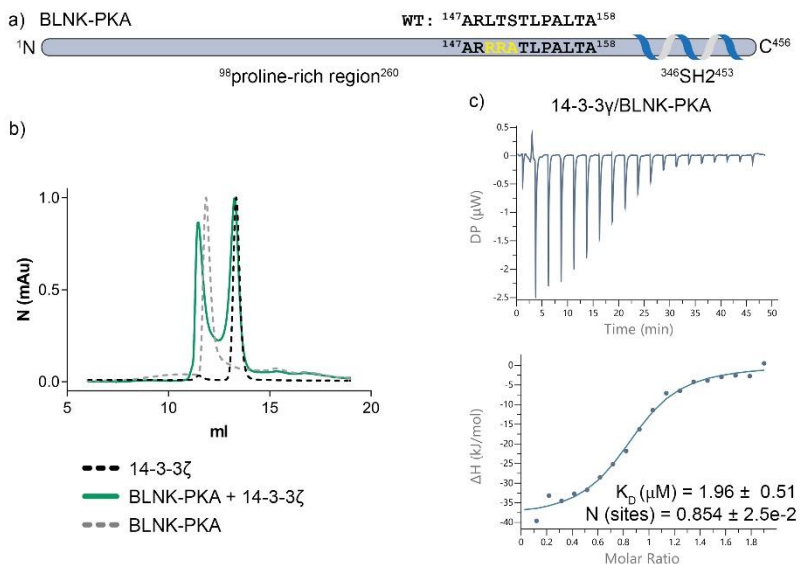


Figure 2.6 | Analysis of the BLNK-PKA construct. a) Cartoon representation of the mutated BLNK-PKA construct: L149R, T150R, S151A. The mutations are highlighted with yellow letters. WT: wild type. b) Superposition of size exclusion profiles of 14-3-3 ζ , BLNK-PKA and their complex. c) ITC experiment of 14-3-3 γ titrated over BLNK-PKA. The assay confirms the binding between 14-3-3 proteins and BLNK-PKA.

The K_D values calculated from the ITC experiment is remarkably close to the ones generated from the ITC experiments performed on the BLNKpT152 peptide. The K_D for the BLNK systems are 1.4 μ M for the 14-3-3 γ /BLNKpT152 system and 1.9 μ M for the 14-3-3 γ /BLNK-PKA system

A shorter construct of BLNK-FL, BLNK-SH2, was also expressed and purified to enable future structural studies or potentially high-throughput screening for modulators of the 14-3-3/BLNK interaction. The rationale behind the truncation was to remove as much disordered regions as possible for structural studies, while keeping the key Thr152 residue for the binding to 14-3-3 as well as the ordered SH2 domain, of which a structure has been deposited in the PDB (2EO6)³⁷. The expression yield of BLNK-SH2 was higher than that of BLNK-FL or BLNK-PKA (50 mg per L BLNK-SH2, 1 mg per L BLNK-

FL/BLNK-PKA), so for HTS it could be a good compromise between using the full-length protein and a short synthetic peptide. The BLNK-SH2 construct could readily be phosphorylated by HPK1 (Figure S 2.4c). ITC measurements confirmed that binding to 14-3-3 γ was only observed when the construct was phosphorylated, with a K_D of 13 μ M (Figure 2.7b). Interestingly, this is ten-fold weaker than the affinity of the pT152 peptide.

The final purification step chromatograms of all the constructs mentioned above are reported in the supporting information along with the SDS-PAGES of the protein peaks content to allow to check the sample quality (Figure S 2.5).

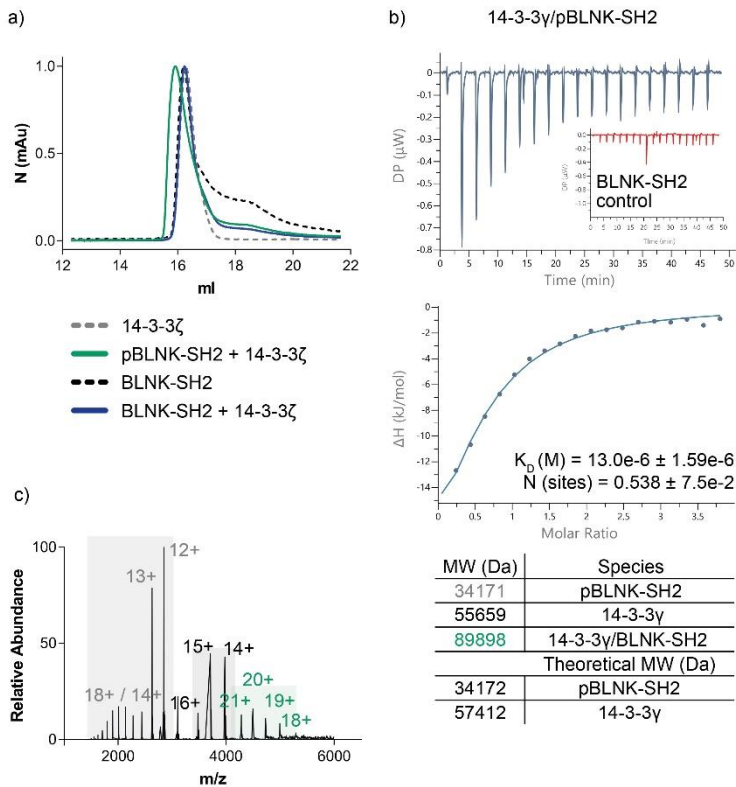


Figure 2.7 | Binding of the pBLNK-SH2 construct to 14-3-3 proteins. a) Size exclusion chromatograms superposition of the samples: 14-3-3 ζ /BLNK-SH2 and 14-3-3 ζ /pBLNK-SH2. The mAu intensity has been normalized. The elution profile of the single proteins has also been reported for comparison. b) ITC direct binding assays of pBLNK-SH2 and BLNK-SH2 to 14-3-3 γ . c) Native mass spectrometry spectrum of the 14-3-3 γ /pBLNK-SH2 complex. The experimental calculated molecular weight of the complex is reported on the graph and below the theoretical molecular weight of the single components as reference.

To investigate the gatekeeper model at a protein level, an *in vitro* phosphorylation using the kinase AKT has been attempted on BLNK-SH2 and pBLNK-SH2. Unfortunately, no phosphorylation on BLNK-SH2 has been detected upon incubation with AKT and ATP in addition to the one already present due to HPK1. It was therefore not possible to determine affinities of BLNK-SH2 to 14-3-3 in the presence of one (pT152 or pS285) or two phosphorylations (both pT152 and pS285). This is illustrative of the difficulty of producing recombinant proteins with multiple, site-specific phosphorylation events, and the reason it is often necessary to resort to shorter synthetic peptides.

2.3 Conclusions and Perspectives

Our findings offer a first insight into the BLNK/14-3-3 PPI from a biophysical and structural standpoint. We observed that phosphorylated pT152 and pS285 provide cooperative binding to 14-3-3 according to the gatekeeper model, where pT152 provides the stronger anchoring interaction, and pS285 can further increase the affinity. The work using four BLNK protein constructs confirmed that the interaction with 14-3-3 indeed occurs in a phosphorylation-dependent manner. The BLNK-FL, BLNK-PKA and BLNK-SH2 can be used for a more in-depth analysis aimed to understand the binding of BLNK to 14-3-3 proteins.

In theory, the 14-3-3/BLNK interaction could be a target for drug discovery as stabilising the interaction is expected to enhance proteolytic BLNK degradation. This should decrease the immune response, a desired effect in the context of many inflammatory and autoimmune conditions. While stabilising protein interactions is not a commonly used approach, it holds great potential in terms of selectivity³⁸, and has been shown to be feasible for 14-3-3 interactions as well as several others^{39,40}. With the generation of an understanding of the binding mechanism, as well as the generation of key reagents, our work has provided a solid basis to start the discovery of small-molecule stabilisers of the 14-3-3/BLNK interaction.

2.4 Material and Methods

Peptide synthesis

The BLNKpT152 peptide was synthesized via Fmoc solid-phase peptide synthesis by an Intavis MultiPep RSi peptide synthesizer exploiting a Rink amide AM resin (Novabiochem, 0.59 mmol/g loading). The acetylated version was acetylated (1:1:3 Ac₂O, Pyridine/NMP) at the N-terminus and the FITC-labelled one was functionalized with Fluorescein Isothiocyanate (FITC, Sigma-Aldrich) after a β -alanine linker introduced via Fmoc chemistry at the N-terminus. BLNKpT152 was purified using a preparative LC-MS system composed by an LCQ Deca XP Max (Thermo Finnigan) ion-trap mass spectrometer, a Surveyor auto sampler, a Surveyor photodiode detector array (PDA) (Thermo Finnigan) and a PrepFC fraction collector (Gilson Inc). Purification column: Waters reverse-phase C18 Atlantis T3 prep OBD, 5 μ M, 150 x 19 mm column in linear gradients of H₂O/CH₃CN/0.1%TFA. The peptides BLNKpS285 and BLNKpT152pS285 were ordered with purity >95% from GenScript.

Protein expression and purification

14-3-3 isoforms FL and Δ C and BLNK-FL, BLNK-E (T152E), BLNK-PKA (L149R, T150R, S151A) and BLNK-SH2 (143-456) were expressed with a (His)₆/(His)₆-SUMO tag in Nico21(DE3) competent cells with a pPROEX-Htb/pCDFDuet-1 vector in 2TY media. The BLNK-PKA construct was transformed together with the vector pACYC encoding for the Protein Kinase A (PKA). The purification was carried out by affinity chromatography on Nickel columns (HisTrap HP, 5 mL). The tags were cleaved with TEV/SUMO hydrolase. The proteins were then loaded again on Nickel columns to remove any uncleaved protein. A final purification step was performed loading the proteins on a size-exclusion chromatography column (HiLoad 26/600 Superdex 75 pg). The BLNK-E and BLNK-PKA were additionally loaded onto a monoS 5/50 GL cation exchange column for an additional purification step. All purification steps were performed on an ÄKTA pure protein purification system (Cytiva).

Fluorescence polarization and isothermal titration calorimetry

FP binding assays were carried out on Corning 384-well 3575 plates, serially diluting (2-fold) 14-3-3 isoforms in the presence of 10 nM FITC-labelled peptides. Proteins and peptides were diluted from their stock concentration in assay buffer (50 mM Tris pH 7.5, 150 mM NaCl, 5mM MgCl₂, 0.05% v/v Tween-20). The data were collected on a PHERAstar FSX plate reader (BMG Labtech) with an λ_{exc} 485 nm, λ_{em} 520 nm FP filter setting. For K_D calculation the background polarization was removed from all values and the data were fitted with a “One site - Specific binding model” and a “Two sites - Specific binding model” on GraphPad Prism version 8.1.1 for Windows, GraphPad Software, La Jolla California USA, www.graphpad.com. Each data point is the average of a triplicate measurement, standard deviation is reported as error bars. ITC measurements were performed on a PEAQ-ITC (Malvern) dissolving the peptides in assay buffer (50 mM Tris pH 7.5, 150 mM NaCl, 5mM MgCl₂, 0.05% v/v Tween-20) and dialysing the protein in the same buffer to minimise buffer mismatch. The optimal peptides and protein concentrations were chosen simulating the experiment on the MicroCal PEAQ-ITC Analysis Software (Malvern) according to the predicted K_D . The peptides were titrated into the cell containing the protein following a series of 18-2 μ L injections at 25 °C (reference power 5 μ cal/sec, stir speeds 750 rpm, initial delay 60 s, spacing 150 s). The data were analysed on the MicroCal PEAQ-ITC Analysis Software (Malvern).

X-ray protein crystallography

For protein crystallisation, a C-terminally truncated version of 14-3-3 σ was used (14-3-3 $\sigma\Delta$ C, Δ C=28 C-terminal AA)²⁸. The binary complex was prepared mixing 14-3-3 $\sigma\Delta$ C 10/12/15 mg/ml and BLNKpT152 at a 1:1 and 1:1.2 ratio and then incubated at 4 °C, O/N (dilution buffer: 20 mM Hepes pH 7.5, 2 mM MgCl₂). The crystallization drops were dispensed in 1:1 protein to crystallisation condition ratio (0.5 μ L + 0.5 μ L). pH over PEG gradients grid crystallisation conditions: 95 mM Hepes pH 7.1-7.7, 24-29% PEG400, 190 mM CaCl₂, Glycerol 5%. The plate was incubated at 4 °C and crystals grew in 5 to 10 days and were observed in most of the crystallisation conditions. The data were collected by harvesting and mounting the crystals on an in-house MicroMax-003 X-ray generator (Rigaku) kept under a constant flux of liquid nitrogen (77 K) and with a wavelength of 1.541 Å. The diffraction pattern was collected using a PILATUS3 R 200K detector (Rigaku). The diffraction data were processed with XDS⁴¹ and AIMLESS^{42,43}.

The structure was solved by molecular replacement using a 14-3-3 ζ structure as search model (PDB ID: 3MHR), with PHASER)^{28,44}. The initial structure was then refined using COOT⁴⁵ and PHENIX⁴⁶. The data collection and refinement statistics of the solved structure are reported in Table S1. The structure is deposited in the PDB with the ID: 6YLU. All figures were generated using PyMOL (The PyMOL Molecular Graphics System, Version 1.2r3pre, Schrödinger, LLC).

Analytical SEC and mass spectrometry

All protein complexes (pBLNK-FL/14-3-3 ζ , BLNK-FL/14-3-3 ζ , BLNK-SH2/14-3-3 ζ , pBLNK-SH2/14-3-3 ζ , BLNK-E/14-3-3 ζ , BLNK-PKA/14-3-3 ζ) were incubated at a 1:1 molar ratio for 2 h at 4°C. The samples were then injected in an ÄCTA pure system on a Superdex 200 10/300 GL column, flow 0.5 ml/min, running buffer 20 mM Hepes pH 7.5, 150 mM NaCl, 2mM DTT. BLNK-FL and BLNK-SH2 were phosphorylated *in vitro* by incubating them O/N at room temperature in their storage buffer supplemented by 0.75 mM ATP, 20 mM MgCl₂ and HPK1 kinase (Thermo Fisher Scientific) in a ratio kinase:protein, 1:3000. Possible phosphorylations were checked by LC-MS. LC-MS experiments were performed on a Waters Acquity UPLC-Xevo G2 ToF LCMS system, operated by MassLynx software. Typically, 5 μ L of protein solution concentrated approximately 1 mg/mL was injected in reverse phase UPLC system using the following conditions: Waters Acquity UPLC BEH300 C4, 2.1 x 100mm, 1.7 μ M particle size analytical column; Solvent A: 0.1% HCOOH in H₂O, Solvent B: 0.1% HCOOH in CH₃CN; flow rate 0.3 mL/min; gradient: 0 min, 5% B; 5 min, 60% B; 6 min, 95% B. Mass spectrometry data were collected over the m/z range 100-5000 Th, with a scan rate of 0.5 seconds. The mass spectrometer was calibrated over this mass range using NaI clusters. Native MS experiment was run on the 14-3-3 ζ /pBLNK-FL complex on a Thermo Fisher Exactive Plus EMR MS fitted with an Advion Nanomate chip-based nanoESI instrument for sample introduction. Prior to analysis, protein sample was buffer exchanged into 50 mM ammonium acetate, pH 6.9 using 2 pre-washed Zeba desalting columns (7KDa MWCO, Thermo Fisher Scientific). The Exactive Plus MS was operated in EMR mode, with trap gas set at 6.0 and source, C-trap and collision energies optimised for improved transmission of protein complexes as necessary. Data were collected over the m/z range 3500-7000 Th. The MS was calibrated using CsI clusters up to approx. m/z 11,000 Th. ITC direct binding assay were performed on pBLNK-SH2 as described before.

2.5 Supporting Information

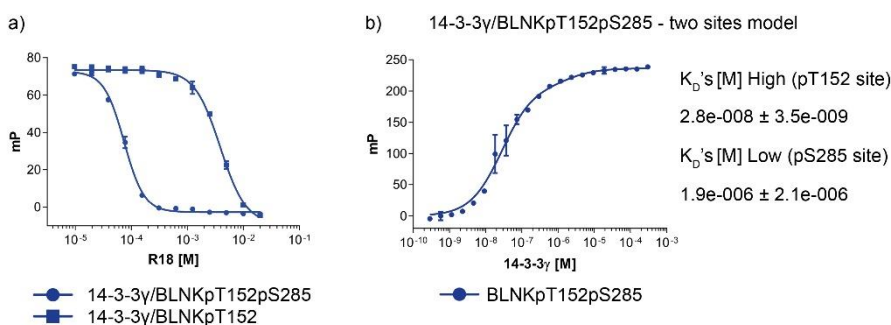


Figure S 2.1 | Fluorescence polarization curves of the R18 control on the 14-3-3 γ /BLNKpT152 and 14-3-3 γ /BLNKpT152pS285 systems and two sites model fitting of the 14-3-3 γ /BLNKpT152pS285 system. a) Inhibition curve originated from the titration of R18 on the 14-3-3 γ /BLNKpT152 and 14-3-3 γ /BLNKpT152pS285 systems. b) 14-3-3 γ /BLNKpT152pS285 data fitted with a “two-sites binding model”. The model calculates a higher K_D attributable to the pThr152 site and a lower K_D attributable to the pSer285 site. K_D values are reported associated with their standard error.

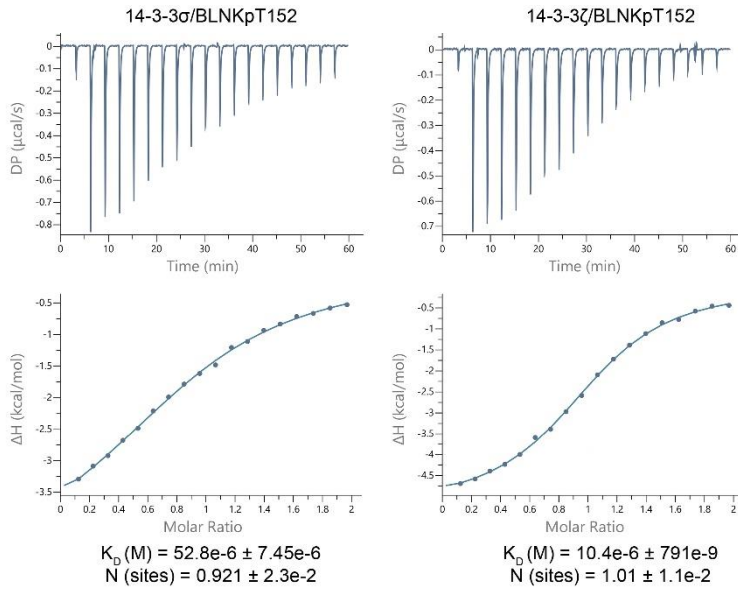
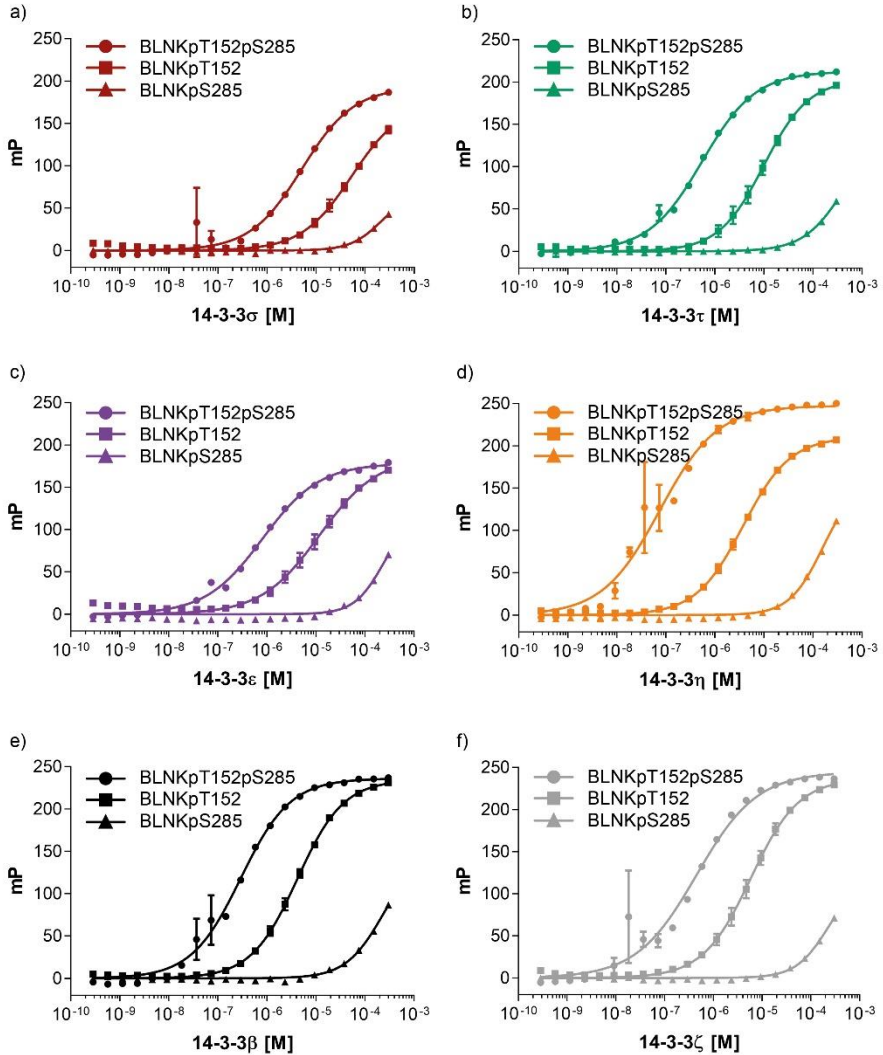


Figure S 2.2 | Isothermal titration calorimetry binding assays of the 14-3-3 σ /BLNKpT152 (left) and 14-3-3 ζ /BLNKpT152 (right).



	BLNKpT152	BLNKpS285 (estimates)	BLNKpT152pS285
γ	$1.4\text{e-}006 \pm 1.2\text{e-}007$	$1.1\text{e-}004 \pm 2.3\text{e-}005$	$3.7\text{e-}008 \pm 3.3\text{e-}009$
σ	$3.9\text{e-}005 \pm 3.6\text{e-}006$	$8.5\text{e-}004 \pm 3.7\text{e-}004$	$5.1\text{e-}006 \pm 8.7\text{e-}007$
τ	$9.5\text{e-}006 \pm 3.1\text{e-}007$	$5.6\text{e-}004 \pm 7.8\text{e-}005$	$5.5\text{e-}007 \pm 2.6\text{e-}008$
ϵ	$8.2\text{e-}006 \pm 9.7\text{e-}007$	$2.3\text{e-}003 \pm 5.6\text{e-}003$	$8.1\text{e-}007 \pm 6.2\text{e-}008$
η	$3.5\text{e-}006 \pm 1.2\text{e-}007$	$3.2\text{e-}004 \pm 7.4\text{e-}005$	$7.5\text{e-}008 \pm 1.1\text{e-}008$
β	$3.9\text{e-}006 \pm 1.2\text{e-}007$	$3.8\text{e-}004 \pm 6.8\text{e-}005$	$2.9\text{e-}007 \pm 2.4\text{e-}008$
ζ	$5.3\text{e-}006 \pm 2.4\text{e-}007$	$7.2\text{e-}004 \pm 2.2\text{e-}004$	$4.5\text{e-}007 \pm 8.8\text{e-}008$

Figure S 2.3 | Superposition of the fluorescence polarization binding curves of the peptides BLNKpT152pS285 (higher affinity), BLNKpT152 (moderate affinity) and BLNKpS285 (low affinity) performed on every human 14-3-3 isoform.

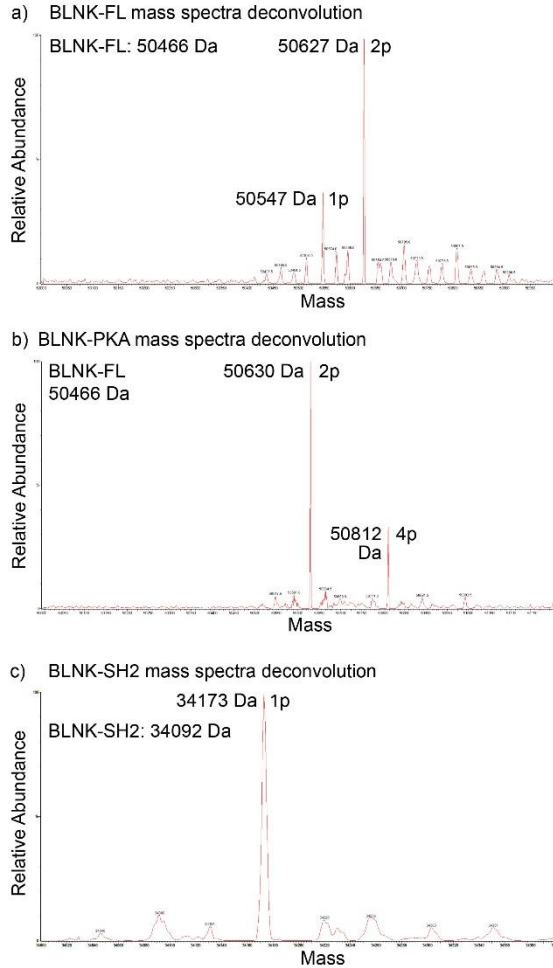


Figure S 2.4 | Deconvolution of the MS spectra of pBLNK-FL, BLNK-PKA and pBLNK-SH2. The expected molecular weight of the proteins in absence of phosphorylation is reported at the top left of the spectra for reference and has been used to calculate the number of phosphorylation events. a) Deconvolution of the pBLNK-FL MS spectra b) Deconvolution of the BLNK-PKA MS spectra c) Deconvolution of the pBLNK-SH2 MS spectra.

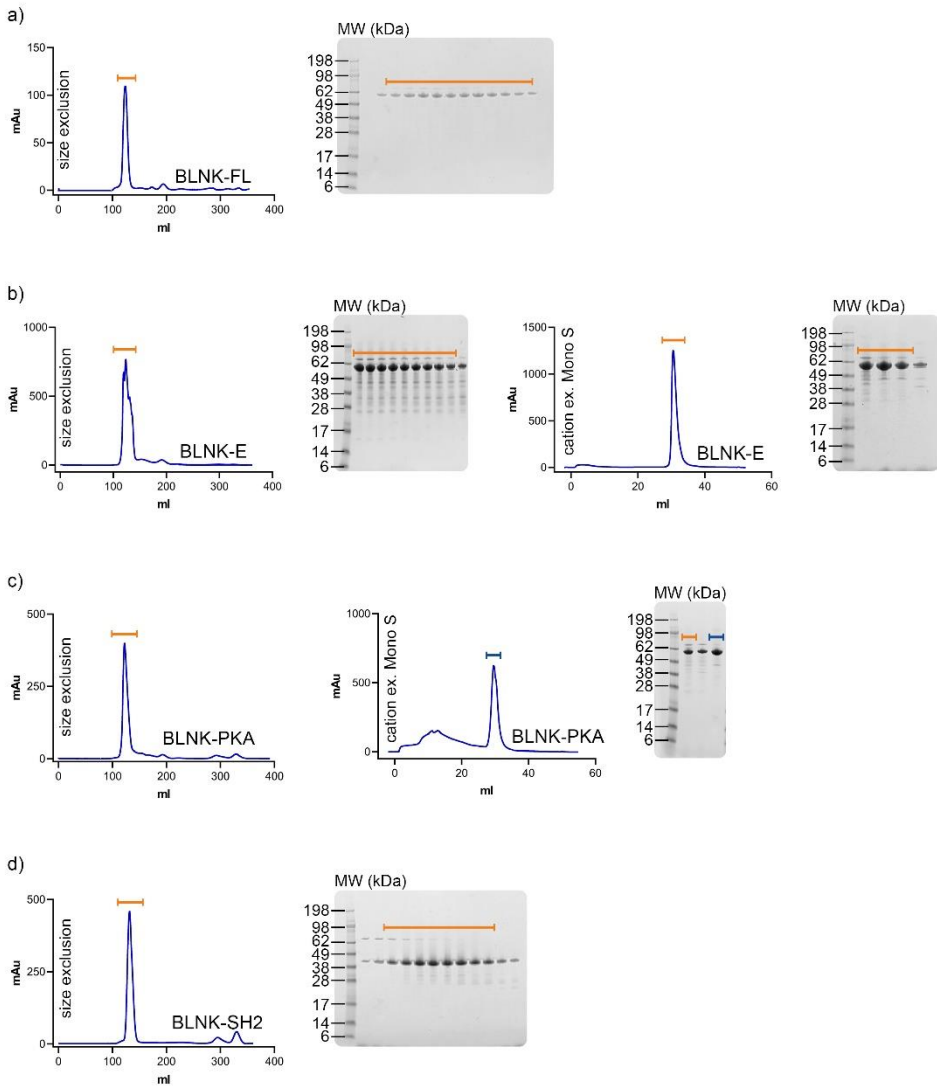


Figure S 2.5 | Last purification steps of the constructs BLNK-FL, BLNK-E, BLNK-PKA and BLNK-SH2. a) SEC profile and SDS-PAGE of the BLNK-FL construct. b) SEC and cation exchange profiles and SDS-PAGE of the BLNK-E construct. c) SEC and cation exchange profiles and SDS-PAGE of the BLNK-PKA construct. d) SEC profile and SDS-PAGE of the BLNK-SH2 construct.

Table S 2.1| Data collection and refinement statistics of the 14-3-3 σ /BLNKpT152 crystal structure. Values in the parenthesis represent the higher resolution shell.

Data collection	
Space group	C222 ₁
Cell dimensions	
a, b, c, (Å)	82.25, 112.11, 62.52
α , β , γ (°)	90, 90, 90
Resolution (Å)	26.63-1.88 (1.93-1.88)
R _{merge}	0.12 (0.34)
<I/ σ (I)>	8.8 (3.8)
Completeness (%)	99.9 (100.0)
Multiplicity	5.1 (4.8)
CC (1/2)	0.99 (0.91)
Refinement	
Resolution (Å)	26.63-1.88
No. Reflections	23758
R _{work} /R _{free}	0.15/0.21
No. Atoms	
Protein	2058
Water	387
B-factors	
Protein	13.55
Water	26.39
R.M.S.D.	
Bond lengths (Å)	0.006
Bond angles (°)	0.805
Ramachandran statistics (%)	
Favoured	98.74
Allowed	1.26
Outliers	0.00

2.6 References

- 1 Fu, C., Turck, C. W., Kurosaki, T. & Chan, A. C. BLNK: a central linker protein in B cell activation. *Immunity* **9**, 93-103 (1998).
- 2 Koretzky, G. A., Abtahian, F. & Silverman, M. A. SLP76 and SLP65: complex regulation of signalling in lymphocytes and beyond. *Nat Rev Immunol* **6**, 67-78, doi:10.1038/nri1750 (2006).
- 3 Wu, J. N. & Koretzky, G. A. The SLP-76 family of adapter proteins. *Semin Immunol* **16**, 379-393, doi:10.1016/j.smim.2004.08.018 (2004).
- 4 Tan, J. E., Wong, S. C., Gan, S. K., Xu, S. & Lam, K. P. The adaptor protein BLNK is required for B cell antigen receptor-induced activation of nuclear factor-kappa B and cell cycle entry and survival of B lymphocytes. *J Biol Chem* **276**, 20055-20063, doi:10.1074/jbc.M010800200 (2001).
- 5 Niiro, H. & Clark, E. A. Regulation of B-cell fate by antigen-receptor signals. *Nat Rev Immunol* **2**, 945-956, doi:10.1038/nri955 (2002).
- 6 Kurosaki, T. & Tsukada, S. BLNK: connecting Syk and Btk to calcium signals. *Immunity* **12**, 1-5, doi:10.1016/s1074-7613(00)80153-3 (2000).
- 7 Hashimoto, S. I., Akihiro; Ishiai, Masamichi; Okawa, Katsuya; Yamadori, Tomoki; Matsushita, Masato; Baba, Yoshihiro; Kishimoto, Tadimitsu; Kurosaki, Tomohiro; Tsukada, Satoshi. Identification of the SH2 Domain Binding Protein of Bruton's Tyrosine Kinase as BLNK—Functional Significance of Btk-SH2 Domain in B-Cell Antigen Receptor-Coupled Calcium Signaling. *Blood* **94**, 2357-2364 (1999).
- 8 Chiu, C. W., Dalton, M., Ishiai, M., Kurosaki, T. & Chan, A. C. BLNK: molecular scaffolding through 'cis'-mediated organization of signaling proteins. *EMBO J* **21**, 6461-6472, doi:10.1093/emboj/cdf658 (2002).
- 9 Turner, M. & Billadeau, D. D. VAV proteins as signal integrators for multi-subunit immune-recognition receptors. *Nature Reviews Immunology* **2**, 476-486, doi:10.1038/nri840 (2002).
- 10 Wang, X. *et al.* Down-regulation of B cell receptor signaling by hematopoietic progenitor kinase 1 (HPK1)-mediated phosphorylation and ubiquitination of activated B cell linker protein (BLNK). *J Biol Chem* **287**, 11037-11048, doi:10.1074/jbc.M111.310946 (2012).
- 11 Tsuji, S. *et al.* B Cell Adaptor Containing Src Homology 2 Domain (BASH) Links B Cell Receptor Signaling to the Activation of Hematopoietic Progenitor Kinase 1. *Journal of Experimental Medicine* **194**, 529-539 (2001).
- 12 Sauer, K. *et al.* Hematopoietic progenitor kinase 1 associates physically and functionally with the adaptor proteins B cell linker protein and SLP-76 in lymphocytes. *J Biol Chem* **276**, 45207-45216, doi:10.1074/jbc.M106811200 (2001).
- 13 Liou, J. *et al.* HPK1 Is Activated by Lymphocyte Antigen Receptors and Negatively Regulates AP-1. *Immunity* **12**, 399-408, doi:10.1016/s1074-7613(00)80192-2 (2000).
- 14 Shui, J. W. *et al.* Hematopoietic progenitor kinase 1 negatively regulates T cell receptor signaling and T cell-mediated immune responses. *Nat Immunol* **8**, 84-91, doi:10.1038/ni1416 (2007).
- 15 Chuang, H. C., Wang, X. & Tan, T. H. MAP4K Family Kinases in Immunity and Inflammation. *Adv Immunol* **129**, 277-314, doi:10.1016/bs.ai.2015.09.006 (2016).
- 16 Zhang, Q. *et al.* Inhibited expression of hematopoietic progenitor kinase 1 associated with loss of jumonji domain containing 3 promoter binding contributes to autoimmunity in systemic lupus erythematosus. *Journal of Autoimmunity* **37**, 180-189, doi:https://doi.org/10.1016/j.jaut.2011.09.006 (2011).
- 17 Mohammad, D. K., Nore, B. F., Gustafsson, M. O., Mohamed, A. J. & Smith, C. I. Protein kinase B (AKT) regulates SYK activity and shuttling through 14-3-3 and importin 7. *Int J Biochem Cell Biol* **78**, 63-74, doi:10.1016/j.biocel.2016.06.024 (2016).
- 18 Sluchanko, N. N. & Gusev, N. B. 14-3-3 Proteins and regulation of cytoskeleton. *Biochemistry (Moscow)* **75**, 1528-1546, doi:10.1134/s0006297910130031 (2011).
- 19 Yang, X. *et al.* Structural basis for protein-protein interactions in the 14-3-3 protein family. *Proc Natl Acad Sci U S A* **103**, 17237-17242, doi:10.1073/pnas.0605779103 (2006).
- 20 Mizuno, E., Kitamura, N. & Komada, M. 14-3-3-dependent inhibition of the deubiquitinating activity of UBPY and its cancellation in the M phase. *Exp Cell Res* **313**, 3624-3634, doi:10.1016/j.yexcr.2007.07.028 (2007).

- 21 Dar, A., Wu, D., Lee, N., Shibata, E. & Dutta, A. 14-3-3 proteins play a role in the cell cycle by shielding cdt2 from ubiquitin-mediated degradation. *Mol Cell Biol* **34**, 4049-4061, doi:10.1128/MCB.00838-14 (2014).
- 22 Obsil, T. & Obsilova, V. Structural basis of 14-3-3 protein functions. *Semin Cell Dev Biol* **22**, 663-672, doi:10.1016/j.semcdb.2011.09.001 (2011).
- 23 Stevers, L. M. *et al.* Characterization and small-molecule stabilization of the multisite tandem binding between 14-3-3 and the R domain of CFTR. *Proc Natl Acad Sci U S A* **113**, E1152-1161, doi:10.1073/pnas.1516631113 (2016).
- 24 Molzan, M. & Ottmann, C. Synergistic binding of the phosphorylated S233- and S259-binding sites of C-RAF to one 14-3-3zeta dimer. *J Mol Biol* **423**, 486-495, doi:10.1016/j.jmb.2012.08.009 (2012).
- 25 Yaffe, M. B. How do 14-3-3 proteins work? - Gatekeeper phosphorylation and the molecular anvil hypothesis. *FEBS Letters* **513**, 53-57, doi:10.1016/S0014-5793(01)03288-4 (2002).
- 26 Yaffe, M. B. *et al.* The structural basis for 14-3-3:phosphopeptide binding specificity. *Cell* **91**, 961-971, doi:http://doi.org/10.1016/S0092-8674(00)80487-0 (1997).
- 27 Petosa, C. *et al.* 14-3-3zeta binds a phosphorylated Raf peptide and an unphosphorylated peptide via its conserved amphipathic groove. *J Biol Chem* **273**, 16305-16310, doi:10.1074/jbc.273.26.16305 (1998).
- 28 Schumacher, B., Skwarczynska, M., Rose, R. & Ottmann, C. Structure of a 14-3-3 σ -YAP phosphopeptide complex at 1.15 Å resolution. *Acta Crystallographica Section F Structural Biology and Crystallization Communications* **66**, 978-984, doi:10.1107/S1744309110025479 (2010).
- 29 Stevers, L. M. *et al.* Structural interface between LRRK2 and 14-3-3 protein. *Biochemical Journal* **474**, 1273-1287, doi:10.1042/bcj20161078 (2017).
- 30 Doveston, R. G. *et al.* Small-molecule stabilization of the p53 - 14-3-3 protein-protein interaction. *FEBS Lett* **591**, 2449-2457, doi:10.1002/1873-3468.12723 (2017).
- 31 Rose, R., Rose, M. & Ottmann, C. Identification and structural characterization of two 14-3-3 binding sites in the human peptidylarginine deiminase type VI. *J Struct Biol* **180**, 65-72, doi:10.1016/j.jsb.2012.05.010 (2012).
- 32 Sluchanko, N. N. Association of Multiple Phosphorylated Proteins with the 14-3-3 Regulatory Hubs: Problems and Perspectives. *J Mol Biol* **430**, 20-26, doi:10.1016/j.jmb.2017.11.010 (2018).
- 33 Figurski, D. *Genetic Manipulation of DNA and Protein - Examples from Current Research*. (2013).
- 34 Pearlman, S. M., Serber, Z. & Ferrell, J. E., Jr. A mechanism for the evolution of phosphorylation sites. *Cell* **147**, 934-946, doi:10.1016/j.cell.2011.08.052 (2011).
- 35 Gogl, G. *et al.* Dual Specificity PDZ- and 14-3-3-Binding Motifs: A Structural and Interactomics Study. *Structure* **28**, 747-759 e743, doi:10.1016/j.str.2020.03.010 (2020).
- 36 Chernik, I. S., Seit-Nebi, A. S., Marston, S. B. & Gusev, N. B. Small heat shock protein Hsp20 (HspB6) as a partner of 14-3-3gamma. *Mol Cell Biochem* **295**, 9-17, doi:10.1007/s11010-006-9266-8 (2007).
- 37 Sano, R., Hayashi, F., Kurosaki, C., Yoshida, M., Yokoyama, S., RIKEN Structural Genomics/Proteomics Initiative (RSGI). Solution structure of the SH2 domain from mouse B-cell linker protein BLNK. doi:10.2210/pdb2e06/pdb.
- 38 Ottmann, C. Protein-Protein Interactions. *Drug Discov Today Technol* **24**, 1-2, doi:10.1016/j.ddtec.2017.11.008 (2017).
- 39 Milroy, L. G., Grossmann, T. N., Hennig, S., Brunsveld, L. & Ottmann, C. Modulators of protein-protein interactions. *Chem Rev* **114**, 4695-4748, doi:10.1021/cr400698c (2014).
- 40 Stevers, L. M. *et al.* Modulators of 14-3-3 Protein-Protein Interactions. *J Med Chem* **61**, 3755-3778, doi:10.1021/acs.jmedchem.7b00574 (2018).
- 41 Kabsch, W. Integration, scaling, space-group assignment and post-refinement. *Acta Crystallogr D Biol Crystallogr* **66**, 133-144, doi:10.1107/S0907444909047374 (2010).
- 42 Evans, P. R. An introduction to data reduction: space-group determination, scaling and intensity statistics. *Acta Crystallogr D Biol Crystallogr* **67**, 282-292, doi:10.1107/S090744491003982X (2011).
- 43 Winn, M. D. *et al.* Overview of the CCP4 suite and current developments. *Acta Crystallogr D Biol Crystallogr* **67**, 235-242, doi:10.1107/S0907444910045749 (2011).
- 44 McCoy, A. J. *et al.* Phaser crystallographic software. *J Appl Crystallogr* **40**, 658-674, doi:10.1107/S0021889807021206 (2007).

- 45 Emsley, P. & Cowtan, K. Coot: model-building tools for molecular graphics. *Acta Crystallogr D Biol Crystallogr* **D60**, 2126-2132, doi:10.1107/S0907444904019158 (2004).
- 46 Adams, P. D. *et al.* PHENIX: a comprehensive Python-based system for macromolecular structure solution. *Acta Crystallogr D Biol Crystallogr* **66**, 213-221, doi:10.1107/S0907444909052925 (2010).

The Native MS experiments were performed by Dr.Rebecca Burnely and Dr. Victoria Ellis.

Chapter 3

A Structural and Biophysical Characterization of the 14-3-3/SLP76 Protein-Protein Interaction

Abstract

The SH2 domain-containing protein of 76 kDa, SLP76, is an important adaptor protein that coordinates a complex protein network downstream of T-cell receptors (TCR), ultimately regulating the immune response. Upon phosphorylation on Ser376, SLP76 interacts with 14-3-3 adaptor proteins, which leads to its proteolytic degradation. This provides a negative feedback mechanism by which TCR signalling can be controlled. To gain insight into the 14-3-3/SLP76 protein-protein interaction (PPI), we have determined a high-resolution crystal structure of a SLP76 synthetic peptide containing Ser376 with 14-3-3 σ . We then characterized its binding to 14-3-3 proteins biophysically by means of fluorescence polarization and isothermal titration calorimetry. Furthermore, we generated two recombinant SLP76 protein constructs and characterized their binding to 14-3-3. Our work lays the foundation for drug design efforts aimed at targeting the 14-3-3/SLP76 interaction and, thereby, TCR signalling.

This work has been published as: **Soini, L.**, Leysen, S., Davis, J., Westwood, M. & Ottmann, C. The 14-3-3/SLP76 protein-protein interaction in T-cell receptor signalling: a structural and biophysical characterization. *FEBS Letters* 595, 404-414.

3.1 Introduction

The Lymphocyte cytosolic protein 2 (LCP2, Uniprot ID Q13094), also called SH2 domain containing protein of 76 kDa or more briefly SLP76, is an adaptor protein that was first identified in association with Grb2 as part of the T-cell receptors (TCRs) compartment ¹. SLP76 is responsible, along with linker for activation of T cells (LAT) ², for orchestrating the signalling downstream of TCRs by coordinating macromolecular complexes that locate on the cell membrane ^{3,4}. SLP76 associates with signalling proteins such as ITK (Tyrosine-protein kinase ITK/TSK), GADS (GRB2-related adapter protein 2), ADAP (adhesion and degranulation-promoting adapter protein), NCK (Cytoplasmic protein NCK1), PLC γ 1 (Phospholipase C-gamma-1) and HPK1 (Hematopoietic progenitor kinase 1) ⁵. A loss or deficiency in SLP76 results in compromised downstream effects such as calcium flux, cytoskeletal reorganization, RAS activation and NFAT (Nuclear factor of activated T-cells), AP1 transcriptional activity activation ⁶. SLP76-deficient mice show impaired viability and an absent or reduced development of T-cells further demonstrating the importance of this protein in immune signalling ^{7,8}.

Besides its role as a positive regulator of TCR signalling, SLP76 is also involved in a negative feedback mechanism modulating TCR signalling ⁹. Upon phosphorylation of Ser376 by HPK1, SLP76 associates with 14-3-3 adaptor proteins ¹⁰. The interaction with 14-3-3 allows SLP76 to be ubiquitinated by a yet to be determined E3 ligase, and consequently leads to its proteolytic degradation resulting in an attenuation of TCR signalling ¹¹. The association of SLP76 to 14-3-3 proteins appears to be a prerequisite for the degradation to happen. This mechanism reveals a sophisticated way by which TCR signalling can be finely controlled by SLP76 ⁹. Down-regulation of T-cell activation has also been reported via release of SLP76 microclusters from LAT triggered by HPK1 activity, specifically of a 14-3-3/GADS/SLP76 complex. The fate of this SLP76 complex upon release is unknown, but the fact that it might be targeted for degradation has been hypothesized ¹².

14-3-3 proteins are a family of dimeric adaptor proteins, highly conserved and present in all eukaryotic organisms. In humans, the seven isoforms are named with the Greek letters γ , τ , σ , ϵ , η , ζ , β ^{13,14}. With an interactome of roughly 500 binding partners, 14-3-3 proteins play a key role in regulating protein trafficking, signal transduction and the cell cycle engaging with mostly phosphorylated binding partners ¹⁵⁻¹⁷. The various functions that 14-3-3 can play involve protection against dephosphorylation, PPI modulation, regulating subcellular localization and the occlusion or exposure of ubiquitination sites ¹⁸⁻²⁰. In general, interest in the stabilisation of 14-3-3 PPI as an approach to modulating function has expanded considerably in the past few years ²¹. Several reviews on the topic have been published as well as innovative approaches that exploit fragment screening and combinatorial chemistry ²²⁻²⁵. Stabilising the interaction of SLP76 with 14-3-3 could potentially provide a way to reduce TCR signalling by shifting the equilibrium towards more degraded SLP76. In this work, we investigate the 14-3-3/SLP76 PPI using a short SLP76-derived phosphorylated peptide that includes Ser376 and characterize its interaction with 14-3-3 using a range of biophysical and structural techniques. Even though many 14-3-3 interaction partners can possess more than one 14-3-3 binding site ²⁶⁻²⁸, often leading to more complex binding mechanisms like the gatekeeper model ²⁹, we focus our attention solely on the Ser376 site in this work as the only 14-3-3 binding

site reported to be essential to 14-3-3 binding^{9,11}. We also characterise the interaction of 14-3-3 proteins with two SLP76 protein constructs, which can be valuable tool reagents in the context of future hit finding campaigns.

3.2 Results and Discussion

3.2.1 Biophysical characterization of the SLP76pS376 peptide binding to 14-3-3

Several potential 14-3-3 interaction sites on SLP76, including S130, S207, S297, S376 and S410, have previously been investigated by mutational studies. Only the S376A mutation was shown to abolish the interaction with 14-3-3⁹⁻¹¹. An *in silico* analysis using the “14-3-3-Pred” webserver³⁹ further points to Thr341 as a possible 14-3-3 interaction site, but it has not been confirmed that this site is phosphorylated *in vivo*. Therefore, we decided to concentrate our biophysical analysis on the S376 site. A short SLP76 phosphorylated peptide was designed and synthesised (Figure 3.1a). The sequence of the peptide was derived from the natural sequence of the SLP76 full-length protein: FPQSApS³⁷⁶LPPYFS (SLP76pS376). Two versions of the peptide were synthesised. One version, FITC-labelled at the N-terminus, was used for a fluorescence polarization (FP) assay while the other, acetylated at the N-terminus, was generated for an isothermal titration calorimetry assay (ITC). In the FP assay, all seven 14-3-3 isoforms were titrated against a fixed concentration of the FITC-labelled SLP76pS376 peptide. Complete binding curves showed a low micromolar interaction strength ranging from 0.39-3.2 μM (Figure 3.1b). An FP assay control was performed using the R18 14-3-3 inhibitor peptide³¹. The R18 peptide was titrated at a fixed concentration of 14-3-3 γ and SLP76pS376 displacing the latter to generate an inhibition curve (Figure S 3.1). This control confirmed the specificity of the SLP76pS376 peptide for the 14-3-3 amphipathic binding groove in which the R18 peptide is also known to bind (1A38). The γ isoform showed the highest affinity toward the SLP76pS376 peptide and was therefore chosen as a representative isoform in the control displacement assay. The affinity of the SLP76pS376 peptide for the 14-3-3 isoforms could be ranked in the following order: $\gamma > \eta > \beta > \zeta > \tau > \varepsilon > \sigma$ (strongest to weakest). Wang et al. reported a similar ranking order expressed in relative affinities of cellular SLP76 binding to 14-3-3 in GST pull-down assays: $\gamma > \zeta > \eta > \beta > \tau > \varepsilon > \sigma$ (strongest to weakest)¹¹. The binding of the SLP76pS376 peptide was confirmed by a direct ITC assay against the 14-3-3 isoform γ (Figure 3.1c). The estimated K_D from the ITC was 0.6 μM (\pm 0.08 μM). ITC measurements were also performed on the ζ and σ isoforms (Figure S 3.2). The overall ITC affinity trend agrees with the one observed by FP: $\gamma > \zeta > \sigma$ (strongest to weakest).

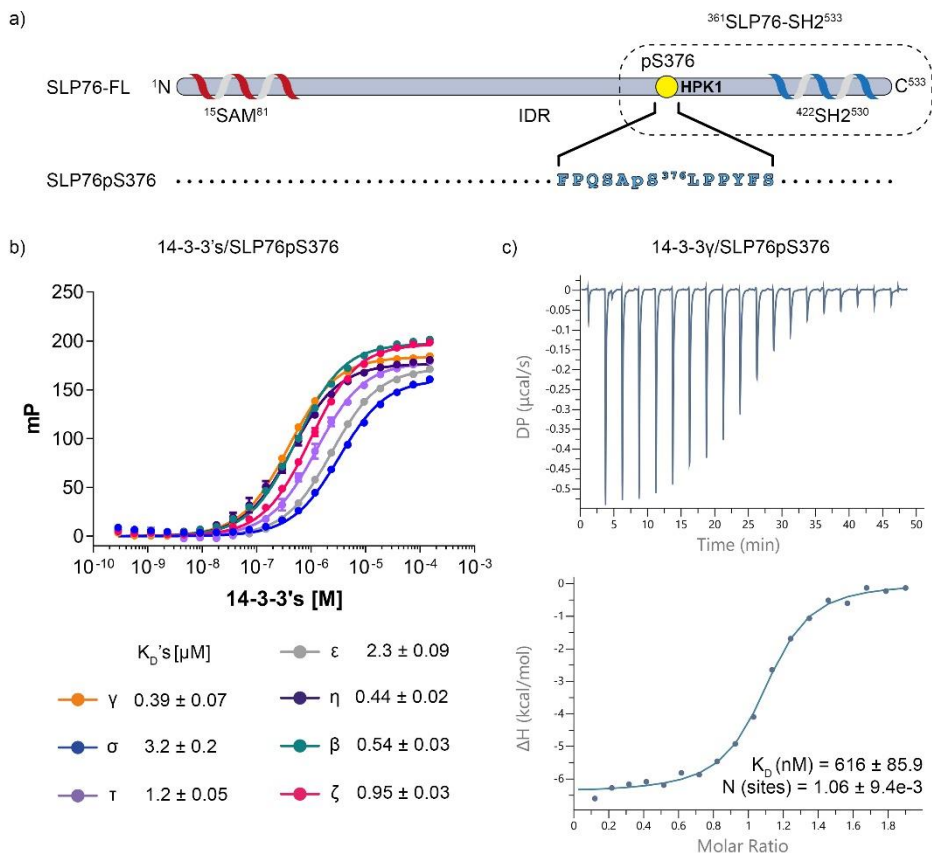


Figure 3.1 | Binding of the SLP76pS376 peptide to 14-3-3 proteins. a) Cartoon representation of the SLP76 protein. SLP76 full-length (SLP76-FL) is formed by a Sterile Alpha Motif (SAM) and Intrinsically Disordered Region (IDR) and an SH2 domain. SLP76-SH2 delineated by the dotted line with the Ser376 highlighted as yellow dot. The sequence of the peptide is reported in blue letters. b) Fluorescence Polarization binding assay of SLP76pS376 to all 14-3-3 isoforms. c) Isothermal Calorimetry Titration assay of SLP76pS376 binding to 14-3-3γ.

3.2.2 Crystal structure of the SLP76pS376 peptide bound to 14-3-3σ

To structurally elucidate the binding of SLP76pS376 to 14-3-3, the peptide was co-crystallized with 14-3-3σΔC. The crystals diffracted to a resolution of 1.53 Å. All data collection and refinement statistics are reported in (Table S 3.1). 14-3-3 proteins form a constitutive dimer with a characteristic cup like shape and two amphipathic binding grooves that can host one or two different binding partners (Figure 3.2a). The asymmetric unit (ASU) of this crystal structure, however, contains one 14-3-3 monomer that accommodates the SLP76pS376 peptide. The 14-3-3 dimer can be reconstituted by applying the space group symmetry operations (Figure 3.2a). The SLP76pS376 peptide could be modelled reliably in the 2Fo-

Fc map displayed within the 14-3-3 binding groove. SLP76pS376 residue Phe371 has been modelled except for the side chain due to lack of electron density (Figure 3.2b). The main anchoring point of the SLP76pS376 peptide to 14-3-3 is the phosphate group on Ser376, which establishes polar contacts with 14-3-3 residues Arg56, Arg129 and Tyr130. More polar bonds are established in the binding groove between SLP76pS376 Ala375, Ser374, Gln373 and 14-3-3 σ residues Asn226, Trp230, Glu182 and Arg60 respectively. An additional hydrophobic contact is provided by the SLP76pS376 Leu377 and 14-3-3 σ Leu222 and Ile219 (Figure 3.2c).

14-3-3 binding motif sequences have been categorized through the years into three main recognition motifs: mode I) RSXpS/TXP, mode II) RXY/FXpS/TXP and mode III) pS/pTX₁₋₂-COOH, where X can be any residue^{14,32}. Although most of the synthetic phosphopeptides that bind 14-3-3 belong to one of those three modes, more and more exceptions to the three classical modes have been reported³³. SLP76pS376 shares Pro378 with modes I and II, the Ser374 with mode I, and a random residue at position -3 from the pSer376 with mode II. However, it differs from classic mode I and II motifs, since there is no arginine at position -3 (mode I) or -4 (mode II).

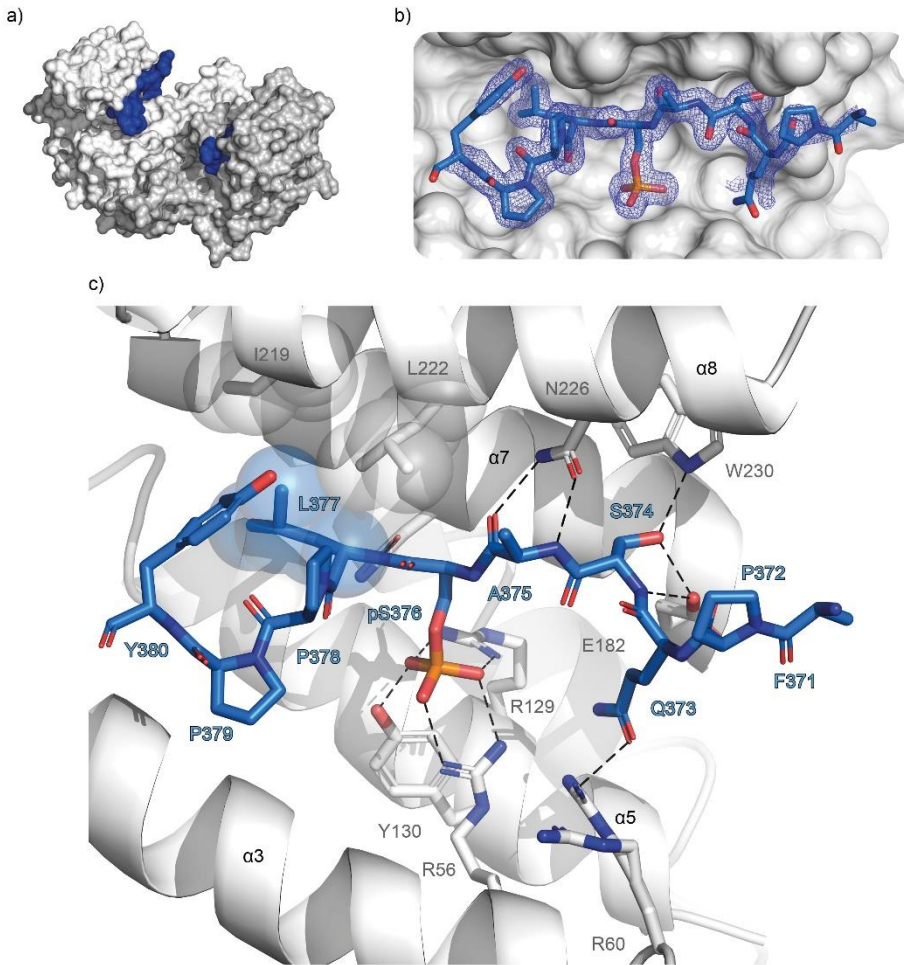


Figure 3.2 | Crystal structure of the 14-3-3 σ /SLP76pS376 binary complex at 1.53 Å resolution. a) The biologically relevant 14-3-3 dimer (reconstituted by applying the space group symmetry operations) is represented as white (one monomer) and grey (one monomer) surface. The SLP76pS376 peptide is represented as blue surface. b) SLP76pS376 peptide bound in the 14-3-3 σ amphipathic binding groove. The SLP76pS376 peptide is represented in blue sticks surrounded by the 2F_o-F_c electron density map contoured at $\sigma=1$. c) Detailed view of the SLP76pS376 peptide (blue sticks) binding to the 14-3-3 σ amphipathic groove (grey cartoon). Polar contacts are represented as black dotted lines and hydrophobic contacts are represented with semi-transparent spheres contoured around the residue side chains.

3.2.3 Interaction of full-length SLP76 constructs with 14-3-3

SLP76 is composed of an N-terminal Sterile Alpha Motif (SAM) acidic region, of which an NMR structure is deposited in the PDB (2EAP), followed by an intrinsically disordered region and a C-terminal SH2 domain (Figure 3.1a). The SH2 domain is a structurally conserved domain which is essential for the association of the kinase HPK1 to SLP76³⁴. The use of synthetic peptides to study 14-3-3 interactions is a practical and well-established approach. A few recent examples include studies of the interaction with SOS1³⁵, USP8³⁶ and LRRK2²⁸. In contrast, studies of 14-3-3 PPI using protein constructs rather than peptides is a less commonly used approach³⁷, since producing larger protein constructs phosphorylated at one or more specific sites is more challenging. Critically, we believe that working with these proteins has the potential to generate additional and more relevant insights than the simpler peptide system.

In this work, we expressed and purified four SLP76 protein constructs using bacterial protein production: a full-length one (SLP76-FL), a phosphomimetic (SLP76-E), a mutated version for PKA co-expression and phosphorylation (SLP76-PKA) and a shorter one containing only the SH2 domain of SLP76 (SLP76-SH2).

SLP76-FL was phosphorylated *in vitro* using the kinase HPK1 (Figure S 3.3a). SLP76-FL was then incubated with 14-3-3 ζ in its phosphorylated form (pSLP76-FL) and in its non-phosphorylated form (SLP76-FL). Both protein mixtures were then loaded consecutively on an analytical size-exclusion column (SEC) to investigate whether the phosphorylation on SLP76-FL indeed leads to 14-3-3 binding. The elution profile (Figure 3.3a) for the mixture containing pSLP76-FL shows a considerable shift to the left, indicating a higher hydrodynamic volume and formation of a pSLP76-FL/14-3-3 ζ complex. Fractions of the elution profile were analysed by SDS-PAGE, confirming the formation of a 14-3-3 and phosphorylated SLP76 (Figure 3.3c). The complex formation was additionally studied by native mass spectrometry (Figure 3.3b). The observed molecular mass of 116048 Da suggests that one 14-3-3 dimer binds a single copy of pSLP76-FL.

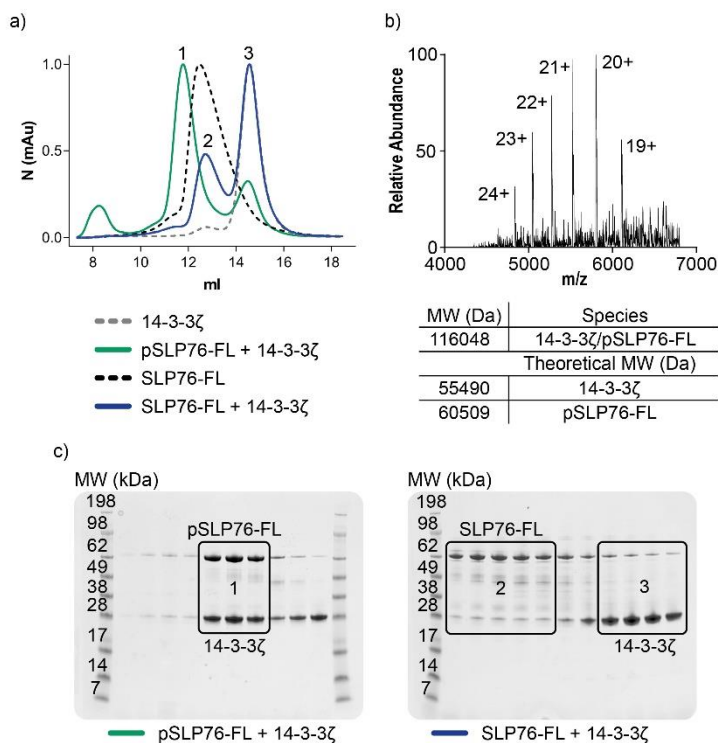


Figure 3.3 | Binding of SLP76-FL to 14-3-3 proteins. a) Superimposed elution profiles for size-exclusion chromatography runs of the 14-3-3 ζ /SLP76-FL and 14-3-3 ζ /pSLP76-FL mixtures. The mAu intensity has been normalized. The elution profile of the single proteins has also been reported for comparison. The samples have been run on an ÄKTA pure system. SLP76-FL and pSLP76-FL at a concentration of 4 mg/ml were mixed with 14-3-3 γ to get to a 1:1 molar ratio. b) Native mass spectrometry spectrum of the complex 14-3-3 ζ /pSLP76-FL. Theoretical and experimental molecular masses are reported on the right of the graph. c) SDS-PAGE analysis for the size-exclusion profiles of the SLP76-FL/14-3-3 ζ and pSLP76-FL/14-3-3 ζ mixtures. The content of peak 1 shows band attributable to 14-3-3 ζ and pSLP76-FL of equal intensity confirming the presence of a complex. The content of peaks 2 and 3 show bands attributable to SLP76-FL and 14-3-3 ζ respectively, eluted at two different elution volumes.

After the successful attempt of generating a phosphorylated version of full-length of SLP76 we wanted to test different strategies that would simplify the reagent generation in the phosphorylation stage. We then expressed and purified a phosphomimetic version of SLP76, SLP76-E (Figure 3.4a), which contained a mutation of the 14-3-3 interaction residue, S376E. We first tested the binding of SLP76-E to 14-3-3 ζ on SEC by mixing the two protein in a 1:1 molar ratio as we did for the SLP76-FL case (Figure 3.4b). No shift of the peak containing the 14-3-3 ζ /SLP76-E mixture was detected, suggesting 14-3-3 ζ and SLP76-E do not interact. This was confirmed using an ITC assay by titrating 14-3-3 γ onto SLP76-E (Figure 3.4c). No

binding curve was detected, hence confirming that phosphorylation of 14-3-3 binding partners is essential for binding.

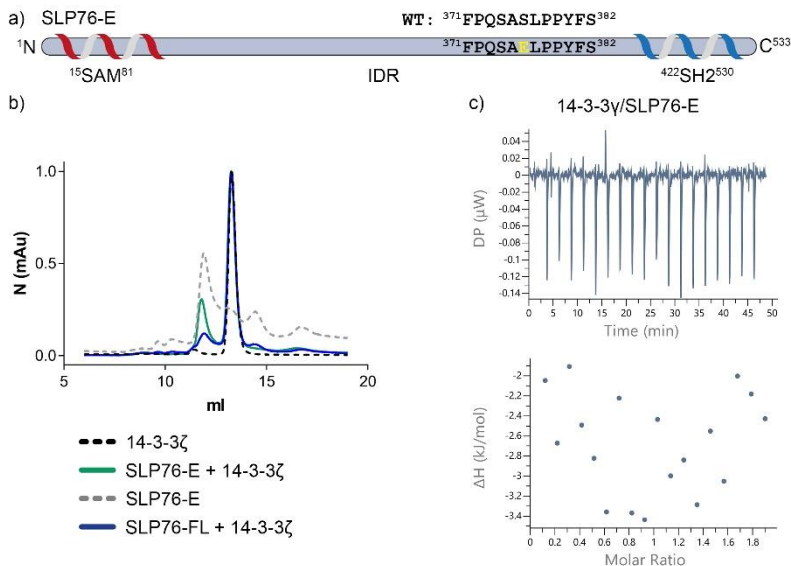


Figure 3.4 | Analysis of the SLP76-E construct. a) Cartoon representation of the mutated SLP76 phosphomimetic construct: S376E. The mutation is highlighted with yellow letters. WT: wild type. b) Superposition of size exclusion profiles of single 14-3-3 ζ , SLP76-E and their complexes. The elution volumes of the single proteins taken as a reference superpose exactly to the proteins when mixed, suggesting that no 14-3-3 ζ /SLP76-E complex has formed. c) ITC experiment of 14-3-3 γ titrated on SLP76-E. The assay shows very little heat formation attributable to the titration and no binding curve, confirming that no interaction occurs between 14-3-3 proteins and SLP76-E.

The same workflow of experiment was applied on the third construct, SLP76-PKA. SLP76-PKA was mutated to be able to be recognized by the kinase PKA and therefore being phosphorylated in the expression phase (Figure 3.5a). A deconvolution of the mass spectra of SLP76-PKA confirming that several phosphorylation events took place is reported in the supporting information (Figure S 3.3b). A binding test performed on SEC revealed a left shift towards higher hydrodynamic volumes of the peak containing the protein mixture composed of SLP76-PKA and 14-3-3 ζ , suggesting the possible formation of a complex (Figure 3.5b). The binding was confirmed by ITC titrating 14-3-3 γ onto SLP76-PKA (Figure 3.5c).

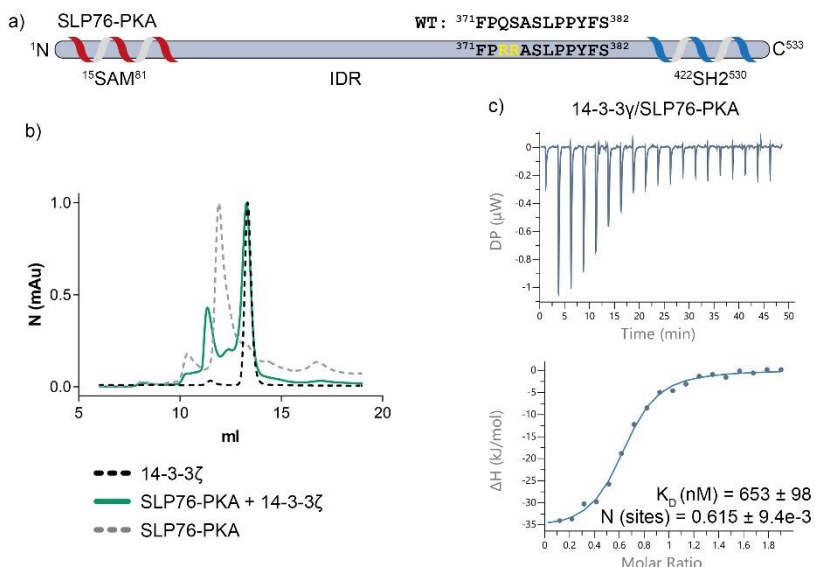


Figure 3.5 | Analysis of the SLP76-PKA construct. a) Cartoon representation of the mutated SLP76-PKA construct: Q373R, S374R. The mutations are highlighted with yellow letters. WT: wild type. b) Superposition of size exclusion profiles of single 14-3-3 ζ , SLP76-PKA and their complex. The elution volumes of the sample containing mixed 14-3-3 ζ and SLP76-PKA is shifted to smaller elution volumes compared to the single proteins taken as a reference, suggesting that a 14-3-3 ζ / SLP76-PKA complex has formed. c) ITC experiment of 14-3-3 γ titrated on SLP76-PKA. The assay confirms the binding between 14-3-3 proteins and SLP76-PKA.

The K_D calculated from the ITC binding assay was 653 nM, remarkably close to the one calculated using the SLP76pS376 peptide, 616 nM.

3.2.4 Biophysical analysis of the interaction of 14-3-3 with a truncated SLP76-SH2 (361-533) construct

Intent on future structural analysis beyond the synthetic peptide, as well as high-throughput screening for modulators of the 14-3-3 SLP76 interaction, we evaluated a truncated version of SLP76, SLP76-SH2. The rationale for its design was this construct contains less intrinsically disordered regions, which should facilitate crystallisation. Furthermore, the SLP76-SH2 construct provides a more convenient system to work with in terms of yield (around 50 mg/L) and ease of phosphorylation while preserving key interactions with 14-3-3 (Figure S 3.3c). Although not the full-length protein, we would consider SLP76-SH2 as a better screening tool than a short synthetic peptide with the potential to provide small-molecule binding sites beyond the smaller interaction surface of the 14-3-3 – phosphopeptide complex. Following the same approach as with the full-length construct, the interaction of phosphorylated and non-phosphorylated SLP76 with 14-3-3 was compared using analytical size-exclusion chromatography. Again, a higher molecular weight species was observed for the mixture containing

pSLP76-SH2 compared to SLP76-SH2 (Figure 3.3a). Native mass spectrometry has been performed on the 14-3-3 γ /pSLP76-SH2 complex confirming the binding (Figure 3.3b).

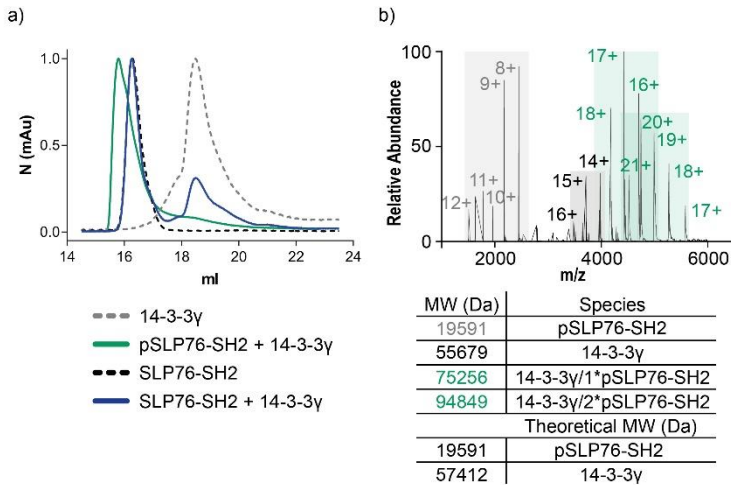


Figure 3.6 | Binding of SLP76-SH2 to 14-3-3 proteins. a) Superimposed elution profiles for size-exclusion chromatography runs on the 14-3-3 γ /SLP76-SH2 and 14-3-3 γ /pSLP76-SH2 mixtures. The mAu intensity has been normalized. The elution profile of the single proteins has also been reported for comparison. The samples were run on an Agilent 1100 Series HPLC Value System. SLP76-SH2 and pSLP76-SH2 were diluted down to a concentration of 1 μ g/ml and were mixed with 14-3-3 γ to get to a 1:1 molar ratio. b) Native mass spectrometry spectrum of the complex 14-3-3 γ /pSLP76-SH2. Theoretical and experimental molecular masses are reported on the right of the graph.

3.2.5 pSLP76-SH2/14-3-3 γ complex K_D and stoichiometry determination

The K_D and the stoichiometry of the 14-3-3 γ /pSLP76-SH2 complex was determined by ITC and SPR. The K_D estimated by ITC was found to be 46.7 nM (\pm 12.5 nM) (Figure 3.7a), an increase by 13-fold when compared to the 14-3-3 γ /SLP76pS376 peptide, 0.6 μ M (\pm 0.08 μ M). To confirm the results obtained from the size exclusion experiment (Figure 3.3c), SLP76-SH2 (non-phosphorylated) was also titrated into 14-3-3 γ and as expected, no binding was observed (Figure 3.7a). The stoichiometry for the 14-3-3 γ /pSLP76-SH2 complex calculated from ITC is close to 1, suggesting that 2 copies of pSLP76-SH2 occupy both sites on one 14-3-3 γ dimer.

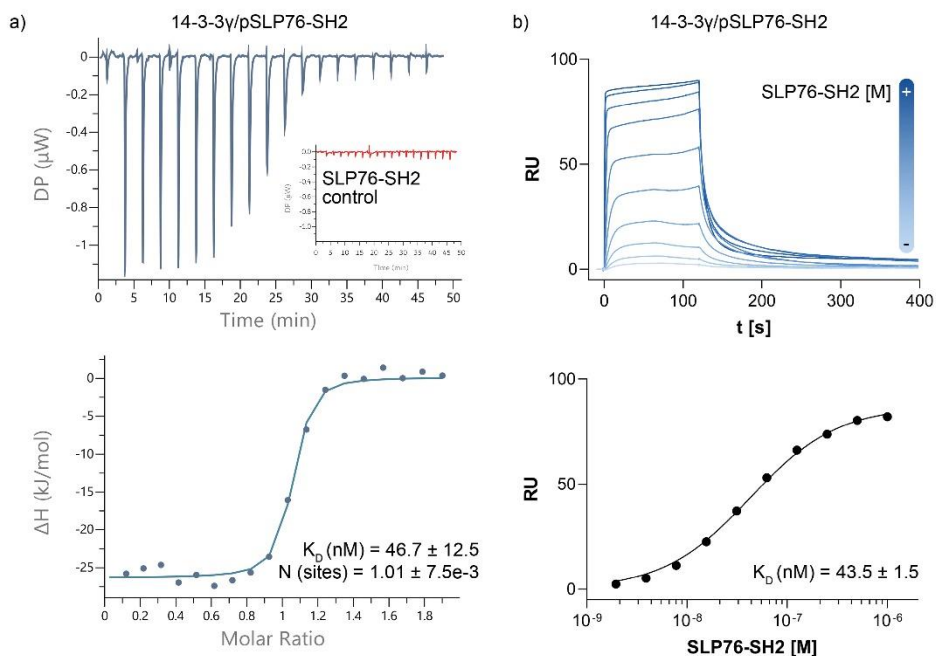


Figure 3.7 | K_D and stoichiometry determination of the complex 14-3-3γ/pSLP76-SH2 by ITC and SPR. a) Direct Isothermal Calorimetry Titration assay of pSLP76-SH2 binding to 14-3-3γ. The control is reported for reference in red and represent a titration of SLP76-SH2 non-phosphorylated on 14-3-3γ. b) Sensorgrams of pSLP76-SH2 flowing over immobilized 14-3-3γ. The binding curve points has been taken from the sensorgrams reference points at equilibrium and fitted in GraphPad. The experiment has been performed in triplicates, only one repetition is reported in the figure for illustrative purposes. The K_D is reported with the associated standard error calculated from the individual measurements.

The binding between pSLP76-SH2 and 14-3-3γ was also characterised by SPR. 14-3-3γ was immobilized on a NTA chip exploiting the double N-terminal (His)₆-tag. Regeneration steps were therefore easily performed and fresh protein was then immobilized at every cycle. Increasing concentrations of pSLP76-SH2 were flowed over 14-3-3γ and the K_D was then measured via steady state approach (Figure 3.7b). The resultant K_D value of 43.5 nM (± 1.5 nM) correlates well with the affinity measured by ITC. The stoichiometry by SPR could be calculated with the following formula: $N = (RU_{pSLP76-SH2} / RU_{14-3-3\gamma}) \cdot (MW_{14-3-3\gamma} / MW_{pSLP76-SH2})$ which is used to predict the maximal response of the assay ³⁸. Where N represents the stoichiometry, $RU_{pSLP76-SH2}$ the maximal response provided by pSLP76-SH2 binding to 14-3-3γ, $RU_{14-3-3\gamma}$ the amount of 14-3-3γ immobilised on the chip and MW the molecular weight of the two protein (14-3-3γ as monomer). Introducing the values in the formula of the sensorgrams at saturation, we could calculate a stoichiometry value close to 0.8, in agreement with the stoichiometry values calculated by ITC: one copy of pSLP76-SH2 per 14-3-3γ monomer. This result is also supported by

native mass spectrometry which showed the presence of species with two SLP76-SH2 molecules binding a 14-3-3 dimer (Figure 3.3d).

The final purification step chromatograms of all the constructs mentioned above are reported in the supporting information along with the SDS-PAGEs of the protein peaks content to allow to check the sample quality (Figure S 3.4).

3.3 Conclusions

In this work we provided structural and biophysical data on the interaction of 14-3-3 with SLP76. We used a short synthetic SLP76 phosphorylated peptide to characterize the binding of SLP76 Ser376 to 14-3-3 isoforms and have shown through X-ray crystallography how it anchors SLP76 to 14-3-3. The 14-3-3 binding site is not a classical mode I or mode II, but rather shares features of both ^{14,32}. To date, more and more exceptions to the three classical binding modes have been reported ³³.

SLP76 has been shown to be an important actor downstream of TCR signalling and its interaction with 14-3-3 could therefore be an attractive target for therapeutic intervention with small molecules. Theoretically, stabilisation of this PPI could increase proteolytic degradation of SLP76, strengthening the negative feedback mechanism which could be a desirable outcome in various autoimmune and inflammatory conditions ³⁹. To lay the foundation for the discovery of such stabilizers, we also generated four recombinant SLP76 protein constructs and characterized them using native MS, SEC, ITC and SPR. Three constructs out of the four generated were found to bind to 14-3-3 proteins. The phosphomimetic construct, SLP76-E, could have represented the easiest way to obtain a full-length, “ready to use” binding partner, but unfortunately it did not bind to 14-3-3. This finding highlights the importance of phosphorylation in the context of 14-3-3 binding. In our opinion, these protein constructs should provide more relevant tools than shorter synthetic SLP76 peptides when performing HTS campaigns, with the opportunity to discover druggable binding sites beyond the 14-3-3 amphipathic binding pocket.

3.4 Material and Methods

Peptide Synthesis

The SLP76pS376 peptide, FPQSApS³⁷⁶LPPYFS, was synthesized *via* Fmoc solid-phase peptide synthesis by an Intavis MultiPep RSi peptide synthesizer exploiting a Rink amide AM resin (Novabiochem, 0.59 mmol/g loading). The acetylated version was acetylated (1:1:3 Ac₂O, Pyridine/NMP) at the N-terminus and the FITC-labelled one was functionalized with Fluorescein Isothiocyanate (FITC, Sigma-Aldrich) after a β -alanine linker introduced *via* Fmoc chemistry at the N-terminus. SLP76pS376 was purified using a preparative LC-MS system composed by an LCQ Deca XP Max (Thermo Finnigan) ion-trap mass spectrometer, a Surveyor auto sampler, a Surveyor photodiode detector array (PDA) (Thermo Finnigan) and a PrepFC fraction collector (Gilson Inc). Purification column: Waters reverse-phase C18 Atlantis T3 prep OBD, 5 μ M, 150 x 19 mm column in linear gradients of H₂O/CH₃CN/0.1%TFA. The R18 peptide, PHCVPRDLSWLDLEANMCLP, was ordered from Sigma-Aldrich, purity \geq 98% (HPLC).

Protein Expression and Purification

14-3-3 isoforms γ , τ , σ , ϵ , η , ζ , β FL and 14-3-3 Δ C (Δ C=17 C-terminal AA) were expressed with a (His)₆-tag in NiCo21(DE3) competent cells, from a pPROEX-Htb vector in 2TY media. The purification was carried out by affinity chromatography on Nickel columns (HisTrap HP, 5 mL). The tags were cleaved with a TEV protease. The proteins were then loaded again on Nickel columns to remove any non-cleaved protein. A final purification step was performed by loading the proteins on a size-exclusion chromatography column (HiLoad 26/600 Superdex 75 pg) equilibrated in 20 mM TRIS-HCl pH 7.5, 150 mM NaCl, 2 mM DTT.

SLP76-FL (1-533), SLP76-SH2 (361-533), SLP76-E (1-533; S376E) and SLP76-PKA (1-533; Q373R, S374R) were expressed with a (His)₆-SUMO tag in NiCo21(DE3) competent cells from a pCDFDuet-1 vector in 2TY media. The SLP76-PKA construct was transformed together with the vector pACYC encoding for the Protein Kinase A (PKA). Cultures were incubated at 37 °C until OD₆₀₀ reached the value of 3.5. The temperature was then dropped to 18 °C until the OD₆₀₀ reached the value of 4.0. A feed solution at the final concentrations of 50 mM MOPS sodium salt pH 7.2, 1 mM MgCl₂, 1 mM MgSO₄ and 2% Glycerol was added to the cultures before inducing expression by adding IPTG to a final concentration of 200 μ M. Protein expression was carried overnight at the temperature of 18 °C. The protein purification was carried out through affinity chromatography as for 14-3-3 proteins. The tags were cleaved with SUMO hydrolase. A final purification step was performed by loading the proteins on a size-exclusion chromatography column (HiLoad 26/600 Superdex 75 pg) equilibrated in 20 mM HEPES pH 7.5, 150 mM NaCl, 2 mM DTT. The SLP76-E and SLP76-PKA were additionally loaded onto a monoQ 5/50 GL cation exchange column for an additional purification step. All purification steps were performed on an ÄKTA pure protein purification system (Cytiva). SLP76-FL and SLP76-SH2 were phosphorylated *in vitro* by incubating them overnight at room temperature in their storage buffer, 20 mM HEPES pH 7.5, 150 mM NaCl, 2 mM DTT, supplemented by 0.75 mM ATP, 20 mM MgCl₂ and HPK1 kinase (Thermo Fisher Scientific) with a kinase:protein weight ratio of 1:3000. Possible phosphorylations were checked by LC-MS. For complex formation pSLP76-FL and SLP76-FL were incubated with 14-3-3 ζ and pSLP76-SH2 and SLP76-SH2 were incubated with 14-3-3 γ at a 1:1 molar ratio for 2 h at 4°C (one SLP76 copy per 14-3-3 monomer, hence 14-3-3 saturation). The SLP76-FL/14-3-3 ζ complexes were injected in an ÄKTA pure system on a Superdex 200 10/300 GL. The SLP76-SH2/14-3-3 γ , SLP76-E/14-3-3 ζ and SLP76-PKA/14-3-3 ζ complexes were injected on an Agilent 1100 Series HPLC Value System system on a Superdex 200 Increase 10/300 GL column, flow 0.5 ml/min, running buffer 20 mM HEPES pH 7.5, 150 mM NaCl, 2 mM DTT.

Fluorescence Polarization and Isothermal Titration Calorimetry

FP binding assays were carried out on Corning 384-well 3575 plates, serially diluting (2-fold) 14-3-3 isoforms in the presence of 10 nM FITC-labelled peptide. Proteins and peptide were diluted from their stock concentration in assay buffer (50 mM Tris pH 7.5, 150 mM NaCl, 5 mM MgCl₂, 0.05% v/v Tween-20). The data were collected on a PHERAstar FSX plate reader (BMG Labtech) with a λ_{ex} 485 nm, λ_{em} 520 nm FP filter setting. For K_D calculation the background polarization was removed from all values and the data were fitted with a “One site - Specific binding model” on GraphPad Prism version 8.1.1 for Windows, GraphPad Software, La Jolla California USA, www.graphpad.com. Each data point is the

average of a triplicate measurement, standard deviation is reported as error bars. ITC measurements were performed on a PEAQ-ITC (Malvern) dissolving the peptides in assay buffer (50 mM Tris pH 7.5, 150 mM NaCl, 5 mM MgCl₂, 0.05% v/v Tween-20) and dialysing the protein in the same buffer to minimise buffer mismatch. The optimal peptide and protein concentrations were chosen simulating the experiment on the MicroCal PEAQ-ITC Analysis Software (Malvern) according to the predicted K_D . The peptides were titrated into the cell containing the protein using a series of 18 injections 2 μ L each at 25 °C (reference power 5 μ cal/sec, stir speed 750 rpm, initial delay 60 s, spacing 150 s). The data were analysed on the MicroCal PEAQ-ITC Analysis Software (Malvern).

X-ray protein crystallography

For protein crystallisation, a C-terminally truncated version of 14-3-3 σ was used (14-3-3 $\sigma\Delta$ C, Δ C=17 C-terminal AA)⁴⁰. The binary complex was prepared mixing 14-3-3 $\sigma\Delta$ C at 10 mg/ml with SLP76pS376 at a 1:1 and 1:1.2 molar ratio, followed by overnight incubation then at 4 °C (dilution buffer: 20 mM HEPES pH 7.5, 2 mM MgCl₂). The crystallization drops were dispensed in 1:1 protein to crystallisation condition ratio (0.5 μ L + 0.5 μ L). pH over PEG gradients grid crystallisation conditions: 95 mM HEPES pH 7.1-7.7, 24-29% PEG400, 190 mM CaCl₂, Glycerol 5%. The plate was incubated at 4 °C and crystals grew in 5 to 10 days and were observed in most of the crystallisation conditions. The data were collected on the I04 Beamline at the Diamond Light Source. The diffraction data were processed with XDS⁴¹ and AIMLESS^{42,43}. The structure was solved by molecular replacement using PHASER, with a 14-3-3 σ structure as search model (PDB ID: 3MHR),^{40,44}. The initial structure was then refined using COOT⁴⁵ and PHENIX⁴⁶. The structure is deposited in the PDB with accession code 6ZCJ. All figures were generated using PyMOL (The PyMOL Molecular Graphics System, Version 1.2r3pre, Schrödinger, LLC).

Mass spectrometry

LC-MS experiments were performed on a Waters Acquity UPLC-Xevo G2 ToF LCMS system, operated by MassLynx software. Typically, 5 μ L of protein solution concentrated to 1 mg/mL was injected in reverse phase UPLC system using the following conditions: Waters Acquity UPLC BEH300 C₄, 2.1 x 100mm, 1.7 μ M particle size analytical column; Solvent A: 0.1% HCOOH in H₂O, Solvent B: 0.1% HCOOH in CH₃CN; flow rate 0.3 mL/min; gradient: 0 min, 5% B; 5 min, 60% B; 6 min, 95% B. Mass spectrometry data were collected over the m/z range 100-5000 Th, with a scan rate of 0.5 seconds. The mass spectrometer was calibrated over this mass range using NaI clusters. Native mass spectrometry experiment was run on the 14-3-3 ζ /pBLNK-FL complex on a Thermo Fisher Exactive Plus EMR MS fitted with an Advion Nanomate chip-based nanoESI instrument for sample introduction. Prior to analysis, protein sample was buffer exchanged into 50 mM ammonium acetate, pH 6.9 using 2 pre-washed Zeba desalting columns (7 kDa MWCO, Thermo Fisher Scientific). The Exactive Plus MS was operated in EMR mode, with trap gas set at 6.0 and source, C-trap and collision energies optimised for improved transmission of protein complexes as necessary. Data were collected over the m/z range 3500-7000 Th. The MS was calibrated using CsI clusters up to approximately m/z 11,000 Th.

Surface Plasmon Resonance

SPR experiments were performed on a Biacore T200 (Cytiva). The running and diluting buffer used was HBS-P (10 mM HEPES pH 7.4, 150 mM NaCl, 0.05% P20). 14-3-3 γ was immobilised on a Sensor Chip NTA (Cytiva) at about 150 RUs exploiting the interaction between the Ni²⁺ charged chip and the double (His)₆-tag present on 14-3-3 γ . SLP76-SH2 was serially diluted from 1 μ M and flowed over the immobilised 14-3-3 γ at 30 μ L/min for 120 s before allowing dissociation for 6 minutes. The top SLP76-SH2 concentration was calculated to give a maximum response of approximately 100 RUs. After every cycle, the chip was washed with EDTA and Ni²⁺ and 14-3-3 γ re-injected for the next cycle. The binding experiment of SLP76-SH2 on 14-3-3 γ was performed in triplicates and the K_D was determined with the steady state affinity model. Reference subtracted data was exported and fitted with a "One site - Specific binding model" on GraphPad Prism version 8.1.1 for Windows, GraphPad Software, La Jolla California USA, www.graphpad.com.

3.5 Supporting Information

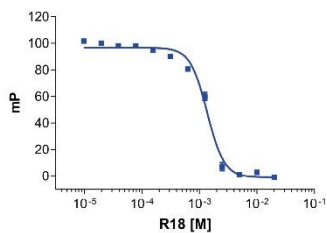


Figure S 3.1 | FP curve of the R18 peptide control on the 14-3-3 γ /SLP76pS376 system.

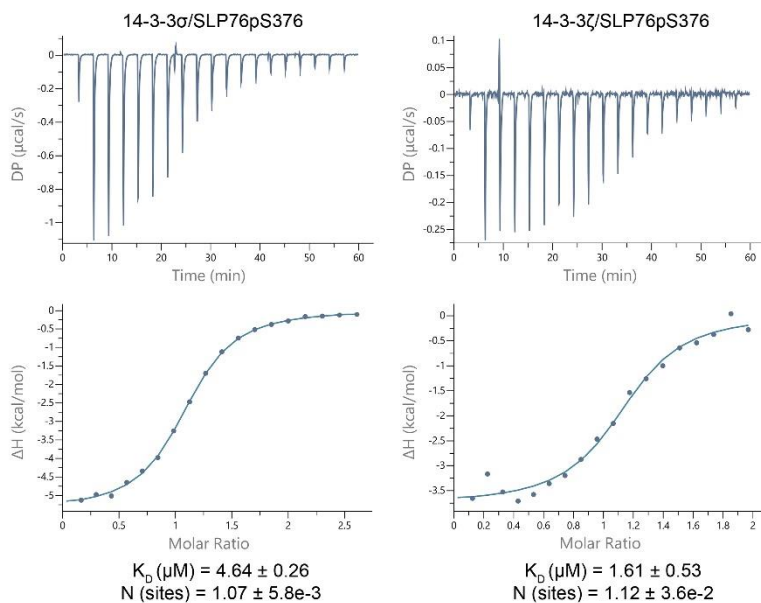


Figure S 3.2 | Additional ITC measurements of 14-3-3 σ /SLP76pS376 (left) and 14-3-3 ζ /SLP76pS376 (right).

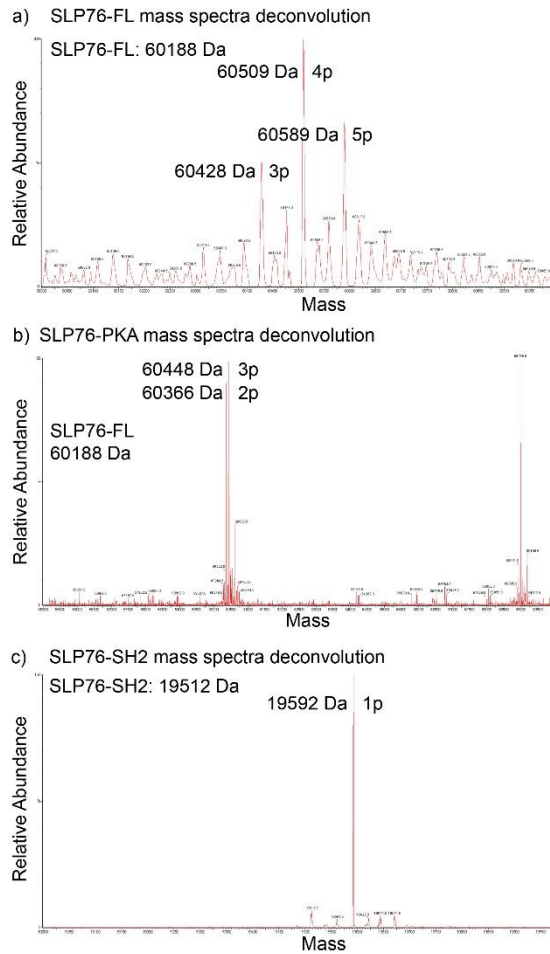


Figure S 3.3 | Deconvolution of the MS spectra of pSLP76-FL, SLP76-PKA and pSLP76-SH2. The expected molecular weight of the proteins in absence of phosphorylation is reported at the top left of the spectra for reference and has been used to calculate the number of phosphorylation events. a) Deconvolution of the pSLP76-FL MS spectra b) Deconvolution of the SLP76-PKA MS spectra c) Deconvolution of the p SLP76-SH2 MS spectra.

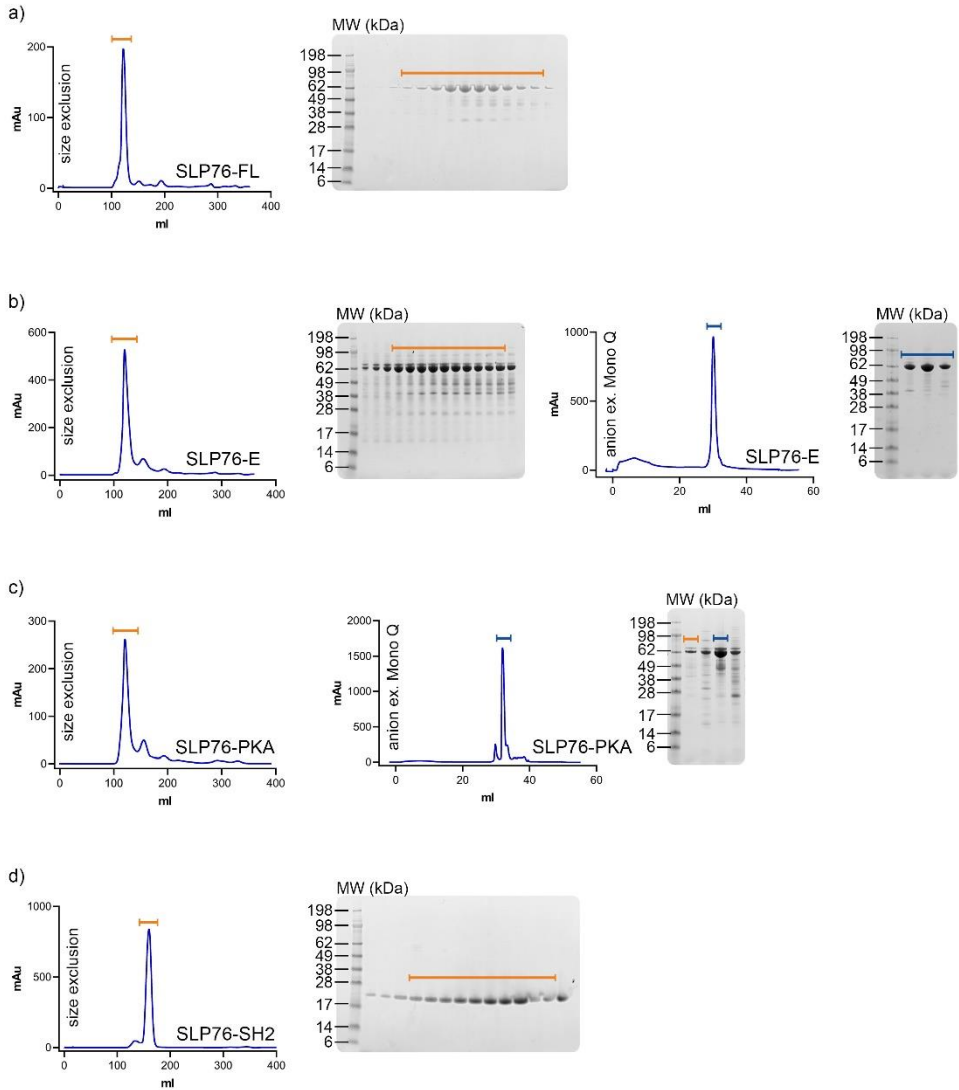


Figure S 3.4 | Last purification steps of the constructs SLP76-FL, SLP76-E, SLP76-PKA and SLP76-SH2. a) SEC profile and SDS-PAGE of the SLP76-FL construct. b) SEC and cation exchange profiles and SDS-PAGE of the SLP76-E construct. c) SEC and cation exchange profiles and SDS-PAGE of the SLP76-PKA construct. d) SEC profile and SDS-PAGE of the SLP76-SH2 construct.

Table S 3.1: Data collection and refinement statistics of the 14-3-3 σ /SLP76pS376 crystal structure.

Data collection	
Space group	C222 ₁
Cell dimensions	
a, b, c, (Å)	82.10, 111.87, 62.4
Resolution (Å)	66.19-1.53 (1.56-1.53)
R _{merge} (%)	0.035 (0.43)
<I/σ(I)>	20.1 (1.6)
Completeness (%)	99.1 (90.1)
Multiplicity	5.8 (2.5)
CC (1/2)	1.00 (0.78)
Refinement	
Resolution (Å)	66.19-1.53
No. Reflections	43290
R _{work} /R _{free}	0.17/0.19
No. Atoms	
Protein	2041
Water	314
B-factors(Å ²)	
Protein	27.54
Water	38.43
R.M.S.D.	
Bond lengths (Å)	0.008
Bond angles (°)	0.922
Ramachandran statistics (%)	
Favoured	98.74
Allowed	1.26
Outliers	0.00

3.6 References

- 1 Jackman, J. K. *et al.* Molecular cloning of SLP-76, a 76-kDa tyrosine phosphoprotein associated with Grb2 in T cells. *J Biol Chem* **270**, 7029-7032, doi:10.1074/jbc.270.13.7029 (1995).
- 2 Zhang, W., Sloan-Lancaster, J., Kitchen, J., Tribble, R. P. & Samelson, L. E. LAT: The ZAP-70 Tyrosine Kinase Substrate That Links T Cell Receptor to Cellular Activation. *Cell* **92**, 83-92, doi:10.1016/s0092-8674(00)80901-0 (1998).
- 3 Wu, J. N. & Koretzky, G. A. The SLP-76 family of adapter proteins. *Semin Immunol* **16**, 379-393, doi:10.1016/j.smim.2004.08.018 (2004).
- 4 Samelson, L. E. Signal transduction mediated by the T cell antigen receptor: the role of adapter proteins. *Annu Rev Immunol* **20**, 371-394, doi:10.1146/annurev.immunol.20.092601.111357 (2002).
- 5 Clements, J. L. Known and potential functions for the SLP-76 adapter protein in regulating T-cell activation and development. *Immunol Rev* **191**, 211-219, doi:10.1034/j.1600-065x.2003.00002.x (2003).
- 6 Koretzky, G. A., Abtahian, F. & Silverman, M. A. SLP76 and SLP65: complex regulation of signalling in lymphocytes and beyond. *Nat Rev Immunol* **6**, 67-78, doi:10.1038/nri1750 (2006).
- 7 Clements, J. L. *et al.* Requirement for the leukocyte-specific adapter protein SLP-76 for normal T cell development. *Science* **281**, 416-419, doi:10.1126/science.281.5375.416 (1998).
- 8 Pivniouk, V. *et al.* Impaired viability and profound block in thymocyte development in mice lacking the adaptor protein SLP-76. *Cell* **94**, 229-238, doi:10.1016/s0092-8674(00)81422-1 (1998).
- 9 Di Bartolo, V. *et al.* A novel pathway down-modulating T cell activation involves HPK-1-dependent recruitment of 14-3-3 proteins on SLP-76. *J Exp Med* **204**, 681-691, doi:10.1084/jem.20062066 (2007).
- 10 Shui, J. W. *et al.* Hematopoietic progenitor kinase 1 negatively regulates T cell receptor signaling and T cell-mediated immune responses. *Nat Immunol* **8**, 84-91, doi:10.1038/ni1416 (2007).
- 11 Wang, X. *et al.* Attenuation of T cell receptor signaling by serine phosphorylation-mediated lysine 30 ubiquitination of SLP-76 protein. *J Biol Chem* **287**, 34091-34100, doi:10.1074/jbc.M112.371062 (2012).
- 12 Lasserre, R. *et al.* Release of serine/threonine-phosphorylated adaptors from signaling microclusters down-regulates T cell activation. *J Cell Biol* **195**, 839-853, doi:10.1083/jcb.201103105 (2011).
- 13 Aitken, A. 14-3-3 proteins: a historic overview. *Semin Cancer Biol* **16**, 162-172, doi:10.1016/j.semcancer.2006.03.005 (2006).
- 14 Obsil, T. & Obsilova, V. Structural basis of 14-3-3 protein functions. *Semin Cell Dev Biol* **22**, 663-672, doi:10.1016/j.semcdb.2011.09.001 (2011).
- 15 Mackintosh, C. Dynamic interactions between 14-3-3 proteins and phosphoproteins regulate diverse cellular processes. *Biochem J* **381**, 329-342, doi:10.1042/BJ20031332 (2004).
- 16 Johnson, C. *et al.* Visualization and biochemical analyses of the emerging mammalian 14-3-3-phosphoproteome. *Mol Cell Proteomics* **10**, M110 005751, doi:10.1074/mcp.M110.005751 (2011).
- 17 Sluchanko, N. N. & Gusev, N. B. 14-3-3 Proteins and regulation of cytoskeleton. *Biochemistry (Moscow)* **75**, 1528-1546, doi:10.1134/s0006297910130031 (2011).
- 18 Sluchanko, N. N. Reading the phosphorylation code: binding of the 14-3-3 protein to multivalent client phosphoproteins. *Biochem J* **477**, 1219-1225, doi:10.1042/BCJ20200084 (2020).
- 19 Wang, X. *et al.* Down-regulation of B cell receptor signaling by hematopoietic progenitor kinase 1 (HPK1)-mediated phosphorylation and ubiquitination of activated B cell linker protein (BLNK). *J Biol Chem* **287**, 11037-11048, doi:10.1074/jbc.M111.310946 (2012).
- 20 Dar, A., Wu, D., Lee, N., Shibata, E. & Dutta, A. 14-3-3 proteins play a role in the cell cycle by shielding cdt2 from ubiquitin-mediated degradation. *Mol Cell Biol* **34**, 4049-4061, doi:10.1128/MCB.00838-14 (2014).
- 21 Andrei, S. A. *et al.* Stabilization of protein-protein interactions in drug discovery. *Expert Opin Drug Discov* **12**, 925-940, doi:10.1080/17460441.2017.1346608 (2017).
- 22 Wolter, M. *et al.* Fragment-Based Stabilizers of Protein-Protein Interactions through Imine-Based Tethering. *Angew Chem Int Ed Engl*, doi:10.1002/anie.202008585 (2020).

- 23 Guillory, X. *et al.* Fragment-based Differential Targeting of PPI Stabilizer Interfaces. *J Med Chem* **63**, 6694-6707, doi:10.1021/acs.jmedchem.9b01942 (2020).
- 24 Sijbesma, E. *et al.* Identification of Two Secondary Ligand Binding Sites in 14-3-3 Proteins Using Fragment Screening. *Biochemistry* **56**, 3972-3982, doi:10.1021/acs.biochem.7b00153 (2017).
- 25 Sijbesma, E. *et al.* Site-Directed Fragment-Based Screening for the Discovery of Protein-Protein Interaction Stabilizers. *J Am Chem Soc* **141**, 3524-3531, doi:10.1021/jacs.8b11658 (2019).
- 26 Molzan, M. & Ottmann, C. Synergistic binding of the phosphorylated S233- and S259-binding sites of C-RAF to one 14-3-3zeta dimer. *J Mol Biol* **423**, 486-495, doi:10.1016/j.jmb.2012.08.009 (2012).
- 27 Stevers, L. M. *et al.* Characterization and small-molecule stabilization of the multisite tandem binding between 14-3-3 and the R domain of CFTR. *Proc Natl Acad Sci U S A* **113**, E1152-1161, doi:10.1073/pnas.1516631113 (2016).
- 28 Stevers, L. M. *et al.* Structural interface between LRRK2 and 14-3-3 protein. *Biochemical Journal* **474**, 1273-1287, doi:10.1042/bcj20161078 (2017).
- 29 Yaffe, M. B. How do 14-3-3 proteins work? - Gatekeeper phosphorylation and the molecular anvil hypothesis. *FEBS Letters* **513**, 53-57, doi:10.1016/S0014-5793(01)03288-4 (2002).
- 30 Madeira, F. *et al.* 14-3-3-Pred: improved methods to predict 14-3-3-binding phosphopeptides. *Bioinformatics* **31**, 2276-2283, doi:10.1093/bioinformatics/btv133 (2015).
- 31 Petosa, C. *et al.* 14-3-3zeta binds a phosphorylated Raf peptide and an unphosphorylated peptide via its conserved amphipathic groove. *J Biol Chem* **273**, 16305-16310, doi:10.1074/jbc.273.26.16305 (1998).
- 32 Yaffe, M. B. *et al.* The structural basis for 14-3-3:phosphopeptide binding specificity. *Cell* **91**, 961-971, doi:http://doi.org/10.1016/S0092-8674(00)80487-0 (1997).
- 33 Johnson, C. *et al.* Bioinformatic and experimental survey of 14-3-3-binding sites. *Biochem J* **427**, 69-78, doi:10.1042/BJ20091834 (2010).
- 34 Sauer, K. *et al.* Hematopoietic progenitor kinase 1 associates physically and functionally with the adaptor proteins B cell linker protein and SLP-76 in lymphocytes. *J Biol Chem* **276**, 45207-45216, doi:10.1074/jbc.M106811200 (2001).
- 35 Ballone, A., Centorrino, F., Wolter, M. & Ottmann, C. Structural characterization of 14-3-3zeta in complex with the human Son of sevenless homolog 1 (SOS1). *J Struct Biol* **202**, 210-215, doi:10.1016/j.jsb.2018.01.011 (2018).
- 36 Centorrino, F., Ballone, A., Wolter, M. & Ottmann, C. Biophysical and structural insight into the USP8/14-3-3 interaction. *FEBS Lett* **592**, 1211-1220, doi:10.1002/1873-3468.13017 (2018).
- 37 Sluchanko, N. N. Association of Multiple Phosphorylated Proteins with the 14-3-3 Regulatory Hubs: Problems and Perspectives. *J Mol Biol* **430**, 20-26, doi:10.1016/j.jmb.2017.11.010 (2018).
- 38 Lin, S., Shih-Yuan Lee, A., Lin, C.-C. & Lee, C.-K. Determination of Binding Constant and Stoichiometry for Antibody-Antigen Interaction with Surface Plasmon Resonance. *Current Proteomics* **3**, 271-282, doi:10.2174/157016406780655586 (2006).
- 39 Ottmann, C. Protein-Protein Interactions. *Drug Discov Today Technol* **24**, 1-2, doi:10.1016/j.ddtec.2017.11.008 (2017).
- 40 Schumacher, B., Skwarczynska, M., Rose, R. & Ottmann, C. Structure of a 14-3-3 σ -YAP phosphopeptide complex at 1.15 Å resolution. *Acta Crystallographica Section F Structural Biology and Crystallization Communications* **66**, 978-984, doi:10.1107/s1744309110025479 (2010).
- 41 Kabsch, W. Integration, scaling, space-group assignment and post-refinement. *Acta Crystallogr D Biol Crystallogr* **66**, 133-144, doi:10.1107/S0907444909047374 (2010).
- 42 Evans, P. R. An introduction to data reduction: space-group determination, scaling and intensity statistics. *Acta Crystallogr D Biol Crystallogr* **67**, 282-292, doi:10.1107/S090744491003982X (2011).
- 43 Winn, M. D. *et al.* Overview of the CCP4 suite and current developments. *Acta Crystallogr D Biol Crystallogr* **67**, 235-242, doi:10.1107/S0907444910045749 (2011).
- 44 McCoy, A. J. *et al.* Phaser crystallographic software. *J Appl Crystallogr* **40**, 658-674, doi:10.1107/S0021889807021206 (2007).
- 45 Emsley, P. & Cowtan, K. Coot: model-building tools for molecular graphics. *Acta Crystallogr D Biol Crystallogr* **D60**, 2126-2132, doi:10.1107/S0907444904019158 (2004).
- 46 Adams, P. D. *et al.* PHENIX: a comprehensive Python-based system for macromolecular structure solution. *Acta Crystallogr D Biol Crystallogr* **66**, 213-221, doi:10.1107/S0907444909052925 (2010).

The Native MS experiments were performed by Dr.Rebecca Burnely and Dr. Victoria Ellis. The SPR experiments were performed in collaboration and under the supervision of Dr. Mara Westwood.

Chapter 4

TR-FRET and FP Assay Development for the discovery of 14-3-3/SLP76 PPI stabilisers

Abstract

Assay development is an important step in the lead generation phase of every drug discovery project. It is essential that the chosen assay reach the standards of reproducibility and robustness that would allow to unequivocally detect variations attributable to compounds exposure. In this chapter, a Time-Resolved Fluorescence Energy Transfer (TR-FRET) assay has been developed on the 14-3-3 γ /SLP76-SH2 system. The assay will be implemented to run a High Throughput Screening (HTS) and in the subsequent phases of hits characterization. Additionally, a second Fluorescence Polarization assay has been validated on the SLP76pS376 shorter peptidic system. This assay will be used complementary to the TR-FRET one in the second phase of hits characterization.

4.1 Introduction

In this chapter the steps that have been performed on the 14-3-3 γ /SLP76-SH2 and on the 14-3-3 γ /SLP76pS376 systems to validate the assays for the identification of small molecule stabilisers will be described.

4.1.1 Fluorescence Resonance Energy Transfer principles

Fluorescence Resonance Energy Transfer, most commonly referred to as FRET, is a non-radiative transfer of energy that occurs from an excited donor molecule to a matched acceptor molecule as a consequence of a close proximity between the two (typically 10 to 100 Å) ^{1,2}.

The FRET phenomenon can be implemented in the detection and characterisation of interactions between biomolecules like proteins, provided they are labelled with the appropriate FRET pair of acceptor and donor. The proximity of the two molecules results in a FRET signal, which is directly proportional to the amount and strength of the interacting molecules ³. One downside of FRET, especially when applied to assays designed to identify modulators of a PPI, is that the compounds are often excited alongside with the donor molecule. This causes an additional read-out from the compounds that are not necessarily hits, resulting in false positives.

Time-Resolved Fluorescence Electron Transfer, TR-FRET, compensates for that issue by making large use of lanthanides as donor molecules which are known for their extended fluorescence lifetime ^{4,5}. One great advantage of longer fluorescent emission is that it can allow a delayed detection of the signal read-out. This gives time to the shorter fluorescent emissions, originating from either compounds or other macromolecules, to decay ⁶. The rapid development of FRET related technologies in the last decades allowed to combine the FRET phenomenon with the TR-FRET technology, giving rise to Homogeneous Time Resolved Fluorescence, or HTRF ⁷. HTRF exploits a ratiometric read-out by calculating the ratio of the fluorescence of the acceptor over the fluorescence of the donor (Figure 4.1). Calculating the ratio of the two emission wavelengths instead of using a single wavelength, allows to compensate for well to well differences which could lead to misleading results ⁷. Media variability and signal interference are cancelled and only the read-out of the interaction under investigation is taken into consideration.

This technology is now widely used for the detection and characterization of biomolecular interactions and can be implemented in high throughput screenings campaigns ^{7,8}.

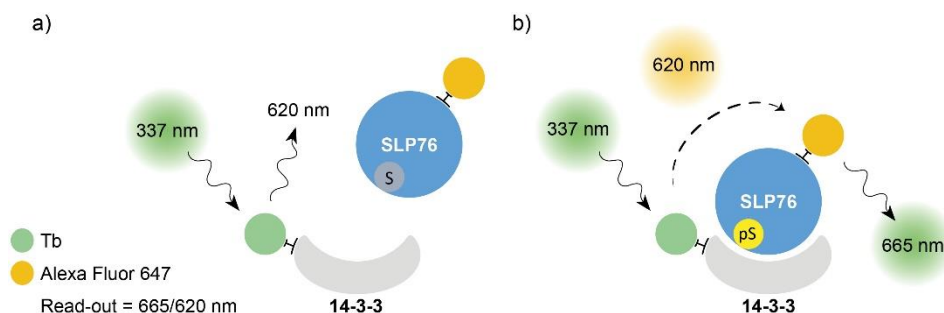


Figure 4.1 | Cartoon representation of the HTRF setup implemented in this work. The two proteins of interest, SLP76 and 14-3-3 γ have been labelled with Tb and AF647 respectively to generate a suitable matched pair of donor molecule (Tb) and acceptor molecule (AF647). a) The donor molecule, Tb labelled 14-3-3, is excited at the proper wavelength of 337 nm. However, because the corresponding acceptor is not in the proximity (no binding) no signal is detected. b) SLP76 bound to 14-3-3 brings the acceptor molecule AF647 close to the donor, allowing energy transfer from one to the other. A radiation with the wavelength of 665 nm is consequently emitted to generate a detectable signal. The read-out is the ratio of the light emitted at 665 nm over the light emitted at 620 nm.

4.1.2 14-3-3 inhibitor R18 as a tool to probe 14-3-3 PPIs

A peptidic inhibitor of 14-3-3 was identified by phage display⁹. The antagonist is a 20-mer peptide, called R18, with the following amino acid sequence: PHCVPRDLSWLDLEANMCLP. R18, it was shown to inhibit the 14-3-3/Raf-1 protein-protein interaction without showing any 14-3-3 isoform selectivity¹⁰. R18 binds to 14-3-3 τ , 14-3-3 β and 14-3-3 ζ with \approx 80 nM affinity⁹. Its tight binding to 14-3-3 regardless of the isoform makes it a valuable tool to probe 14-3-3 PPIs. In the context of this work, the R18 peptide has been used in the preliminary assay development process of an HTS for the identification of the SLP76/14-3-3 γ PPI stabilisers.

A crystal structure of the R18 peptide has been solved in complex with 14-3-3 ζ ¹¹. The crystal structure elucidates how R18 binds to 14-3-3 ζ *via* its canonical amphipathic groove, which most of the time accommodates biologically relevant phosphorylated motifs. The structural binding characterization also explains how R18 acts as an inhibitor of 14-3-3 proteins exploiting a WLDLE motif for binding to 14-3-3 proteins. In Figure 4.2 a superposition has been performed between the 14-3-3 ζ /R18 crystal structure (PDB ID: 1A38) and the 14-3-3 σ /SLP76 crystal structure solved as part of the work presented in this thesis (PDB ID: 6ZCJ). Although the superposition occurs between two different 14-3-3 isoforms, the 14-3-3 residues involved in the binding of the R18 and SLP76 peptides within the amphipathic groove are conserved among all 7 isoforms. From the picture it is possible to observe how the R18 peptide in yellow occupies the same position as, in this case, the SLP76-derived synthetic peptide (Figure 4.2). At the appropriate concentration, the R18 peptide can therefore displace 14-3-3 binding partners by replacing them in the canonical binding site.

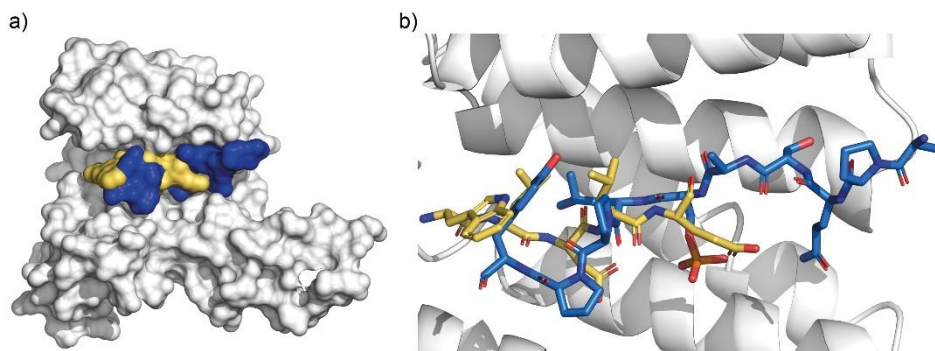


Figure 4.2 | Superposition of the 14-3-3 ζ /R18 (1A38) and the 14-3-3 σ /SLP76 (6ZCJ) crystal structures. a) Surface representation of R18 and SLP76 bound to 14-3-3. 14-3-3 σ is represented as white surface, the R18 peptide is represented as yellow surface and the SLP76 peptide is represented as blue surface. b) Sticks and cartoon representation of R18, SLP76 and 14-3-3 σ respectively. SLP76 peptide (blue sticks) is bound to 14-3-3 σ . The R18 peptide (yellow sticks) superposed on the 14-3-3 σ /SLP76 structure occupies the same spot as the SLP76 peptide, revealing the inhibitory mechanism of R18.

4.2 Results and Discussion

4.2.1 Preliminary binding tests of SLP76-SH2 to 14-3-3 γ and titration of SLP76-SH2 over 14-3-3 γ defines the final 14-3-3 γ assay concentration

SLP76-SH2 was initially titrated against different concentrations of 14-3-3 γ (0.1, 0.3, 1, 3 and 10 nM) to test whether the binding would occur in an HTRF setup using labelled SLP76-SH2 and 14-3-3 γ (Figure 4.3). The HTRF signal raised proportionally to the increase in concentration of SLP76-SH2, as expected in the case of a binding event. However, the titration curves showed a certain degree of non-specific binding at higher SLP76-SH2 concentrations, due to the high concentration of fluorophore present in solution. The titration curves in fact do not show a plateau but a rather sharp and constant linear signal increase (Figure 4.3). In order to understand whether the nature of this PPI would provide an appreciable specific signal increase under this HTRF setup, the same assay was repeated in the presence of R18 at 10 μ M (Figure 4.4). From Figure 4.4 it is possible to observe how non-specific binding affects the shape of the titration curves. By being a 14-3-3 inhibitor, the R18 peptide at that concentration is supposed to compete with SLP76-SH2 and completely prevent its binding to 14-3-3 γ . All the signal generated by that titration curve can therefore be associated with non-specific binding. Consequently, the subtraction of the values of the curve in the presence of R18 (non-specific) from the values of the curve in absence of it (non-specific + specific) generates a curve which is attributable only to the specific binding of 14-3-3 γ and SLP76-SH2 (Figure 4.4).

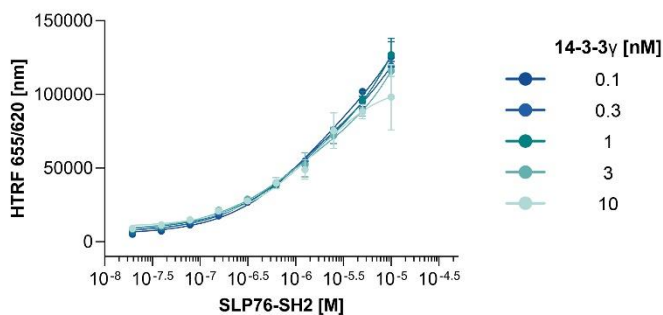


Figure 4.3 | Binding saturation assay obtained by titrating SLP76-SH2 over different concentrations of 14-3-3 γ .

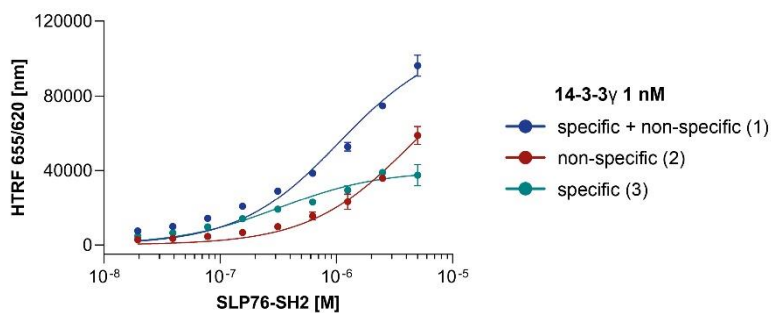


Figure 4.4 | Illustration of the non-specific binding effect observed for SLP76-SH2 binding to 14-3-3 γ at 1 nM. The blue curve represents the totality of the binding: SLP76-SH2 binding specifically to 14-3-3 γ with the addition of non-specific binding. The red curve represents the same titration curve with the addition of a constant concentration of R18, at 10 μ M. The trend of the curve is linear and directly proportional to the increase of fluorophore attached to SLP76-SH2. The aquamarine curve represents the subtraction of curve 2 from curve 1, generating a specific binding curve.

In order to define the optimal concentration of Tb-labelled 14-3-3 γ to use in the HTS (High Throughput Screening), the binding saturation assay at different 14-3-3 γ concentrations was repeated in the presence of 10 μ M R18 (Figure 4.5). The final 14-3-3 γ concentration was chosen considering the assay stability and reagent consumption. Since Tb-labelled samples are expensive we wanted to minimise the amount of 14-3-3 γ -Tb used in every step of the assay development, the HTS and the follow-up of hits. The concentration chosen was 1 nM because it generated the first stable curve of the series with a calculated K_D comparable to 3 and 10 nM of Tb-labelled 14-3-3.

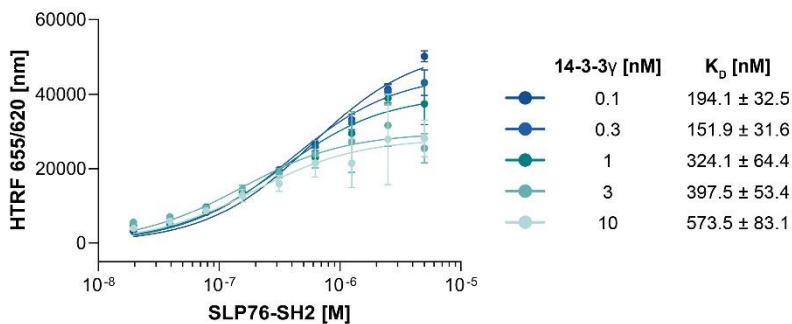


Figure 4.5 | Binding saturation assay obtained by titrating SLP76-SH2 over different concentrations of 14-3-3γ. For each curve, the non-specific binding signal has been subtracted.

Up to this point, the work has been carried out in parallel with another 14-3-3 protein target which is described in this thesis: BLNK. Like SLP76, BLNK is involved in an analogous pathway downstream of BCRs. Given our interest in the identification of small molecule stabilisers of addressable biological targets, we performed these initial assay development stages on BLNK as well.

As for SLP76, a shorter construct of BLNK has been designed, expressed and purified, BLNK-SH2. The two constructs showed a remarkable degree of analogy in terms of the success in the challenging and demanding processes of production, purification and phosphorylation *in vitro*. It was then logical to work on both constructs in parallel in order to maximise the chances of success. BLNK-SH2 was labelled with AF-647 as SLP76-SH2 and titrated on a fixed 14-3-3γ concentration. The same identical titration was repeated in the presence of R18 to assess the contribution of non-specific binding (Figure 4.6). At this point, a comparison with SLP76-SH2 was necessary to spot potential differences and to identify the best construct to focus on for the next steps.

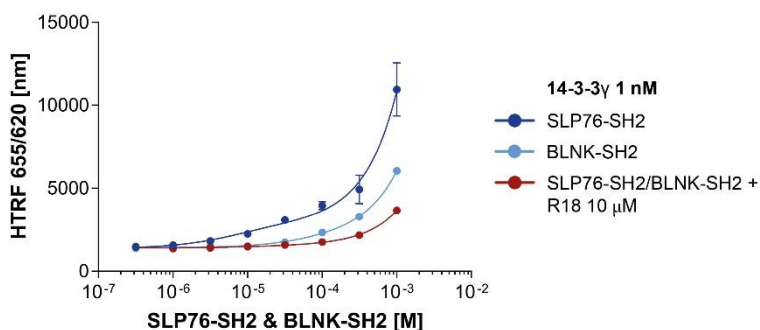


Figure 4.6 | Comparison of the binding assay of SLP76-SH2 and BLNK-SH2 to 14-3-3γ in the presence and absence of R18.

The assay clearly showed that R18 is capable of inhibiting both interactions. The signal is in fact significantly lower in the presence of R18. It is also possible to notice how SLP76-SH2 at the same concentration as BLNK-SH2 generates a higher signal. This is most likely attributable to the higher affinity of SLP76-SH2 to 14-3-3 γ compared to BLNK-SH2. The signal generated from BLNK-SH2 is unfortunately too small and the assay window between the non-specific and specific signal too narrow. BLNK-SH2 does not possess the ideal features that would allow us to keep working on it. One could argue that it could be easier to identify small molecule stabilisers of a PPI with a lower affinity, because the room to improve that affinity would be higher. However, it is also necessary to consider the practicalities and consumables that a delicate experiment such as an HTS requires. Our preference was therefore to prioritize the SLP76-SH2 project.

4.2.2 R18 competitive assay validates the assay and defines its final concentrations

Reversible competitive inhibition is a condition that applies when given an enzyme and a substrate, or a protein “A” and a protein “B”, their interaction can be reversibly inhibited. The higher the inhibitor concentration, the more substrate or protein is displaced from its binding site. As the reaction reversible, the ligand has the same effect as the inhibitor if we look at it from the opposite perspective ¹². The relationship between inhibitor and substrate/protein is therefore strictly related to their concentration and is described by the Cheng-Prusoff equation ¹³. In order to validate the assay and define the SLP76-SH2 concentration to use in the HTS, a competitive inhibition assay has been implemented, exploiting the R18 inhibitor.

The assay has been designed in a way that identical titrations of SLP76-SH2 against 14-3-3 γ are repeated in the presence of increasing concentrations of R18 inhibitor (Figure 4.7). From a minimum of 0 μ M, as a reference, to a maximum of 10 μ M where the SLP76-SH2/14-3-3 γ interaction is completely blocked. The assay has been fitted with a competitive inhibition model (the Cheng-Prusoff equation) from which it was possible to calculate the K_D of the SLP76-SH2/14-3-3 γ interaction as well as the K_i , the R18 inhibition constant to the SLP76-SH2/14-3-3 γ interaction. The calculated K_D , 524.1 nM \pm 48.5 nM, provided the SLP76-SH2 concentration to use in the HTS. The value was in the later stages approximated to 600 nM. The calculated R18 K_i , 9.1 nM \pm 0.7 nM, provided an additional confirmation of the quality of the assay since the value could be compared with the number already present in the literature: \approx 80 nM ^{9,11}. The R18 peptide competitively inhibits the SLP76-SH2/14-3-3 γ system, therefore validating the assay (Figure 4.7).

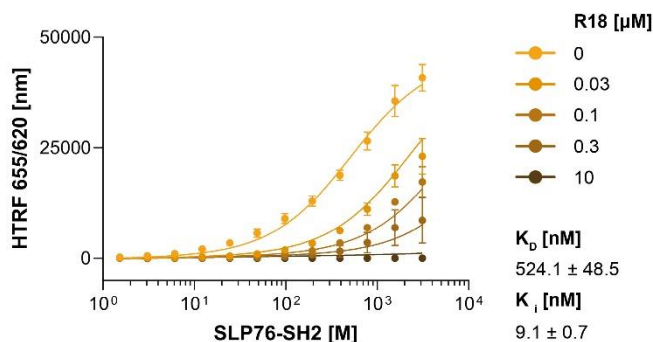


Figure 4.7 | R18 Competitive inhibition assay using R18. Identical titrations of SLP76-SH2 on 14-3-3γ were performed, in the presence of increasing R18 concentrations. The R18 peptide was tested at concentrations between 0 μM and 10 μM. Each curve is colour coded from light orange to dark orange respectively. The K_D and the K_I calculated from the model are reported below the legend.

4.2.3 R18 inhibition assay and DMSO tolerance defines final assay conditions and Z'

The SLP76-SH2 and 14-3-3γ concentrations to use in the HTS were determined and the HTRF assay has been validated. An additional assay allowed us to test for the DMSO tolerance of the system and to calculate the R18 IC₅₀'s in the presence of 0 %, 1 %, 2 % and 5 % DMSO.

The assay was essentially an R18 inhibition assay. R18 was titrated against constant SLP76-SH2 and 14-3-3γ concentrations: 600 nM and 1 nM respectively. These concentrations are the ones that will be used in the actual HTS (Figure 4.8). The assay plate setup was also designed to be as close as possible to the final assay having the first two columns dedicated to the DMSO control, and the last two columns dedicated to the negative control, R18 at 1 μM (Figure 4.8a). The R18 was added to columns 3 to 22 dissolved in 100% DMSO, mimicking the addition of a small molecule dissolved in 100% DMSO, an important detail in an assay development process. The correct dilutions provided the desired final DMSO concentration in the wells.

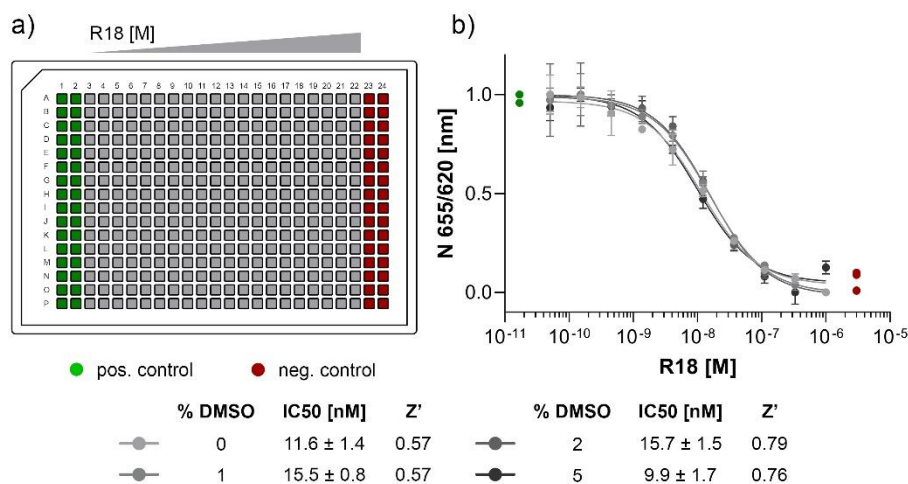


Figure 4.8 | Assay plate setup and R18 inhibition assay fitting curves. a) A cartoon representation of an assay plate shows the standard assay setup for this stage. Columns 1 and 2 contain the DMSO control composed of either 0%, 1%, 2% or 5% DMSO. Columns 23 and 24 contain the R18 negative control, composed of R18 at 1 μM in either 0%, 1%, 2% or 5% DMSO. The HTRF signal has been normalised to 1 for the maximum response (green dots) and to 0 for the minimum one (red dots).

The fitting curves allowed to calculate R18 IC₅₀s in the presence of different percentages of DMSO. The calculated values resulted to be all within a 1-fold difference to one another, despite the presence of increasing concentrations of DMSO. This provided a first confirmation of the robustness of the assay. The plate columns dedicated to the controls allowed to calculate the Z', an important statistical parameter used to determine any assay quality based on their controls¹⁴. The Z' can be calculated with the following formula: $Z' = 1 - [(3\sigma_{c+} + 3\sigma_{c-}) / (\mu_{c+} - \mu_{c-})]$ where σ_{c+} and σ_{c-} are the standard deviations of the DMSO control and the negative control respectively, and μ_{c+} and μ_{c-} are the mean of the DMSO control and the negative control respectively. The Z' factor can only take values between 0 and 1. An excellent assay normally has Z' values between 0.5 and 1, and ensures that the assay possesses a good enough signal window to identify potential hits¹⁴.

All the Z' factor values calculated for the SLP76-SH2/14-3-3 γ interaction at the varying DMSO percentages met the expectations in terms of assay quality (Figure 4.8b). Moreover, the assay showed to be more stable, having higher Z' factor values, towards higher DMSO concentrations. This situation is ideal because an assay that can take higher DMSO concentration is more likely to avoid compounds precipitation providing more range to the assay.

Altogether, the results obtained from this R18 inhibition assay ultimately defined the assay conditions and assessed its robustness.

4.2.4 Automated liquid handling tests complete the final assay development process

A High Throughput Screening that involves tens of thousands of small molecules is a delicate process. It should be avoided having to repeat the assay because of piece of equipment failures. Automated liquid handling robots therefore need to be tested in advance multiple times to assure their proper function under the same assay conditions that has been defined in the previous steps. Every single step needs to be as close as possible to the actual screening. The Z' factor is again used to evaluate the quality of the assay.

A few plates containing the protein mixture at the defined concentrations, the DMSO control, the negative control and 5% DMSO mimicking the compounds over all the rest of the plates, have been tested in few different days (Figure 4.9). Despite the Z' factors calculated for all the tests indicating ideal assay conditions, test 1 and 2 showed a drifting effect towards the end of the plate. The specific trend the drifting effect took indicated a potential serial fault in pipetting and/or a sealing defect rather than aleatory events. Drifting effects like that could seriously impair the process of hit selection of an HTS and could question the entire fate of the experiment. The faults were addressed promptly, and further tests (3 and 4) have been performed to confirm their resolution. The assay was demonstrated to be robust enough, also after overnight incubation at room temperature (Figure 4.9).

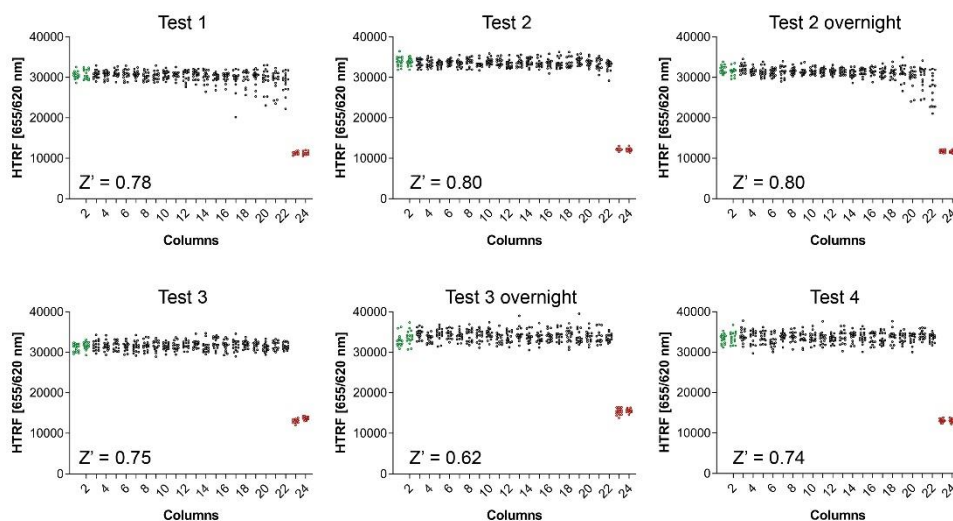


Figure 4.9 | Automated liquid handling plate tests. The graph plots represent the plate read-outs. The green dots represent the DMSO controls, which in this case are formally identical to the other wells being all supplemented with 5% DMSO. The red dots represent the R18 negative control.

4.2.5 Fluorescence polarization assay validation for 14-3-3 γ /SLP76pS376 and 14-3-3 γ /BLNKpT152

The fluorescence polarization assay was developed starting by titrating 14-3-3 γ on different constant concentrations of SLP76pS376 FITC labelled peptide: 10, 50 and 100 nM (Figure 4.10a) in order to define the assay concentrations. The 14-3-3 γ isoform was chosen for consistency with the HTS work. The K_D calculated from the fitting curves showed to be very comparable. We have therefore chosen the lowest concentration of labelled peptide to use in the further steps of the assay: 10 nM. To validate the assay and DMSO tolerance we used the R18 peptide as we did before (Figure 4.10b, c). The R18 peptide was titrated in an inhibition assay on constant 14-3-3 γ /peptide concentrations in the presence of 0 %, 1 %, 2 % and 5 % DMSO. IC₅₀s values and Z' factors were calculated based on this assay. We also validated the 14-3-3 γ /BLNKp152 system (Figure 4.10c) with the intent to use it as a counter screen for compounds testing. The R18 peptide showed to inhibit both systems in all the DMSO concentrations tested. The IC₅₀s values calculated from the inhibition curves were all comparable and were in the low micromolar range. The values for the 14-3-3 γ /BLNKpT152 system were slightly higher in all DMSO concentration and that is explained by the fact that the concentration of 14-3-3 γ in that specific assay was 2 μ M rather than 600 nM (as for the 14-3-3 γ /SLP76pS376 system). IC₅₀s values depend in fact on the assay conditions. Both assays were designed in a way that allowed to calculate Z' factors. The first two and last two columns of the assay plates were in fact dedicated to the DMSO and the negative control (R18 10 μ M) respectively. Regardless of the DMSO concentrations all the Z' factors calculated were higher than 0.75 with the one at 5% DMSO, higher than 0.91. These tests qualified the assays as excellent, sensible and robust enough to detect variations attributable to potential compound titrations.

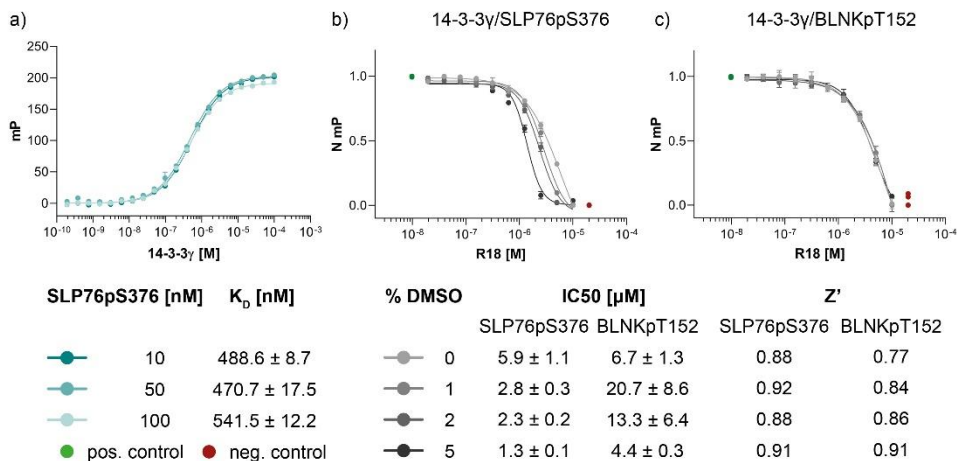


Figure 4.10 | Assay development steps for the 14-3-3 γ /SLP76pS376 and 14-3-3 γ /BLNKpT152 systems. a) Binding saturation curves of 14-3-3 γ on different concentrations of labelled peptide. K_D values are reported below. b), c) R18 inhibition assays for the 14-3-3 γ /SLP76pS376 and 14-3-3 γ /BLNKpT152 systems. IC₅₀'s values and Z' factors are reported below. The green dots represent the positive control and the red dots represent the negative control. The dots are the result of

the average of the read-out of 16 wells of the first two and last two columns of the plate and they have been used in the Z' factor calculation.

4.3 Conclusions

In this chapter we implemented and developed a TR-FRET assay aimed at the identification of modulators of the 14-3-3/SLP76 PPI. A BLNK construct was tested as well in the initial stages of the assay development process. However, it did not prove to be a good candidate to bring further into the HTS steps. The extended use of the commercially available 14-3-3 inhibitor R18 proved to be useful on few different aspects. Firstly, it allowed to discriminate between non-specific and specific FRET signal. Secondly, it was used in a competitive inhibition assay to validate the screening assay and to determine the final assay concentrations. Finally, it was used to determine DMSO tolerance, assay robustness and it will be used as the assay control in every phase of the HTS and follow-up of the hits.

A fluorescent polarization assay was also validated for two peptidic targets: SLP76pS376 and BLNKpT152. The intent will be to use it as additional tool to test compounds active in the primary TR-FRET assay to identify potential connections between the SLP76-SH2 system and the SLP76pS376 peptide system.

4.4 Material and Methods

TR-FRET manual assay development steps: 14-3-3 γ and SLP76-SH2 concentration determination

For all the initial assays, Corning 384-well 3574 assay plates were used. AF647 labelled SLP76-SH2 was titrated from a top concentration of 10 μ M, 5 μ M and 3 μ M following a 2 or 3-fold dilution against fixed concentrations of Tb labelled 14-3-3 γ : 0.1 nM, 0.3 nM, 1 nM, 3 nM and 10 nM. Identical titrations were performed in the constant presence of R18 at 10 μ M to identify the non-specific signal. The non-specific signal was then subtracted from the total read-out before the fitting to generate the specific signal. For the R18 competitive inhibition assay, AF647 labelled SLP76-SH2 was titrated from a top concentration of 3 μ M following a 2-fold dilution against Tb labelled 14-3-3 γ at 1 nM. Every single titration was repeated in the presence of constant concentrations of R18 at 0 μ M, 0.03 μ M, 0.1 μ M, 0.3 μ M and 10 μ M. The titration in the presence of R18 at 10 μ M was subtracted from all the others generating specific signal. All the reagents were diluted in the assay buffer: 50 mM Tris pH 7.5, 150 mM NaCl, 5mM MgCl₂, 0.05% v/v Tween-20 and mixed in the Corning 384-well 3574 assay plate to reach the final assay volume of 30 μ L, that is 10 μ L per reagent (Tb labelled 14-3-3, AF647 labelled SLP76-SH2 and R18). The data were collected on a PHERAstar FSX plate reader (BMG Labtech) with an λ_{ex} of 337 nm, λ_{em} of 665 nm and 620 nm HTRF filter setting. All the data were exported in GraphPad Prism version 8.1.1 for Windows (GraphPad Software, La Jolla California USA, www.graphpad.com). The data were fitted with “One site - Specific binding model”, “One site - Total binding model” and “Competitive inhibition binding model”. Each data point is the average of a triplicate or quadruplicate measurement, the standard deviation is reported as error bars.

TR-FRET automated assay development steps: DMSO tolerance and assay robustness determination

For the R18 inhibition and DMSO tolerance assay, columns 1 and 2 of four Corning 384-well 3574 assay plates were pre-filled with 2 μ L of 0%, 20%, 40% and 100% DMSO in assay buffer, using a Multidrop Dispenser (ThermoScientific). The assay buffer contained 50 mM Tris pH 7.5, 150 mM NaCl, 5mM MgCl₂ and 0.05% v/v Tween-20. Similarly, columns 23 and 24 were pre-filled with 2 μ L of R18 peptide dissolved at 20 μ M in the assay buffer containing 0%, 20%, 40% and 100% DMSO. 40 μ L of protein mixture, composed of 14-3-3 γ -Tb at 1 nM and SLP76-SH2-AF647 at 600 nM in assay buffer, were added to columns 1, 2, 23 and 24 with a Multidrop Dispenser (ThermoScientific). This way, final concentrations of 1 μ M R18 and 0%, 1%, 2% and 5% DMSO were reached.

For generating the inhibition curve, R18 was pre-diluted following a 2-fold dilution series from a top concentration of 20 μ M. 2 μ L of the R18 dilution series in assay buffer containing 0%, 20%, 40% and 100% DMSO were added in duplicates from column 3 to column 22 of the assay plate. 40 μ L of the protein mixture in assay buffer were consequently added on top, to give four inhibition curves at 0%, 1%, 2% and 5% DMSO. The data were collected on a PHERAstar FSX plate reader (BMG Labtech) with an λ_{ex} 337 nm, λ_{em} 665 nm and 620 nm HTRF filter setting. All the data were exported in GraphPad Prism version 8.1.1 for Windows (GraphPad Software, La Jolla California USA, www.graphpad.com). Before fitting, the data were normalised defining the negative control, R18 columns 23 and 24, as 0 and the DMSO control, columns 1 and 2, as 1. The data were fitted with a “Dose-response - inhibition binding model”. Each data point is the average of a duplicate measurement, the standard deviation is reported as error bars. Z' factors were calculated from the DMSO control (columns 1 and 2) and negative control (columns 23 and 24).

Assay robustness was tested by preparing Corning 384-well 3574 assay plates pre-filled with a Multidrop Dispenser (ThermoScientific) as described above. 2 μ L of 100% DMSO were dispensed throughout the entire plate, except for columns 23 and 24 which were filled with 2 μ L of R18 peptide dissolved at 20 μ M in 100% DMSO. 40 μ L of protein mixture in assay buffer were added to all the wells. 30 μ L were then transferred by a Biomek FXP Automated Workstation (Beckman Coulter) into a new set of Corning 384-well 3574 assay plates to get the final assay conditions and volumes. The plates were sealed and incubated with gently shaking for 4h before reading the plates. Additional readings to check robustness were performed after overnight incubation as well. The data were collected on a PHERAstar FSX plate reader (BMG Labtech) with an λ_{ex} 337 nm, λ_{em} 665 nm and 620 nm HTRF filter setting. All the data were exported in GraphPad Prism version 8.1.1 for Windows (GraphPad Software, La Jolla California USA,

www.graphpad.com), and plotted on columns over read-out graphs. Z' factors were calculated from the DMSO control (columns 1 and 2) and negative control (columns 23 and 24).

Fluorescence Polarization validation assay for SLP76pS376 and BLNKpT152

FP binding saturation curves on 14-3-3 γ /SLP76pS376 were performed as described in Chapter 3. For the R18 inhibition and DMSO tolerance assay, columns 1 and 2 of four Corning 384-well 3574 assay plates were filled with 10 μ L of assay buffer (50 mM Tris pH 7.5, 150 mM NaCl, 5 mM MgCl₂, 0.05% v/v Tween-20) containing DMSO at the final concentration of 0%, 1%, 2% and 5%; 10 μ L SLP76pS376 and BLNKpT152 FITC-labelled at 10 nM; 10 μ L 14-3-3 γ -FL at 600 nM for the SLP76pS376 case and 2 μ M for the BLNKpT152 case for a final volume of 30 μ L. Columns 23 and 24 contained the same volumes and concentrations of FITC-labelled peptides and 14-3-3 γ with the addition of R18 at 10 μ M diluted in buffer containing DMSO at the final concentration of 0%, 1%, 2% and 5%. FITC-labelled peptides and 14-3-3 γ were added at columns 3 to 22 in the same volumes and concentrations. Finally, an R18 2-fold dilution series from a top concentration of 10 μ M was added in 10 μ L to provide the titration inhibition curve at different DMSO concentration (buffer, 1%, 2% and 5%). The data were collected on a PHERAstar FSX plate reader (BMG Labtech) with an λ_{ex} 485 nm, λ_{em} 520 nm FP filter setting. For K_D calculation the background polarization was removed from all values and the data were fitted with a "One site - Specific binding model" on GraphPad Prism version 8.1.1 for Windows (GraphPad Software, La Jolla California USA, www.graphpad.com). For the R18 inhibition curves the data were normalized setting 0 as the maximum R18 inhibition achieved and 1 the DMSO control. The data were fitted with a "[Inhibitor] vs. response - Variable slope (four parameters) model". Each data point is the average of a triplicate measurement, standard deviation is reported as error bars.

4.5 References

- 1 Sahoo, H. Förster resonance energy transfer – A spectroscopic nanoruler: Principle and applications. *Journal of Photochemistry and Photobiology C: Photochemistry Reviews* **12**, 20-30, doi:10.1016/j.jphotochemrev.2011.05.001 (2011).
- 2 Valeur, B. & Berberan-Santos, M. N. *Molecular Fluorescence*. (2012).
- 3 Piston, D. W. & Kremers, G. J. Fluorescent protein FRET: the good, the bad and the ugly. *Trends Biochem Sci* **32**, 407-414, doi:10.1016/j.tibs.2007.08.003 (2007).
- 4 Selvin, P. R. Principles and biophysical applications of lanthanide-based probes. *Annu Rev Biophys Biomol Struct* **31**, 275-302, doi:10.1146/annurev.biophys.31.101101.140927 (2002).
- 5 Bazin, H., Trinquet, E. & Mathis, G. Time resolved amplification of cryptate emission: a versatile technology to trace biomolecular interactions. *J Biotechnol* **82**, 233-250, doi:10.1016/s1389-0352(01)00040-x (2002).
- 6 Degorce, F. *et al.* HTRF: A technology tailored for drug discovery - a review of theoretical aspects and recent applications. *Curr Chem Genomics* **3**, 22-32, doi:10.2174/1875397300903010022 (2009).
- 7 Degorce, F. HTRF((R)): pioneering technology for high-throughput screening. *Expert Opin Drug Discov* **1**, 753-764, doi:10.1517/17460441.1.7.753 (2006).
- 8 Milroy, L. G., Grossmann, T. N., Hennig, S., Brunsvelde, L. & Ottmann, C. Modulators of protein-protein interactions. *Chem Rev* **114**, 4695-4748, doi:10.1021/cr400698c (2014).
- 9 Wang, B. *et al.* Isolation of high-affinity peptide antagonists of 14-3-3 proteins by phage display. *Biochemistry* **38**, 12499-12504, doi:10.1021/bi991353h (1999).
- 10 Thorson, J. A. *et al.* 14-3-3 proteins are required for maintenance of Raf-1 phosphorylation and kinase activity. *Mol Cell Biol* **18**, 5229-5238, doi:10.1128/mcb.18.9.5229 (1998).
- 11 Petosa, C. *et al.* 14-3-3zeta binds a phosphorylated Raf peptide and an unphosphorylated peptide via its conserved amphipathic groove. *J Biol Chem* **273**, 16305-16310, doi:10.1074/jbc.273.26.16305 (1998).
- 12 Kenakin, T. P. *Pharmacology in drug discovery and development: Understanding drug response: Second edition*. (2016).
- 13 Yung-Chi, C. & Prusoff, W. H. Relationship between the inhibition constant (KI) and the concentration of inhibitor which causes 50 per cent inhibition (I₅₀) of an enzymatic reaction. *Biochemical Pharmacology* **22**, 3099-3108, doi:10.1016/0006-2952(73)90196-2 (1973).
- 14 Zhang, J. H., Chung, T. D. & Oldenburg, K. R. A Simple Statistical Parameter for Use in Evaluation and Validation of High Throughput Screening Assays. *J Biomol Screen* **4**, 67-73, doi:10.1177/108705719900400206 (1999).

The TR-FRET assay development was performed under the supervision of Dr. Martin Redhead. Dr. Martin Redhead developed the R18 competitive inhibition model used for the determination of the final assay conditions.

Chapter 5

Identification of Molecular Glues of the SLP76/14-3-3 Protein-Protein Interaction

Abstract

The stabilisation of protein-protein interactions (PPIs) through molecular glues is a novel and promising approach in drug discovery. In stark contrast to research in protein-protein inhibition the field of stabilisation remains underdeveloped with comparatively few examples of small-molecule stabilisers of PPIs reported to date. At the same time interest in identifying molecular glues has received recent sustained interest, especially in the fields of targeted protein degradation and 14-3-3 PPIs. The hub-protein 14-3-3 has a broad interactome with more than 500 known protein partners which presents a great opportunity for therapeutic intervention. In this study we have developed an HTRF assay suitable for HTS of the 14-3-3/SLP76 PPI and have completed a proof of concept screen against a chemically diverse library of 20K molecules. The adaptor protein SLP76 has been reported to interact with 14-3-3 proteins downstream of the TCR playing an important role in mediating its own proteasomal degradation. We believe that stabilisation of this PPI could be exploited to potentiate degradation of SLP76 and therefore inhibit TCR signalling. This would represent an interesting alternative to other approaches in the field of targeted protein degradation. Here we disclose novel stabilisers of the 14-3-3/SLP76 PPI across multiple different chemotypes. Based on the early results presented here we would recommend this approach to find molecular glues with broad applicability in the field of 14-3-3 PPIs.

Part of this work will be published as: **Soini, L.**, Redhead, M., Westwood, M., Leysen, S., Davis, J., and Ottmann, C. Identification of molecular glues of the SLP76/14-3-3 protein-protein interaction.

5.1 Introduction

Inhibition of protein-protein interactions has become an established approach in drug discovery and has delivered successful examples to the market and in clinical trials ¹⁻³. In contrast, the stabilisation of Protein-Protein Interactions (PPI) remains a relatively novel field in drug discovery but has seen a considerable increase in interest over the last two decades. Although stabilising PPIs is considered a challenging approach, it has significant advantages. The binding epitopes generated at the interface of two different target surfaces confer an intrinsically higher potential for selectivity and theoretically even modest enhancements of the affinity of an already occurring PPI could lead to useful levels of activity ⁴. The natural immunosuppressant products Cyclosporine and FK506 were among the first reported examples of molecular glues, although their mechanism of action was elucidated retrospectively ⁵⁻⁷. Most recently, small-molecule approaches have been pursued. PROTACs (Proteolysis Targeting Chimeras) are classes of bifunctional small molecules that promote proximity between an ubiquitin ligase and a substrate protein, leading to the degradation of the latter ⁸⁻¹¹. Smaller, monovalent molecules grouped under the IMiDs drug class, capable of promoting the ubiquitination of substrates targeting them for degradation, have also been described with thalidomide and lenalidomide the main examples ¹²⁻¹⁵. The ability to target proteins for degradation using small molecules has expanded the range of accessible new targets previously considered to be undruggable^{16,17}.

So far, rationally designed small molecules aimed at the stabilisation of a PPI between an E3 ligase and its specific interaction partner has been the direct route to enhance protein degradation ¹⁸⁻²¹. However, mechanisms that indirectly promote protein degradation might be an alternate approach to find novel, therapeutically useful chemical matter. Protein degradation can be modulated via ubiquitination ²², phosphorylation ^{23,24}, acetylation ²⁵, sumoylation ²⁶, or, as some studies have suggested, via interaction with adaptor proteins such as 14-3-3 ²⁷⁻³¹. 14-3-3 proteins are a family of eukaryotic adaptor proteins that are known for recognizing specific pSer/pThr containing motifs on binding partners ^{32,33}. In humans, they are present in seven isoforms (β , γ , σ , ζ , η , ϵ and τ). Composed of alpha helices and loops they can form either homo and hetero dimers ³⁴. 14-3-3 proteins have a remarkable interactome with up to 500 binding partners ³⁵ and are involved in a plethora of biological processes which include apoptosis, cellular trafficking, cell-cycle and signal transduction ³⁶. With a role as a central hub protein this makes the 14-3-3 family drug targets of huge, but as yet unrealised, potential ³⁷. Among the most important related diseases to 14-3-3 and therapeutically relevant binding partners are: cancer (p53) ³⁸, Parkinson's Disease (LRRK2) ^{39,40}, Alzheimer's Disease (Tau) ⁴¹ and Cystic Fibrosis (CTRF) ^{42,43}. The stabilisation of 14-3-3 PPIs has been an area of active research since the natural product Fusicoccin-A (FC-A), a wilt-inducing phytotoxin produced by the fungus *Phomopsis amygdali*, was first identified as a 14-3-3/H⁺-ATPase PPI stabiliser ^{44,45}. Cotylenin-A (CN-A), a remarkably similar compound to FC-A has also been reported to stabilise 14-3-3 PPIs ^{46,47}. The natural products Fusicoccin-A and Cotylenin-A showed very good stabilisation properties and physiological activity on the 14-3-3/ H⁺-ATPase system, theoretically opening the way for natural products derivatives that could improve binding properties and introduce selectivity for other systems ^{45,47,48}. However, their chemical complexity and properties make them challenging to progress as potential drug candidates. Biosynthesis, total synthesis and semi-synthesis are under

investigation, but are far from being completely actualised⁴⁹⁻⁵¹. Pyrroldone-1 was the first 14-3-3 stabiliser identified via High Throughput Screening (HTS), providing the possibility of more easily optimisable starting points amenable to rational design⁵²⁻⁵³. Fragment-based approaches have also been pursued⁵⁴⁻⁵⁶. Despite these successful examples of 14-3-3 PPI stabilisers the field is still significantly lacking in novel chemotypes to stimulate development of the next generation of PPI stabilisers. In this study we have developed a Homogenous Time-Resolved Fluorescence (HTRF) assay suitable for HTS on the 14-3-3/SLP76 PPI and have completed a proof of concept screen against a chemically diverse library of 20K molecules. Previous screening approaches have relied on short phopshopeptides to mimic the 14-3-3 protein partner which, although convenient, have significant limitations. Pivotal to our approach was to commit to using an SLP76 protein construct which we believe is both more relevant and opens the possibility of finding molecular glues beyond the small binding epitope of the peptide. 14-3-3 has been reported to interact with the protein SLP76 *via* one specific phosphorylation site located on SLP76, Ser376^{57,58}. SLP76 is an adaptor protein that orchestrates the signalling downstream of TCRs helping to modulate the immune response^{59,60}. The SLP76 phosphorylation on Ser376 is performed by the kinase HPK1 (Hematopoietic progenitor kinase 1) and revealed a sophisticated negative feedback mechanism by which TCR signalling is modulated. The binding of 14-3-3 to SLP76 seems to mediate the proteasomal degradation of the latter which results in a negative regulation of TCR signalling. We believe that stabilisation of the 14-3-3/SLP76 PPI by means of a small molecule could therefore increase SLP76 degradation. An enhancement of the negative regulation of the TCR signalling could be beneficial in the context of autoimmune and inflammatory conditions mainly driven by over activated T-cells.

In order to find stabilisers of the 14-3-3/SLP76 PPI we generated a protein system composed of full-length 14-3-3 γ and a 20 KDa phosphorylated SLP76 construct. This introduced a higher degree of complexity since 14-3-3 PPIs are more typically investigated using 12-mer synthetic peptides to mimic the 14-3-3 binding partner. We then developed and ran an HTRF-HTS (Homogeneous Time Resolved Fluorescence High Throughput Screening) on the UCB “Diversity Set” of 20,000 small molecules. The “Diversity Set” is a subset of the larger UCB HTS compound collection specifically selected for lead-like molecular properties and chemical diversity. We also used an unrelated PPI that shared the same FRET pair as the 14-3-3 γ /SLP76 system as a counterscreen, which allowed us to identify specific potential stabilisers of this interaction. The hits found were further characterised performing HTRF dose-response and dose-ratio assays and the stabilisation effect orthogonally confirmed by SPR.

5.2 Results and Discussion

5.2.1 Primary HTRF HTS Screening of 20,000 Small Molecules against the 14-3-3 γ /SLP76 PPI

The performance of the initial single point screening of the 20,000 molecule UCB Diversity Deck against the 14-3-3 γ /SLP76 PPI system is shown in (Figure 5.1a). The peptide R18 is a well characterised inhibitor of 14-3-3 PPIs^{61,62} and was therefore chosen as the assay negative control and was also an

important reagent used during assay validation. Unfortunately, there are no reported stabilisers of 14-3-3/SLP76 interactions and therefore no true positive controls. Of course, the fundamental aim of this work was to discover molecular glues of this interaction which can then be used as starting points and tool compounds to evaluate the therapeutic potential of stabilising the complex. The cut-off for selection of hits in the first round of screening was set at 20% stabilisation (or -20% inhibition) at a concentration of 100 μ M with the reference control set at 100% inhibition and all the screening outcomes normalised accordingly (Figure 5.1b).

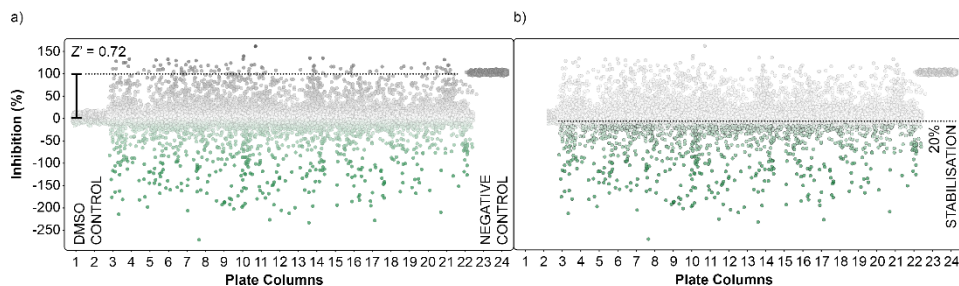


Figure 5.1 | Graphical representation of the High Throughput Screening performance. a) Dots representation of the HTS in the plate format. Potential inhibitors are represented as grey dots, potential stabilisers are represented as green dots. DMSO control and negative control are grouped in plate columns 1, 2 and 23, 24 respectively. The calculated overall Z' factor for the assay was 0.72. b) An initial cut-off of 20% stabilisation was used to select hits to follow-up.

The cut-off expressed in number of standard deviations of the DMSO control from the mean was $4 \cdot SD_{DMSO}$ (or $30 \cdot SD_{DMSO}$ calculated using raw data). The cut-off chosen from the primary screen left us with 1136 hits, roughly 5% of the initial 20,000 molecules. Of these 1136 small molecules, 660 repeated in a confirmatory screen with the same cut-off threshold; roughly 3% of the initial 20,000 compounds. These 660 hits were subsequently tested in an assay using IL17/receptor as an unrelated PPI which shared the same FRET acceptor/donor pair as the 14-3-3 γ /SLP76 system (Figure 5.2a).

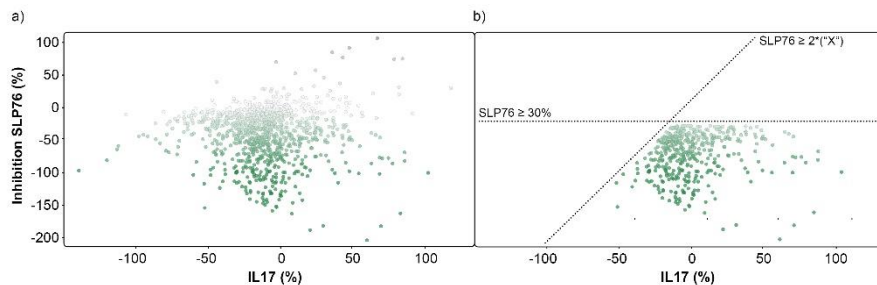


Figure 5.2 | Graphical representation of the repeated 1136 hits tested on 14-3-3/SLP76 and IL17/IL17R. a) Representation of the hits expressed as percent inhibition against 14-3-3 γ /SLP76 and IL17/IL17R. Potential 14-3-3 γ /SLP76 stabilisers are represented as green dots. b) Selection conditions

applied to the hits were to retain compounds that showed an effect on SLP76 \geq -30% and simultaneously at least a two-fold greater stabilisation than IL17 PPI, SPL76 \geq 2*IL17.

The matched FRET pair counter screen was specifically introduced to reduce the number of false positive hits and to focus on molecules that selectively stabilised the 14-3-3 γ /SLP76 system. Using this counter screen, we were able to further refine compounds of most interest to 428 hits as summarised in Figure 5.2b. The hits selected in this way were then ranked according to their inhibition ratio (%inhibition SLP76/%inhibition IL17), with the most selective compounds (highest ratios) prioritised for further study. This allowed us to further focus our efforts on a shortlist of 64 compounds which demonstrated little to no stabilisation of the counter-screen system with the results of this triage process summarised in Figure 5.3a.

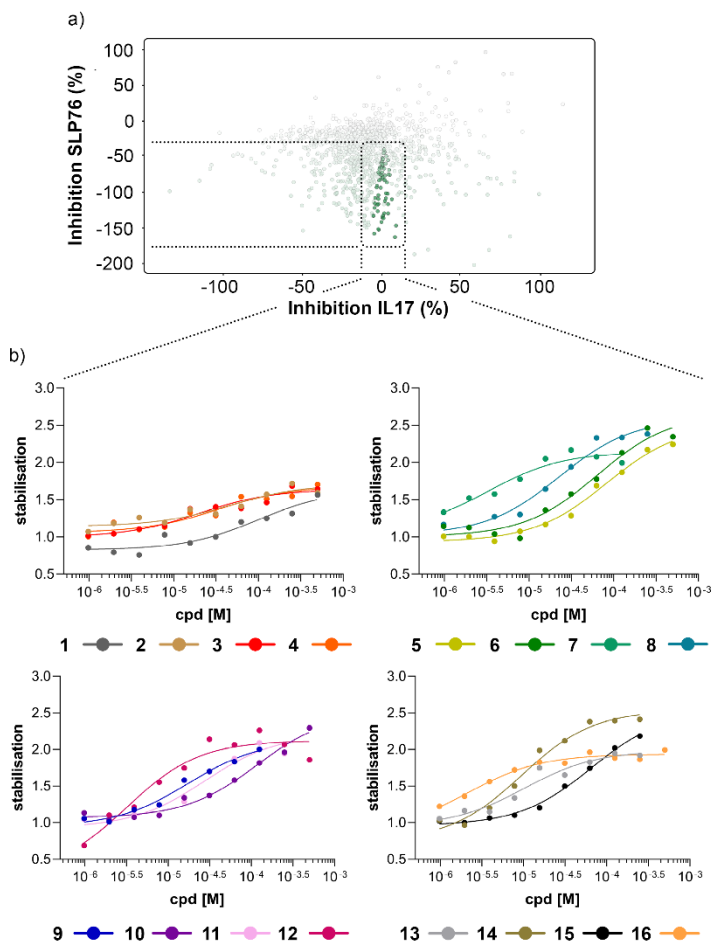


Figure 5.3 | Representation of the 64 small molecules selected on the basis of SLP76 stabilisation and IL17/IL17R counter-screen and 14-3-3 γ /SLP76 dose response curves for the best 16 compounds. a) Selection of 64 small molecules represented as green dots within dotted lines. b) Dose response curves of the best 16 out of the 64 compounds tested. Estimated EC₅₀ values for every compound are reported in Table 5.1.

5.2.2 HTRF Dose-response Assay on the Selected 64 Compounds

The compounds which appeared selective in the single point screening were tested as dose responses on 14-3-3 γ /SLP76 (Figure 5.3b). Of the 64 tested in dose response, 30 did not show any dose-response effect. Of the remaining 34 compounds, 16 were selected as the most promising hits to follow up based on EC₅₀ values (Table 5.1). All 16 compounds demonstrated a concentration dependent increase in HTRF signal as a result of the binding of the molecules to the 14-3-3/SLP76 complex. EC₅₀ values estimated from the fitting curves were between 2.2 and 110 μ M (Figure 5.3b). These 16 compounds were re-tested in dose response using 10mM DMSO stock solutions freshly prepared from solid and pleasingly they were

all confirmed as stabilisers of the 14-3-3 γ /SLP76 PPI system (Figure 5.4c). To test whether the concentration-dependent effect would influence other PPI systems as well, the compounds were also tested on IL17/IL17R as an unrelated PPI (Figure 5.4a) and on the 14-3-3 ζ /p27 system (Figure 5.4b) as an example of another 14-3-3 PPI. In all cases the same FRET pair was used to label the different protein systems.

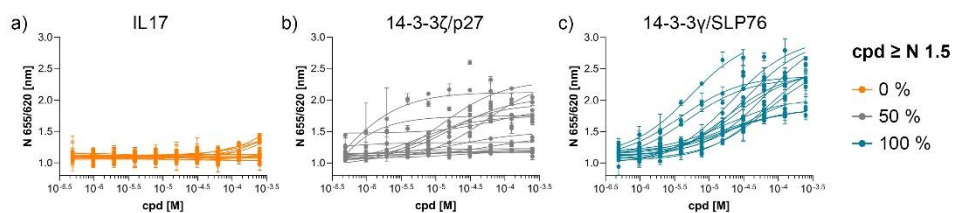


Figure 5.4 | Comparison of the dose response assay of the 16 compounds on the systems IL17/IL17R, 14-3-3 ζ /p27 and 14-3-3 γ /SLP76. a) dose response of the 16 compounds on IL17/IL17R. None of the compounds showed an effect on IL17/IL17R. b) dose response of the 16 compounds on 14-3-3 ζ /p27. 8 out of 16 compounds showed an effect greater than 1.5 normalised response. c) All 16 compounds repeated on 14-3-3 γ /SLP76.

None of the 16 compounds showed an effect on IL17/IL17R, as expected from the primary counter screen assay. However, eight compounds showed a dose-response effect on the 14-3-3 ζ /p27 system that exceeded the normalised response of 1.5, with 2.0 being the theoretical maximal response. This evidence indicates that these compounds are not specifically selective for the 14-3-3 γ /SLP76 PPI and provides an opportunity for further exploration. Although the key objective of this study was to find selective stabilisers of the 14-3-3 γ /SLP76 interaction, the prospect of finding generic 14-3-3 PPI stabilisers would be of general benefit to research in this area. Furthermore, if the binding site of these compounds could be characterised it would open the possibility to rationally build in selectivity for different 14-3-3 protein-protein interactions through structure-based drug design.

5.2.3 Orthogonal SPR Confirmation on the selected 16 Compounds

Of the 16 hit compounds 13 were tested in an orthogonal SPR assay in which each compound was flowed with SLP76 over 14-3-3 γ immobilised on the chip. Runs at different concentrations of compound were compared to the runs in absence of compound. Of the 13 compounds tested this way, 8 showed a difference in off-rate indicative of increased binding of SLP76 to 14-3-3 γ and were subsequently tested at multiple concentrations to establish a concentration-dependent effect. All 8 compounds proved to be dose responsive leading to a concentration-dependent increase in mass on the chip. The effect of the compounds on 14-3-3 γ /SLP76 was measured by calculating the percentage of SLP76 remained on the chip after the dissociation phase and immediately before: $RU (\%) = RU_{5 \text{ sec before dissociation}} / RU_{+240 \text{ sec after dissociation}}$. EC₅₀ values are reported only in the cases in which the extrapolated dose-response

curves reached saturation. In the other cases, the RU (%) mass increase in the presence of compound was reported.

5.2.4 Analysis of hit compounds

The structures of all 16 hits and data from all assays used to triage the compounds are summarised in Table 5.1. Of the 16 compounds tested by HTRF in dose response, compounds **1**, **2**, **3**, **4**, **7**, **8**, **12** were orthogonally confirmed by SPR and of those, compounds **1**, **2**, **3**, **4** were selective for 14-3-3 γ /SLP76 over 14-3-3 ζ /p27. Ten of the sixteen hit compounds could be grouped into four structurally distinct chemotypes with the remaining 6 compounds singleton hits. Compounds **1** and **2** belong to an interesting benzo-fused tricyclic oxazolidinone system. Both compounds were selective for the 14-3-3 γ /SLP76 interaction with similar activities and no observed stabilisation in the 14-3-3 ζ /p27 HTRF assay. The stabilising effect of these compounds was orthogonally confirmed and equipotent by SPR (Figure 5.5a). These oxazolidinones have good lead-like properties with low MW, PSA and good AlogP (Table S 2) which makes them excellent candidates for hit expansion. The presence of a chiral centre offers the prospect to investigate if there is an enantiomeric preference in stabilisation.

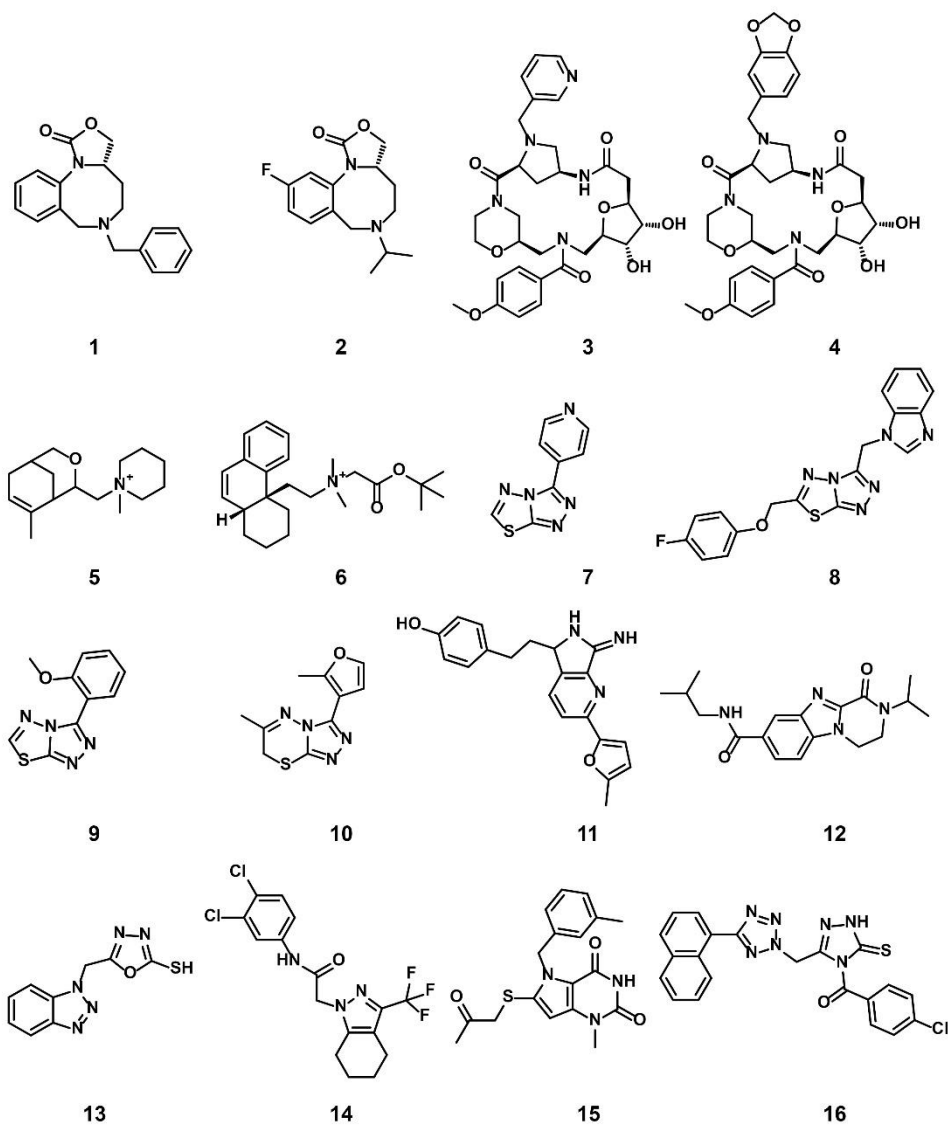


Table 5.1 | Summary table of the 16 compounds identified from the HTRF dose-response assay.

Molecule	HTRF EC ₅₀ (μM)		HTRF K _D improvement	SPR EC ₅₀ (μM) / RU (%)
	14-3-3γ/SLP76	14-3-3ζ/p27	14-3-3γ/SLP76	14-3-3γ/SLP76
1	19.1 ± 7.7	IA*	3.3 x [†]	66.4 RU (%)◊
2	18.6 ± 5.5	IA*	4.1 x [†]	67.6 RU (%)◊
3	14.4 ± 1.9	IA*	2.2 x [†]	36.1 ± 6.5 μM
4	17.4 ± 4.9	IA*	3.4 x [†]	26.8 ± 12.9 μM
5	71.1 ± 23.9	IA*	4.7 x [†]	NS**

6	33.5 ± 10.7	IA*	Nm‡	Ns**
7	5.3 ± 1.9	IA*	4.4 x†	5.2 ± 1.9 μM
8	69.1 ± 22.6	53.9 ± 17.1	3.5 x†	61.2 RU (%)◇
9	24.5 ± 5.8	5.8 ± 2.2	1.3 x†	58.7 RU (%)◇
10	70.1 ± 8.7	16.5 ± 10.6	1.7 x†	Ns**
11	29.7 ± 21.8	128.9 ± 70.5	Nm‡	Nm‡
12	3.8 ± 1.2	0.43 ± 0.37	5.2 x†	8.1 ± 5.9 μM
13	4.9 ± 1.1	IA*	1.1 x†	Ns**
14	21.2 ± 11.3	12.6 ± 14.4	14.6 x†	Ns**
15	17.1 ± 5.2	11.6 ± 6.1	Nm‡	Nm‡
16	1.2 ± 0.7	80.6 ± 53.4	1.8 x†	Nm‡

*IA: inactive <x% stabilisation observed at top concentration (250 μM); ‡Nm: not measured; † n-fold 14-3-3γ/SLP76 K_D improved in presence of increasing concentration of small molecule; **Ns: no stabilisation observed in SPR; ◇ RU (%) of mass increase in the presence of 200 μM of compounds.

An equally interesting chemotype are the 16-membered macrocyclic compounds **3** and **4** which were also shown to be selective for the 14-3-3γ/SLP76 system as well as being orthogonally confirmed in the SPR assay (Figure 5.5b). Although the macrocycles show very similar levels of activity in the 14-3-3γ/SLP76 HTRF assay to compounds **1** and **2**, they both appear to perform better in the SPR stabilisation assay. The macrocycles lie outside the range of conventional lead-like properties with MW of 609 and 652 respectively, highly polarity (AlogP -1.3 and -0.5) and with PSA around 150 which could impact cell permeability. However, this should not preclude a more detailed investigation and indeed these compounds could give valuable insight as tools for future structural studies.

The third group of hits, compounds **5** and **6**, are characterised by having a quaternary positively charged amine group. Both showed activity in the 14-3-3γ/SLP76 HTRF assay although with modest EC₅₀s and were selective over 14-3-3ζ/p27. However, neither of these two compounds were confirmed in SPR with no observable stabilisation effect.

The fourth group of compounds: **7**, **8**, **9** and **10** all share a triazolothiadiazole heteroaromatic scaffold or in the case of Compound **10** the closely related triazolothiadiazine structure. This set of compounds is especially attractive in that they have low MW with good molecular properties in fragment space and have significant potential for further exploration. It is also notable that these compounds form the largest structurally related cluster of SLP76 stabilisers from the UCB Diversity Deck. Compound **7** is the stand-out hit as a selective 14-3-3γ/SLP76 stabiliser with EC₅₀ of 5.3 μM, a fourfold increase in K_D and no measurable modulation of the 14-3-3ζ/p27 system. Compound **7** also has a strong concentration dependence in off-rate in SPR when compared to other compounds in this group (e.g. Compound **10** demonstrates no observable stabilisation in the SPR assay). With a MW of only 203 Compound **7** demonstrates remarkable modulation of the 14-3-3γ/SLP76 system and is a priority for further focussed hit expansion. What is even more interesting is that the closely related analogues in this group are also able to stabilise the 14-3-3ζ/p27 PPI to a lesser or greater extent. This opens up the intriguing possibility that these compounds could be generic modulators of 14-3-3 protein-protein interactions, with the potential to tune-in selectivity for a specific protein pair. This speculation would of course require a larger confirmatory study to expand both the chemical matter around these scaffolds and the numbers of 14-3-3 PPIs tested. For these compounds to be general stabilisers of the 14-3-3 PPIs it is reasonable to expect

that they are interacting with a conserved pocket on the 14-3-3 protein. Compound **8** is the closest analogue of **7** and is a weak and equipotent stabiliser of both the 14-3-3 γ /SLP76 and 14-3-3 ζ /p27 systems. Compounds **9** and **10** in contrast show a modest level of selectivity in stabilising 14-3-3 ζ /p27 over 14-3-3 γ /SLP76.

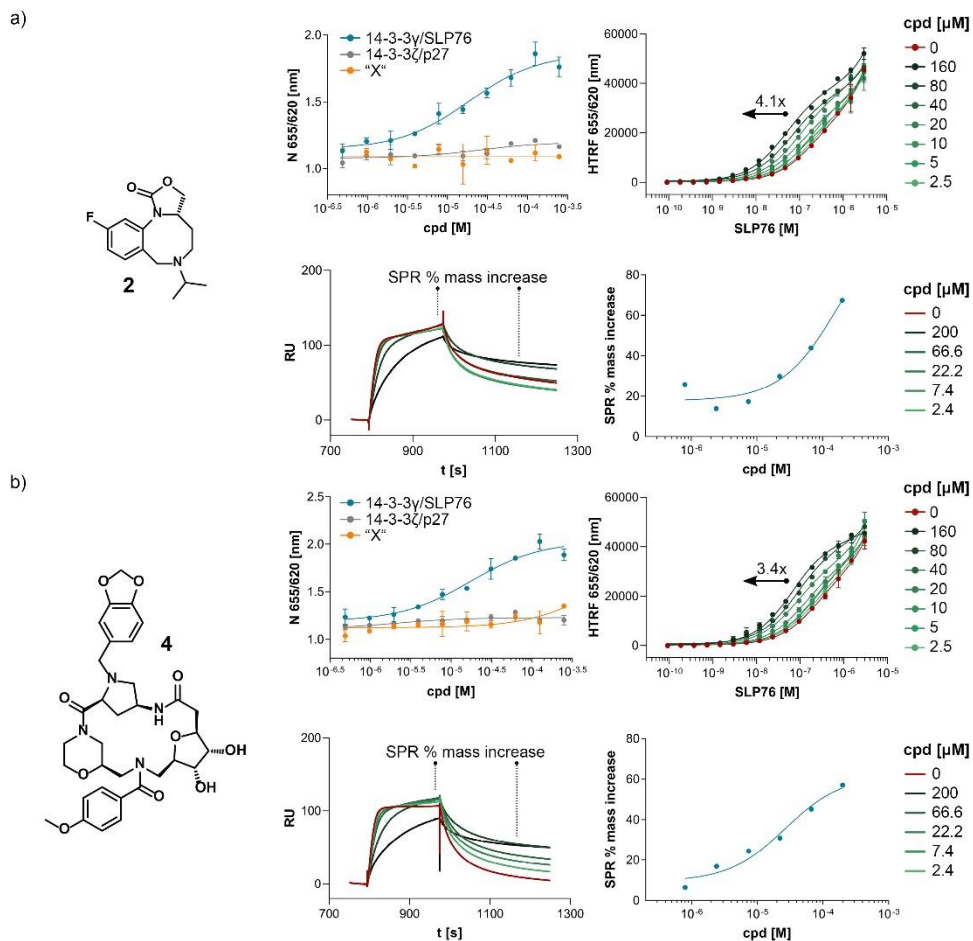


Figure 5.5 | Combined set of assays example for the Compound 2 and 4. a) HTRF dose response comparison of the three systems used. HTRF dose ratio assay on the 14-3-3 γ /SLP76-SH₂ system. The arrow represents the increment in potency upon increasing compound concentration. Sensorgrams generated by SLP76-SH₂ flowing over 14-3-3 γ in absence (as reference) and in the presence of different concentration of compounds. The plot of the reference points taken from the sensogram used to generate dose-response curves is reported to the right. The reference points before and after the dissociation phase are highlighted in the sensograms (bottom left). b) The same set of assays are repeated on compound **4**.

The last group of compounds are six singleton hits Compounds **11** to **16** which, with the exception of compound **13** are able to stabilise both the 14-3-3 γ /SLP76 and 14-3-3 ζ /p27 systems. The dihydropyrazino[1,2-a]benzimidazole, compound **12**, is the most potent stabiliser of 14-3-3 ζ /p27 tested with an EC₅₀ of 0.43 μ M, almost 8-fold selective over 14-3-3 γ /SLP76 (EC₅₀ of 3.2 μ M). This hit is also the only compound in the group of singletons that showed a measurable stabilisation of 14-3-3 γ /SLP76 by SPR with EC₅₀ 8.1 μ M. With ability to modulate both systems and with excellent molecular properties, Compound **12** should be followed-up in greater detail. The last compound we would highlight is Compound **14** which is another attractive chemical starting point for further investigation. Although this compound provides modest stabilisation EC₅₀s for both the 14-3-3 γ /SLP76 and 14-3-3 ζ /p27 systems (EC₅₀ 21.2 μ M and 16.6 μ M respectively), it shows the highest improvement in SLP76 HTRF K_D at 14-fold. However, this stabilisation was not confirmed in the SPR assay. The full set of assays per compound is reported in the Supplementary Information (Figure S 5.2).

5.2.5 Hit expansion by focused screening of derivative libraries

Compounds **1**, **2** and **3**, **4** identified in the HTS campaign were among our preferred hits from the UCB Diversity Library with activity only on the 14-3-3 γ /SLP76-SH2 system and selective in the counter screens. The hits were confirmed in an orthogonal SPR assay and were attractive starting points for further investigation. In addition, these hits belong to two different chemotypes for which a large number of analogues were available from the wider UCB compound collection. We therefore decided to screen a selection of these derivative compounds first in a single point TR-FRET screen followed by dose-response for the most potent compounds.

In contrast to the original HTS campaign, we used Compound **16** as a positive control which we selected from the best 16 hits. Compound **16** is a potent stabiliser of the SLP76/14-3-3 interaction with good selectivity in the p27/14-3-3 counter screen. All the data were subsequently normalised fixing the stabilisation provided by 50 μ M of compound **16** as the maximum response (100% stabilisation). Compound **16** generated the maximum response in the dose-response assay at this concentration (Figure 5.3b). The derivatives were tested at a single concentration of 20 μ M, five times lower compared to the HTS where the compounds were tested at 100 μ M (Figure 5.6). Given the derivatives were chosen for their structural similarity to the hits **1**, **2**, **3** and **4**, using a lower starting concentration allowed us to focus only on compounds with similar or better activity.

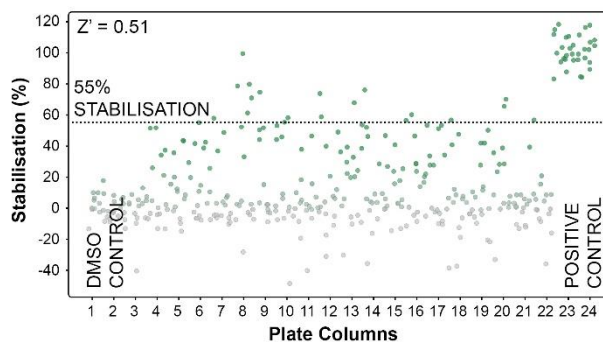


Figure 5.6 | Single point screening of a derivative library. The read-out of the screening has been displayed by representing every single compound as a coloured dot. A colour gradient from grey to green discriminates progressively the activity of the compounds from null (grey) to active (green). The first two columns contained the DMSO control (5% DMSO), while the last two columns contained the positive control (compound **16**, at 50 μ M). The assay achieved a Z' factor of 0.51 based on the control responses and was considered suitable to support derivative screening. The 16 most active compounds were selected as hits to follow up in dose-response studies which correspond to a minimum of 55% stabilisation with reference to the positive control.

The derivative screening set was composed of 312 compounds across the two main chemotypes (Figure 5.7). Scaffolds A, B and C are grouped in the same family sharing the 8-membered 1,5-diazocane heterocycle. Scaffold D consists of a macrocycle with two substituents, R5 and R6 (60 compounds). Although a proper structure-activity relationship (SAR) study is not possible solely on the basis of single point screening, some qualitative considerations are still worth mentioning.

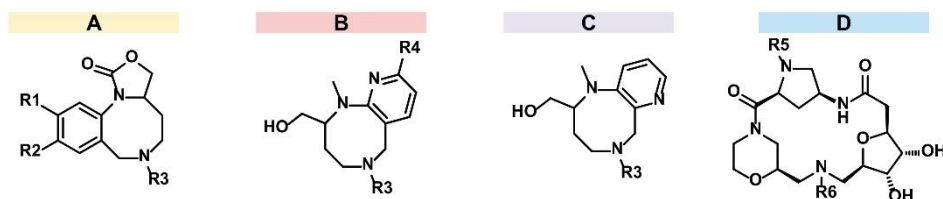


Figure 5.7 | The four different scaffolds that compose the derivative library. The family composed of scaffolds A, B and C which make up 252 members of the library whereas scaffold D has 60 analogues.

The first general observation is that the derivative library is highly enriched with stabilisers of the 14-3-3 γ /SLP76 PPI (Figure 5.8). Given that these were analogues specifically selected for hit expansion this is not unexpected but does increase confidence in the scaffolds as a productive set for further

investigation. Of course, if very few analogues had been active then it would have significantly lowered confidence in these as useful series. There is a good dynamic range of stabilisation across the compounds with a distribution of activities from weak to strong stabilisers including some inactives. This is another hallmark of an emerging SAR and adds to the interest in these chemotypes. The activity of each compound in the single point screen coloured by scaffold is shown in Figure 5.8.

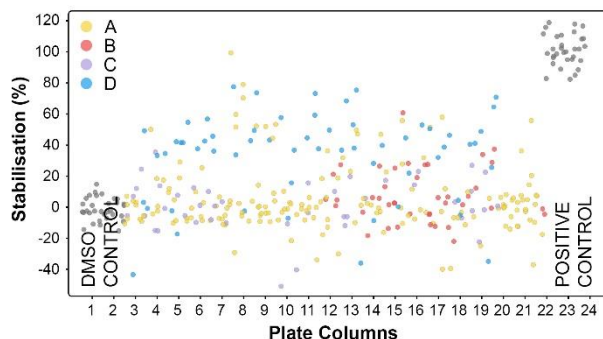


Figure 5.8 | Single point screening of a derivative library. The picture displays the same screening performance that is showed above but with the read-out colour coded depending on the scaffold A (yellow), B (red), C (purple) or D (light blue).

Scaffold A had the greatest number of analogues available and makes up over half of the derivative library screened. This scaffold has analogues with the strongest stabilisation effect compared with positive control and a range of activity from strong stabilisation to inactive. Scaffold A has 21 compounds with greater than an arbitrary threshold of 30% stabilisation and 14 with more than 50%. Compound **17** from this set is the strongest stabiliser across the entire derivative library screened. Variation of R1 (R1 = H, Me or F) and R2 (R2 = H, OMe) is tolerated with examples of each showing some stabilisation. It is clear, however, that R2 = H is preferred over methoxy with matched pairs consistently and significantly favouring a hydrogen substituent in this position. Looking at matched pairs for R1, there is a strong preference for rank order for % stabilisation F > Me > H with the best stabilisers all bearing the Fluoro substituent and Hydrogen quite a weak effect. However, the strongest effect observed in Scaffold A was the nature of R3. Of the compounds tested in this class 103 were simple amide or urea derivatives at this position and none of these analogues showed any significant level of stabilisation. We therefore conclude, for the moment, that the weakly basic sp³ amine is important for activity. Of course, obvious analogues to make would be nitrogen atom substitutions (O, S and C) to further explore this hypothesis. Scaffolds B and C, despite sharing the 8-membered 1,5-diazocane ring, are considerably different from the Scaffold A. This is remarked by the fact that the Scaffold B appears only once among the highest activity compounds with Compound **21** having a stabilisation of 61%. All other compounds in this class had an activity of less than 37%, most having no appreciable activity at all. Analogues of Scaffold C, however, never appear among the most active compounds with the best analogue only achieving a stabilisation of 37%. Out of the 84 analogues from Scaffolds B and C, 67 demonstrated less than 20% stabilisation and

only a single compound showed more than 40% stabilisation. Although there is not the perfect matched analogue to compare with Scaffolds B and C, we would conclude that the carbamate cycle of Scaffold A has to play an important role in engaging the 14-3-3 γ /SLP76 system. Regarding the macrocycles of scaffold D, is worth mentioning that only a few are present at the lower end of the activity ranking. Despite the fact they make up only 60 compounds out of 312 in the library, 42 show an activity of 30% or more. In fact, 40 of the 70 most active compounds are macrocycles. The higher complexity and 3-dimensionality of the molecule might better fulfil the requirements of an ideal molecular glue.

The 16 most active compounds had an activity of between 98% and 57% (Figure 5.9), (Table 5.2, Table 5.3). We decided to test these 16 in dose-response assays. All the compounds selected for the dose-response assays resulted in a stimulation fitting curve from which it was possible to calculate EC₅₀ values (Figure 5.10), (Table 5.2, Table 5.3). Even though these compounds were tested at lower concentrations and still showed remarkable activity, the EC₅₀s of the derivatives did not improve dramatically compared to the original compounds identified in the HTS. The 8-membered ring scaffold compounds (**17**, **18**, **19**, **20**, **21**, **22**) generated EC₅₀s in the same range as compounds **1** and **2**. The macrocycle compounds, however, generated a wider EC₅₀ range, with compounds **23**, **24**, **25**, **28**, **29** and **30** showing EC₅₀ values below 10 μ M. This is a marginal improvement of the EC₅₀s observed for the original HTS compounds.

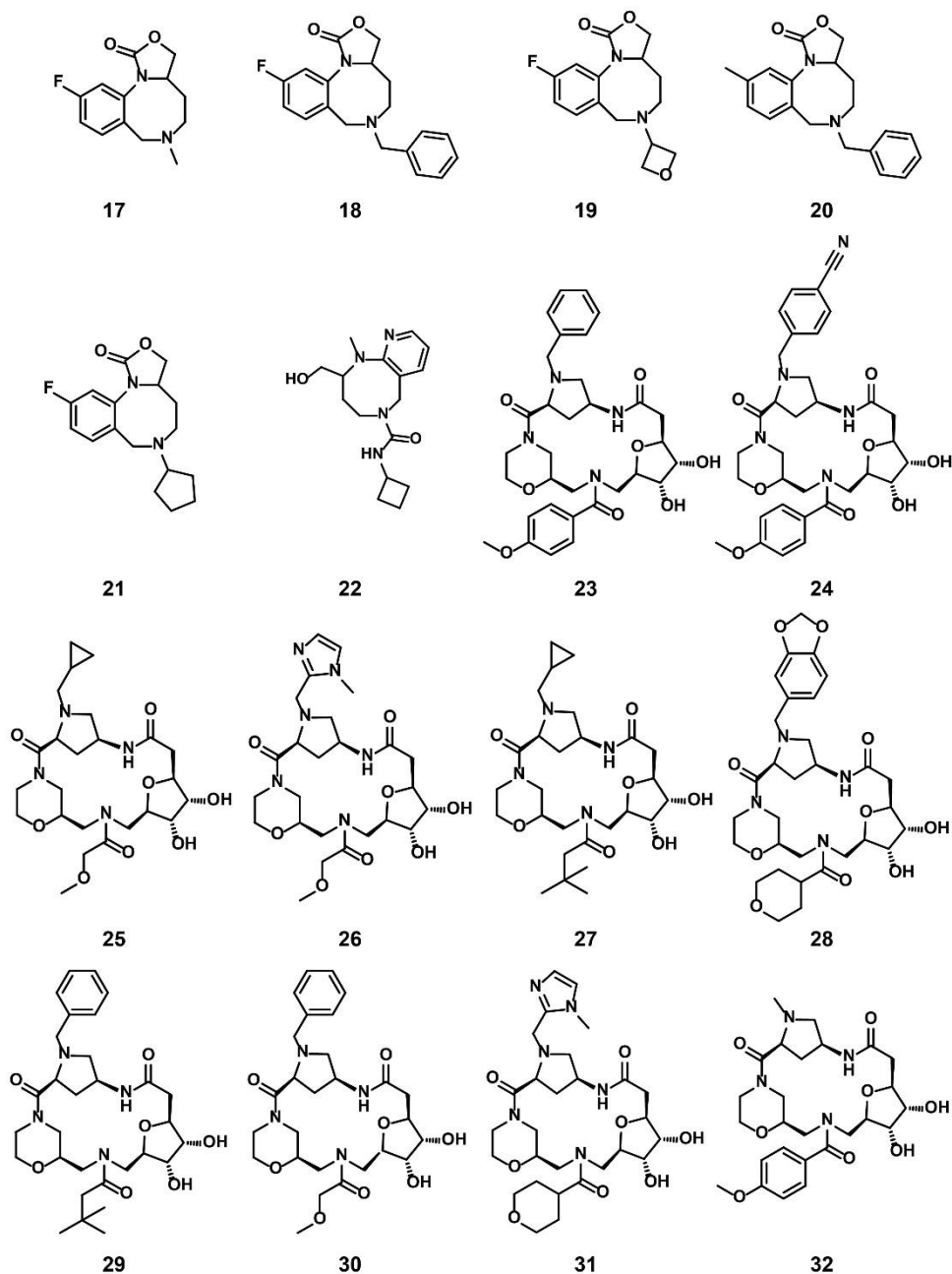


Figure 5.9 | Structures of the best 16 compounds chosen for the dose-response assay.

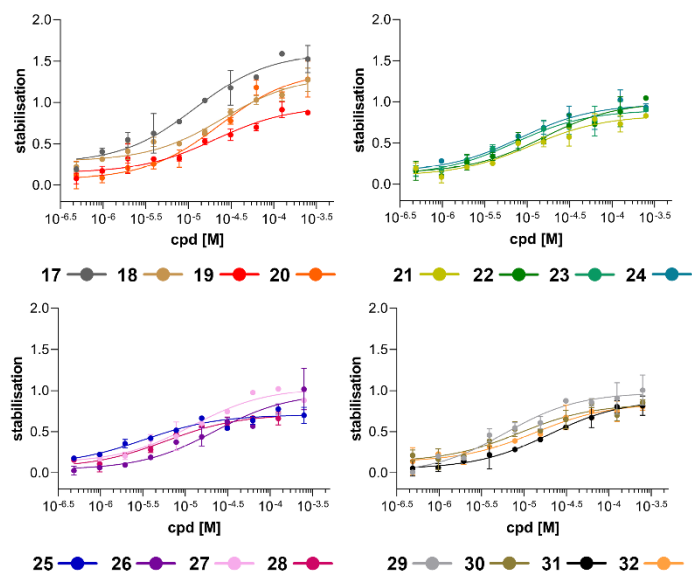


Figure 5.10 | Dose-response fitting curves of the best 16 derivatives identified. The read-out was normalised against compound **16** to give 1.0 as maximum response.

In Table 5.2, the EC₅₀ values are reported for the Scaffold A and B derivatives along with the original compounds identified in the HTS **1**, and **2**. Regarding Scaffold A, we can observe that the fluorine substituent is the most desirable substituent to have as R1. Compounds bearing a fluorine in this position were clearly the most preferred from the single point data although the sole methyl analogue tested in dose response, Compound **20**, has a comparable EC₅₀. As discussed above, analogues bearing a hydrogen substituent in R2 are consistently the highest-ranking compounds for Scaffolds A and B. As previously discussed, Scaffold A does not tolerate an amide or urea substituent at R3. Indeed, all active compounds for Scaffold A have relatively simple lipophilic alkyl or benzyl substituents. There does not, however, seem to be a strong SAR with regard to the nature of these substituents; all have very similar EC₅₀s. The best compound in this set is Compound **17** with the highest maximal stabilisation and EC₅₀ of 12 μM. It is notable that Compound **17** is also the simplest analogue across all Scaffold A compounds screened and therefore represents the most interesting analogue to focus on for future studies. It delivers high levels of stabilisation with similar or better activity to the original hit compounds with greater atom efficiency. It is worth mentioning that the “naked” scaffold (R1 = H; R2 = H; R3 = CH₃) is also present in the derivative library with an activity of only 11%. Therefore, the substituents listed in Table 5.2 are definitely making a significant contribution to the observed binding. As discussed above, scaffolds B and C are scarcely present in the higher part of the activity ranking. Regarding scaffold D, the macrocycles, there is a high degree of tolerance for different substituents in R5 and R6 with no strong SAR arising. EC₅₀ values are reported in Table 5.3 along with the original compounds identified in the HTS **3**, and **4**. It is likely, therefore, that the ring system as whole is making the largest contribution with less sensitivity to variation

at these positions. The better stabilisers tend to favour lipophilic benzyl and cyclopropylmethyl substituents at R5, although the imidazolyl substituent stands out as an example of a more polar group (Compounds **26** and **31**). A similarity lack of sensitivity seems to be apparent in R6 with a range of different amide groups tolerated. We would judge the best Scaffold D analogues to be Compounds **23-25** and **28-30** all demonstrating EC₅₀s < 10 μM a modest improvement on the original hit compounds. We would further focus on those compounds that deliver the highest level of stabilisation (E_{max}) with the greatest atom efficiency. In this regard Compounds **25** and **27** are the most interesting with a small cyclopropylmethyl group in R5 and small amide group in R6. It is interesting to mention that 3 macrocycles demonstrated apparent inhibition (negative activity) with the common factor being a small R5 alkyl substituent combined with an isopropylurea or pivaloyl amide group at R6. Looking back at the single point data it appears that it is the combination rather than individual substituents that lead to this effect. The individual substituents combined with other groups can lead to good stabilisation.

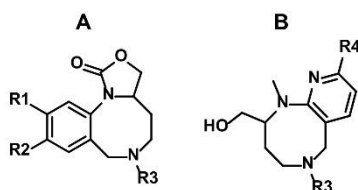
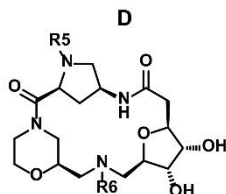
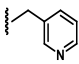
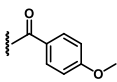
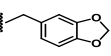
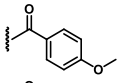
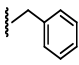
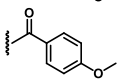
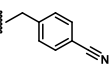
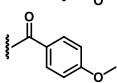
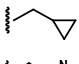
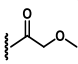
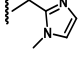
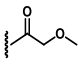
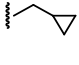
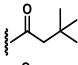
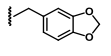
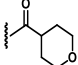
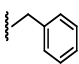
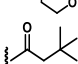
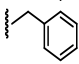
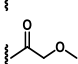
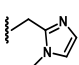
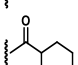

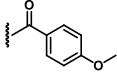


Table 5.2 | EC₅₀ values for the compounds **1**, **2** and **17** to **22**.

Scaffold	Molecule	Stabilisation (%) [*]	EC ₅₀ (μM)	R1	R2	R3	R4
			14-3-3γ/SLP76				
A	1	Nr [‡]	19.1 ± 7.7				
	2	Nr [‡]	18.6 ± 5.5				
	17	98	12.1 ± 3.2				
	18	80	25.4 ± 7.1				
	19	70	20.5 ± 7.5				
	20	57	15.4 ± 5.8				
	21	60	11.1 ± 4.3				
B	22	61	23.4 ± 6.2				

^{*} Percent stabilisation of 14-3-3γ/SLP76 FRET assay at 20 μM; [‡]Nr: not reported. These compounds were identified in the original HTS, hence an activity number would be not comparable in this context.


 Table 5.3 | EC₅₀ values for the compounds **3**, **4** and **23** to **32**.

Scaffold	Molecule	Stabilisation (%) [*]	EC ₅₀ (μM)		R5	R6
			14-3-3γ/SLP76			
D	3	Nr ‡	14.4 ± 1.9			
	4	Nr ‡	17.4 ± 4.9			
	23	78	7.1 ± 1.8			
	24	76	8.1 ± 2.9			
	25	74	3.2 ± 1.5			
	26	73	22.1 ± 9.3			
	27	71	12.2 ± 4.1			
	28	68	5.8 ± 1.6			
	29	65	5.9 ± 1.8			
	30	59	8.8 ± 3.9			
	31	57	19.9 ± 2.4			
	32	57	13.4 ± 3.1			

^{*} Percent stabilisation of 14-3-3γ/SLP76 FRET assay at 20 μM; ‡Nr: not reported. These compounds were identified in the original HTS, hence an activity number would be not comparable in this context.

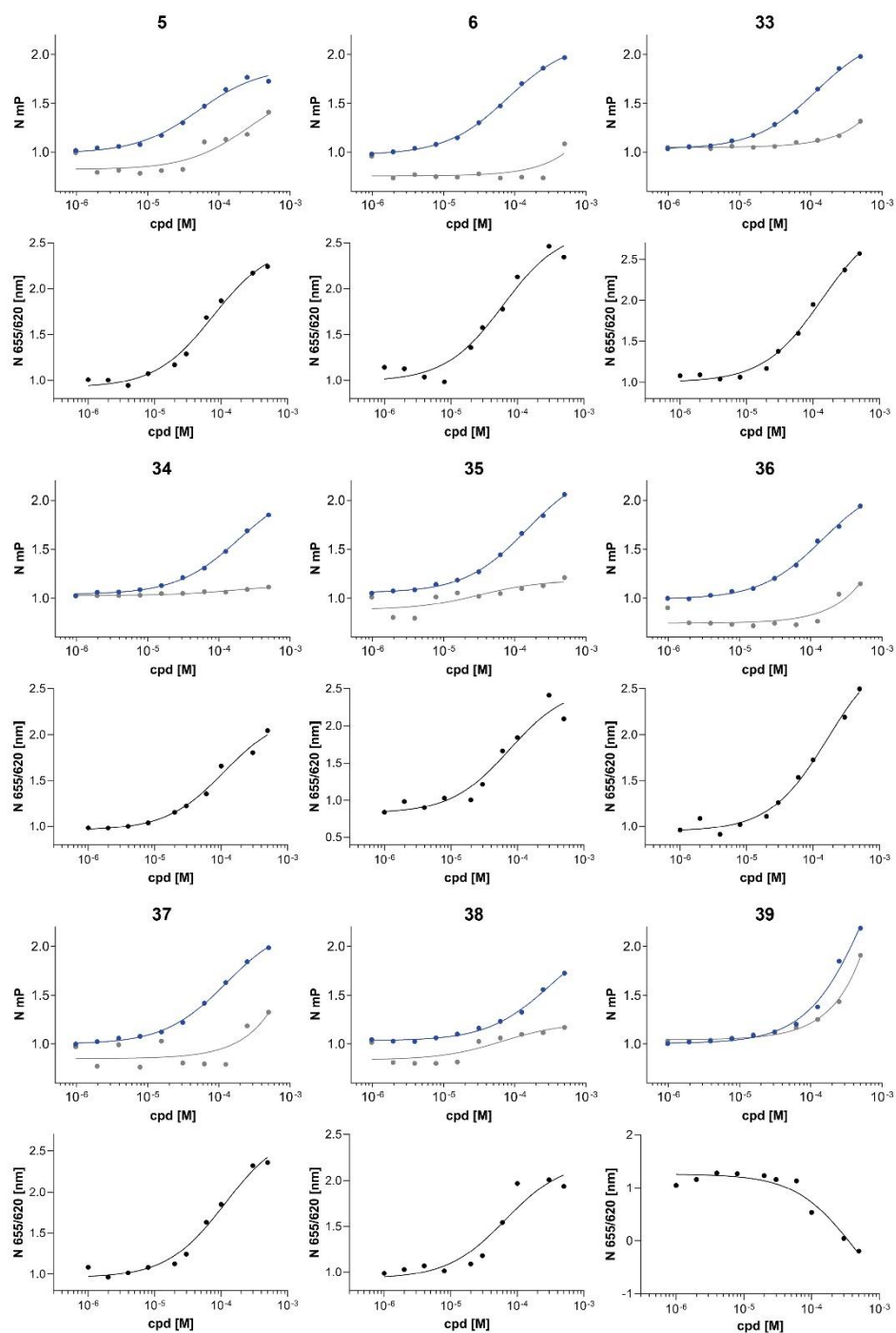
5.2.6 Fluorescence polarization dose-response assay of compounds identified in the HTS on the SLP76 and BLNK peptide systems

In the past decades, the drug discovery field has made huge steps forward in the identification of hits and lead compounds, thanks to the improvement in library design and screening technologies⁶³. These technologies, as well as structure-based drug design approaches, played fundamental roles in lead compound optimization and in the understanding of their binding mechanism to their targets^{64,65}.

Structural information on the interaction between proteins and their ligands can be extremely valuable for the success of a drug discovery project. However it is not always easy to obtain.⁶⁶ In the 14-3-3 field, the structural path seems to be more practicable than others, relatively speaking. However, this is only true if when using short phosphorylated peptides to represent larger and more complex 14-3-3 clients, as it is easier to obtain crystals of those in complex with 14-3-3. In contrast, it is much more difficult to use longer constructs, such as protein domains or actual full-length partners. Of the tens of 14-3-3 structures deposited in the PDB, only 6 show 14-3-3 in complex with longer binding partners⁶⁷ (Figure 1.4). While 14-3-3 has a rigid structure, its binding partners often contain intrinsically disordered regions that bring a disadvantageous entropic contribution to the crystallisation process, making the determination of these structures extremely challenging⁶⁸.

With this in mind, we decided to test some of the molecules identified in the HTS, in a dose-response assay on the 14-3-3 γ /SLP76pS376 peptide system. The testing on the peptide system, might provide new information of the mechanism of binding and could help identify the molecules most amenable to structural studies. In order to do so, the FP assay developed in Chapter 4 was used.

The 64 single point hits identified in the HTS were tested in dose-response on the peptide systems to check whether a connection between the SLP76 peptide system and the SLP76-SH2 system could be found. Compounds active on both would be ideal tests in crystallographic studies with the SLP76pS376 peptide. The 64 compounds were tested also on the 14-3-3 γ /BLNKpT152 for counter screening. Of the 64, the 16 most active ones were selected, and the assay was repeated (Figure 5.11). The stimulation curves for the fluorescence polarization derived from the 14-3-3 γ /SLP76pS376 system were superimposed on the ones generated from the 14-3-3 γ /BLNKpT152 system to compare compound activity (Figure 5.11). For compounds **5**, **6**, **33**, **34**, **35**, **36**, **37** the difference between the two systems appeared clear. The consistency of the control (see Chapter 4 for Z' factors) and the evidences provided by the BLNKpT152 counterscreen, suggest that they are having a genuine effect. From compound **39** to **46**, instead, the difference between the two titration curves is less obvious. For comparison, the dose-response curves derived from the HTRF assay on 14-3-3 γ /SLP76-SH2 were also reported below to the FP assay curves (Figure 5.11).



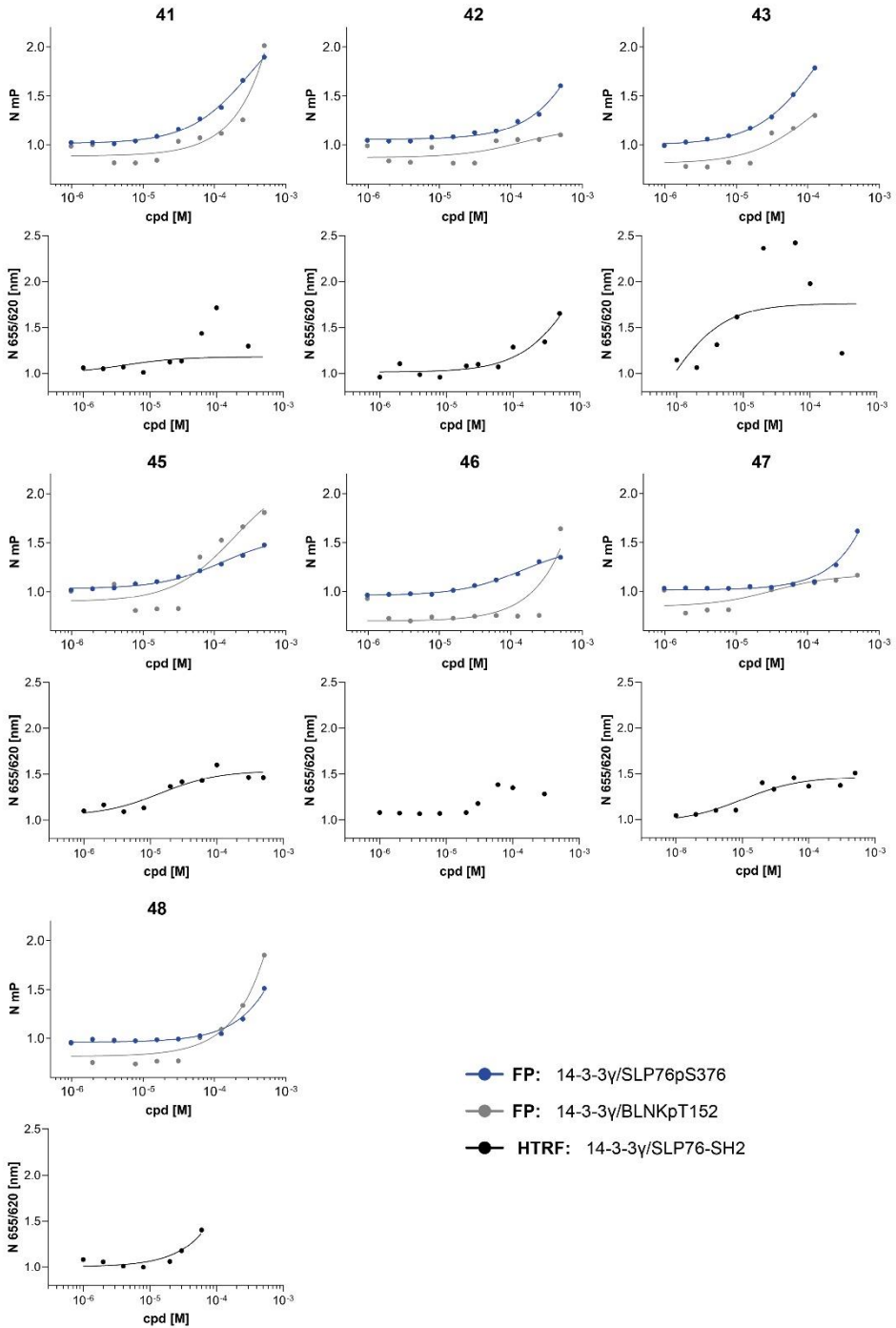


Figure 5.11 | FP and HTRF dose-response assays on a selection of the most active compounds for the 14-3-3 γ /SLP76pS376 system. For each compound identified with a number, the graph on the top shows the dose-response for the FP assay while the graph on the bottom shows the dose-response for the HTRF assay. All the read-outs were normalised using the R18 peptide as reference (o).

The structures of the compounds are reported in Figure 5.12. It is interesting to notice how compounds **5**, **6**, **33**, **37** and **42** share the feature of a positively charged quaternary amine. EC₅₀ values are reported in Table 5.4 for both FP and HTRF dose-response for compounds **5** and **6**. The EC₅₀ values calculated by the two different techniques appear to be comparable.

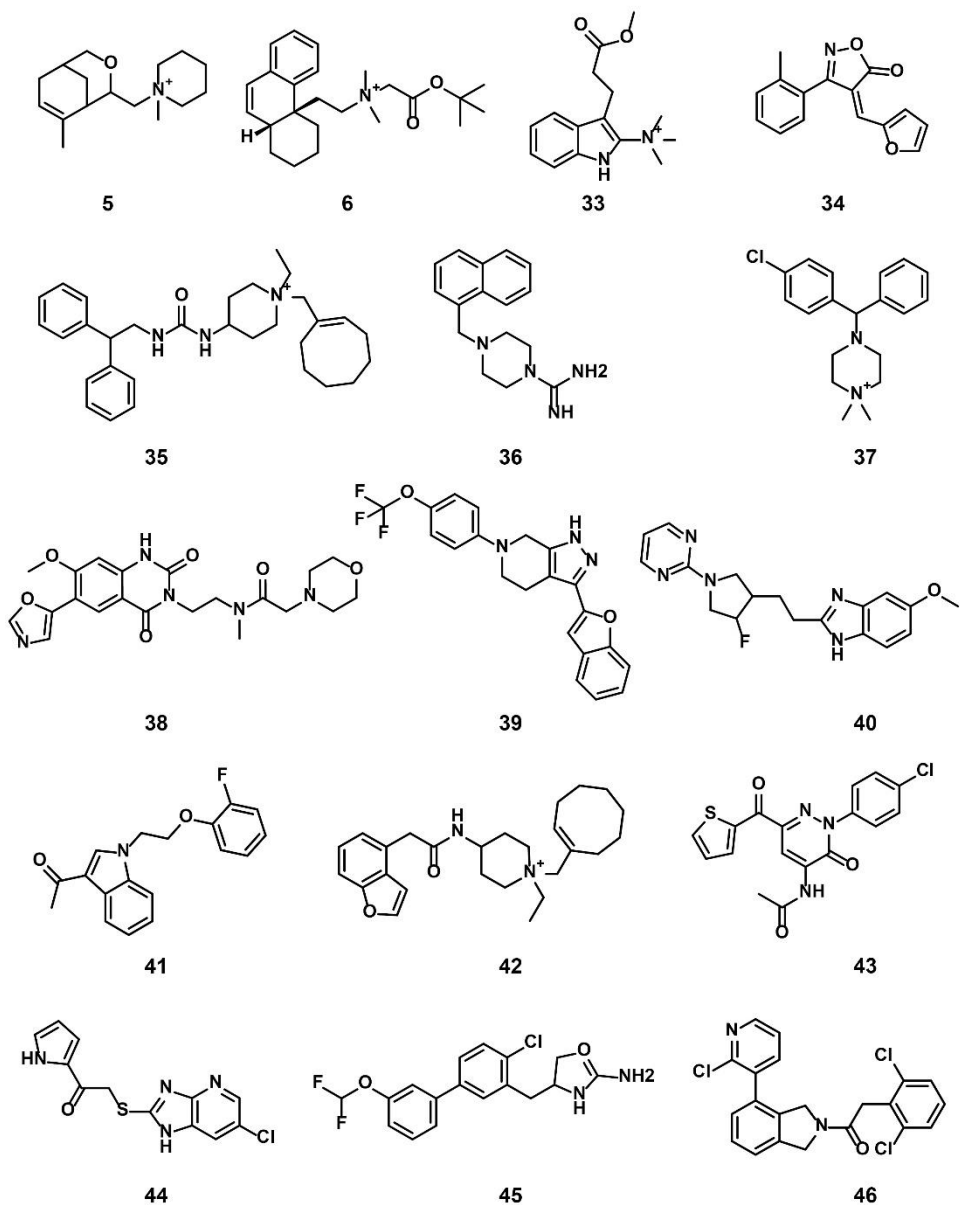


Figure 5.12 | Chemical structures of the 16 compounds selected from the FP assay performed on the 14-3-3 γ /SLP76pS376 peptide system.

Table 5.4 | EC₅₀'s values for the compounds **5**, **6** and **33** to **46**.

Molecule	FP EC ₅₀ (μM)		HTRF EC ₅₀ (μM)
	14-3-3γ/SLP76pS376	14-3-3γ/BLNKpT152	14-3-3γ/SLP76
5	51.6 ± 9.6	Nd*	75.5 ± 14.9
6	78.8 ± 4.1	Nd*	60.8 ± 19.8

*Nd: not determined

Compounds **1**, **2**, **3** and **4** (Table 5.1) proved to be among the most interesting compounds active on the 14-3-3γ/SLP76-SH2 system. The screening of a library of derivatives of the two scaffolds opened new paths for future work on these molecules. Being among the 64 compounds tested on the 14-3-3γ/SLP76pS376 system it was logical to give them special consideration when analysing the data of the FP dose-response assay. The four compounds generated a flat response in the assay (Figure 5.13a). Therefore, perhaps these four compounds engage a binding pocket formed by the contact of 14-3-3γ and SLP76-SH2 which is no longer present in the 14-3-3γ/SLP76pS376 system. An interaction between 14-3-3 and a phosphorylated peptide provides considerably less exposed contact surface compared to an interaction formed by 14-3-3 and a second larger protein construct, diminishing the locations in which a compound could to stabilise the complex.

Finally, the 14-3-3γ/SLP76pS376 and the 14-3-3γ/BLNKpT152 systems were tested against Fusicoccin-A (FC-A). FC-A, a natural fungal toxin, has often been used as a reference and as a tool compound for the stabilisation of 14-3-3 PPIs^{42,48,69}. The titration of FC-A on the 14-3-3γ/SLP76pS376 and the 14-3-3γ/BLNKpT152 systems showed to inhibit rather than enhance the interaction, suggesting that the FC-A molecule could displace the peptides from their binding pockets at higher concentrations (Figure 5.13b). Given the availability of structural information generated in this thesis and scientific literature, we tried to rationalize the observation by superposing the 14-3-3σ/SLP76-S376⁷⁰, the 14-3-3σ/BLNKpT152⁷¹ and the 14-3-3σ/p53/FC-A crystal structures⁶⁹ (Figure 5.13c). The 14-3-3σ/p53/FC-A crystal structure is a ternary complex formed by a p53 derived synthetic peptide and the molecule FC-A⁶⁹. From the superposition it is possible to see how FC-A generates a clash with SLP76pS376 tyrosine (in blue) and how one of FC-A hydroxyl group points directly towards a BLNKpT152 proline (in yellow), making them unlikely to co-exist simultaneously inside the 14-3-3 binding groove (Figure 5.13c). The insights from this structural analysis can explain why FC-A does not behave as a binder of the binary 14-3-3γ/SLP76pS376 and 14-3-3γ/BLNKpT152 complexes.

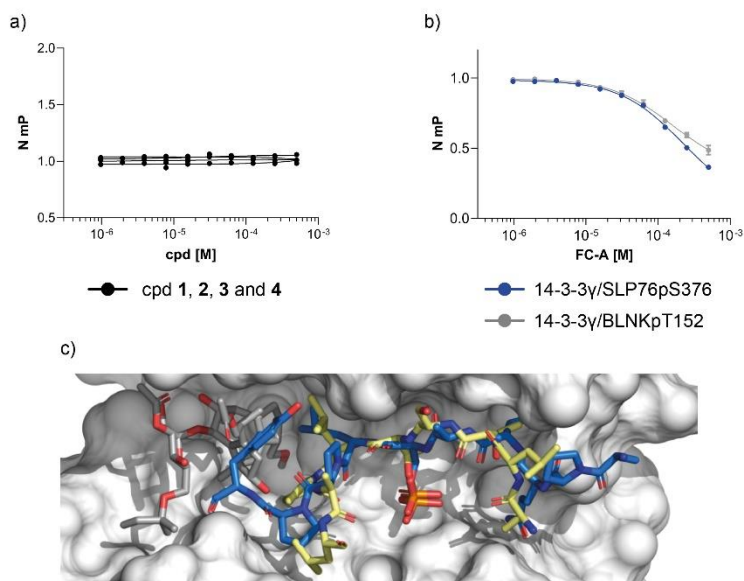


Figure 5.13 | FP dose-response assay of compounds 1, 2, 3, 4 and FC-A, and superposition analysis of SLP76pS376, BLNKpT152 and FC-A crystal structures. a) Titration of compounds 1, 2, 3 and 4 on the 14-3-3 γ /SLP76pS376 system. b) Titration of FC-A on the 14-3-3 γ /SLP76pS376 and 14-3-3 γ /BLNKpT152 systems. c) Superposition of the 14-3-3 σ (white surface) crystal structures in complex with SLP76pS376 (6ZCJ, blue sticks), BLNKpT152 (6YLU, yellow sticks) and p53 (peptide not shown) stabilised by FC-A (5MXO, grey sticks).

5.2.7 Crystallographic attempts to generate a ternary complex of the 14-3-3/SLP76 PPI

Several crystallographic experiments were implemented in order to try to generate a crystal structure of a ternary complex composed of 14-3-3 σ , the SLP76pS376 peptide and one of the compounds identified as active towards the 14-3-3/SLP76 PPI. The soaking technique was used. Ideally, the best 14-3-3 isoform to conduct the study would be the same isoform used in the assay, which is 14-3-3 γ . Crystallisation attempts of this isoform with the SLP76pS376 peptide were made and generated crystals in a few different conditions. However, these crystals never provided a high enough resolution and/or were not robust enough to tolerate DMSO required for the soaking process.

In place of 14-3-3 γ we decided to move to the more robust 14-3-3 σ /SLP76pS376 system. Although we are considering two different isoforms, the 14-3-3 binding groove is conserved among all the isoforms. The choice of using a different isoform that best suits crystallographic purposes is therefore reasonable. A grid screen of 14-3-3 σ crystallization conditions was already known but a test on small volumes was performed nonetheless to identify the best PEG400 concentration and pH range to allow the scaling up of the crystallisation drops: PEG400 28%, pH 6.9. A high number of crystallization drops containing 14-3-3 σ /SLP76pS376 crystals were generated in 2 and 4 μ L drops (Figure 5.14).

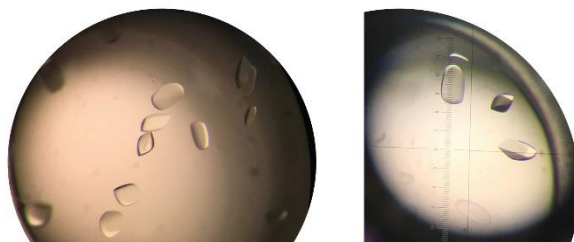


Figure 5.14 | 14-3-3 σ /SLPpS376 crystals exploited in the soaking process of small molecules.

Compounds **1, 2, 3, 4, 5, 6, 7, 8, 9, 10, 12, 13, 16, 33, 34, 35, 36, 37, 42** were soaked into the 14-3-3 σ /SLP76pS376 crystals in concentrations that varied from 10 mM to 50 mM and 10% final DMSO. Unfortunately, despite the high resolution of the generated structures (1.4 to 1.8 Å), no extra electron density was ever detected. To date, there is still no structural evidence of the compounds identified in the assays bound to a 14-3-3/SLP76 complex available. More crystallisation trials are planned, and co-crystallisation will also be considered instead of soaking.

5.2.8 Complex formation for the crystallisation attempts of longer 14-3-3 binding partners

In parallel to the SLP76pS376 peptide work, crystallisation trials have been attempted on the longer 14-3-3 binding partners: pSLP76-SH2 and pBLNK-SH2. Crystal structures of these complexes would be quite exceptional in the 14-3-3 field. When it comes to crystallisation trials, every additional parameter exponentially increases the possible sets of combinations for the crystallisation plates ⁷². Among the main parameters that one has to consider when designing a crystallisation experiment are: the chosen number of sparse matrix screens, the incubation temperature (usually 4 °C or 18 °C), the sample/crystallisation cocktail ratio and the method used to reach supersaturation ⁷³. Even with one single protein complex to crystallise, the combination of these four parameters could lead to hundred if not thousands of different conditions. Since there are seven 14-3-3 isoforms, identifying hit conditions can be very laborious. The sample preparation and the choice of which 14-3-3 partner construct to use is also critical for the success of the experiment. As mentioned above, most 14-3-3 clients contain intrinsically disordered regions, and the scouting for the identification of the best “crystallizable” protein construct is another parameter to take into consideration.

With all this considered the choice of parameters for the crystallisation experiments of 14-3-3 in complex with pSLP76-SH2 and pBLNK-SH2 were somewhat arbitrary. The protein chosen for the experiments were: 14-3-3 γ , 14-3-3 σ clu3, pSLP76-SH2 and pBLNK-SH2. 14-3-3 σ clu3 is a mutated construct of 14-3-3 σ (E75A, E76A, K77A). The construct, described by Sluchanko et al. ⁷⁴, helped in the resolution of the crystal structure of full-length HSPB6 with 14-3-3 σ (PDB ID: 5LTW). These mutations were made following a SER (surface entropy reduction) approach ⁷⁵. A second construct, 14-3-3 σ clu1,

carrying mutations K159A, K160A, E161A was also purified, but not used in crystallisation trials so far. The protein complexes were prepared by mixing 14-3-3 γ , and 14-3-3 σ clu3 proteins with BLNK-SH2 or SLP76-SH2 in a 1:1 ratio. The complexes were then loaded onto a size-exclusion column for an additional polishing step. The chromatograms for 14-3-3 γ /pSLP76-SH2, 14-3-3 σ clu3/pSLP76-SH2 and 14-3-3 γ /pBLNK-SH2 are shown in Figure 5.15. SDS-PAGE gels were performed to check the content of the collected fractions. For the 14-3-3 γ /pSLP76-SH2 and 14-3-3 σ clu3/pSLP76-SH2 complexes, a smaller peak at higher elution volumes reveals the presence of SLP76-SH2 which has been eluted as a single protein. This suggests that either pSLP76-SH2 completely saturated the 14-3-3 binding sites, or a small portion of pSLP76-SH2 was not successfully phosphorylated during the reagent preparation process and consequently did not bind to 14-3-3. In either case, the size-exclusion purification step contributed to making the sample more homogeneous, a desirable feature in crystallisation trials.

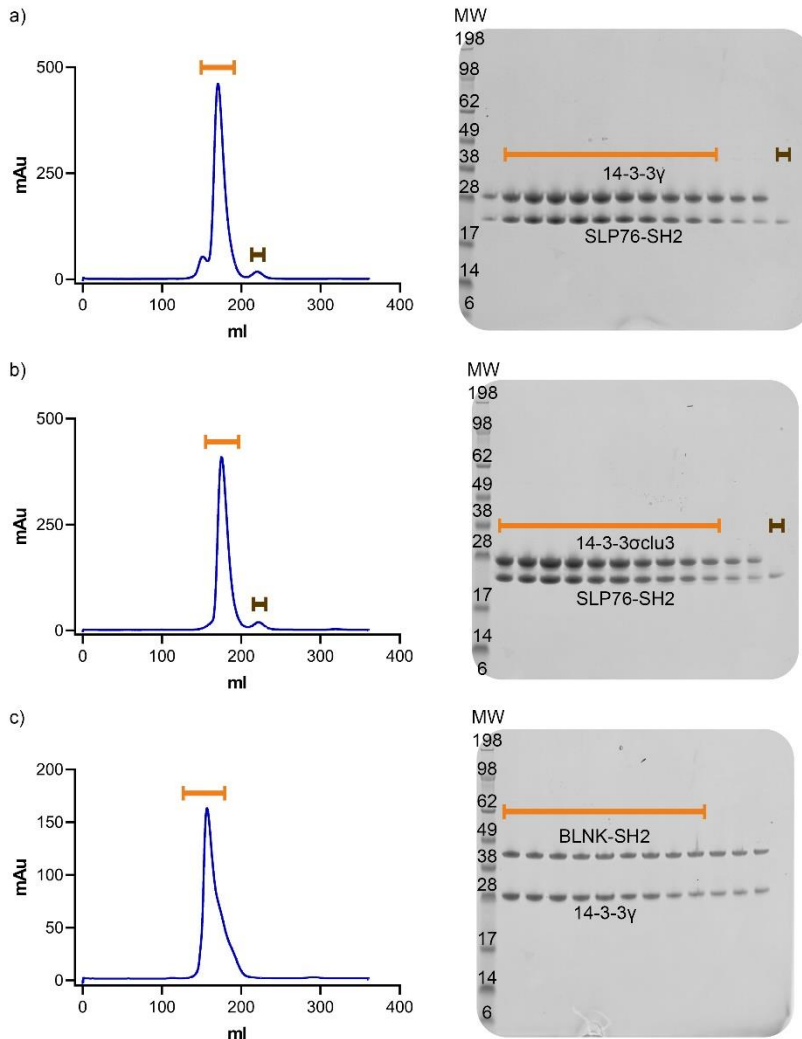


Figure 5.15 | Size exclusion profiles of 14-3-3 in complex with binding partners and SDS-PAGE analysis of the collected fractions. a) Size-exclusion profile of the 14-3-3 γ /SLP76-SH2 complex. the SDS-PAGE confirms the complex formation, showing two distinct bands corresponding to the two different proteins under the main peak (orange bar). A smaller peak at higher elution volumes shows SLP76-SH2 eluted alone. b) Size-exclusion profile and SDS-PAGE analysis of the 14-3-3 σ clu3/SLP76-SH2 complex. c) Size-exclusion profile and SDS-PAGE analysis of the 14-3-3 γ /BLNK-SH2 complex.

The protein complex samples were then dispensed over 24 sparse matrix screens (Table 5.5) and stored at 18 °C.

Table 5.5 | Sparse matrix screens used in the crystallography campaign.

Sparse matrix screens			
Classic*	AmSO ₄ *	JCSG Core I*	MbClass*
Classic Lite*	PACT*	JCSG Core II*	MbClass II*
pH Clear*	Lite*	JCSG Core III*	LMB‡
pH Clear II*	PEGs*	JCSG Core IV*	Morpheus‡
ComPAS*	PEGs II*	JSCG +*	WizardCryo‡
MPDs*	ProteinComplex*	BCS*	BCS‡

*: Qiagen; ‡: Molecular Dimension

Despite the observation that a few drops contained potential starting points for crystal optimisation, none of the complexes described above lead to a crystal structure. Optimisation has been attempted on the 14-3-3 σ cl α 3/pSLP76-SH2 complex, but these attempts never led to crystals of the required quality and/or size for harvesting and data collection. Obtaining high resolution structures remains a key goal of this research, however we were not able to achieve this goal within the course of this work.

5.3 Conclusions

In this study we have developed and performed a high-throughput screen of a chemically diverse 20,000 small molecule library to discover molecular glues of the 14-3-3 γ /SLP76 protein-protein interaction. The use of counter screens with a related 14-3-3/p27 system and an unrelated PPI with matched fluorophores allowed us to reduce false positives and identify specific modulators of both 14-3-3 protein-protein interactions. The outcome was that we were able to find 16 novel stabilisers of the 14-3-3 γ /SLP76 complex across a range of different chemotypes with good lead-like properties to support future research. Of these 16 hits, six compounds (Compounds **1 - 5** and Compound **7**) achieved our principal objective of selective stabilisation of 14-3-3 γ /SLP76 with orthogonal confirmation in SPR and are a priority for further exploration. Of equal interest were a group of compounds that modulated both the 14-3-3 systems tested and offer the intriguing possibility that these molecules may be of general utility in the field of 14-3-3 research. These preliminary results already hint that selectivity may be achievable in this group of compounds with Compound **12** one of the most interesting compounds for further investigation which stabilised the 14-3-3/p27 system with an EC₅₀ of 430 nM.

To the best of our knowledge this is the first report in the field of 14-3-3 PPIs to use a phosphorylated protein construct in an HTS HTRF format. In our opinion, such protein constructs have greater relevance than the short synthetic phosphopeptides that have been extensively used to represent the client protein in the 14-3-3 field to date. Although these phosphopeptides remain valuable tools to enable rapid early investigation of new 14-3-3 PPIs, they have inherent limitations as screening systems to find modulators of these interactions. By contrast working with full-length/truncated versions of phosphorylated 14-3-3

binding partners substantially extends the opportunity to discover druggable binding sites beyond the 14-3-3 amphipathic binding pocket. In this regard we believe that the results in this study support wider use as an approach to find molecular glues of 14-3-3 protein-protein interactions. Of course, the novel 14-3-3 stabilisers we report in this paper remain early hits and should still be treated cautiously. There is a need to continue to characterise these compounds to understand where they bind and how they stabilise the 14-3-3 ternary complex. Our priority will be to use X-ray crystallography and NMR to locate and rationalise the binding of the small molecules identified here. This will open the path for future optimisation of these molecules to tune and increase their stabilisation effect and ultimately demonstrate a therapeutically useful function.

Additionally, we screened a library of 312 derivatives of two chemotypes identified in the HTS campaign. The compounds were tested first in a single point TR-FRET and the best 16 compounds were tested in a dose-response assay. All 16 compounds were shown to be good stabilisers of the 14-3-3 γ /SLP76 PPI and were able to produce complete dose-response curves from which EC₅₀ values could be derived. Screening of analogues from the wider UCB library has therefore expanded the number of hits for further study and increased confidence in Scaffolds A and D for further exploration. The optimisation of stabilisers is inherently more challenging than classic orthosteric inhibitors. In orthosteric PPI inhibition for instance, the modification of a substituent might determine in a clearer way whether the compound binds or not. The pocket is usually more defined and the interaction simpler, making the optimisation of binding intrinsically easier. With stabilisation on the other hand, the small molecule has to act as a molecular glue. Therefore, the SAR cannot be expected to be simple linear combinations of different groups but will probably be more complex given that we are trying to optimise the interacting surfaces of two binding partners than a single protein. Changes made during optimisation of the molecules are as likely to disrupt rather than improve the stability of the complex. In addition, the EC₅₀ alone cannot be considered the only activity parameter to focus on but must be done in tandem with the degree to which each compound can stabilise the protein system (e.g. K_D improvement as judged by dose ratio experiments).

Nonetheless, the molecules identified have proved to be promising hits and valuable tools to develop better PPI stabilisers. This now requires a major synthetic effort to further define the SAR around these scaffolds, preferably combined with structural information to optimise these compounds. The deliberate deletion or addition of specific substituents and the consequent comparison with the simplest or minimally active molecule in biophysical assays would certainly give insight in the structure-activity relationship.

In the attempt of obtaining structural data on some of the hits, a fluorescence polarization assay was performed using the 14-3-3 γ /SLP76pS376 peptide system and the active molecule soaked into 14-3-3 σ /SLP76pS376 crystals. So far, structural data on the hits identified in this work are still elusive. Attempts in generating a complex of 14-3-3 with a longer binding partner (pSLP76-SH2 and pBLNK-SH2) has been performed as well. However, the generation of such protein complex crystal structures in the 14-3-3 field remains a challenge. More experiments will be set up in the future and different strategies will be applied. Among these, the 4°C temperature and different sample to crystallisation cocktail ratio will be tried. Co-crystallisation experiments with potential stabilisers could be tried as well. If the compounds

can significantly stabilise the 14-3-3 complex, it is conceivable that this could help crystallisation. Although speculative and very sample consuming this experiment could be implemented in stages focussing on a small number of the best stabilisers from each chemotype discovered in this work.

5.4 Material and Methods

Protein Expression and Purification

14-3-3 γ and SLP76 were expressed respectively with a (His)₆ and (His)₆-SUMO tag in Nico21(DE3) competent cells, in 2TY media. The purification was carried out by affinity chromatography on Nickel columns (HisTrap HP, 5 mL). The tags were cleaved with TEV or SUMO protease. The proteins were then loaded again on Nickel columns to remove any uncleaved protein. A final purification step was performed loading the proteins on a size-exclusion chromatography column (HiLoad 26/600 Superdex 75 pg). All purification steps were performed on an ÄKTA pure protein purification system (Cytiva). SLP76 was phosphorylated *in vitro* by incubating overnight at room temperature in its storage buffer supplemented by 0.75 mM ATP, 20 mM MgCl₂ and HPK1 kinase (Thermo Fisher Scientific) with a kinase:protein ratio of 1:3000. Phosphorylation status was checked by LC-MS. The expression, purification and phosphorylation of the SLP76 construct (SLP76-SH2) has been described before.⁷⁰

Protein labelling

14-3-3 γ was labelled with Tb cryptate: LanthaScreen™ Amine Reactive Tb Chelate, (PV3582, ThermoFisher). SLP76 was labelled with AF647: Alexa Fluor™ 647 carboxylic acid, succinimidyl ester, A37573 ThermoFisher). Before labelling, the protein buffers were exchanged to sodium carbonate buffer at pH 9.0 to allow deprotonation of amine groups. The proteins were subsequently diluted down to 50 μ M with sodium carbonate buffer, and a 7-fold and 5-fold excess of Tb cryptate and AF647 were added to 14-3-3 γ and SLP76 respectively. The mixtures were left in the dark for 1h at room temperature. After labelling, the buffers were ultimately exchanged to assay buffer (50 mM Tris pH 7.5, 150 mM NaCl, 5 mM MgCl₂, 0.05% v/v Tween-20). All the buffer exchange steps were performed with Zeba™ Spin Desalting Columns, 7K MWCO, 0.5 mL (ThermoFisher) and P-10 Desalting Columns (Cytiva) for higher volumes.

Homogeneous Time-Resolved Fluorescence Assay Development and High Throughput Screening

384-well Greiner plates (Ref. 784201) were pre-filled with 2 μ L of compounds at 2 mM, 100% DMSO, except for columns 1,2, 23 and 24. Columns 1,2 were filled with 2 μ L of DMSO while columns 23, 24 were filled with 2 μ L of the 14-3-3 inhibitor R18 at 20 μ M using a Multidrop Dispenser (ThermoScientific). Next, 40 μ L of protein mixture containing Tb-labelled 14-3-3 γ at 1 nM and AF647 labelled SLP76 at 600 nM in assay buffer (50 mM Tris pH 7.5, 150 mM NaCl, 5 mM MgCl₂, 0.05% v/v Tween-20) were added using a Multidrop Dispenser (ThermoScientific). Hence, the final assay concentrations were 14-3-3 γ -Tb at 1 nM, SLP76-AF647 at 600 nM, compounds at 100 μ M, R18 at 1 μ M, and DMSO at 5% v/v. To perform the assay, 30 μ L volumes were then transferred using a Biomek FX^P Automated Workstation (Beckman Coulter) into Corning 384-well 3574 assay plates. The plates were incubated at room temperature with gentle shaking for 4 h. Finally, the data were collected on a PHERAstar FSX plate reader (BMG Labtech) with an λ_{ex} 337 nm, λ_{em} 665 nm and 620 nm HTRF filter setting. The data were exported in IDBS ActivityBase (IDBS) where they were normalised setting the R18 negative control as 100% inhibition and the DMSO control as 0%. Negative percentage values were therefore associated with a stabilisation of the 14-3-3 γ /SLP76 interaction. The threshold of -20% inhibition (or 20% stabilisation) was chosen to select the hits to follow up. The selected hits were retested on 14-3-3 γ /SLP76 and were also tested against an unrelated protein pair (IL-17/receptor) in a similar assay setup. Only the ones that had an effect on 14-3-3 γ /SLP76 and not on the IL-17/IL17 receptor system were selected. All the assays were performed as described above.

For the single point derivatives library screening the compounds came in 384-well Greiner plates (Ref. 784201) filled with 10 μ L at 10 mM. A dilution was performed with a Multidrop Dispenser (ThermoScientific) to 400 μ M adding DMSO to the same plate. Columns 1, 2, 23 and 24 were empty upon delivery and were filled separately with DMSO (1 and 2) and compound **16** 1 mM (23 and 24) identified in the original HTS with a Multidrop Dispenser (ThermoScientific). 40 μ L of protein mixture, 14-3-3 γ -Tb 1 nM and SLP76-AF647 600 nM in assay buffer (50 mM Tris pH 7.5, 150 mM NaCl, 5mM MgCl₂, 0.05% v/v Tween-20) were added with a Multidrop Dispenser (ThermoScientific) into a Corning 384-well 3574 assay plate. 2 μ L of compounds, DMSO and positive control were transferred from the logistic plate to the Corning 384-well assay plate with a CyBio Felix liquid handler (Analytic Jena), to give final compound concentrations of 20 μ M for the derivatives and 50 μ M for the positive control. The plate was incubated

with gentle shaking for 4 h at room temperature. The data were collected on a PHERAstar FSX plate reader (BMG Labtech) with an λ_{exc} 337 nm, λ_{em} 665 nm and 620 nm HTRF filter setting. The data were exported in Excel where they were normalised, setting compound **16** as 100% stabilisation and the DMSO control as 0%.

Homogeneous Time-Resolved Fluorescence dose-response and dose-ratio

384-well Greiner plates (Ref. 784201) were pre-filled with 40 μL of compounds at 10 mM, 100% DMSO in column 3. Columns 1,2 and 4 to 22 were filled with 20 μL of 100 % DMSO with a Multidrop Dispenser (ThermoScientific). 2-fold dilutions of the compounds were carried over from column 3 to 22, with a CyBio FeliX liquid handler (analytikjena). 2 μL of R18 peptide at 20 μM was added to columns 23 and 24 of the Corning 384-well 3574 final assay plates with a Multidrop Dispenser (ThermoScientific). 40 μL of protein mixture, containing Tb labelled 14-3-3 γ at 1 nM and AF647 labelled SLP76 at 600 nM in assay buffer (50 mM Tris pH 7.5, 150 mM NaCl, 5 mM MgCl₂, 0.05% v/v Tween-20) were added with a Multidrop Dispenser (ThermoScientific) into the Corning 384-well 3574 final assay plates. 2 μL of compounds along with the DMSO control were then transferred with a CyBio FeliX liquid handler (analytikjena) from the 384-well Greiner plates (Ref. 784201) to the final Corning 384-well 3574 assay plates. This resulted in final assay concentrations of: Tb labelled 14-3-3 γ at 1 nM, AF647 labelled SLP76 at 600 nM, compound concentrations between 500 and 50 μM following a 2-fold dilution, and R18 peptide at 1 μM in 5% DMSO. The dose-response on the first 64 compounds was performed in singlet from a 500 μM top concentration. The repetition on the best 16 compounds was performed in duplicates from a 250 μM top concentration. A dose-response assay on an unrelated 14-3-3 ζ /p27 HTRF protein pair was performed as described above. Incubation, data acquisition and normalisation were performed as described above. For EC₅₀ estimation, the data were fitted with a “log(agonist) vs. response (three parameters)” model on GraphPad Prism version 8.1.1 for Windows, GraphPad Software, La Jolla California USA, www.graphpad.com. In the case of duplicates, each data point is the average of a duplicate measurement, standard deviation is reported as error bars.

Dose-ratio assays were carried out on Corning 384-well 3575 plates, serially diluting (2-fold) SLP76-AF647 in the presence of 14-3-3 γ -Tb 1 nM from a top concentration of 3 μM . Each protein titration was performed in the presence of a fixed concentration of compound. A set of 8 titration curves per compound (160, 80, 40, 20, 10, 5, 2.5, 0 μM) were performed. Proteins and R18 peptide were diluted from their stock concentration in assay buffer (50 mM Tris pH 7.5, 150 mM NaCl, 5mM MgCl₂, 0.05% v/v Tween-20). Incubation and data acquisition were performed as described above. One titration series of SLP76-AF647 on 14-3-3 γ was performed in the constant presence of R18 10 μM that completely inhibits the interaction. For data analysis the background FRET signal generated by the titration in the presence of R18 10 μM was removed from all values. K_D values for each curve were estimated and comparison with the different concentration of compounds were made. The data were fitted with a “One site – specific” model on GraphPad Prism version 8.1.1 for Windows, GraphPad Software, La Jolla California USA, www.graphpad.com. Each data point is the average of a duplicate measurement, standard deviation is reported as error bars.

Surface Plasmon Resonance

SPR experiments were performed on a Biacore T200 (Cytiva). The Sensor Chip NTA was validated as previously reported by Soini et al.⁷⁰. A DMSO tolerance at 2% and 5% was performed in the same way (Figure S 5.1). For compounds testing, the compounds were pre-incubated with SLP76, in final DMSO concentration of 5%. The compounds were tested at a single concentration of 100 μM and at multiple concentrations following a 3-fold dilution from a top concentration of 100 μM with SLP76 at the saturation concentration of 250 nM. A second set of experiments were performed at multiple concentrations of compound following a 3-fold dilution from a top concentration of 200 μM with SLP76 around the K_D concentration of 40 nM. The SLP76/compound mixtures were flowed over the immobilised 14-3-3 γ at 30 $\mu\text{L}/\text{min}$ for 180 s before allowing dissociation for 5 minutes. After every cycle, the chip was washed with EDTA and Ni²⁺ and 14-3-3 γ re-injected for the next cycle. The compound effects were measured by calculating the percentage of SLP76 remained on the chip after the dissociation phase and right before: $\text{RU} (\%) = \text{RU}_{5 \text{ sec before dissociation}} / \text{RU}_{+240 \text{ sec after dissociation}}$. RU response points relative to +240 sec after dissociation were also plotted and EC₅₀ values were extrapolated when possible. The data were fitted with a “One site – specific” model on GraphPad Prism version 8.1.1 for Windows, GraphPad Software, La Jolla California USA, www.graphpad.com.

Fluorescence Polarization dose-response assay

384-well Greiner plates (Ref. 784201) were pre-filled with 40 μ L of compounds at 10 mM, 100% DMSO in column 3. Columns 1,2 and 4 to 22 were filled with 20 μ L of 100 % DMSO with a Multidrop Dispenser (ThermoScientific). 2-fold dilutions of the compounds were carried over from column 3 to 22, with a CyBio Felix liquid handler (analytikjena). 2 μ L of R18 peptide at 200 μ M was added to columns 23 and 24 of the Corning 384-well 3575 final assay plates with a Multidrop Dispenser (ThermoScientific). 40 μ L of protein mixtures, containing 14-3-3 γ at 600 nM and SLP76pS376 FITC labelled peptide at 10 nM in assay buffer (50 mM Tris pH 7.5, 150 mM NaCl, 5 mM MgCl₂, 0.05% v/v Tween-20) or 14-3-3 γ at 2 μ M and BLNKpT152 FITC labelled peptide at 10 nM in assay buffer were added with a Multidrop Dispenser (ThermoScientific) into the Corning 384-well 3575 final assay plates. 2 μ L of compounds along with the DMSO control were then transferred with a CyBio Felix liquid handler (analytikjena) from the 384-well Greiner plates (Ref. 784201) to the final Corning 384-well 3575 assay plates. This resulted in final assay concentrations of: 14-3-3 γ at 600 nM, SLP76pS376 FITC labelled peptide at 10 nM or 14-3-3 γ at 2 μ M, BLNKpT152 FITC labelled peptide at 10 nM, compound concentrations between 500 and 50 μ M following a 2-fold dilution, and R18 peptide at 10 μ M in 5% DMSO. The data were collected on a PHERAstar FSX plate reader (BMG Labtech) with a λ ex 485 nm, λ em 520 nm FP filter setting. Data normalization was performed as described above. For EC₅₀ estimation, the data were fitted with a "log(agonist) vs. response (three parameters)" model on GraphPad Prism version 8.1.1 for Windows, GraphPad Software, La Jolla California USA, www.graphpad.com. In the case of duplicates, each data point is the average of a duplicate measurement, and standard deviation is reported as error bars.

Crystallography

14-3-3 σ /SLP76pS376 crystals were generated as described in Chapter 3. Compounds **1, 2, 3, 4, 5, 6, 7, 8, 9, 10, 12, 13, 16, 33, 34, 35, 36, 37, 42** were soaked at a final DMSO concentration of 10% and final compound concentrations between 50 mM and 10 mM. The final concentrations were obtained adding 0.4 μ L of compound to 4 μ L crystallization drops. The crystallization plates were stored back at 4 °C. The crystals were frozen at two different time points: 48 h and 7 days after the soaking process started. Data collection and structure solving was performed as described in Chapter 3.

Generation of protein complexes for crystallographic trials was performed by mixing SLP76-SH2 or BLNK-SH2 with 14-3-3 γ Δ C and 14-3-3 σ clu3, at a 1:1.2 molar ratio respectively. Three complexes were generated this way: 14-3-3 γ Δ C/SLP76-SH2, 14-3-3 σ clu3/SLP76-SH2 and 14-3-3 γ Δ C/BLNK-SH2. The complexes were left for an incubation time of 1 h in ice and consequently loaded onto a HiLoad 26/600 200pg size-exclusion column (Cytiva). SDS-PAGEs were performed on the collected fractions to confirm complex formation. The crystallization drops were dispensed by a mosquito robot (SPT Labtech) in 1:1 protein complex to crystallization condition ratio (0.4 μ L + 0.4 μ L) using 24 commercially available screens. The crystallization plates were stored in a Rock Imager (Formulatrix) at 18 °C.

5.5 Supporting Information

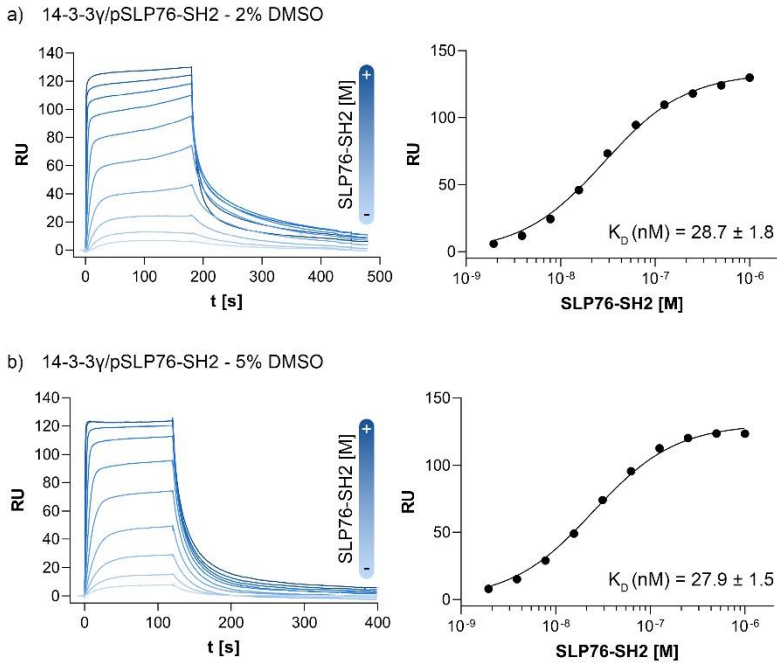
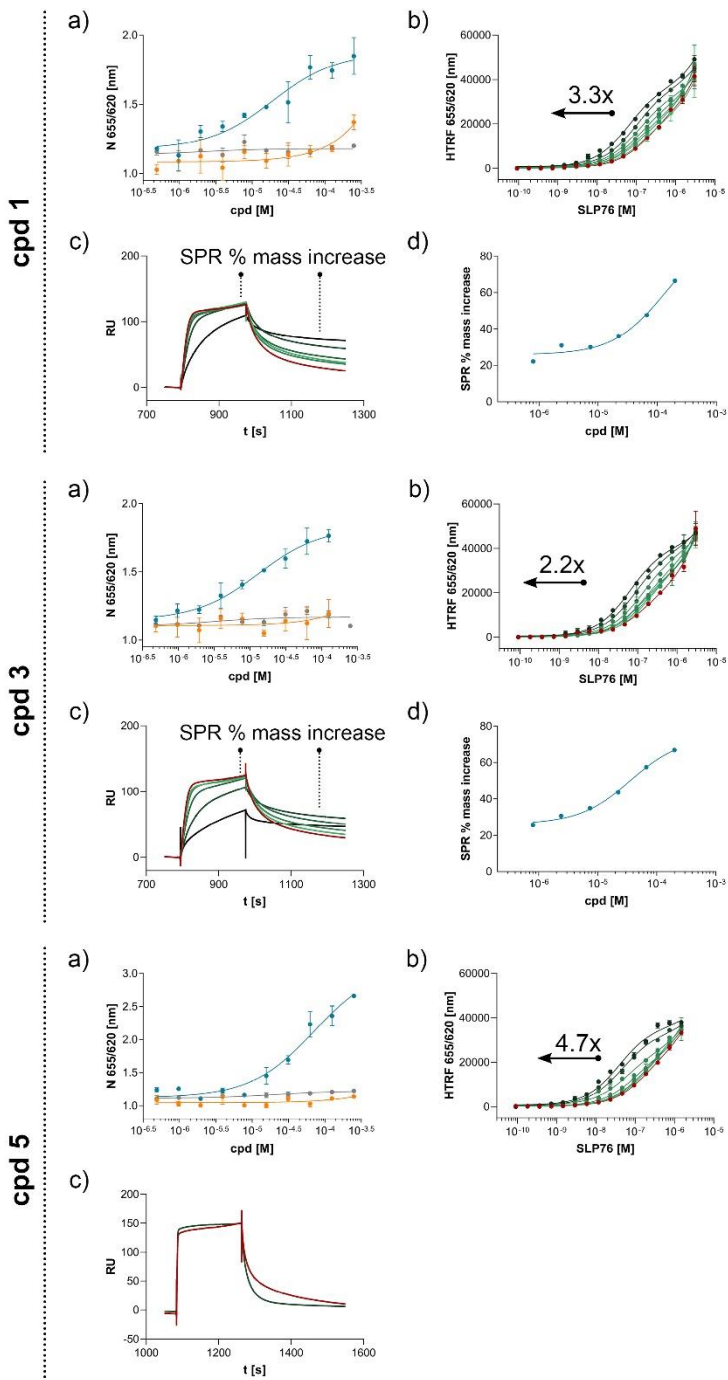
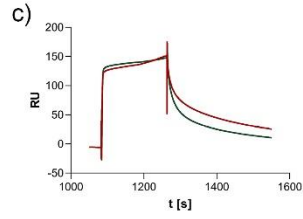
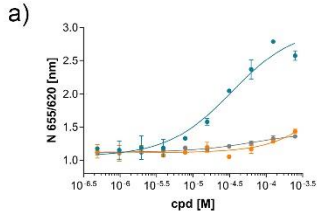


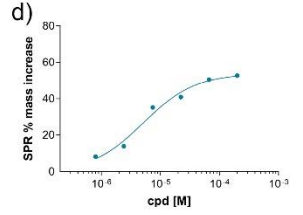
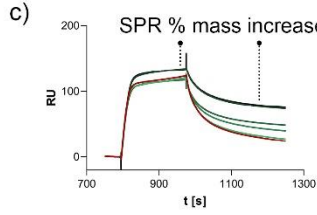
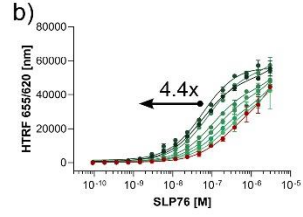
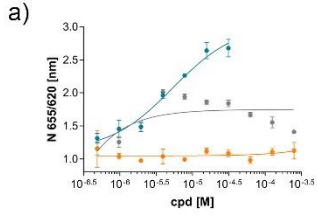
Figure S 5.1 | SPR binding assay of SLP76-SH2 to 14-3-3 γ at different DMSO concentrations. a) Sensorgram and respective binding curve extrapolated from reference points at equilibrium of SLP76-SH2 flowing over 14-3-3 γ in the presence of 2% DMSO. b) Sensorgram and respective binding curve extrapolated from reference points at equilibrium of SLP76-SH2 flowing over 14-3-3 γ in the presence of 5% DMSO. The K_D values has been extrapolated from the fitting model (One site - Specific binding model' on GraphPad Prism version 8.1.1 for Windows; GraphPad Software, www.graphpad.com.) and showed to be comparable the one to the other confirming a DMSO tolerance of the 14-3-3 γ /SLP76-SH2 system in an SPR context. A K_D value calculated by Soini et al. in absence of DMSO (43 nM) is also comparable and along the previous results validate the chip surface for further studies ⁷⁰.



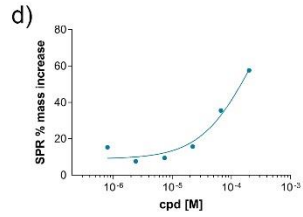
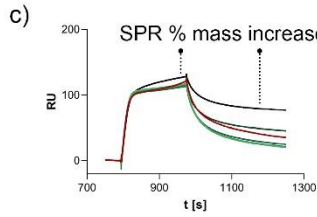
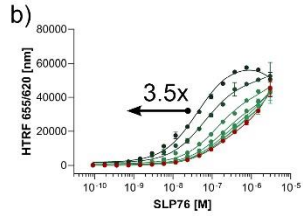
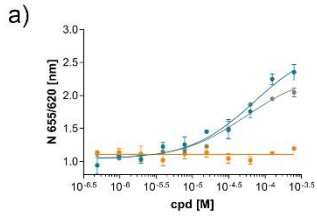
cpd 6

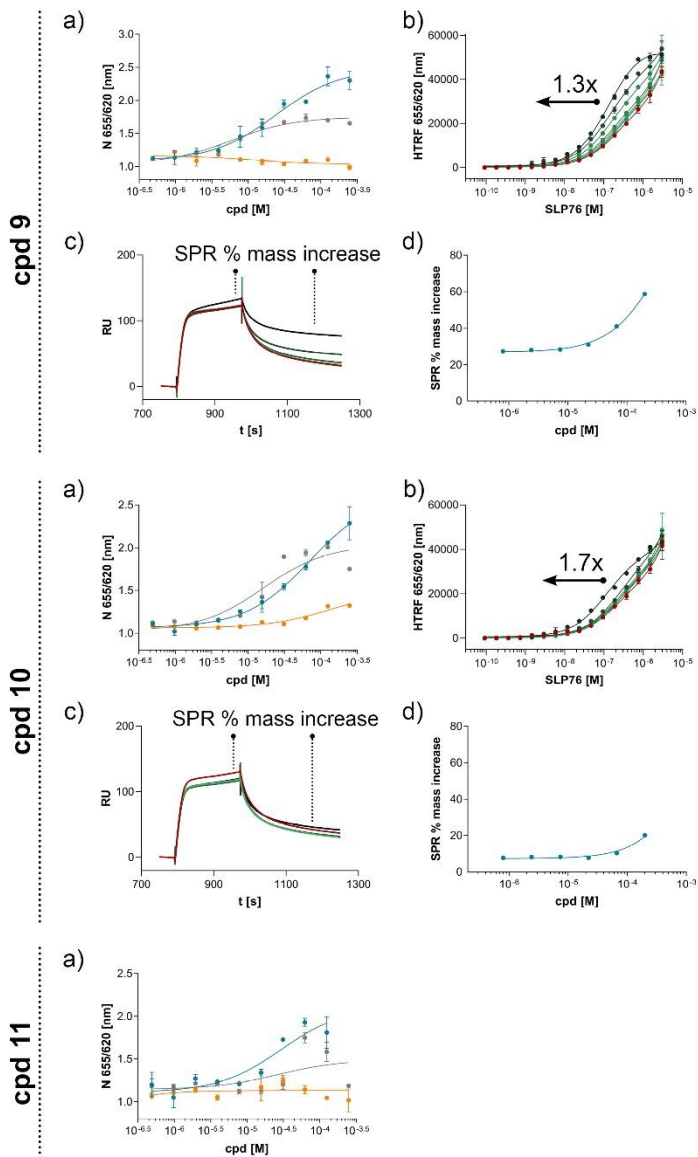


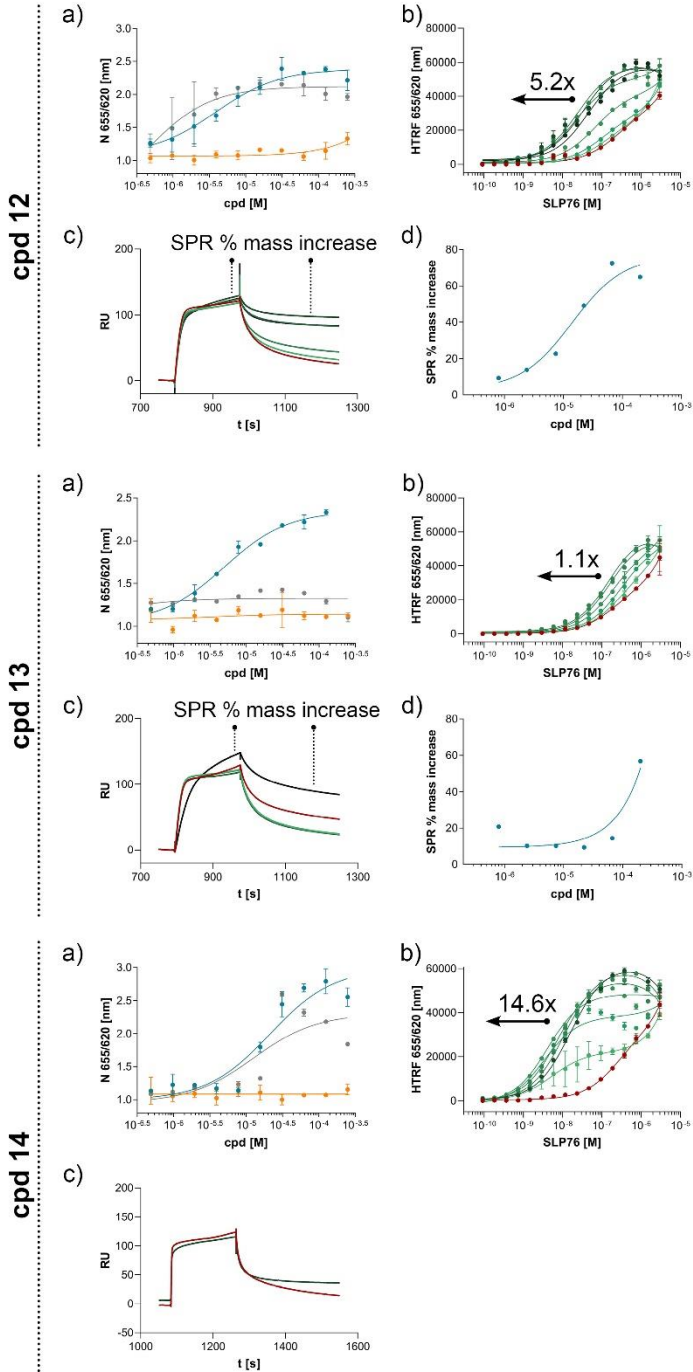
cpd 7



cpd 8







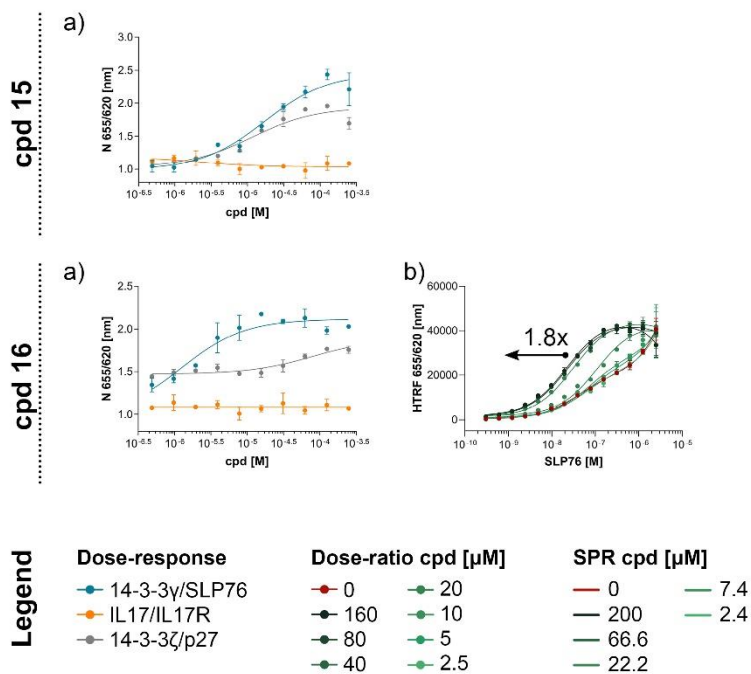


Figure S 5.2 | Set of assays for Compounds 1-16. a) HTRF dose-response comparison. b) HTRF dose-ratio assay with EC₅₀ fold increase. c) Sensorgrams at different compound concentrations. d) Plot and fitting curve derived from the sensorgram reference points showed in c).

Table S 2 | Compounds molecular properties.

Cpd. ID	MW (Da)	ALog P *	TPSA (Å²) ‡	CAS Number	IUPAC Name	Supplier
1	308.4	3.18	32.8	1797577-90-2	(6S)-9-benzyl-4-oxa-2,9-diazatricyclo[9.4.0.02,6]pentadeca-1(11),12,14-trien-3-one	AnalytiCon Discovery, GmbH
2	278.3	2.53	32.8	1796930-73-8	(6S)-14-fluoro-9-propan-2-yl-4-oxa-2,9-diazatricyclo[9.4.0.02,6]pentadeca-1(15),11,13-trien-3-one	AnalytiCon Discovery, GmbH
3	609.7	-1.32	154.2	n/a	(3S,6S,10S,11R,12S,13R,17R)-11,12-dihydroxy-15-(4-methoxybenzoyl)-4-(pyridin-3-ylmethyl)-18,22-dioxa-1,4,7,15-tetrazatetracyclo[15.3.1.13,6.110,13]tricosane-2,8-dione	AnalytiCon Discovery, GmbH
4	652.7	-0.41	159.5	n/a	(3S,6S,10S,11R,12S,13R,17R)-4-(1,3-benzodioxol-5-ylmethyl)-11,12-dihydroxy-15-(4-methoxybenzoyl)-18,22-dioxa-1,4,7,15-tetrazatetracyclo[15.3.1.13,6.110,13]tricosane-2,8-dione	AnalytiCon Discovery, GmbH
5	250.4	1.42	9.2	738575-09-2	1-methyl-1-[(8-methyl-3-oxabicyclo[3.3.1]non-7-en-2-yl)methyl]piperidin-1-ium	ChemBridge Corporation
6	400.5	3.32	35.5	692728-26-0	2-[(4aS,10aR)-6-methoxy-2,3,4,10a-tetrahydro-1H-phenanthren-4a-yl]ethyl-dimethyl-[2-[(2-methylpropan-2-yl)oxy]-2-oxoethyl]azanium	Chemieliva Pharmaceutical Product List
7	203.2	0.30	84.2	133847-06-0	3-pyridin-4-yl-[1,2,4]triazolo[3,4-b][1,3,4]thiadiazole	ChemBridge Corporation
8	380.4	2.99	98.3	791806-06-9	3-(benzimidazol-1-ylmethyl)-6-[(4-fluorophenoxy)methyl]-[1,2,4]triazolo[3,4-b][1,3,4]thiadiazole	Specs
9	232.3	1.44	80.5	1432902-04-9	3-(2-methoxyphenyl)-[1,2,4]triazolo[3,4-b][1,3,4]thiadiazole	Specs
10	234.3	1.29	81.5	892690-26-5	6-methyl-3-(2-methylfuran-3-yl)-7H-[1,2,4]triazolo[3,4-b][1,3,4]thiadiazine	Specs

Identification of Molecular Glues of the SLP76/14-3-3 Protein-Protein Interaction

11	333.4	3.76	82.1	n/a	4-[2-[7-imino-2-(5-methylfuran-2-yl)-5,6-dihydropyrrolo[3,4-b]pyridin-5-yl]ethyl]phenol	Chempartner
12	328.4	2.32	67.2	n/a	N-(2-methylpropyl)-1-oxo-2-propan-2-yl-3,4-dihydropyrazino[1,2-a]benzimidazole-8-carboxamide	ChemDiv
13	233.2	1.69	108.4	136715-68-9	5-(benzotriazol-1-ylmethyl)-1,3,4-oxadiazole-2-thiol	Maybridge, Ltd.
14	392.2	5.20	46.9	332943-31-4	N-(3,4-dichlorophenyl)-2-[3-(trifluoromethyl)-4,5,6,7-tetrahydroindazol-1-yl]acetamide	Specs
15	358.4	2.43	109.6	303973-50-4	3-methyl-7-[(3-methylphenyl)methyl]-8-(2-oxopropylsulfanyl)purine-2,6-dione	ENAMINE Ltd.
16	447.9	4.65	120.4	144338-89-6	(4-chlorophenyl)-[3-[(5-naphthalen-1-yltetrazol-2-yl)methyl]-5-sulfanylidene-1H-1,2,4-triazol-4-yl]methanone	Specs

* AlogP, calculated in Pipeline Pilot (Dassault Systemes) v 19; † Topological Polar Surface Area, calculated in Pipeline Pilot (Dassault Systemes) v 19.

5.6 References

- 1 Bier, D., Thiel, P., Briels, J. & Ottmann, C. Stabilization of Protein-Protein Interactions in chemical biology and drug discovery. *Prog Biophys Mol Biol* **119**, 10-19, doi:10.1016/j.pbiomolbio.2015.05.002 (2015).
- 2 Arkin, M. R., Tang, Y. & Wells, J. A. Small-molecule inhibitors of protein-protein interactions: progressing toward the reality. *Chem Biol* **21**, 1102-1114, doi:10.1016/j.chembiol.2014.09.001 (2014).
- 3 Lu, H. *et al.* Recent advances in the development of protein–protein interactions modulators: mechanisms and clinical trials. *Signal Transduction and Targeted Therapy* **5**, doi:10.1038/s41392-020-00315-3 (2020).
- 4 Ottmann, C. Protein-Protein Interactions. *Drug Discov Today Technol* **24**, 1-2, doi:10.1016/j.ddtec.2017.11.008 (2017).
- 5 Schreiber, S. L. The Rise of Molecular Glues. *Cell* **184**, 3-9, doi:10.1016/j.cell.2020.12.020 (2021).
- 6 Schreiber, S. L. Immunophilin-sensitive protein phosphatase action in cell signaling pathways. *Cell* **70**, 365-368, doi:10.1016/0092-8674(92)90158-9 (1992).
- 7 Liu, J. *et al.* Calcineurin is a common target of cyclophilin-cyclosporin A and FKBP-FK506 complexes. *Cell* **66**, 807-815, doi:10.1016/0092-8674(91)90124-h (1991).
- 8 Neklesa, T. K., Winkler, J. D. & Crews, C. M. Targeted protein degradation by PROTACs. *Pharmacol Ther* **174**, 138-144, doi:10.1016/j.pharmthera.2017.02.027 (2017).
- 9 Zhou, X., Dong, R., Zhang, J. Y., Zheng, X. & Sun, L. P. PROTAC: A promising technology for cancer treatment. *Eur J Med Chem* **203**, 112539, doi:10.1016/j.ejmech.2020.112539 (2020).
- 10 Schneckloth, A. R., Puchault, M., Tae, H. S. & Crews, C. M. Targeted intracellular protein degradation induced by a small molecule: En route to chemical proteomics. *Bioorganic & Medicinal Chemistry Letters* **18**, 5904-5908, doi:10.1016/j.bmcl.2008.07.114 (2008).
- 11 Buckley, D. L. *et al.* Targeting the von Hippel-Lindau E3 ubiquitin ligase using small molecules to disrupt the VHL/HIF-1 α interaction. *J Am Chem Soc* **134**, 4465-4468, doi:10.1021/ja209924v (2012).
- 12 Somers, G. F. Pharmacological properties of thalidomide (alpha-phthalimido glutarimide), a new sedative hypnotic drug. *Br J Pharmacol Chemother* **15**, 111-116, doi:10.1111/j.1476-5381.1960.tb01217.x (1960).
- 13 Fink, E. C. & Ebert, B. L. The novel mechanism of lenalidomide activity. *Blood* **126**, 2366-2369, doi:10.1182/blood-2015-07-567958 (2015).
- 14 Lopez-Girona, A. *et al.* Cereblon is a direct protein target for immunomodulatory and antiproliferative activities of lenalidomide and pomalidomide. *Leukemia* **26**, 2326-2335, doi:10.1038/leu.2012.119 (2012).
- 15 Ito, T. *et al.* Identification of a primary target of thalidomide teratogenicity. *Science* **327**, 1345-1350, doi:10.1126/science.1177319 (2010).
- 16 Crews, C. M., Georg, G. & Wang, S. Inducing Protein Degradation as a Therapeutic Strategy. *J Med Chem* **59**, 5129-5130, doi:10.1021/acs.jmedchem.6b00735 (2016).
- 17 Zhang, Y., Loh, C., Chen, J. & Mainolfi, N. Targeted protein degradation mechanisms. *Drug Discov Today Technol* **31**, 53-60, doi:10.1016/j.ddtec.2019.01.001 (2019).
- 18 Valeur, E., Narjes, F., Ottmann, C. & Plowright, A. T. Emerging modes-of-action in drug discovery. *Medchemcomm* **10**, 1550-1568, doi:10.1039/c9md00263d (2019).
- 19 Feng, J. J. & Zhang, C. A two-pronged attack. *Nat Chem Biol* **16**, 1154-1155, doi:10.1038/s41589-020-0647-1 (2020).
- 20 Che, Y., Gilbert, A. M., Shanmugasundaram, V. & Noe, M. C. Inducing protein-protein interactions with molecular glues. *Bioorg Med Chem Lett* **28**, 2585-2592, doi:10.1016/j.bmcl.2018.04.046 (2018).
- 21 Hughes, S. J. & Ciulli, A. Molecular recognition of ternary complexes: a new dimension in the structure-guided design of chemical degraders. *Essays Biochem* **61**, 505-516, doi:10.1042/EBC20170041 (2017).
- 22 Glickman, M. H. & Ciechanover, A. The ubiquitin-proteasome proteolytic pathway: destruction for the sake of construction. *Physiol Rev* **82**, 373-428, doi:10.1152/physrev.00027.2001 (2002).
- 23 Swaney, D. L. *et al.* Global analysis of phosphorylation and ubiquitylation cross-talk in protein degradation. *Nat Methods* **10**, 676-682, doi:10.1038/nmeth.2519 (2013).

- 24 Yamada, Y. & Sato, F. Tyrosine phosphorylation and protein degradation control the transcriptional activity of WRKY involved in benzyloisoquinoline alkaloid biosynthesis. *Scientific Reports* **6**, doi:10.1038/srep31988 (2016).
- 25 Nguyen, K. T., Mun, S.-H., Lee, C.-S. & Hwang, C.-S. Control of protein degradation by N-terminal acetylation and the N-end rule pathway. *Experimental & Molecular Medicine* **50**, 1-8, doi:10.1038/s12276-018-0097-y (2018).
- 26 Miteva, M., Keusekotten, K., Hofmann, K., Praefcke, G. J. & Dohmen, R. J. Sumoylation as a signal for polyubiquitylation and proteasomal degradation. *Subcell Biochem* **54**, 195-214, doi:10.1007/978-1-4419-6676-6_16 (2010).
- 27 Wang, X. *et al.* Attenuation of T cell receptor signaling by serine phosphorylation-mediated lysine 30 ubiquitination of SLP-76 protein. *J Biol Chem* **287**, 34091-34100, doi:10.1074/jbc.M112.371062 (2012).
- 28 Wang, X. *et al.* Down-regulation of B cell receptor signaling by hematopoietic progenitor kinase 1 (HPK1)-mediated phosphorylation and ubiquitination of activated B cell linker protein (BLNK). *J Biol Chem* **287**, 11037-11048, doi:10.1074/jbc.M111.310946 (2012).
- 29 Mizuno, E., Kitamura, N. & Komada, M. 14-3-3-dependent inhibition of the deubiquitinating activity of UBPY and its cancellation in the M phase. *Exp Cell Res* **313**, 3624-3634, doi:10.1016/j.yexcr.2007.07.028 (2007).
- 30 Cornell, B., Wachi, T., Zhukarev, V. & Toyo-Oka, K. Regulation of neuronal morphogenesis by 14-3-3epsilon (Ywhae) via the microtubule binding protein, doublecortin. *Hum Mol Genet* **25**, 4405-4418, doi:10.1093/hmg/ddw270 (2016).
- 31 Cornell, B. & Toyo-Oka, K. 14-3-3 Proteins in Brain Development: Neurogenesis, Neuronal Migration and Neuromorphogenesis. *Front Mol Neurosci* **10**, 318, doi:10.3389/fnmol.2017.00318 (2017).
- 32 Yaffe, M. B. *et al.* The structural basis for 14-3-3:phosphopeptide binding specificity. *Cell* **91**, 961-971, doi:http://doi.org/10.1016/S0092-8674(00)80487-0 (1997).
- 33 Aitken, A. 14-3-3 proteins: a historic overview. *Semin Cancer Biol* **16**, 162-172, doi:10.1016/j.semcancer.2006.03.005 (2006).
- 34 Obsil, T. & Obsilova, V. Structural basis of 14-3-3 protein functions. *Semin Cell Dev Biol* **22**, 663-672, doi:10.1016/j.semcdb.2011.09.001 (2011).
- 35 Johnson, C. *et al.* Visualization and biochemical analyses of the emerging mammalian 14-3-3-phosphoproteome. *Mol Cell Proteomics* **10**, M110 005751, doi:10.1074/mcp.M110.005751 (2011).
- 36 Hermeking, H. & Benzinger, A. 14-3-3 proteins in cell cycle regulation. *Seminars in Cancer Biology* **16**, 183-192, doi:10.1016/j.semcancer.2006.03.002 (2006).
- 37 Zhao, J., Meyerkord, C. L., Du, Y., Khuri, F. R. & Fu, H. 14-3-3 proteins as potential therapeutic targets. *Semin Cell Dev Biol* **22**, 705-712, doi:10.1016/j.semcdb.2011.09.012 (2011).
- 38 Danes, C. G. *et al.* 14-3-3 Down-regulates p53 in Mammary Epithelial Cells and Confers Luminal Filling. *Cancer Research* **68**, 1760-1767, doi:10.1158/0008-5472.Can-07-3177 (2008).
- 39 Muda, K. *et al.* Parkinson-related LRRK2 mutation R1441C/G/H impairs PKA phosphorylation of LRRK2 and disrupts its interaction with 14-3-3. *Proceedings of the National Academy of Sciences* **111**, E34-E43, doi:10.1073/pnas.1312701111 (2013).
- 40 Dzamko, N. *et al.* Inhibition of LRRK2 kinase activity leads to dephosphorylation of Ser910/Ser935, disruption of 14-3-3 binding and altered cytoplasmic localization. *Biochemical Journal* **430**, 405-413, doi:10.1042/bj20100784 (2010).
- 41 Sadik, G. *et al.* Phosphorylation of tau at Ser214 mediates its interaction with 14-3-3 protein: implications for the mechanism of tau aggregation. *Journal of Neurochemistry* **108**, 33-43, doi:10.1111/j.1471-4159.2008.05716.x (2009).
- 42 Stevers, L. M. *et al.* Characterization and small-molecule stabilization of the multisite tandem binding between 14-3-3 and the R domain of CFTR. *Proc Natl Acad Sci U S A* **113**, E1152-1161, doi:10.1073/pnas.1516631113 (2016).
- 43 Liang, X. *et al.* Phosphorylation-dependent 14-3-3 protein interactions regulate CFTR biogenesis. *Mol Biol Cell* **23**, 996-1009, doi:10.1091/mbc.E11-08-0662 (2012).
- 44 Ballio, A. *et al.* Fusicoccin: a New Wilting Toxin produced by *Fusicoccum amygdali* Del. *Nature* **203**, 297-297, doi:10.1038/203297a0 (1964).
- 45 Oecking, C., Eckerskorn, C. & Weiler, E. W. The fusicoccin receptor of plants is a member of the 14-3-3 superfamily of eukaryotic regulatory proteins. *FEBS Letters* **352**, 163-166, doi:10.1016/0014-5793(94)00949-x (1994).
- 46 Molzan, M. *et al.* Stabilization of physical RAF/14-3-3 interaction by cotylenin A as treatment strategy for RAS mutant cancers. *ACS Chem Biol* **8**, 1869-1875, doi:10.1021/cb4003464 (2013).

- 47 Ottmann, C. *et al.* A structural rationale for selective stabilization of anti-tumor interactions of 14-3-3 proteins by cotylenin A. *J Mol Biol* **386**, 913-919, doi:10.1016/j.jmb.2009.01.005 (2009).
- 48 Ottmann, C. *et al.* Structure of a 14-3-3 coordinated hexamer of the plant plasma membrane H⁺-ATPase by combining X-ray crystallography and electron cryomicroscopy. *Mol Cell* **25**, 427-440, doi:10.1016/j.molcel.2006.12.017 (2007).
- 49 Milroy, L. G., Brunsvelde, L. & Ottmann, C. Stabilization and inhibition of protein-protein interactions: the 14-3-3 case study. *ACS Chem Biol* **8**, 27-35, doi:10.1021/cb300599t (2013).
- 50 Williams, D. R., Robinson, L. A., Nevill, C. R. & Reddy, J. P. Strategies for the synthesis of fusicocanes by Nazarov reactions of dolabelladienones: total synthesis of (+)-fusicauritone. *Angew Chem Int Ed Engl* **46**, 915-918, doi:10.1002/anie.200603853 (2007).
- 51 Toyomasu, T. *et al.* Fusicoccins are biosynthesized by an unusual chimera diterpene synthase in fungi. *Proc Natl Acad Sci U S A* **104**, 3084-3088, doi:10.1073/pnas.0608426104 (2007).
- 52 Rose, R. *et al.* Identification and structure of small-molecule stabilizers of 14-3-3 protein-protein interactions. *Angew Chem Int Ed Engl* **49**, 4129-4132, doi:10.1002/anie.200907203 (2010).
- 53 Bosica, F. *et al.* Design of Drug-Like Protein-Protein Interaction Stabilizers Guided By Chelation-Controlled Bioactive Conformation Stabilization. *Chemistry* **26**, 7131-7139, doi:10.1002/chem.202001608 (2020).
- 54 Sijbesma, E. *et al.* Site-Directed Fragment-Based Screening for the Discovery of Protein-Protein Interaction Stabilizers. *J Am Chem Soc* **141**, 3524-3531, doi:10.1021/jacs.8b11658 (2019).
- 55 Guillory, X. *et al.* Fragment-based Differential Targeting of PPI Stabilizer Interfaces. *J Med Chem* **63**, 6694-6707, doi:10.1021/acs.jmedchem.9b01942 (2020).
- 56 Wolter, M. *et al.* Fragment-Based Stabilizers of Protein-Protein Interactions through Imine-Based Tethering. *Angew Chem Int Ed Engl*, doi:10.1002/anie.202008585 (2020).
- 57 Shui, J. W. *et al.* Hematopoietic progenitor kinase 1 negatively regulates T cell receptor signaling and T cell-mediated immune responses. *Nat Immunol* **8**, 84-91, doi:10.1038/ni1416 (2007).
- 58 Di Bartolo, V. *et al.* A novel pathway down-modulating T cell activation involves HPK-1-dependent recruitment of 14-3-3 proteins on SLP-76. *J Exp Med* **204**, 681-691, doi:10.1084/jem.20062066 (2007).
- 59 Samelson, L. E. Signal transduction mediated by the T cell antigen receptor: the role of adapter proteins. *Annu Rev Immunol* **20**, 371-394, doi:10.1146/annurev.immunol.20.092601.111357 (2002).
- 60 Koretzky, G. A., Abtahian, F. & Silverman, M. A. SLP76 and SLP65: complex regulation of signalling in lymphocytes and beyond. *Nat Rev Immunol* **6**, 67-78, doi:10.1038/nri1750 (2006).
- 61 Wang, B. *et al.* Isolation of high-affinity peptide antagonists of 14-3-3 proteins by phage display. *Biochemistry* **38**, 12499-12504, doi:10.1021/bi991353h (1999).
- 62 Petosa, C. *et al.* 14-3-3zeta binds a phosphorylated Raf peptide and an unphosphorylated peptide via its conserved amphipathic groove. *J Biol Chem* **273**, 16305-16310, doi:10.1074/jbc.273.26.16305 (1998).
- 63 Pereira, D. A. & Williams, J. A. Origin and evolution of high throughput screening. *Br J Pharmacol* **152**, 53-61, doi:10.1038/sj.bjp.0707373 (2007).
- 64 Andricopulo, A. D., Salum, L. B. & Abraham, D. J. Structure-based drug design strategies in medicinal chemistry. *Curr Top Med Chem* **9**, 771-790, doi:10.2174/156802609789207127 (2009).
- 65 Kalyanamoorthy, S. & Chen, Y. P. Structure-based drug design to augment hit discovery. *Drug Discov Today* **16**, 831-839, doi:10.1016/j.drudis.2011.07.006 (2011).
- 66 Leissing, T. M., Luh, L. M. & Cromm, P. M. Structure driven compound optimization in targeted protein degradation. *Drug Discovery Today: Technologies*, doi:10.1016/j.ddtec.2020.11.005 (2020).
- 67 Sluchanko, N. N. Association of Multiple Phosphorylated Proteins with the 14-3-3 Regulatory Hubs: Problems and Perspectives. *J Mol Biol* **430**, 20-26, doi:10.1016/j.jmb.2017.11.010 (2018).
- 68 Sluchanko, N. N. & Bustos, D. M. Intrinsic disorder associated with 14-3-3 proteins and their partners. *Prog Mol Biol Transl Sci* **166**, 19-61, doi:10.1016/bs.pmbts.2019.03.007 (2019).
- 69 Doveston, R. G. *et al.* Small-molecule stabilization of the p53 - 14-3-3 protein-protein interaction. *FEBS Lett* **591**, 2449-2457, doi:10.1002/1873-3468.12723 (2017).

-
- 70 Soini, L., Leysen, S., Davis, J., Westwood, M. & Ottmann, C. The 14-3-3/SLP76 protein-protein interaction in T-cell receptor signalling: a structural and biophysical characterization. *FEBS Lett*, doi:10.1002/1873-3468.13993 (2020).
- 71 Soini, L., Leysen, S., Davis, J. & Ottmann, C. A biophysical and structural analysis of the interaction of BLNK with 14-3-3 proteins. *J Struct Biol* **212**, 107662, doi:10.1016/j.jsb.2020.107662 (2020).
- 72 McPherson, A. & Gavira, J. A. Introduction to protein crystallization. *Acta Crystallogr F Struct Biol Commun* **70**, 2-20, doi:10.1107/S2053230X13033141 (2014).
- 73 Ng, J. T., Dekker, C., Reardon, P. & von Delft, F. Lessons from ten years of crystallization experiments at the SGC. *Acta Crystallogr D Struct Biol* **72**, 224-235, doi:10.1107/S2059798315024687 (2016).
- 74 Sluchanko, N. N. *et al.* Structural Basis for the Interaction of a Human Small Heat Shock Protein with the 14-3-3 Universal Signaling Regulator. *Structure* **25**, 305-316, doi:10.1016/j.str.2016.12.005 (2017).
- 75 Goldschmidt, L., Cooper, D. R., Derewenda, Z. S. & Eisenberg, D. Toward rational protein crystallization: A Web server for the design of crystallizable protein variants. *Protein Sci* **16**, 1569-1576, doi:10.1110/ps.072914007 (2007).

The TR-FRET HTS was performed under the supervision of Dr. Martin Redhead. The SPR experiments were performed in collaboration and under the supervision of Dr. Marta Westwood.

Chapter 6

Structural and Biophysical characterization of the GADS/14-3-3 PPI

Abstract

The GRB-2 related adaptor protein 2, GADS, is one of the adaptor proteins that regulates the signalling pathways downstream of TCR. GADS is being recruited on the Linker for activation of T cells, LAT, where it is responsible to bridge the interaction with another crucial TCR signalling molecule, SLP76. Several studies report a model in which the adaptor protein 14-3-3 is responsible for the uncoupling of the GADS/SLP76 complex anchored on LAT. The uncoupling occurs upon HPK1 phosphorylation on SLP76 Ser376 and GADS Thr262, two sites that 14-3-3 uses to dock onto. It has been suggested this complex could be targeted for degradation therefore causing attenuation of TCR signalling. This work focuses on the characterization of the reported 14-3-3 interaction site on GADS, pThr262. A novel crystal structure of a binary complex of a 12-mer GADSpT262 peptide in complex with 14-3-3 σ is presented, supported by biophysical binding data. Additionally, few GADS and SLP76 constructs have been tested for solubility in prevision of future structural studies on the 14-3-3/GADS/SLP76 PPI.

6.1 Introduction

The GRB2-related adaptor protein 2 (Uniprot ID O75791), more briefly known as GADS, is an adaptor protein that was first identified as an Shc proteins binder via tyrosine phosphorylated residues ¹. Its structure is closely related to the GRB2 (Growth factor receptor bound-2) and GRAP proteins (Grb2-related adaptor protein) ¹. GADS is expressed throughout all the hematopoietic compartment and immune cells and is responsible for the nucleation of regulatory multimolecular protein complexes ². Upon T-cell receptor activation, these adaptor protein complexes, are responsible for the regulation and tuning of downstream effects such as Ca²⁺ flux, activation of the Ras-Erk kinase pathway and cytoskeleton reorganization ²⁻⁴. GADS-deficient mice showed an impaired thymocytes proliferation ⁵. Moreover, GADS has also been linked to lymphoid disease in the BCR-ABL pathway by facilitating the interactions with other signalling molecules ⁶.

More in dept, GADS is responsible of making a bridge between the adaptor proteins LAT (Linker for activation of T cells) and SLP76 (Lymphocyte cytosolic protein 2) which are tyrosine phosphorylated after T-cell receptor activation. Two studies revealed that GADS and SLP76 are also involved in a more complex cooperative binding mechanism involving a SLP76/GADS complex, resulting in a negative regulation of T-cell signalling ^{7,8}. A model has been proposed where the HPK1 kinase is responsible for the uncoupling of the SLP76/GADS complex from LAT, and consequently a downregulation of TCR signalling (Figure 6.1). The uncoupling would occur *via* 14-3-3 docking onto the phosphorylated sites by HPK1, i.e. Thr262 and Ser376 on GADS and SLP76 ⁸. The scaffolding activity of 14-3-3 proteins that dock simultaneously onto two binding partners is a known concept although only few examples are reported ^{9,10}. The fate of the 14-3-3/GADS/SLP76 complex is yet unknown, but it has been speculated that the complex could be targeted for degradation. Interestingly, a negative feedback mechanism involving Ser376 HPK1 phosphorylation on SLP76 and consequent 14-3-3 binding leading to SLP76 degradation and TCR signalling attenuation has already been reported ^{11,12}. The addition of GADS to the equation certainly complicates the existing proposed mechanism. However, it could also provide a new entry point for the modulation of PPI downstream TCR, opening up new perspectives.

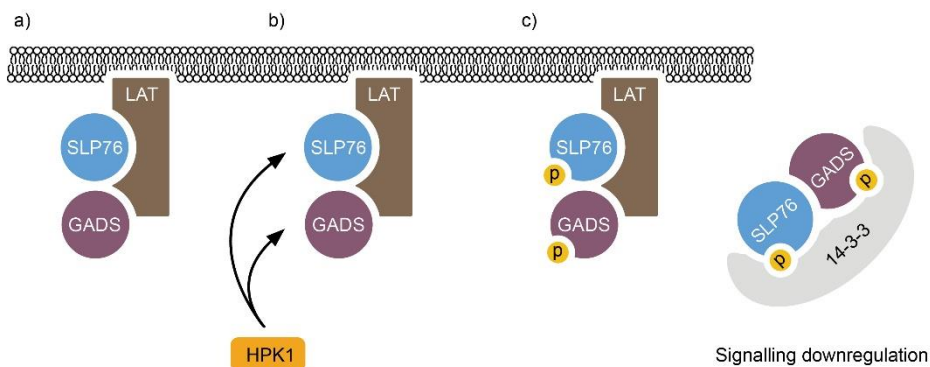


Figure 6.1 | Cartoon representation of the GADS regulation model. a) GADS and SLP76 are recruited to LAT and form signalling complexes. b) HPK1 is recruited by SLP76 and phosphorylate GADS T262 and SLP76 S376. c) 14-3-3 binds to the phosphorylation sites on SLP76 and GADS uncouple them from LAT and downregulating TCR signalling.

The interaction between GADS and SLP76 occurs between the C-terminal SH3 domain of GADS and a specific motif on SLP76: $^{237}\text{R-X-X-K}^{240}$ ¹³. The interaction has been further investigated by generating a solution structure of the GADS SH3 C-terminal domain in complex with a short derived SLP76 peptide containing the $^{237}\text{R-X-X-K}^{240}$ motif and two crystal structures (PDB ID: 1H3H, 1OEB, 2DoN)¹⁴⁻¹⁶.

In this work, we investigate the nature of the interaction between 14-3-3 proteins and GADS. By means of a GADS derived 12-mer synthetic peptide containing the suggested 14-3-3 interaction site, pThr262, we characterize the interaction biophysically exploiting Fluorescence Polarization and Isothermal Titration Calorimetry. We proceed by generating the first crystal structure of a GADS peptide in complex with 14-3-3 σ . Finally, in preparation of future work on this PPI involving longer protein constructs, we express and perform protein solubility tests on few GADS and SLP76 constructs.

6.2 Results and Discussion

6.2.1 Binding characterization of the GADSpT262 peptide and 14-3-3 proteins

The structure of GADS is composed of an N-terminal and C-terminal SH3 domains (SH3-N and SH3-C) flanking a central SH2 domain. The SH2 domain and the SH3-C domain are separated by an intrinsically disordered region, with the 14-3-3 binding site, Thr262, situated just before the SH3-C domain (Figure 6.2a)¹. Still, a small angle X-ray scattering (SAXS) study of full-length GADS showed that GADS adopts a globular structure¹⁷.

In order to characterize the interaction between 14-3-3 proteins and GADS, a 11-mer synthetic phosphorylated peptide was designed starting from the native GADS sequence, GADSpT262: HRRHpT262DPVQLQ (Figure 6.2a). The peptide contains 4 residues before and 6 residues after the 14-3-3 anchor point, Thr262. Short phosphorylated peptides mimicking the interaction point of larger 14-3-3 clients represent a useful tool to begin the biophysical and structural investigation on a specific 14-3-3 PPI. Two versions of the same peptide were ordered: a FITC-labelled one for fluorescence polarization studies and an acetylated one for isothermal titration calorimetry assays and X-ray protein crystallography.

The FITC-labelled version of the GADSpT262 peptide was first tested against all 14-3-3 isoforms. K_D values were calculated from fitting curves and were estimated to be in the micromolar range: 1.8-33.9 μM (Figure 6.2b). These K_D values are in agreement with the affinities that others synthetic phosphorylated peptides show towards 14-3-3 proteins¹⁸⁻²¹. An assay validation was performed exploiting the R18 peptide, a known 14-3-3 inhibitor, to confirm that the polarization signal was indeed attributable to a binding event²². The validation was performed on the 14-3-3 γ isoform (Figure S 6.1).

The binding towards 14-3-3 proteins was orthogonally confirmed by isothermal titration calorimetry by testing the GADSpT262 peptide against 14-3-3 γ (Figure 6.2c). The calculated K_D was 1.13 $\mu\text{M} \pm 0.07$ μM which compared very well with the K_D calculated by the FP being just within the 2-fold difference.

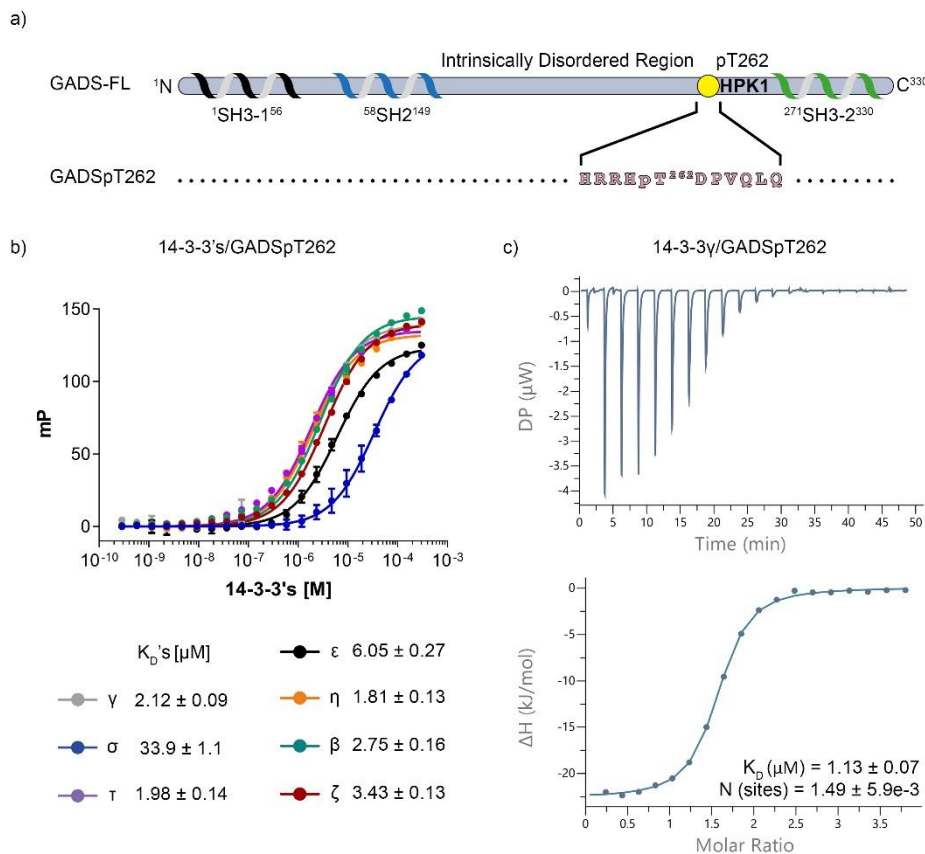


Figure 6.2 | Binding of 14-3-3 proteins to the GADSpT262 peptide. a) Cartoon representation of GADS-FL and the GADSpS262 peptide sequence. GADS is composed of three separate domains SH3-1, SH2 and SH3-2. SH2 and SH3-2 domains are separated by an intrinsically disordered region. b) Fluorescence polarization assay of the binding of 14-3-3 proteins to the GADSpT262 peptide. The calculated K_D are reported below the graph. c) Isothermal titration calorimetry assay of the 14-3-3 γ bound to the GADSpT262 peptide.

6.2.2 Structural characterization of the GADSpT262/14-3-3 σ binary complex

After the confirmation of the binding of the GADSpT262 peptide to 14-3-3 proteins, we wanted to elucidate the mechanism of binding of the latter to 14-3-3. All the 14-3-3 isoforms bound to GADSpT262, as shown in the fluorescence polarization assay (Figure 6.2b). However, the 14-3-3 σ isoform is known to produce crystals with high-resolution diffraction. We therefore crystallised the GADSpT262 peptide with 14-3-3 σ and the crystals diffracted to a resolution of 1.9 Å. Data collection and refinement statistics are reported in (Table 6.1). Solving the structure allowed to identify the GADSpT262 peptide bound to a 14-3-3 σ monomer (Figure 6.3a), this binary complex also constitutes the asymmetric unit of the crystal. The

electron density, displayed by the $2F_o - F_c$ map, allowed to model 7 out of 11 residues of the peptide (Figure 6.3b). As expected, the peptide bound to 14-3-3 σ determined that the binding occurs *via* the canonical 14-3-3 amphipathic binding groove. The phosphorylated Thr262 provides the major anchor point for the peptide, exploiting polar contacts with 14-3-3 residues Lys49, Arg56, Arg129 and Tyr130. Additional polar contacts are established between GADSpT262 Asp263, His261 and Arg260 with 14-3-3 σ Asn 175, Asp225, Asn226 and Glu182 (Figure 6.3c).

Table 6.1: Data collection and refinement statistics of the 14-3-3 σ /GADSpT262 crystal structure.

Data collection	
Space group	C222 ₁
Cell dimensions	
a, b, c, (Å)	82.31, 111.91, 62.57
Resolution (Å)	29.29-1.90 (1.94-1.90)
R _{merge} (%)	0.044 (0.55)
<I/σ(I)>	21.1 (2.4)
Completeness (%)	98.1 (89.7)
Multiplicity	5.4 (3.5)
CC (1/2)	0.98 (0.62)
Refinement	
Resolution (Å)	28.29-1.9
No. Reflections	22692
R _{work} /R _{free}	0.17/0.19
No. Atoms	
Protein	2093
Water	273
B-factors(Å ²)	
Protein	26.25
Water	34.87
R.M.S.D.	
Bond lengths (Å)	0.004
Bond angles (°)	0.63
Ramachandran statistics (%)	
Favoured	98.31
Allowed	1.69
Outliers	0.00

Values in parenthesis represent the high-resolution shell.

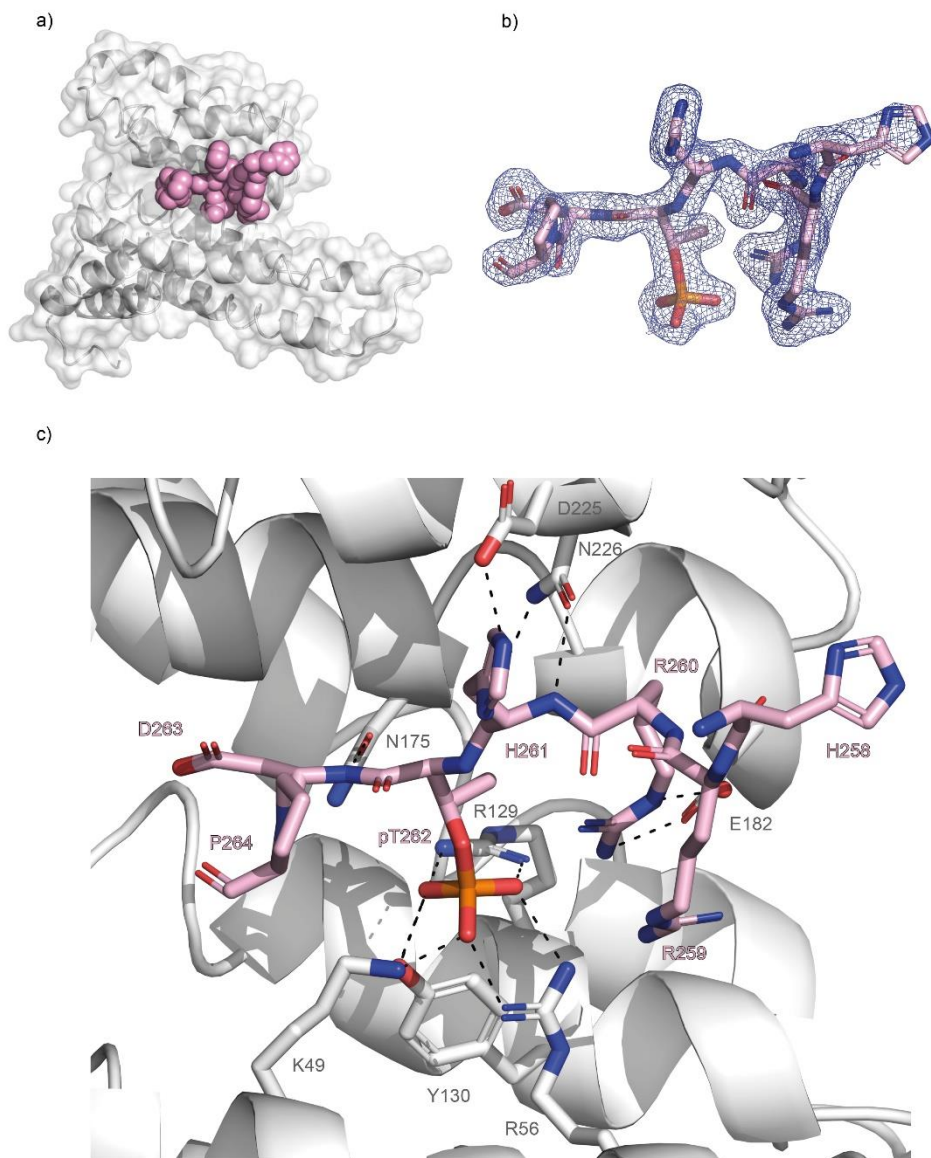


Figure 6.3 | Crystal structure of the GADSpT262 bound to 14-3-3. a) Asymmetric unit of the crystal structure. 14-3-3 is represented as white surface (60% transparency) and grey cartoon highlighting its secondary structure formed by α -helices and loops. The GADSpT262 peptide is represented as pink spheres. b) Stick representation of the GADSpT262 peptide (pink) with its 2Fo-Fc maps contoured at $\sigma=1$. c) Stick representation of the GADSpT262 peptide (pink) bound to the 14-3-3 binding groove. 14-3-3 is represented as white α -helices. The 14-3-3 residues interacting with the GADSpT262 peptide are represented with their side chains in grey sticks. Polar contacts are represented as dotted black lines.

6.2.3 Expression and solubility tests of few SLP76 and GADS protein constructs

TCR signalling and the modulation of its downstream effects which lead to the immune response is a very complex and concerted network of PPI²³. GADS and SLP76 embody part of this complexity. Along with 14-3-3, in fact, they are part of a suggested cooperative mechanism triggered by HPK1 that negatively regulate TCR signalling⁸. It is therefore important to characterize the interactions of these proteins and their ability to make complexes *in vitro*. We then expressed 8 systems, by single or as co-expression experiments: GADS-FL, SLP76-2, GADS-FL + SLP76-2, GADS-SH3, GADS-SH3 + SLP76-2, GADS-PKA, GADS-PKA + PKA, GADS-PKA + PKA + 14-3-3 ϵ -FL. The *E. coli* cultures of each system were lysed and four sample for each system were loaded on an SDS-PAGE to check the solubility of the protein of interest: the whole cell lysate before induction, the whole cell lysate after induction, the soluble fraction after the induction and the insoluble fraction after the induction (Figure 6.4). The first two constructs tested, GADS-FL and SLP76-2, a shorter version of SLP76-FL, were found to be insoluble. This was also the case upon co-expression of the two (Figure 6.4a). Columns 4, 8 and 12 of the first SDS-PAGE (Figure 6.4a) shows a band that identifies the entire amount of the expressed protein in the insoluble fractions. A shorter version of GADS protein, GADS-SH3, containing the 14-3-3 and SLP76 binding site, the phosphorylated pThr262 and the SH3 domain, was on the contrary found mainly in the soluble fraction (Figure 6.4b). GADS-SH3 was also co-expressed with SLP76-2. The comparison between the co-expression and the single SLP76-2 expression revealed a very light band possibly attributable to SLP76-2 (Figure 6.4b), column 23. A very small portion of SLP76-2 could have been rescued by GADS-SH3 present in the soluble fraction. This, however, would require a follow-up and confirmation. Finally, a GADS-PKA construct with a D263V mutation, which allows PKA phosphorylation of the pT262 site, has been also expressed (Figure 6.4c). The construct resulted in soluble expression like the GADS-SH3. A co-expression of 14-3-3 ϵ -FL and GADS-PKA showed that both the proteins successfully expressed in the soluble fraction.

The incorporation of phosphorylated Ser/Thr or Tyr in a specific position of protein substrates is a challenging process. Several biochemical methods have been implemented such as: total chemical synthesis, semi synthesis, and unnatural amino acid incorporation²⁴. PKA co-expression is another method that can be used to phosphorylate proteins, on condition that these targets are PKA substrates. If not, the phosphorylation can often be achieved by mutating the residues surrounding the site to phosphorylate, to create the PKA recognition motif: RRXS/TY where X can be any residue and Y is a hydrophobic amino acid. If protein mutations alter the native protein sequence, they most of the time do not introduce modification that would impair the substance of any biological analysis. If multiple, PKA phosphorylation sites are present, site-specific phosphorylation can of course not be guaranteed, unless for example Ser to Ala mutations are introduced at the unwanted sites.

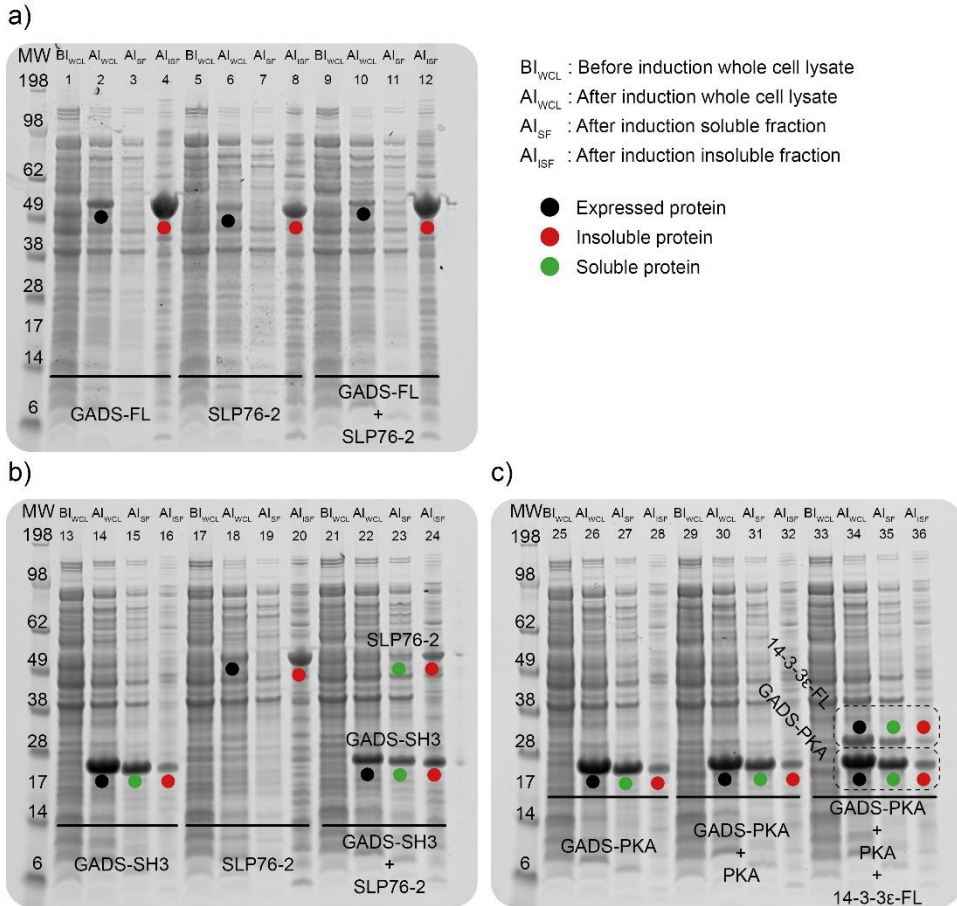


Figure 6.4 | SDS-PAGEs analysis of the GADS and SLP76 protein expression constructs. The legend indicates all the sample types and the coloured dots highlight the relevant bands on the gels. Every gel contains three expression systems and for each one of them four samples are loaded. Every single sample is numbered for easier identification. a) GADS-FL, SLP76-2 and GADS-FL + SLP76-2 are loaded on the gel. All three systems have been found in the expressed fraction but none of them has been found in the soluble fraction. b) GADS-SH3, SLP76-2 and GADS-SH3 + SLP76-2 systems are loaded on the gel. GADS-SH3 had been found in the soluble fraction and a small amount SLP76-2 can be observed in the soluble fraction only when co-expressed with GADS-SH3. c) GADS-PKA, GADS-PKA + PKA and GADS-PKA + PKA + 14-3-3 ϵ -FL are loaded on the gel. Both GADS-PKA and GADS-PKA + PKA systems has been found in the soluble fraction. The co-expression with 14-3-3 ϵ -FL revealed that 14-3-3 ϵ -FL can be expressed along with GADS-PKA and PKA, in the soluble fraction

6.3 Conclusions

In this work we report the first biophysical and structural characterization of the interaction between a GADS-derived synthetic peptide and 14-3-3 proteins. The GADSpT262 peptide containing the phosphorylated Thr262, which was already reported to be responsible for 14-3-3 binding ⁸, shows micromolar affinity to 14-3-3. The novel 14-3-3 σ /GADSpT262 crystal structure confirms that the binding occurs *via* the canonical 14-3-3 binding groove.

GADS has been reported to be part of a complex cooperative mechanism downstream TCRs, which involves SLP76 and 14-3-3 ⁸. Therefore, in order to have a reasonably simple access to longer protein constructs instead of short phosphorylated peptides, a variety of expression constructs have been tested for solubility. The objective was to allow structural characterization of the 14-3-3, GADS and SLP76 PPIs using larger protein constructs in the future. The solubility tests performed on the expressed constructs revealed that GADS-SH3 and GADS-PKA are promising constructs and that a purification process could start from here. A co-expression of GADS-PKA with 14-3-3 ϵ -FL also revealed that the generation of protein complexes right from the expression and purification stage could also happen. The success of the formation of the complex would need to be confirmed in the purification stages. The possibility of expressing and purifying protein complexes from the *E. coli* lysates without having to reconstitute them *in vitro* from individual components could be helpful for structural studies. It would still be interesting to attempt co-expression of 14-3-3 with PKA mutants of SLP76-2 and full-length GADS, to investigate if 14-3-3 can rescue them to the soluble fraction.

6.4 Material and Methods

GADS and SLP76 constructs cell transformation, expression and solubility test

NiCo21(DE3) (Thermo Scientific) competent cells were transformed by heat shock with the expression vectors encoding for (His)₆-SUMO-GADS-FL (1-330) (pETDuetTM-1, selectable marker: Ampicillin), (His)₆-SUMO-GADS-SH3 (254-330) (pETDuetTM-1, selectable marker: Ampicillin), (His)₆-SUMO-GADS-SH3-PKA (254-330, D263V) (pETDuetTM-1, selectable marker: Ampicillin), (His)₆-SUMO-SLP76-2 (337-533) (pETDuetTM-1, selectable marker: Streptomycin), Strep-14-3-3-ε-FL (pPRoeX-Htb, selectable marker: Streptomycin) and PKA (pACYC, selectable marker: chloramphenicol). ≈ 100 ng of DNA were added to the competent cells and then put in ice for 20 min. A thermal shock was then applied (42 °C, 30 s) followed by incubation on ice for 3 min. 900 μL of SOC medium were added at the cells and incubated under stirring for 1 h at 37 °C. 100 μL of cells were spread on the agar plates, the rest of the cells were spun down (5000 rpm, 5 min), the majority of the medium removed and the pellet formed resuspended in ≈ 100/200 μL of medium. The resuspended cells were spread on agar plates which were incubated O/N at 37 °C. The agar plates were supplemented with 100 μg/mL of Ampicillin, 100 μg/mL of Streptomycin and 25 μg/mL of Chloramphenicol for the single and the double transformations. For the triple transformation, ≈ 33 μg/mL, 33 μg/mL and 8 μg/mL of Ampicillin, Streptomycin and Chloramphenicol were used respectively. 500 mL 2TY cultures supplemented with the final concentrations used for the plates were seeded at OD₆₀₀ = 0.1 from O/N cultures in 200 mL 2TY supplemented with antibiotic in the same way (37 °C, 210 rpm). O/N cultures were created from one colony picked from a freshly transformed plate of cells. Cultures were incubated until the OD₆₀₀ reached the value of 3.5 (37 °C, 170 rpm, 4/5 h). OD measurements were performed using a 1 in 10 dilution of the culture. The temperature set was then dropped to 18 °C, 170 rpm, 30 min. When the OD₆₀₀ reached the value of 4.0, 500 μL of culture was sampled, and centrifuged for 5 min. at 5000 rpm in a tabletop centrifuge. The OD is referred to below as OD_{600 before induction}. The supernatant was removed, and the pellet was stored at -20 °C until the next day. It is referred to below as the pellet before induction (BI). Then, 25 ml of a 20X feed solution (500 mM MOPS sodium salt pH 7.2, 20 mM MgCl₂, 20 mM MgSO₄ and 40% v/v Glycerol) was added to the 500 ml cultures. In addition, IPTG was added to a final concentration of 200 μM. The next day, the OD₆₀₀ of the cultures were measured, using a 1 in 40 dilution of the culture for the measurement. This measurement will be referred to below as OD_{600 after induction}. From the culture, a volume, calculated by using the following formula: $V (\mu\text{L}) = 500 \mu\text{L} / (\text{OD}_{600 \text{ after induction}} / \text{OD}_{600 \text{ before induction}})$ was taken. A bacterial pellet, referred to as after induction (AI), was then harvested as described above. 200 μL of BugBuster Master Mix (Thermo Fisher) was added to the BI and AI pellets. The samples were slowly stirred for 20 min incubation at room temperature, 30 μL of samples were taken and 10 μL of Loading Dye (4X) were added. These samples are referred to as whole cell lysate (WCL) BI and AI. The remaining of the AI sample was centrifuged for 20 min at 13000 rpm in a tabletop centrifuge, to separate the lysate in a soluble (SF) and insoluble (ISF) fraction. 10 μL of the soluble fraction was taken out and 10 μL of Loading Dye (4X) were added. The supernatant was removed from the rest of the AI sample and the pellet, if present, was dissolved in 170 μL of Loading Dye (1X). All the samples were denatured at 95 °C for 5 min and loaded on an SDS-PAGE for analysis.

14-3-3 protein purification

14-3-3 isoforms γ, τ, σ, ε, η, ζ, β FL and 14-3-3 Δ C (Δ C=231-248) were expressed with a (His)₆-tag in NiCo21(DE3) competent cells, from a pPRoeX-Htb vector in 2TY media. The purification was carried out by affinity chromatography on Nickel columns (HisTrap HP, 5 mL). The tags were cleaved with a TEV protease. The proteins were then loaded again on Nickel columns to remove any non-cleaved protein. A final purification step was performed by loading the proteins on a size-exclusion chromatography column (HiLoad 26/600 Superdex 75 pg) equilibrated in 20 mM TRIS-HCl pH 7.5, 150 mM NaCl, 2 mM DTT. All purification steps were performed on an ÄKTA pure protein purification system (Cytiva). The 14-3-3 FL versions were used in the biophysical assays and the 14-3-3 Δ C construct was used for crystallography purposes.

The peptide GADSpT262 (HRRHpT262DPVQLQ) was ordered with purity >95% from GenScript in an N-terminal acetylated version and in an N-terminal FITC-Ahx labelled version. The R18 peptide, PHCVPRDLSWLDLEANMCLP, was ordered from Sigma-Aldrich, purity ≥98% (HPLC).

Fluorescence Polarization and Isothermal Titration Calorimetry

FP binding assays were carried out on Corning 384-well 3575 plates, serially diluting (2-fold) 14-3-3 isoforms in the presence of 10 nM FITC-labelled peptides. Proteins and peptides were diluted from their stock concentration in assay buffer (50 mM Tris pH 7.5, 150 mM NaCl, 5 mM MgCl₂, 0.05% v/v Tween-20). The data were collected on a PHERAstar FSX plate reader (BMG Labtech) with an λ_{ex} 485 nm, λ_{em} 520 nm FP filter setting. For K_D calculation the background polarization was removed from all values and the data were fitted with a “One site - Specific binding model” and “Specific binding with hill slope” on GraphPad Prism version 8.1.1 for Windows, GraphPad Software, La Jolla California USA, www.graphpad.com. Each data point is the average of a triplicate measurement and the standard deviation is reported as error bars. ITC measurements were performed on a PEAQ-ITC (Malvern) dissolving the peptides in assay buffer (50 mM Tris pH 7.5, 150 mM NaCl, 5 mM MgCl₂, 2mM 2-mercaptoethanol, 0.05% v/v Tween-20) and dialysing the protein in the same buffer to minimise buffer mismatch. The optimal peptide and protein concentrations were chosen after simulating the experiment on the MicroCal PEAQ-ITC Analysis Software (Malvern) according to the predicted K_D . The peptides were titrated into the cell containing the protein using a series of 18 injections 2 μL each at 25 °C (reference power 5 $\mu\text{cal}/\text{sec}$, stir speed 750 rpm, initial delay 60 s, spacing 150 s). The data were analysed on the MicroCal PEAQ-ITC Analysis Software (Malvern).

X-ray protein crystallography

For protein crystallisation, a C-terminally truncated version of 14-3-3 σ was used (14-3-3 $\sigma\Delta\text{C}$, $\Delta\text{C}=17$ C-terminal AA)²⁵. The binary complexes were prepared mixing 14-3-3 $\sigma\Delta\text{C}$ at 10-15 mg/ml with GADSpT262 at a 1:1 and 1:1.2 molar ratio, followed by overnight incubation at 4 °C (dilution buffer: 20 mM HEPES pH 7.5, 2 mM MgCl₂). The crystallization drops were dispensed in 1:1 protein to crystallisation condition ratio (0.5 μL + 0.5 μL). A focused crystallisation screen was used. The conditions contained a constant concentration of 5% (v/v) glycerol and 190 mM CaCl₂, while PEG400 was screened between 24-29% (v/v) and the pH of the 95 mM HEPES buffer was varied at 7.1, 7.3, 7.5 and 7.7. The plate was incubated at 4 °C and crystals grew in 5 to 10 days and were observed in most of the crystallisation conditions. Diffraction data were collected on the I04 Beamline at the Diamond Light Source. The data were processed with XDS²⁶ and AIMLESS^{27,28}. The structure was solved by molecular replacement using PHASER, with a 14-3-3 σ structure as search model (PDB ID: 3MHR),^{25,29}. The initial structure was then refined using COOT³⁰ and PHENIX³¹. All figures were generated using PyMOL (The PyMOL Molecular Graphics System, Version 1.2r3pre, Schrödinger, LLC).

6.5 Supporting Information

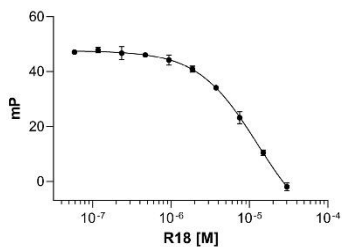


Figure S 6.1| Validation assay for the 14-3-3/GADS interaction. The R18 peptide is titrated on constant concentrations of 14-3-3 γ and GADSpT262 peptide inhibiting the interaction therefore validating the binding.

6.6 References

- 1 Liu, S. K. & McGlade, C. J. Gads is a novel SH2 and SH3 domain-containing adaptor protein that binds to tyrosine-phosphorylated Shc. *Oncogene* **17**, 3073-3082, doi:10.1038/sj.onc.1202337 (1998).
- 2 Liu, S. K., Berry, D. M. & McGlade, C. J. The role of Gads in hematopoietic cell signalling. *Oncogene* **20**, 6284-6290, doi:10.1038/sj.onc.1204771 (2001).
- 3 Liu, S. K., Fang, N., Koretzky, G. A. & McGlade, C. J. The hematopoietic-specific adaptor protein gads functions in T-cell signaling via interactions with the SLP-76 and LAT adaptors. *Curr Biol* **9**, 67-75, doi:10.1016/s0960-9822(99)80017-7 (1999).
- 4 Bilal, M. Y. *et al.* GADS is required for TCR-mediated calcium influx and cytokine release, but not cellular adhesion, in human T cells. *Cell Signal* **27**, 841-850, doi:10.1016/j.cellsig.2015.01.012 (2015).
- 5 Yoder, J. *et al.* Requirement for the SLP-76 adaptor GADS in T cell development. *Science* **291**, 1987-1991, doi:10.1126/science.1057176 (2001).
- 6 Gillis, L. C., Berry, D. M., Minden, M. D., McGlade, C. J. & Barber, D. L. Gads (Grb2-related adaptor downstream of Shc) is required for BCR-ABL-mediated lymphoid leukemia. *Leukemia* **27**, 1666-1676, doi:10.1038/leu.2013.40 (2013).
- 7 Houtman, J. C. *et al.* Binding specificity of multiprotein signaling complexes is determined by both cooperative interactions and affinity preferences. *Biochemistry* **43**, 4170-4178, doi:10.1021/bi035731i (2004).
- 8 Lasserre, R. *et al.* Release of serine/threonine-phosphorylated adaptors from signaling microclusters down-regulates T cell activation. *J Cell Biol* **195**, 839-853, doi:10.1083/jcb.201103105 (2011).
- 9 Chatterjee, D., Zhiping, L. L., Tan, S. M. & Bhattacharjya, S. Interaction Analyses of the Integrin beta2 Cytoplasmic Tail with the F3 FERM Domain of Talin and 14-3-3zeta Reveal a Ternary Complex with Phosphorylated Tail. *J Mol Biol* **428**, 4129-4142, doi:10.1016/j.jmb.2016.08.014 (2016).
- 10 Obsil, T. & Obsilova, V. Structural basis of 14-3-3 protein functions. *Semin Cell Dev Biol* **22**, 663-672, doi:10.1016/j.semcdb.2011.09.001 (2011).
- 11 Di Bartolo, V. *et al.* A novel pathway down-modulating T cell activation involves HPK-1-dependent recruitment of 14-3-3 proteins on SLP-76. *J Exp Med* **204**, 681-691, doi:10.1084/jem.20062066 (2007).
- 12 Wang, X. *et al.* Attenuation of T cell receptor signaling by serine phosphorylation-mediated lysine 30 ubiquitination of SLP-76 protein. *J Biol Chem* **287**, 34091-34100, doi:10.1074/jbc.M112.371062 (2012).
- 13 Berry, D. M., Nash, P., Liu, S. K. W., Pawson, T. & McGlade, C. J. A High-Affinity Arg-X-X-Lys SH3 Binding Motif Confers Specificity for the Interaction between Gads and SLP-76 in T Cell Signaling. *Current Biology* **12**, 1336-1341, doi:10.1016/s0960-9822(02)01038-2 (2002).
- 14 Liu, Q. & Li, S. S. 1H, 13C and 15N resonance assignments of Gads C-terminal SH3 domain in complex with an RXXK motif-containing peptide derived from SLP-76. *J Biomol NMR* **24**, 161-162, doi:https://doi.org/10.1016/S1097-2765(03)00046-7 (2002).
- 15 Liu, Q. *et al.* Structural basis for specific binding of the Gads SH3 domain to an RxxK motif-containing SLP-76 peptide: a novel mode of peptide recognition. *Mol Cell* **11**, 471-481, doi:10.1016/s1097-2765(03)00046-7 (2003).
- 16 Dimasi, N. Crystal structure of the C-terminal SH3 domain of the adaptor protein GADS in complex with SLP-76 motif peptide reveals a unique SH3-SH3 interaction. *Int J Biochem Cell Biol* **39**, 109-123, doi:10.1016/j.biocel.2006.07.003 (2007).
- 17 Moran, O., Roessle, M. W., Mariuzza, R. A. & Dimasi, N. Structural features of the full-length adaptor protein GADS in solution determined using small-angle X-ray scattering. *Biophys J* **94**, 1766-1772, doi:10.1529/biophysj.107.116590 (2008).
- 18 Soini, L., Leysen, S., Davis, J., Westwood, M. & Ottmann, C. The 14-3-3/SLP76 protein-protein interaction in T-cell receptor signalling: a structural and biophysical characterization. *FEBS Lett*, doi:10.1002/1873-3468.13993 (2020).
- 19 Soini, L., Leysen, S., Davis, J. & Ottmann, C. A biophysical and structural analysis of the interaction of BLNK with 14-3-3 proteins. *J Struct Biol* **212**, 107662, doi:10.1016/j.jsb.2020.107662 (2020).
- 20 Centorrino, F., Ballone, A., Wolter, M. & Ottmann, C. Biophysical and structural insight into the USP8/14-3-3 interaction. *FEBS Lett* **592**, 1211-1220, doi:10.1002/1873-3468.13017 (2018).

- 21 Ballone, A., Centorrino, F., Wolter, M. & Ottmann, C. Structural characterization of 14-3-3zeta
in complex with the human Son of sevenless homolog 1 (SOS1). *J Struct Biol* **202**, 210-215,
doi:10.1016/j.jsb.2018.01.011 (2018).
- 22 Petosa, C. *et al.* 14-3-3zeta binds a phosphorylated Raf peptide and an unphosphorylated
peptide via its conserved amphipathic groove. *J Biol Chem* **273**, 16305-16310,
doi:10.1074/jbc.273.26.16305 (1998).
- 23 Koretzky, G. A., Abtahian, F. & Silverman, M. A. SLP76 and SLP65: complex regulation of
signalling in lymphocytes and beyond. *Nat Rev Immunol* **6**, 67-78, doi:10.1038/nri1750
(2006).
- 24 Chen, Z. & Cole, P. A. Synthetic approaches to protein phosphorylation. *Current Opinion in
Chemical Biology* **28**, 115-122, doi:10.1016/j.cbpa.2015.07.001 (2015).
- 25 Schumacher, B., Skwarczynska, M., Rose, R. & Ottmann, C. Structure of a 14-3-3 σ -YAP
phosphopeptide complex at 1.15 Å resolution. *Acta Crystallographica Section F Structural
Biology and Crystallization Communications* **66**, 978-984, doi:10.1107/s1744309110025479
(2010).
- 26 Kabsch, W. Integration, scaling, space-group assignment and post-refinement. *Acta
Crystallogr D Biol Crystallogr* **66**, 133-144, doi:10.1107/S0907444909047374 (2010).
- 27 Evans, P. R. An introduction to data reduction: space-group determination, scaling and
intensity statistics. *Acta Crystallogr D Biol Crystallogr* **67**, 282-292,
doi:10.1107/S090744491003982X (2011).
- 28 Winn, M. D. *et al.* Overview of the CCP4 suite and current developments. *Acta Crystallogr D
Biol Crystallogr* **67**, 235-242, doi:10.1107/S0907444910045749 (2011).
- 29 McCoy, A. J. *et al.* Phaser crystallographic software. *J Appl Crystallogr* **40**, 658-674,
doi:10.1107/S0021889807021206 (2007).
- 30 Emsley, P. & Cowtan, K. Coot: model-building tools for molecular graphics. *Acta Crystallogr D
Biol Crystallogr* **D60**, 2126-2132, doi:10.1107/S0907444904019158 (2004).
- 31 Adams, P. D. *et al.* PHENIX: a comprehensive Python-based system for macromolecular
structure solution. *Acta Crystallogr D Biol Crystallogr* **66**, 213-221,
doi:10.1107/S0907444909052925 (2010).

Chapter 7

The characterization of potential 14-3-3 interaction sites on the bone regulator protein Schnurri-3

Abstract

14-3-3 proteins regulate many intracellular processes and their ability to bind in subtly different fashion to the numerous partner proteins provides attractive drug targeting points for a range of diseases. Schnurri-3 is a suppressor of mouse bone formation and a candidate target for novel osteoporosis therapeutics so it is of interest to determine whether it interacts with 14-3-3. In this work, we identified potential 14-3-3 interaction sites on mammalian Schnurri-3 by an *in silico* analysis of its protein sequence. Using fluorescence polarization, isothermal titration calorimetry and X-ray crystallography we show that synthetic peptides containing either phosphorylated Thr869 or Ser542 can indeed interact with 14-3-3, with the latter capable of forming an interprotein disulphide bond with 14-3-3 σ ; a hitherto unreported phenomenon.

Part of this work will be published as: **Soini, L.**, Leysen, S., Crabbe, T., Davis, J. & Ottmann, C. The identification and structural analysis of potential 14-3-3 interaction sites on the bone regulator protein Schnurri-3.

7.1 Introduction

14-3-3 proteins are a family of regulatory adaptor proteins with an interactome currently estimated to include almost 500 binding partners¹. They facilitate cellular processes like signal transduction, cellular trafficking, apoptosis and cell-cycle regulation²⁻⁴. 14-3-3 proteins are expressed in all eukaryotic cells and human compartments, reaching a remarkable percentage of 1% of the soluble brain proteins⁵. In humans, seven isoforms (β , γ , σ , ζ , η , ϵ and τ) of 14-3-3 exist. They share a high degree of homology and are known to form homodimers and heterodimers. Structurally, each 14-3-3 monomer is formed by 9 α -helices connected by short loops, which confers a high degree of rigidity when docking onto binding partners^{6,7}.

The binding of 14-3-3 proteins to their protein partners occurs via recognition of specific consensus motifs that includes a phosphorylated serine or threonine. So far, three of these motifs have been defined: mode I) RSXpS/pTXP, mode II) RXY/FXpS/pTXP and mode III) pS/pTX₁₋₂-COOH⁸. X represents any residue and mode III motifs are situated on the C-terminus of the binding partner. However, many exceptions to these motifs have also been identified⁹. Tens of crystal structures of 14-3-3 proteins bound to these motifs under the form of synthetic phosphorylated peptides are reported in the PDB¹⁰, and together provide an important resource that can be exploited for the understanding and modulation of 14-3-3 Protein-Protein Interactions (PPIs).

Regulation of osteoblast activity is essential for the preservation of bone homeostasis¹¹. Schnurri3 (SHN3), also known as Transcription Factor HIVEP3 has been identified as a key inhibitory regulator of osteoblast activity in the context of mouse postnatal skeletal remodelling¹². It has been proposed that this is achieved via interaction with the MAPK ERK1/2 and suppression of kinase activity critical to pro-osteogenic signalling pathways^{13,14}, though it remains unclear how MAPK or pathway specificity is achieved. Mice lacking critical residues in SHN3's MAPK binding motif or mice treated to reduce expression of endogenous SHN3 nevertheless displayed few phenotypic changes beyond increased adult bone mass, identifying SHN3 as an attractive drug target for osteoporosis and fracture repair treatments¹⁵.

The interaction of SHN3 with kinases opens up the possibility that its function is more specifically regulated by phosphorylation and binding to 14-3-3 proteins. To initiate investigations, we performed an *in silico* analysis and found 18 potential 14-3-3 interaction sites in human SHN3, only 2 of which were conserved in the mouse sequence. Phosphorylated synthetic peptides of these 2 consensus motifs were found to interact with 14-3-3 *in vitro* and their binding mode was further characterised by X-ray crystallography. Of particular interest, we observed that the motif built around Ser542 in human SHN3 can become covalently associated to 14-3-3 σ via an interprotein disulphide bond.

7.2 Results and Discussion

7.2.1 In silico analysis of the SHN3 protein sequence

To identify potential 14-3-3 sites on SHN3 (Uniprot ID Q5T1R4), we performed a sequence analysis using the 14-3-3-Pred webserver¹⁶. Of all the serine and threonine identified within the SHN3 sequence, 18 scored the highest values to be selected as potential 14-3-3 binding sites (Table 7.1). Among these 18 we focused our attention on the ones that more closely resembled the mode I and mode II 14-3-3 binding motifs, having an arginine at position -3/-4 and a proline at position +2 from the Ser/Thr that is phosphorylated. Particular focus has been given to the Pro +2 which has been reported to be of crucial importance for 14-3-3 recognition^{6,8,17}. Following this strategy, a more detailed analysis was performed on the sites Ser542, Thr869, Ser1894, Thr1401 and Thr2339. Since sequence conservation in different species often correlates with biological function, an alignment of the human and mouse (*Mus musculus*) SHN3 sequences was performed. This strategy also prioritises motifs that can be investigated for function in genetically engineered model organisms. The alignment revealed that only Ser542 and Thr869 were conserved in mouse, and therefore we concentrated our *in vitro* experiments on these sites.

Table 7.1: 14-3-3 putative binding sites identified on SHN3 by the 14-3-3-Pred webserver.

pS/pT Site	Sequence	Conservation*	Proline +2	Mode I/II)**
399	YFSRSE(pSer)AEQQVS	-	-	Hybrid
490	VKPRRS(pSer)LSRRSM	-	-	Hybrid
542	PLLRSH(pSer)MPSAAC	Y	Y	I) (Arg -3; Pro +2)
793	GKERRT(pThr)SKEISV	-	-	Hybrid
794	KERRTT(pSer)KEISVI	-	-	Hybrid
869	EPDRPD(pThr)EPEPPP	Y	Y	I) (Arg -3; Pro +2)
892	WPQRSQ(pThr)LAQLPA	-	-	Hybrid
933	PLSRSP(pSer)QESNVN	-	-	Hybrid
948	GSSRSA(pSer)FERDDH	-	-	Hybrid
993	EMRRSA(pSer)EQSPNV	-	-	Hybrid
1012	TETRSK(pSer)FDYGSL	-	-	Hybrid
1050	FLVRQA(pSer)LSRPPE	-	-	Hybrid
1401	YLRVPV(pThr)LPERKG	-	Y	II) (Arg -4; Pro +2)
1625	HADRRS(pSer)VYAGWC	-	-	Hybrid
1894	HALRAD(pSer)SPILGP	-	Y	I) (Arg -3; Pro +2)
1986	PLARKH(pSer)LTKNDS	-	-	Hybrid
2339	ESPRAP(pThr)NPEPSA	-	Y	I) (Arg -3; Pro +2)
2354	PLDRSS(pSer)VGCLAE	-	-	Hybrid

* Conservation has been tested against mouse ** Mode I) RSXpS/pTXP; Mode II) RXY/FXpS/pTXP

7.2.2 Biophysical characterization of the SHN3pS542 and SHN3pT869 peptides to 14-3-3 proteins

To investigate potential 14-3-3 interaction sites on a given protein, short synthetic phosphorylated peptides derived from their native sequences can be studied in biophysical assays. This circumvents the challenges associated with producing full length proteins, phosphorylated at specific sites, with sufficient amounts and purity. Several examples employing this approach are reported in the literature¹⁸⁻²⁰. Two peptides derived from the SHN3 protein sequence were designed: SHN3pS542 (LLRSHpS542MPSAAC) and SHN3pT869 (PDRPDpT869EPEPPP).

The binding of the SHN3 peptides to 14-3-3 proteins was first characterised with a fluorescence polarization assay exploiting a Fluorescein Isothiocyanate (FITC) version of the peptides. 14-3-3 proteins, in their full-length versions, were titrated on fixed concentration of peptides in order to generate a polarization attributable to a binding event. For the SHN3pS542 peptide all the 14-3-3 isoforms bound to the peptide, generating full titration curves from which it was possible to calculate affinities in the low micromolar range: from 0.5 to 2 μM (Figure 7.1a). 14-3-3 σ however, generated a curve which underwent a considerable left shift towards higher affinities compared to the other isoforms generating a nM affinity: 26 nM \pm 2 nM (Figure 7.1a). In contrast, The SHN3pT869 peptide failed to provide full titration curves as only a modest FP signal was observed at the top concentrations. It was therefore not possible to calculate K_D values (Figure 7.1b). The SHN3pT869 peptide can be considered as a very weak 14-3-3 binder.

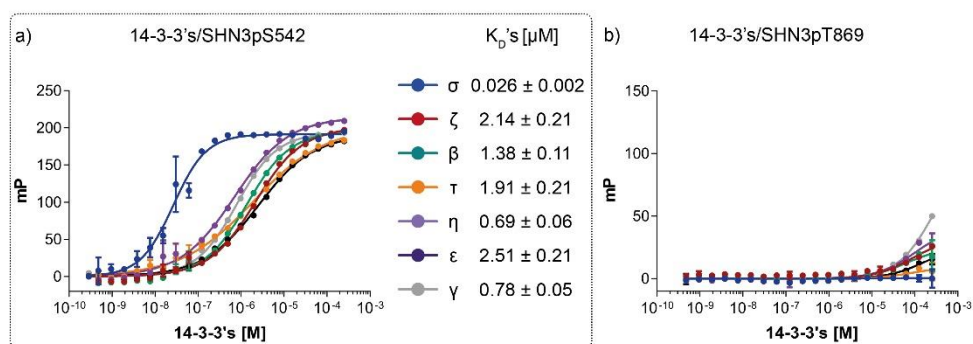


Figure 7.1 | Fluorescence polarization assays of the SHN3 peptides with all human 14-3-3 isoforms. a), b) Titration curves of 14-3-3 proteins titrated over constant concentration of SHN3 peptide. K_D values are reported on the right for the SHN3pS542 peptide.

The binding of SHN3pS542 to 14-3-3 was further characterised by ITC. The peptide was tested against the 14-3-3 γ isoform which was taken as a reference for all the other isoforms. The estimated K_D for this assay was 0.69 μM \pm 0.15 μM which matched the one estimated with the FP assay: 0.78 μM \pm 0.05 μM (Figure S 7.1a).

7.2.3 X-ray structural characterization of the SHN3pS542 and SHN3pT869 peptides in complex with 14-3-3 σ

To structurally elucidate the binding of the SHN3pS542 and the SHN3pT869 peptides, they were crystallised with 14-3-3 σ . Despite SHN3pT869 being a very weak binder to 14-3-3 proteins, X-ray crystallography experiments with this peptide were implemented. The 14-3-3 σ isoform was chosen since crystallisation conditions are known that readily produce crystals independent of the peptides being used. Also, we hoped it could provide insight as to why the SHN3pS542 peptide bound stronger to this isoform. High resolution structures for 14-3-3 σ in complex with each peptide were obtained. The data collection and refinement statistics for the solved structures are reported in Table 7.2.

Table 7.2: Data collection and refinement statistics of the 14-3-3 σ /SHN3pS542 and the 14-3-3 σ /SHN3pT869 crystal structure.

Data collection	14-3-3σ/SHN3pS542	14-3-3σ/SHN3pT869
Space group	C222 ₁	C222 ₁
Cell dimensions		
a, b, c, (Å)	82.76, 112.83, 62.93	83.29, 113.63, 63.2
Resolution (Å)	28.46-1.37 (7.52-1.37)	56.72-1.59 (8.68-1.59)
R _{merge} (%)	0.050 (0.32)	0.042 (0.15)
<I/ σ (I)>	14.1 (3.2)	19.3 (5.6)
Completeness (%)	99.9 (99.9)	99.8 (99.7)
Multiplicity	5.2 (3.4)	5.2 (3.5)
CC (1/2)	0.99 (0.84)	0.99 (0.96)
Refinement		
Resolution (Å)	28.46-1.37	56.72-1.59
No. Reflections	61661	40935
R _{work} /R _{free}	0.14/0.16	0.13/0.15
No. Atoms		
Protein	2124	2121
Water	412	394
B-factors(Å ²)		
Protein	17.89	19.66
Water	34.35	35.67
R.M.S.D.		
Bond lengths (Å)	0.018	0.011
Bond angles (°)	1.56	1.02
Ramachandran statistics (%)		
Favoured	97.91	98.32
Allowed	2.09	1.68
Outliers	0.00	0.00

Values in parenthesis represent the high-resolution shell.

For both structures, the asymmetric unit (ASU) is composed of one 14-3-3 σ monomer bound to one copy of peptide (Figure 7.2a, b). The peptide sequences bound to 14-3-3 σ were modelled in the 2F_o-F_c map contoured at $\sigma=1$, which allowed to build 9 residues out of 12 for both SHN3pS542 and SHN3pT869 peptides (Figure 7.2e, f). The two peptides bound to the canonical amphipathic 14-3-3 groove employ the phosphorylated Ser542 and Thr869 as major anchor points. These generate polar contacts with Arg56, Arg129 and Tyr130 from 14-3-3 σ (Figure 7.2c, d). Besides the phosphorylated Ser542 and Thr869, the peptides interact with different residues on 14-3-3 σ . SHN3pT869 establishes polar contacts between its Glu872 and Glu870 with Asn50, Lys122, Lys49 and Asn175 on the C-terminus side of the peptide and between SHN3pT869 Asp868 and Pro867 with Asn226 on the N-terminus side of the peptide (Figure 7.2d). Differently, the SHN3pS542 peptides establishes polar contacts between its His541 and Ser540 and Asn226, Trp230 and Glu182 on the N-terminus side of the peptide (Figure 7.2c). The C-terminus side sees the SHN3pS542 peptide extending over the entire 14-3-3 σ cavity generating contacts between Ala547, Ala546, Ser545 and Met543 with Asn42, Ser45 and Lys122 on 14-3-3 σ .

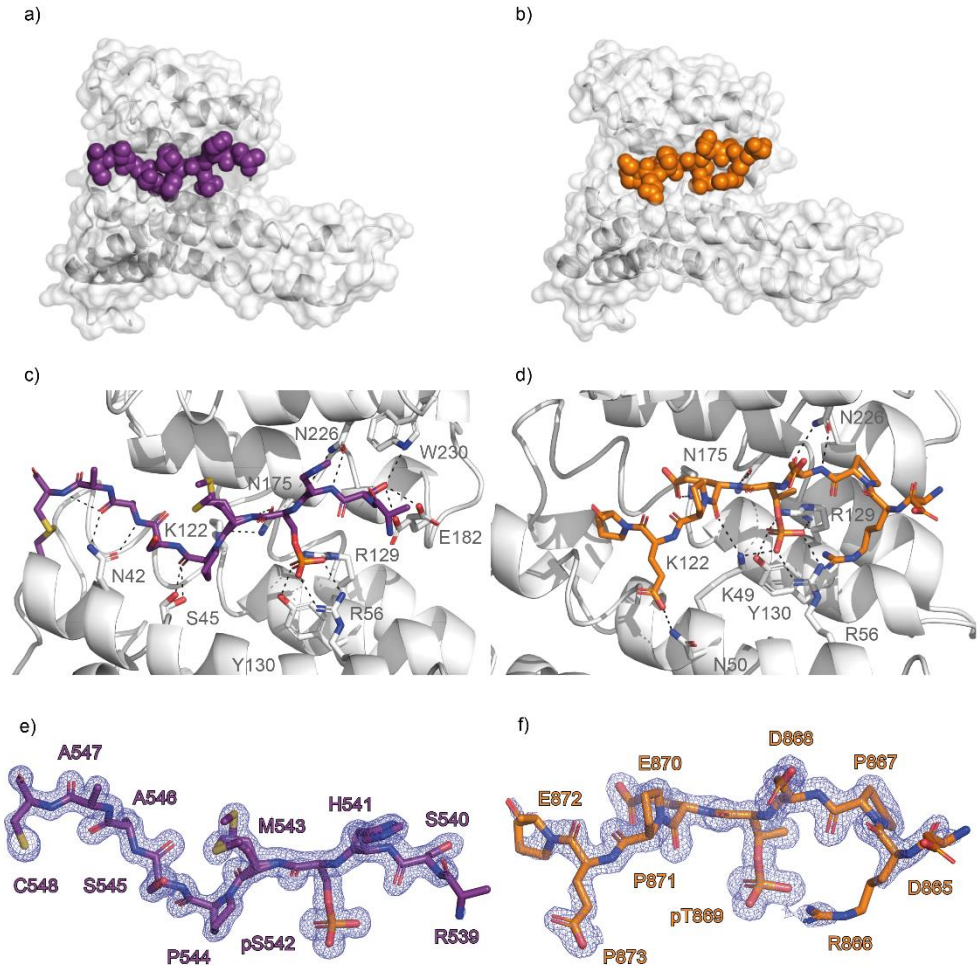


Figure 7.2 | Crystal structures of 14-3-3 σ in complex with the phosphorylated peptides SHN3pS542 and SHN3pT869. a), b) Surface representation of the asymmetric unit of the 14-3-3 σ /SHN3pS542 and SHN3pT869 crystal structure. The 14-3-3 σ monomer is represented as white surface with transparency at 60% and as white cartoon highlighting the secondary structure of 14-3-3 proteins: 9 α -helices and loops connecting them. The SHN3pS542 peptide is represented as purple spheres and the SHN3pT869 peptide is represented as orange ones. c), d) Sticks representation of the SHN3pS542 peptide (purple) and SHN3pT869 peptide (orange) bound to the 14-3-3 σ amphipathic binding groove. Polar bonds are represented as dotted black lines. e), f) Stick representation of the SHN3pS542 peptide (purple) and SHN3pT869 peptide (orange) with their 2Fo-Fc maps contoured at $\sigma=1$. The side chain of the R539 of the SHN3pS542 peptide has not been modelled due to the lack of electron density in the area.

14-3-3 proteins often bind to pSer/pThr located on intrinsically disordered regions inducing a disorder to order transition effect on their binding partners^{21,22}. Therefore, in 14-3-3/phosphopeptide

crystal structures, usually only 3 to 4 amino acids can be modelled on each side of the central pSer/Thr anchoring residue. However, it was possible to model the entire sequence of the SHN3pS542 peptide from pSer542 to Cys548 (Figure 7.2c). The $2F_o - F_c$ map strongly suggests a disulphide bond is formed between Cys548 on SHN3pS542 and Cys38 on 14-3-3 σ . This keeps the peptide rigidly docked close to the 14-3-3 surface, explaining why more of the peptide could be modelled in the electron density. It also explains the observed higher affinity of the SHN3pS542 peptide for the 14-3-3 σ isoform, as the other isoforms do not have a cysteine at the corresponding position in their primary sequence. (Figure S 7.2).

If we compare the two SHN3 peptides bound to 14-3-3 σ it is possible to notice how the covalent disulphide bond acts on the orientation that the SHN3pS542 peptide takes within the 14-3-3 binding groove (Figure 7.3b). The covalent bond in fact forces the peptide to occupy the entire length of the cavity. This evidence was found to be in total agreement with what observed in the FP assay that showed an increase of binding affinity of a 100-fold for 14-3-3 σ compared to the other 14-3-3 isoforms (Figure 7.2c). 14-3-3 proteins possess a remarkable degree of sequence similarity among the isoforms. 14-3-3 σ and 14-3-3 γ are 65% identical, but the degree of similarity can go up to 87% for 14-3-3 η and 14-3-3 γ . However, the Cys38 is present only in the 14-3-3 σ isoform which explains why the disulphide covalent bond could form only with that specific isoform (Figure S 7.2). In contrast, the SHN3pT869 peptide adopts the typical conformation with the proline in the +2 position from pThr869 inducing a turn away from the 14-3-3 binding groove^{8,17}.

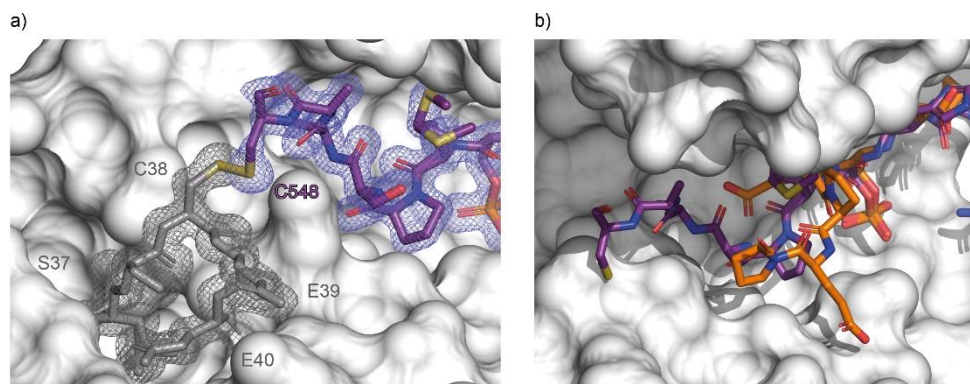


Figure 7.3 | Magnification of the SHN3pS542 and SHN3pT869 peptides bound to 14-3-3 σ .

a) The SHN3pS542 peptide is represented as purple sticks bound covalently through a disulphide bond to 14-3-3 σ Cys38. 14-3-3 σ is represented as white surface and its residues Ser37, Cys38, Glu39 and Glu40 as grey sticks. $2F_o - F_c$ map countered at $\sigma=1$ is coloured in blue for the SHN3pS542 and in grey for 14-3-3 σ suggesting the presence of a disulphide bond between Cys38 and Cys548. b) Superposition of the SHN3pS542 and the SHN3pT869 peptide bound to 14-3-3 σ . The SHN3pS542 peptide (purple) occupies the entire 14-3-3 groove whereas the two consecutive prolines in the SHN3pT869 cause the peptide to turn away from the 14-3-3 groove.

A closer look at the peptide sequences highlights the conclusion that the SHN3pS542 peptide is a pure mode I) binder, while the proline at position -2 from the pT869 site replaces the ideal hydroxylic/aromatic residue. Despite the discovery of exceptions to the canonical binding motifs 9, the presence of an aliphatic residue may be the cause of the weak affinity of the SHN3pT869 peptide to 14-3-3 proteins.

After the observation that the SHN3pS542 peptide binds covalently to 14-3-3 σ in the crystal structure, it was also tested by ITC in its acetylated and FITC-labelled form against the 14-3-3 σ isoform, under reducing conditions to calculate the K_D in the absence of a covalent bond. The estimated K_D 's for both versions of the peptide were very similar: $5.8 \mu\text{M} \pm 1.3 \mu\text{M}$ for the acetylated peptide (Figure S 7.1b) and $4.8 \mu\text{M} \pm 0.8 \mu\text{M}$ for the FITC-labelled one (Figure S 7.1c). This shows that under reducing conditions both peptides had K_D 's placed in the same affinity range as observed by FP for the other 14-3-3 isoforms (Figure 7.1a).

One of the proposed mechanisms that 14-3-3 proteins utilise to dock onto binding partners is the so-called gate-keeper model. In this model it is proposed that at first a stronger site interacts with one binding groove on 14-3-3. This would then cause the second weaker site to be in close proximity to bind to the second 14-3-3 binding groove taking advantage of the avidity effect caused by the first binding event²³⁻²⁶. Having two sites bound to 14-3-3 simultaneously improves the affinity of the whole system. This mechanism of action highlights the fact that there could be many 14-3-3 sites situated on binding partners that would not necessarily be revealed by biophysical techniques such as FP and ITC. They would in fact need to be linked to a first stronger site. The fact that the SHN3pT869 peptide did not show a comparable affinity for 14-3-3 proteins as SHN3pS542 could theoretically be explained by the fact that is part of a more complicated mode of binding such as the gate-keeper model.

7.3 Conclusions

In this work we show that, in the form of 12-mer peptides, the SHN3pS542 and SHN3pT869 sites interact with 14-3-3 proteins *in vitro* and utilise the canonical 14-3-3 binding groove. FP and ITC assays supported the SHN3pS542 binding to all 14-3-3 proteins whereas the SHN3pT869 interaction was only confirmed under the artificially high protein concentrations required to obtain the crystal structure. Significant differences in binding affinity were observed and the SHN3pS542 peptide established a disulphide bond with Cys38, which is present only on 14-3-3 σ isoform. This is the first observation of the phenomenon and it will be interesting to see whether this also occurs within the cellular environment and with full length SHN3. A covalent interaction may define a new biological function to 14-3-3 σ , for example a more permanent 3D-structural determinant for disordered proteins like SHN3.

The findings presented in this paper represent a starting point for investigating the function of any SHN3/14-3-3 PPI, with pS542 the recommended focus. The presence of a proximal reactive cysteine residue may also allow the use of covalent chemical probes to modulate any observed biological functionality^{27,28}.

7.4 Material and Methods

Protein Expression and Purification

14-3-3 isoforms γ , τ , σ , ϵ , η , ζ , β FL (full-length) and 14-3-3 $\sigma\Delta C$ ($\Delta C=231-248$) were expressed with a (His)₆-tag in NiCo21(DE3) competent cells, from a pRoeX-Htb vector in 2TY media. The purification was carried out by affinity chromatography on Nickel columns (HisTrap HP, 5 mL). The tags were cleaved with a TEV protease. The proteins were then loaded again on Nickel columns to remove any non-cleaved protein. A final purification step was performed by loading the proteins on a size-exclusion chromatography column (HiLoad 26/600 Superdex 75 pg) equilibrated in 20 mM TRIS-HCl pH 7.5, 150 mM NaCl, 2 mM DTT. All purification steps were performed on an ÄKTA pure protein purification system (Cytiva). The 14-3-3 FL versions were used in the biophysical assays and the 14-3-3 $\sigma\Delta C$ construct was used for crystallography purposes.

The peptides SHN3pS542 (LLRSHpS542MP5AAC) and SHN3pT869 (PDRPDpT869EPEPPP) were ordered with purity >95% from GenScript in an N-terminal acetylated version and in an N-terminal FITC-Ahx labelled version.

Fluorescence Polarization and Isothermal Titration Calorimetry

FP binding assays were carried out on Corning 384-well 3575 plates, serially diluting (2-fold) 14-3-3 isoforms in the presence of 10 nM FITC-labelled peptides. Proteins and peptides were diluted from their stock concentration in assay buffer (50 mM Tris pH 7.5, 150 mM NaCl, 5 mM MgCl₂, 0.05% v/v Tween-20). The data were collected on a PHERAstar FSX plate reader (BMG Labtech) with an λ_{ex} 485 nm, λ_{em} 520 nm FP filter setting. For K_D calculation the background polarization was removed from all values and the data were fitted with a "One site - Specific binding model" on GraphPad Prism version 8.1.1 for Windows, GraphPad Software, La Jolla California USA, www.graphpad.com. Each data point is the average of a triplicate measurement, standard deviation is reported as error bars. ITC measurements were performed on a PEAQ-ITC (Malvern) dissolving the peptides in assay buffer (50 mM Tris pH 7.5, 150 mM NaCl, 5 mM MgCl₂, 2 mM 2-mercaptoethanol, 0.05% v/v Tween-20) and dialysing the protein in the same buffer to minimise buffer mismatch. The optimal peptide and protein concentrations were chosen simulating the experiment on the MicroCal PEAQ-ITC Analysis Software (Malvern) according to the predicted K_D . The peptides were titrated into the cell containing the protein using a series of 18 injections 2 μ L each at 25 °C (reference power 5 μ cal/sec, stir speed 750 rpm, initial delay 60 s, spacing 150 s). The data were analysed on the MicroCal PEAQ-ITC Analysis Software (Malvern).

X-ray protein crystallography

For protein crystallisation, a C-terminally truncated version of 14-3-3 σ was used (14-3-3 $\sigma\Delta C$, $\Delta C=17$ C-terminal AA)²⁹. The binary complexes were prepared mixing 14-3-3 $\sigma\Delta C$ at 10/15 mg/ml with SHN3pS542 and SHNpT869 at a 1:1 and 1:1.2 molar ratio, followed by overnight incubation at 4 °C (dilution buffer: 20 mM HEPES pH 7.5, 2 mM MgCl₂). The crystallization drops were dispensed in 1:1 protein to crystallisation condition ratio (0.5 μ L + 0.5 μ L). A focused set of crystallisation conditions was used, containing: 95 mM HEPES pH 7.1-7.7, 24-29% PEG400, 190 mM CaCl₂, Glycerol 5%. The plate was incubated at 4 °C and crystals grew in 5 to 10 days and were observed in most of the crystallisation conditions. The data were collected on the Io4 Beamline at the Diamond Light Source. The diffraction data were processed with XDS³⁰ and AIMLESS^{31,32}. The structure was solved by molecular replacement using PHASER, with a 14-3-3 σ structure as search model (PDB ID: 3MHR),^{29,33}. The initial structure was then refined using COOT³⁴ and PHENIX³⁵. The structures are deposited in the PDB with accession code 7B13 for 14-3-3 σ /SHN3pS542 and 7B15 for 14-3-3 σ /SHN3pT869. All figures were generated using PyMOL (The PyMOL Molecular Graphics System, Version 1.2r3pre, Schrödinger, LLC).

7.5 Supporting Information

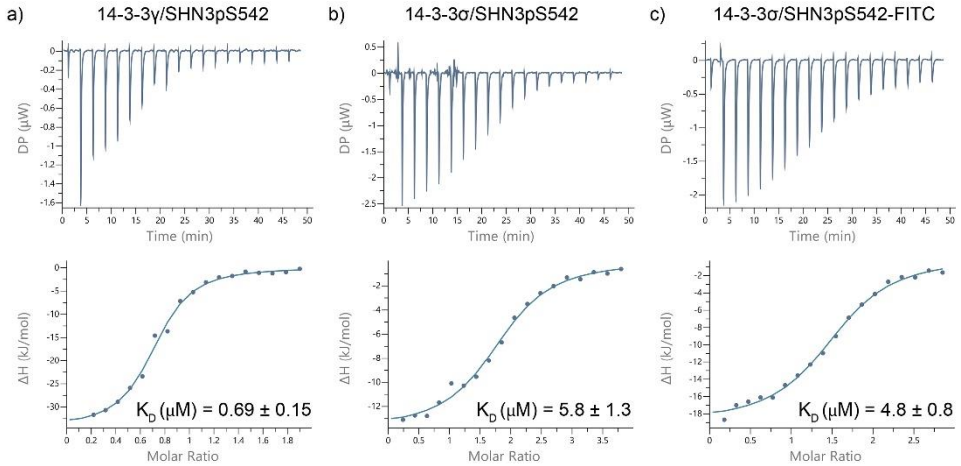


Figure S 7.1 | Isothermal Titration Calorimetry assays of 14-3-3 proteins with SHN3pS542.
a) SHN3pS542 peptide titrated over 14-3-3 γ . b) SHN3pS542 peptide titrated over 14-3-3 σ under reducing conditions. c) SHN3pS542-FITC peptide titrated over 14-3-3 σ .

```

... -38- ...
P31947 |  $\sigma$  --MERASLIQKAKLAEQAERYEDMAAFMKGAVEKGEELS $\color{orange}C$ EERNLLSVAYKNVVGQRAA ... 58
P61981 |  $\gamma$  --MVDREQLVQKARLAEQAERYDDMAAMKNVTEELNEPLSNEERNLLSVAYKNVVGARRSS ... 59
Q04917 |  $\eta$  --MGDREQLLRARLAEQAERYDDMASAMKAVTEELNEPLSNEEDRNLLSVAYKNVVGARRSS ... 59
P31946 |  $\beta$  MTMDKSELVQKAKLAEQAERYDDMAAMKAVTEQGHELSNEERNLLSVAYKNVVGARRSS ... 60
P27348 |  $\tau$  --MEKTELIQKAKLAEQAERYDDMATCMKAVTEQGAELSN EERNLLSVAYKNVVGRRSA ... 58
P62258 |  $\epsilon$  --MDDREDLVYQAKLAEQAERYDEMVESMKKVAGMDVELTVEERNLLSVAYKNVIGARRS ... 59
P63104 |  $\zeta$  --MDKNELVQKAKLAEQAERYDDMAACMKSVTEQGAELSN EERNLLSVAYKNVVGARRS ... 58

```

Figure S 7.2 | Alignment of the initial portion of the sequence of all 14-3-3 isoforms up to the first 58/59/60 residues. Homologues residues are highlighted in green and the Cys38 present only in the 14-3-3 σ isoform is highlighted in yellow.

7.6 References

- 1 Aitken, A. 14-3-3 proteins: a historic overview. *Semin Cancer Biol* **16**, 162-172, doi:10.1016/j.semcancer.2006.03.005 (2006).
- 2 Hermeking, H. & Benzinger, A. 14-3-3 proteins in cell cycle regulation. *Seminars in Cancer Biology* **16**, 183-192, doi:10.1016/j.semcancer.2006.03.002 (2006).
- 3 Mackintosh, C. Dynamic interactions between 14-3-3 proteins and phosphoproteins regulate diverse cellular processes. *Biochem J* **381**, 329-342, doi:10.1042/BJ20031332 (2004).
- 4 Johnson, C. *et al.* Visualization and biochemical analyses of the emerging mammalian 14-3-3-phosphoproteome. *Mol Cell Proteomics* **10**, M110 005751, doi:10.1074/mcp.M110.005751 (2011).
- 5 Cornell, B. & Toyo-Oka, K. 14-3-3 Proteins in Brain Development: Neurogenesis, Neuronal Migration and Neuromorphogenesis. *Front Mol Neurosci* **10**, 318, doi:10.3389/fnmol.2017.00318 (2017).
- 6 Sluchanko, N. N. & Gusev, N. B. 14-3-3 Proteins and regulation of cytoskeleton. *Biochemistry (Moscow)* **75**, 1528-1546, doi:10.1134/s0006297910130031 (2011).
- 7 Obsil, T. & Obsilova, V. Structural basis of 14-3-3 protein functions. *Semin Cell Dev Biol* **22**, 663-672, doi:10.1016/j.semcdb.2011.09.001 (2011).
- 8 Yaffe, M. B. *et al.* The structural basis for 14-3-3:phosphopeptide binding specificity. *Cell* **91**, 961-971, doi:http://doi.org/10.1016/S0092-8674(00)80487-0 (1997).
- 9 Johnson, C. *et al.* Bioinformatic and experimental survey of 14-3-3-binding sites. *Biochem J* **427**, 69-78, doi:10.1042/BJ20091834 (2010).
- 10 Sluchanko, N. N. Association of Multiple Phosphorylated Proteins with the 14-3-3 Regulatory Hubs: Problems and Perspectives. *J Mol Biol* **430**, 20-26, doi:10.1016/j.jmb.2017.11.010 (2018).
- 11 Harada, S. & Rodan, G. A. Control of osteoblast function and regulation of bone mass. *Nature* **423**, 349-355, doi:10.1038/nature01660 (2003).
- 12 Jones, D. C., Wein, M. N. & Glimcher, L. H. in *Osteoimmunology*. (ed Yongwon Choi) 1-13 (Springer US).
- 13 Shim, J. H. *et al.* Schnurri-3 regulates ERK downstream of WNT signaling in osteoblasts. *J Clin Invest* **123**, 4010-4022, doi:10.1172/JCI69443 (2013).
- 14 Kim, J. M. *et al.* The ERK MAPK Pathway Is Essential for Skeletal Development and Homeostasis. *Int J Mol Sci* **20**, doi:10.3390/ijms20081803 (2019).
- 15 Yang, Y. S. *et al.* Bone-targeting AAV-mediated silencing of Schnurri-3 prevents bone loss in osteoporosis. *Nat Commun* **10**, 2958, doi:10.1038/s41467-019-10809-6 (2019).
- 16 Madeira, F. *et al.* 14-3-3-Pred: improved methods to predict 14-3-3-binding phosphopeptides. *Bioinformatics* **31**, 2276-2283, doi:10.1093/bioinformatics/btv133 (2015).
- 17 Rittinger, K. *et al.* Structural analysis of 14-3-3 phosphopeptide complexes identifies a dual role for the nuclear export signal of 14-3-3 in ligand binding. *Mol Cell* **4**, 153-166, doi:10.1016/s1097-2765(00)80363-9 (1999).
- 18 Ballone, A., Centorrino, F., Wolter, M. & Ottmann, C. Structural characterization of 14-3-3zeta in complex with the human Son of sevenless homolog 1 (SOS1). *J Struct Biol* **202**, 210-215, doi:10.1016/j.jsb.2018.01.011 (2018).
- 19 Centorrino, F., Ballone, A., Wolter, M. & Ottmann, C. Biophysical and structural insight into the USP8/14-3-3 interaction. *FEBS Lett* **592**, 1211-1220, doi:10.1002/1873-3468.13017 (2018).
- 20 Rose, R., Rose, M. & Ottmann, C. Identification and structural characterization of two 14-3-3 binding sites in the human peptidylarginine deiminase type VI. *J Struct Biol* **180**, 65-72, doi:10.1016/j.jsb.2012.05.010 (2012).
- 21 Bustos, D. M. & Iglesias, A. A. Intrinsic disorder is a key characteristic in partners that bind 14-3-3 proteins. *Proteins* **63**, 35-42, doi:10.1002/prot.20888 (2006).
- 22 Sluchanko, N. N. & Bustos, D. M. Intrinsic disorder associated with 14-3-3 proteins and their partners. *Prog Mol Biol Transl Sci* **166**, 19-61, doi:10.1016/bs.pmbts.2019.03.007 (2019).
- 23 Molzan, M. & Ottmann, C. Synergistic binding of the phosphorylated S233- and S259-binding sites of C-RAF to one 14-3-3zeta dimer. *J Mol Biol* **423**, 486-495, doi:10.1016/j.jmb.2012.08.009 (2012).
- 24 Obsil, T., Ghirlando, R., Anderson, D. E., Hickman, A. B. & Dyda, F. Two 14-3-3 binding motifs are required for stable association of Forkhead transcription factor FOXO4 with 14-3-3 proteins and inhibition of DNA binding. *Biochemistry* **42**, 15264-15272, doi:10.1021/bi0352724 (2003).

- 25 Kostelecky, B., Saurin, A. T., Purkiss, A., Parker, P. J. & McDonald, N. Q. Recognition of an intra-chain tandem 14-3-3 binding site within PKCepsilon. *EMBO Rep* **10**, 983-989, doi:10.1038/embor.2009.150 (2009).
- 26 Yaffe, M. B. How do 14-3-3 proteins work? - Gatekeeper phosphorylation and the molecular anvil hypothesis. *FEBS Letters* **513**, 53-57, doi:10.1016/s0014-5793(01)03288-4 (2002).
- 27 Sijbesma, E. *et al.* Site-Directed Fragment-Based Screening for the Discovery of Protein-Protein Interaction Stabilizers. *J Am Chem Soc* **141**, 3524-3531, doi:10.1021/jacs.8b11658 (2019).
- 28 Sijbesma, E. *et al.* Fluorescence Anisotropy-Based Tethering for Discovery of Protein-Protein Interaction Stabilizers. *ACS Chem Biol* **15**, 3143-3148, doi:10.1021/acscchembio.0c00646 (2020).
- 29 Schumacher, B., Skwarczynska, M., Rose, R. & Ottmann, C. Structure of a 14-3-3σ-YAP phosphopeptide complex at 1.15 Å resolution. *Acta Crystallographica Section F Structural Biology and Crystallization Communications* **66**, 978-984, doi:10.1107/s1744309110025479 (2010).
- 30 Kabsch, W. Integration, scaling, space-group assignment and post-refinement. *Acta Crystallogr D Biol Crystallogr* **66**, 133-144, doi:10.1107/S0907444909047374 (2010).
- 31 Evans, P. R. An introduction to data reduction: space-group determination, scaling and intensity statistics. *Acta Crystallogr D Biol Crystallogr* **67**, 282-292, doi:10.1107/S090744491003982X (2011).
- 32 Winn, M. D. *et al.* Overview of the CCP4 suite and current developments. *Acta Crystallogr D Biol Crystallogr* **67**, 235-242, doi:10.1107/S0907444910045749 (2011).
- 33 McCoy, A. J. *et al.* Phaser crystallographic software. *J Appl Crystallogr* **40**, 658-674, doi:10.1107/S0021889807021206 (2007).
- 34 Emsley, P. & Cowtan, K. Coot: model-building tools for molecular graphics. *Acta Crystallogr D Biol Crystallogr* **D60**, 2126-2132, doi:10.1107/S0907444904019158 (2004).
- 35 Adams, P. D. *et al.* PHENIX: a comprehensive Python-based system for macromolecular structure solution. *Acta Crystallogr D Biol Crystallogr* **66**, 213-221, doi:10.1107/S0907444909052925 (2010).

Chapter 8

Epilogue

8.1 Introduction

This final chapter takes the opportunity to review what was achieved over the course of this research but also highlight some of the challenges and limitations of our approach raised in the previous chapters. Most importantly we discuss how this research could best be exploited to identify stabilisers of 14-3-3 PPIs with a view to develop therapeutically useful drugs. Using a peptide approach to study 14-3-3 biology and new targets remains a useful complementary tool we possess to discriminate between potentially promising and non-promising targets. Moreover, an outlook will be given on the added value that high-throughput screening using protein constructs performed in this work brings and how we could continue to further validate and develop the novel 14-3-3 stabilisers that were discovered.

8.2 The challenges associated with studying multivalent 14-3-3 interactions and full-length 14-3-3 binding partners

In the early days of 14-3-3 research it became clear that the binding to 14-3-3 proteins was driven almost exclusively by phosphorylated threonine or serine amino acids on the binding partner. The more 14-3-3 binding partners that were discovered, the more sequence patterns started to emerge and these were classified in the three binding modes that have been described in the previous chapters ¹. Although these sequences could be classified into specific recognition motifs, with the expansion of the 14-3-3 interactome, more and more exceptions to the rule were identified. In (Table 8.1) all the peptides characterised in this work were aligned with the three classical 14-3-3 motifs.

Table 8.1: Sequences of the peptides of which binding has been characterised as part of this work. The three modes have been colour-coded and used to determine if the peptide adheres to a specific motif, i.e. blue for mode I), green for mode II), grey for the C-terminal mode III). Mode III) motif have not been characterised in this work. Amino acids not adhering to these motifs are marked in red.

Peptides	Sequence
SLP76pS376	F P Q S A (pS) L P P Y F S
BLNKpT152	A R L T S (pT) L P A L T A
BLNKpS285	R H R G S (pS) H R Q E A V
SHN3pS542	L L R S H (pS) M P S A A C
SHN3pT869	P D R P D (pT) E P E P P P
GADSpT262	H R R H (pT) D P V Q L Q
Modes	
I)	R S X (pX) X P
II)	R X Y/F X (pX) X P
III)	(pX) X ₁₋₂ - COOH

Even among the peptides characterised in this work, it is clear how a clean-cut distinction between the modes cannot be made, except for the SHN3pS542 peptide. However, there is a common feature that

stands out: the proline in position +2 from the pS/pT. Although it is not necessary for binding, its absence in the BLNKpS285 peptide resulted in extremely poor affinity of the peptide for 14-3-3. In the case of the SHN3pT869 however its presence did not rescue the binding to 14-3-3. The categorisation of these sequences into motifs is certainly useful to consider but should not be relied upon too heavily. Indeed, this could lead to either false positives, identifying sequences in rigid non-accessible areas of the binding partner, or false negatives, missing very different sequences from the original motifs ².

When discussing 14-3-3 binding, multivalency must be considered. Focussing only on single phosphorylated peptides and prioritising one binding site over the other based solely on affinity could lead to mistakes since 14-3-3 can simultaneously engage two different sites on its binding partner ³. Often one of the two is too weak to drive the interaction and could therefore be discarded as irrelevant if studied in the absence of another phosphorylated 14-3-3 binding site. More extensive analysis and generation of longer peptides carrying combinations of different phosphorylation sites must therefore be considered. Thermodynamic models describing multivalent 14-3-3 interactions, as well as structural and biophysical studies of multivalent 14-3-3 interactions are present in the literature ⁴⁻⁶. In this work, another example has been provided by the BLNK case in which the pS285 site was found to be a very weak binder, but in combination with the pT152 site the affinity towards 14-3-3 increased dramatically. The pT869 site of SHN3 was also shown to be a very weak binder. Here too, a more extensive analysis of the other potential 14-3-3 interaction sites on SHN3 might reveal additional novel sites and binding modes. As our knowledge of 14-3-3 PPIs continues to expand so does our understanding of the complex interplay of binding sites and isoforms. This necessitates using more complex systems to ensure and avoid an overly reductionist approach.

Although working with peptides representing larger 14-3-3 binding partners has proved to be practical, they only provide a partial view of the actual PPI since short peptides can only engage the most conserved surface on the 14-3-3 proteins, the amphipathic groove. This makes it difficult to investigate isoform selectivity within signalling transduction pathways. More variable areas on 14-3-3, especially α -helices 8 and 9, might be responsible for secondary interactions that can drive specificity toward different binding partners. Therefore, working with peptide systems in HTS to identify modulators of 14-3-3 PPIs has inherent limitations. A first drawback is that potential stabiliser binding sites could be missed, as a smaller interface is probed. Secondly, one risks developing stabilisers which are only active in the context of the peptide, but not of the full-length binding partner. This work partially tries to address these issues by generating and using longer constructs or even full-length versions of 14-3-3 binding partners. Although working with proteins has the advantage of greater relevance, it does come with its own challenges. Assuming the protein of interest can be obtained in sufficient amounts, which may require extensive optimisation of protein expression and purification protocols, a major challenge comes from the fact that the protein needs to be phosphorylated, preferably in a homogeneous and site-specific manner. *In vitro* phosphorylation by the putative native kinase is one approach to obtain the phosphorylated target protein. However, extensive optimisation of the phosphorylation conditions is often required. One has also to consider the kinetics of the enzymatic reaction which can require hours of incubation at room temperature and in the case of already unstable proteins this can translate in considerable sample loss or

deterioration of sample quality. The *in vitro* phosphorylation proved to be successful in this project for the generation of a single phosphorylated species of the SLP76-SH2 construct, which has been implemented in a full-scale screening campaign. *In vitro* phosphorylation of other constructs like BLNK-FL and SLP76-FL were also successful, but multiple phosphorylation events were detected. Although it served the purpose of testing the binding to 14-3-3, more experiments will be required to identify those sites and potentially their physiological relevance. When the native kinase responsible for the phosphorylation of the 14-3-3 binding partner is unknown, or unavailable, a PKA phosphorylation site can be introduced by mutagenesis. This allows the *in vitro* phosphorylation of the target protein using recombinant PKA, or in a cellular context by co-expression of PKA. As at the start of this study, it was not certain that *in vitro* phosphorylation by HPK1 would be successful, the PKA phosphorylation approach was also explored for SLP76 and BLNK. However, as the proteins phosphorylated by HPK1 contained the native protein sequence, this strategy was ultimately preferred.

Another major challenge of working with larger protein constructs or full-length proteins, is that the structural characterization of the interaction and of potential small molecular modulators becomes more difficult. This is a consequence of the significant degree of disordered regions often observed in many 14-3-3 binding partners.

For BLNK, SLP76 and GADS previous studied identified only one site responsible for 14-3-3 binding: Thr152, Ser376 and Thr262 respectively⁷⁻⁹. Knocking out those sites impaired 14-3-3 binding and the downstream signalling. However, it cannot be excluded that more than one phosphorylated site is involved in the binding. Identifying those potential sites might be important to understand how 14-3-3 regulates signalling through its binding. It is particularly difficult to locate those sites since they are not strong enough to engage 14-3-3 alone. The number of sites involved in a 14-3-3 binding event is strictly correlated to the stoichiometry of those complexes. Hence, the stoichiometry is another important parameter that needs to be determined. In this work, the stoichiometry of the studied complexes has been partially elucidated, but has only been unequivocally determined in the case of the SLP76-SH2 construct by ITC and SPR. Two copies of SLP76-SH2 have been determined to bind to one 14-3-3 dimer. Experiments conducted on the full-length construct SLP76-FL and SLP76-PKA, however, suggest that only one copy of these protein bind to 14-3-3. Whether this is due to the larger protein size that can only fit once in the dimer, or due to other phosphorylation sites that engage simultaneously the 14-3-3 dimer will need to be addressed in the future. Interestingly, indications from the ITC performed on BLNK-PKA suggest that two copies of protein bind to 14-3-3. This is counterintuitive given the fact that our data supports that only one copy of the shorter BLNK-SH2 construct binds to 14-3-3.

The contribution that the additional interactions between 14-3-3 and a full-length or smaller construct binding partner bring to the affinity of the complex is another topic that is worth discussing in the context of this thesis. The failed binding test of the two BLNK-E and SLP76-E phospho-mimetics by SEC and ITC confirmed that phosphorylation is essential for binding and that any additional contacts developed between 14-3-3 and these two proteins are not strong enough to rescue this binding. Additional experiments are required also to clarify the difference in affinity between the SLP76 constructs and the SLP76pS376 peptide. The affinity of SLP76pS376 for 14-3-3 γ is 616 nM whereas the affinity of SLP76-

PKA for 14-3-3 γ is 650 nM. Given they are largely identical, one might argue that no affinity contribution comes from the additional contacts generated from a larger 14-3-3/SLP76 interaction. However, the affinity of the shorter SLP76-SH2 construct for 14-3-3 γ is 40 nM, so 15-fold higher. Similar observations were made from the analysis the BLNK constructs. The BLNKpT152 peptide and BLNK-PKA construct had affinities for 14-3-3 γ of 1.4 μ M and 1.9 μ M respectively. Interestingly the affinity of BLNK-SH2 for 14-3-3 γ is 13 μ M which is an opposite trend compare to what observed for the SLP76 constructs. The two SLP76-SH2 and BLNK-SH2 are different in size, 19 kDa and 34 kDa respectively. The molecular weight of an SH2 domain itself is around 12 KDa. The BLNK-SH2 construct therefore has a considerable amount of additional disorder that could interfere with the binding to 14-3-3.

8.3 SLP76 as potential therapeutic target

Drug discovery is an extremely costly and time-consuming process that can take up to 20 years and several billions (€/\$) without a guarantee of success ¹⁰. The steps that have to be considered are many and include target validation, lead generation followed by preclinical and clinical development, and ultimately drug approval ¹¹. Obviously, every single step is crucial for a successful outcome. High-throughput screening (HTS) remains the most commonly used technique and generally applicable technique in hit finding today and is the focus of this work ¹². Hughes et al. ¹¹ described five key general requirements independent from the chosen assay format which should be considered. Those are: a validation of the assay, the reproducibility of the assay, the assay costs, the assay quality identified with the Z factor and the robustness to the solvent used for compounds storage. In the case of the 14-3-3 γ /SLP76-SH2 HTS all these requirements have been fulfilled.

The high-throughput screen developed in this work has general applicability to other 14-3-3 PPIs with the appropriate optimisation. Indirectly, the approach has already been applied to the 14-3-3/p27 PPI which was used as a counter screen during hit triage of the output from the 14-3-3/SLP76 screen. In identifying novel and selective stabilisers of the 14-3-3/SLP76 protein system, using protein constructs rather than peptides, we have achieved a major objective of our research. A key observation is that using the protein system we have found different chemical matter than would have not been found using only the peptide system. Of the 16 best compounds, only two demonstrated activity in both protein-based FRET and FP-labelled peptide assay. This supports the fundamental hypothesis that protein-systems inherently provide a greater opportunity to discover potentially useful hit compounds beyond the canonical 14-3-3 binding site. An unintended but welcome by-product of the 14-3-3/SLP76 screen was the discovery of compounds that also stabilised 14-3-3/p27 PPI, opening up future exploration on this target. More broadly we would expect that extending this screening approach across a wide range of 14-3-3 PPIs we could reasonably expect to find more chemotypes that selectively stabilise specific interactions or indeed those that stabilise multiple 14-3-3 PPIs. In our first proof of concept screen we have at least exposed the potential with the early data already showing tuneable selectivity between SLP76 and p27. As discussed in previous chapters, the generation of high-resolution structural information on 14-3-3/full-length

binding partners PPIs is challenging, and it is still elusive for the 14-3-3/SLP76-SH2. The general applicability of the FRET assay developed here would allow the identification of molecular glues of other 14-3-3 PPI with more potential to crystallise. The obtaining of high-resolution data on any ternary 14-3-3/target/compound complex would be transformational for the development and optimisation of 14-3-3 PPIs stabilisers and/or inhibitors.

The natural follow up of the 14-3-3 γ /SLP76-SH2 project would be to test the hits identified from the HTS in a more complex environment such as cell lines and test them for function. Ten of the sixteen compounds identified from the primary and secondary screening, i.e compounds **1**, **2**, **3**, **4**, **7**, **8**, **9**, **10**, **12** and **13** were tested in Jurkat T-cells exploiting flow cytometry. Our initial hypothesis was that the stabilisation of the 14-3-3/SLP76 complex would increase proteasomal degradation of SLP76. Flow cytometry is an assay that would allow levels of phosphorylated and non-phosphorylated SLP76 in the cell to be monitored upon stimulation of the TCR with anti-CD3 and compare these levels in the presence and absence of the compounds. Two antibodies labelled for flow cytometry detection were ordered: one specific for SLP76 and one for the phosphorylated form of SLP76 at Ser376, the site that triggers the negative feedback mechanism leading to SLP76 degradation. An initial test on cell viability revealed that they tolerate a DMSO concentration of 0.3 % and exposure to 30 μ M compound concentrations. Unfortunately, so far, no SLP76 decrease has been detected upon TCR stimulation and compound exposure. However, the assay development is still at its early days and was unable to be fully developed within the time of this thesis. It also needs to be recognised that the hits from the FRET screen are at their earliest stage of their development and will almost certainly need some optimisation before demonstrating functional effects in cells. We also recognise the importance of additional functional assays to confirm the relevance of the hits from the screen and support continued hit characterisation. Although we believe the FRET assay will prove to be a valuable approach to research in this field, it shares the limitation of any protein-based high-throughput screen. The novel 14-3-3 stabilisers we have identified will only have true value if they can be optimised and demonstrate a useful cellular and ultimately *in vivo* function. Our recommendation as a next step would be to focus on techniques where first you can recapitulate specific stabilisation of the 14-3-3/SLP76 interaction in cells e.g. using a Promega NanoBit® system used widely to study PPIs. In tandem, flow cytometry or other techniques to monitor protein levels should continue to be explored. Given that our ultimate goal was to promote degradation of SLP76 these assays will be key to supporting the next phase of hit characterisation. Only after we have hits that can do this can we move to look at inhibiting T-Cell signalling in human primary cells.

8.3.1 SLP76 involvement in human disease

Although SLP76 has been identified mainly as a critical signal transducer protein downstream TCR, it is an adaptor protein expressed in all the hematopoietic compartment, mast cells, neutrophils, platelets and natural killer cells¹³. It has also been described to play a role downstream of the BCR in the context of Chronic Lymphocytic Leukemia. In particular, aberrant SLP76 expression in Chronic Lymphocytic Leukemia cells correlates with a more aggressive disease course¹⁴. SLP76 has also been recently reported to interact with the Receptor for Advanced Glycation Endproducts (RAGE) in the context of Sepsis.

SLP76 binds through its N-terminal SAM domain to RAGE mediating the signalling to downstream effectors in macrophages. Inhibiting the interaction between RAGE and SLP76, *via* a TAT-SAM fusion peptide, results in blocking the downstream signalling events, therefore prolonging life of mice that underwent cecal ligation and puncture ¹⁵. Although a speculative concept, these two examples highlight how a degrading or inhibiting SLP76 by drugs could result in a beneficial therapeutic effect.

Until recently, the adaptor protein SLP76 has never been directly associated to a human disease condition. In fact, the major studies on SLP76 have been performed on Jurkat cell lines and SLP76-deficient mice. Recently, for the first time, human immunodeficiency due to biallelic mutation in SLP76 has been described resulting in T and B cell immunodeficiency, heavy neutrophil defects and platelet aggregation ¹⁶. The correlation between the SLP76 deficiency and the patient's immune phenotype helped in the understanding of the role of SLP76 and its biology in man.

These findings highlight the importance of SLP76 in the context of the immune response, immunology and human conditions making it a potential drug target for the future.

8.4 References

- 1 Yaffe, M. B. *et al.* The structural basis for 14-3-3:phosphopeptide binding specificity. *Cell* **91**, 961-971, doi:http://doi.org/10.1016/S0092-8674(00)80487-0 (1997).
- 2 Sluchanko, N. N. Association of Multiple Phosphorylated Proteins with the 14-3-3 Regulatory Hubs: Problems and Perspectives. *J Mol Biol* **430**, 20-26, doi:10.1016/j.jmb.2017.11.010 (2018).
- 3 Yaffe, M. B. How do 14-3-3 proteins work? - Gatekeeper phosphorylation and the molecular anvil hypothesis. *FEBS Letters* **513**, 53-57, doi:10.1016/s0014-5793(01)03288-4 (2002).
- 4 Stevers, L. M. *et al.* Characterization and small-molecule stabilization of the multisite tandem binding between 14-3-3 and the R domain of CFTR. *Proc Natl Acad Sci U S A* **113**, E1152-1161, doi:10.1073/pnas.1516631113 (2016).
- 5 Stevers, L. M. *et al.* Structural interface between LRRK2 and 14-3-3 protein. *Biochemical Journal* **474**, 1273-1287, doi:10.1042/bcj20161078 (2017).
- 6 Stevers, L. M., de Vink, P. J., Ottmann, C., Huskens, J. & Brunsveld, L. A Thermodynamic Model for Multivalency in 14-3-3 Protein-Protein Interactions. *J Am Chem Soc* **140**, 14498-14510, doi:10.1021/jacs.8b09618 (2018).
- 7 Wang, X. *et al.* Down-regulation of B cell receptor signaling by hematopoietic progenitor kinase 1 (HPK1)-mediated phosphorylation and ubiquitination of activated B cell linker protein (BLNK). *J Biol Chem* **287**, 11037-11048, doi:10.1074/jbc.M111.310946 (2012).
- 8 Wang, X. *et al.* Attenuation of T cell receptor signaling by serine phosphorylation-mediated lysine 30 ubiquitination of SLP-76 protein. *J Biol Chem* **287**, 34091-34100, doi:10.1074/jbc.M112.371062 (2012).
- 9 Lasserre, R. *et al.* Release of serine/threonine-phosphorylated adaptors from signaling microclusters down-regulates T cell activation. *J Cell Biol* **195**, 839-853, doi:10.1083/jcb.201103105 (2011).
- 10 Kola, I. & Landis, J. Can the pharmaceutical industry reduce attrition rates? *Nat Rev Drug Discov* **3**, 711-715, doi:10.1038/nrd1470 (2004).
- 11 Hughes, J. P., Rees, S., Kalindjian, S. B. & Philpott, K. L. Principles of early drug discovery. *Br J Pharmacol* **162**, 1239-1249, doi:10.1111/j.1476-5381.2010.01127.x (2011).
- 12 Brown, D. G. & Bostrom, J. Where Do Recent Small Molecule Clinical Development Candidates Come From? *J Med Chem* **61**, 9442-9468, doi:10.1021/acs.jmedchem.8b00675 (2018).
- 13 Koretzky, G. A., Abtahian, F. & Silverman, M. A. SLP76 and SLP65: complex regulation of signalling in lymphocytes and beyond. *Nat Rev Immunol* **6**, 67-78, doi:10.1038/nri1750 (2006).
- 14 Dezarella, N. *et al.* SLP76 integrates into the B-cell receptor signaling cascade in chronic lymphocytic leukemia cells and is associated with an aggressive disease course. *Haematologica* **101**, 1553-1562, doi:10.3324/haematol.2015.139154 (2016).
- 15 Yan, Z. *et al.* Targeting adaptor protein SLP76 of RAGE as a therapeutic approach for lethal sepsis. *Nature Communications* **12**, doi:10.1038/s41467-020-20577-3 (2021).
- 16 Lev, A. *et al.* Inherited SLP76 deficiency in humans causes severe combined immunodeficiency, neutrophil and platelet defects. *J Exp Med* **218**, doi:10.1084/jem.20201062 (2021).

The flow cytometry work mentioned in this chapter was performed by Dr. Catherine Simpson.

Summary

Protein-Protein Interactions (PPIs) play a role in almost every essential biological process of the cell: from apoptosis to cell cycle regulation, from subcellular localization to signal transduction and regulation of transcription factors. Since misregulation of PPIs often leads to serious human pathological conditions, targeting them by small molecule inhibitors or stabilisers had consequently become an attractive strategy for the development of novel therapeutic drugs.

The class of regulatory adaptor proteins 14-3-3, facilitate a plethora of cellular processes recognizing phosphorylated sites in motifs present on their binding partner, hence modulating signalling pathways. 14-3-3 proteins have also been correlated to ubiquitination and proteasomal degradation pathways. This thesis work focuses on the identification of molecular glues of 14-3-3 PPIs that could potentially enhance the proteasomal degradation of their binding partners. Additionally, an extensive biophysical and structural characterization of these 14-3-3 binding partners was performed.

In Chapter 2, a structural and biophysical characterization of the 14-3-3 interaction with B-cell linker protein (BLNK) has been performed. BLNK is an adaptor protein that orchestrates signalling downstream of BCR (B-cell receptor) and that has been reported to undergo negative feedback mechanism which ultimately leads to BLNK degradation. This mechanism is mediated by HPK1 phosphorylation of BLNK Thr152 and 14-3-3 binding. A second BLNK site, Ser285, has been suggested to contribute to the 14-3-3/BLNK PPI. The interaction was characterized by means of two BLNK 12-mer synthetic peptides and a long peptide containing both pThr152 and pSer285. The experimental data suggests that BLNK could interact with 14-3-3 *via* a gate-keeper model. Additionally, several BLNK protein constructs were generated, including BLNK-FL, BLNK-SH2, BLNK-PKA and BLNK-E. BLNK-SH2 was identified as a potential construct to use in screening campaigns for the determination of small molecule stabilisers of the 14-3-3/BLNK PPI.

Chapter 3 focuses on the 14-3-3 interaction with the Lymphocyte cytosolic protein 2 (SLP76). SLP76 is a protein that belongs to the same protein family as BLNK but has been described as a regulator of the signalling downstream of TCR (T-cell receptor). Similarly to BLNK, a negative feedback mechanism involving HPK1, that phosphorylates SLP76 Ser376, allowing 14-3-3 binding and subsequent SLP76 proteasomal degradation has been described. Therefore, the characterization of the binding of a 12-mer synthetic peptide mimicking SLP76 has been performed. Since an equally important goal of these preliminary studies was to generate longer protein constructs to be used for the identification of small molecule stabilisers of 14-3-3 PPI, SLP76-FL, SLP76-SH2, SLP76-PKA and SLP76-E protein constructs were generated. The affinity of SLP76-SH for 14-3-3 and the stoichiometry of the its complex with 14-3-3 was also characterized.

In Chapter 4, a TR-FRET (Time Resolved Fluorescence Energy Transfer) assay for the identification of modulators of 14-3-3 PPIs has been developed, using the BLNK-SH2 and SLP76-SH2 protein constructs described in Chapter 1 and Chapter 2. The TR-FRET assay development process was started

on both constructs with the ultimate decision to only focus on SLP76-SH2 as it provided ideal assay conditions.

Chapter 5 implements the TR-FRET developed in Chapter 4 for the 14-3-3 γ /SLP76-SH2 PPI in a full high-throughput screening (HTS) campaign. During the HTS campaign two other protein FRET pairs were used as counter screens: an unrelated one (IL17/IL17R) and a related one (14-3-3 ζ /p27). The HTS and follow-up on the hits allowed to identify 16 stabilisers of the 14-3-3 γ /SLP76-SH2 PPI across a range of different chemotypes. Additionally, a library of derivatives of two of these initial hits was also tested resulting in the identification of additional stabilisers of the 14-3-3 γ /SLP76-SH2 PPI. The hits identified on the 14-3-3 γ /SLP76-SH2 PPI were also tested on the 14-3-3 γ /SLP76pS376 peptide system to provide support for structural studies. However, crystal structures of a ternary complex of the hits identified in this work remain to be determined.

In Chapter 6, a structural and biophysical characterization of another 14-3-3 binding partner involved in TCR signalling, the GRB2-related adapter protein 2 (GADS), has been performed. GADS, like SLP76, orchestrates signalling downstream of TCR and a model has previously been proposed where a ternary complex formed by 14-3-3, SLP76 and GADS might be targeted for degradation. A deeper investigation of the interaction between GADS, SLP76 and 14-3-3 could therefore provide a new entry point for the modulation of TCR signalling.

Chapter 7 explores the interaction with a yet unreported 14-3-3 potential binding partner, the bone regulator protein Schnurri-3 (SHN3). We exploited the 14-3-3-Pred webserver to identify potential 14-3-3 binding motifs on SHN3 *in silico*, after which we focussed on Ser542 and Thr869 as potential binding sites. The two sites were studied using 12-mer synthetic peptides and two novel crystal structures were generated. Our findings revealed that the SHN3pS542 peptide bound covalently to 14-3-3 σ suggesting that it could be the starting point for a more in-depth investigation of the 14-3-3/SH3 PPI.

As a general conclusion, this work identifies new stabilisers of the 14-3-3 γ /SLP76-SH2 PPI. Exploiting, to the best of our knowledge, for the first time a proteinaceous 14-3-3 binding partner in a TR-FRET format HTS. The general applicability of this approach could help in the identification of new modulators of other 14-3-3 PPIs in the future. Additionally, this work extensively expands the structural and biophysical characterization of four 14-3-3 binding partners exploiting short synthetic phosphorylated peptides.

Curriculum Vitae



Lorenzo Soini was born in Rovereto, Italy, the 12th December 1989. He obtained the BSc and the MSc in Chemistry at the University of Padua (Italy). During his master's degree he joined the Erasmus Programme and spent one semester at the Instituto Superior Técnico, Lisbon. The master's graduation project involved the structural characterization of the antiapoptotic protein Bcl-xL. In 2016, he joined the TASPPPI consortium (funded project by the H2020 Marie Curie Actions of the European Commission) as a PhD student at UCB Pharma (Slough, United Kingdom) under the supervision of Dr. Jeremy Davis and Dr. Christian Ottmann. The PhD project dealt with the generation of screening technologies for the identification of molecular glues of 14-3-3 Protein-Protein Interactions and their structural and biophysical characterization. During the PhD, two internships at the Technical University of Eindhoven were conducted. The major results achieved in this PhD project are presented in this thesis.

List of Publications

Soini, L., Leysen, S., Davis, J. & Ottmann, C. A biophysical and structural analysis of the interaction of BLNK with 14-3-3 proteins. *J Struct Biol* 212, 107662, (2020).

Soini, L., Leysen, S., Davis, J., Westwood, M. & Ottmann, C. The 14-3-3/SLP76 protein–protein interaction in T-cell receptor signalling: a structural and biophysical characterization. *FEBS Letters* **595**, 404-414, (2020).

Soini, L., Leysen, S., Crabbe, T., Davis, J. & Ottmann, C. The identification and structural analysis of potential 14-3-3 interaction sites on the bone regulator protein Schnurri-3. *Recently submitted*.

Soini, L., Redhead, M., Westwood, M., Leysen, S., Davis, J., and Ottmann, C. Identification of molecular glues of the SLP76/14-3-3 protein-protein interaction. *Recently submitted*.

Acknowledgments

I would like to thank my supervisors Dr. Jeremy Davis and Dr. Christian Ottmann for giving me the opportunity to work on this challenging and stimulating PhD project. Thank to Dr. Seppe Leysen for guiding me as an advisor through these difficult years and to have always been there for help. I found the writing of this thesis and of the manuscripts one of the toughest tasks I have ever had to perform. So, thank again to Dr. Jeremy Davis and to Dr. Seppe Leysen for the effort you put into what I think it has been quite a painful reviewing process to go through.

Thank to Dr. Martin Redhead for guiding me through the key work of this project (TR-FRET HTS) and to Marta Westwood for helping me in the generation of crucial SPR data. UCB Pharma in Slough has been my home for three years and I would like to acknowledge all the people that contributed to this project: Dr. Tom Crabbe, Dr Alex Macpherson, Dr. Carl Doyle, Prashant Mori, Jan Broadbridge, Dr. Rachel Davis, Dr. Christine Prosser, Adam Hold, Dr. Rebecca Burnley, Dr. Victoria Ellis

Thank you, Kate, Jade and Anna, for supporting me over the years I lived in Slough, for the runs, the chats, the coffees and the movies. A special thank goes to the TASPPPI group with which I shared important years of my life. I would like to thank in particular Dario, Alice, Federica, Sonja, Blaz and Francesco for all the happy moments we spent together and for supporting me as a friend during the difficult times of this PhD.

Finally, a special thank to my family and closest friends for always believing in me.